Cape Peninsula
University of Technology

Heat pumping for cloudy weather and night solar water purification

by

FOUAD M ALKILANI

Thesis submitted in fulfilment of the requirements for the degree

Doctor of Engineering: Mechanical Engineering

in the Faculty of Engineering

at the Cape Peninsula University of Technology

Supervisor: Dr Ouassini Nemraoui

Co-supervisor: Dr Fareed Ismail

Bellville

December 2022

DECLARATION

I, Fouad M Alkilani, declare that the contents of this dissertation/thesis represent my own unaided work, and that the dissertation/thesis has not previously been submitted for academic examination towards any qualification. Furthermore, it represents my own opinions and not necessarily those of the Cape Peninsula University of Technology.

09/12/2022

Signed **Date**

ABSTRACT

As a result of rapid population growth, and the expansion of urbanization, industrial and agricultural activities, the stress on fresh water resources has drastically increased. The limitation of natural drinkable water resources has a negative impact on safety, security and socioeconomic conditions of human societies. The traditional water treatment processes are associated with controversial matters such as environmental issues and economic decline; however, the advanced processes required need a developed infrastructure facility and high initial investment cost.

This research work presents a method that could help individuals in rural areas and small communities to produce their daily needs of potable water. Two types of solar powered heat pump systems were designed and developed to be combined into conventional solar still models, and therefore to overcome the main drawback of conventional solar stills, which is low efficiency. The advanced solar stills make use of the available solar energy to generate electrical and thermal energies, so that heating up water more quickly and recovering the energy losses is possible.

The first proposed system was solar still integrated with a DC vapour compression heat pump system. Outdoor experimental results showed that in summer season of Cape Town, the comparison between the conventional solar still and the proposed one indicated that on a typical day of November (summer season in the southern hemisphere), the water temperature in advanced solar still reached 73 ºC while in conventional one was 57.5 ºC. The daily distillate yield was 6.21 and 2.67 L/m^2 for the advanced and conventional solar still respectively. In the winter season, the conventional solar still performed poorly on a partly cloudy cold day, the maximum water temperature was about 38.5 ºC and the daily distillate yield was 0.215 L/m^2, while the performance of the advanced still was satisfactory, the daily distillate yield was 4.2 L/m^2 at a maximum water temperature of 58.9 ºC. The average of the coefficient of performance (COP) of the vapour compression heat pump system was 3.5.

The second proposed system was a solar still integrated with thermoelectric heat pump system. Outdoor experimental tests were performed to investigate the performance of the system. The results obtained show that the daily distillate yield of the second proposed system was about 4.4 L/m^2, while the conventional one produced 2.1 L/m^2. The maximum value (COP) of the thermoelectric heat pump according to energy balance equations and the principle of thermodynamics for a single-stage heat pump was about 1.9.

ACKNOWLEDGEMENTS

I wish to thank and express my gratitude to

- **Dr Ouassini Nemraoui and Dr Fareed Ismail for their supervision of this thesis.**
- **The staff of the Mechanical Engineering Workshop for their assistance.**

DEDICATION

I would like to dedicate this thesis to my family and friends

Contents

LIST OF FIGURES

LIST OF TABLES

GLOSSARY

Acronyms/Abbreviations	Definition/Explanation
AST	Apparent solar time
AWQ	Atmospheric water generation
BWD	Brackish water desalination
CPUT	Cape Peninsula University of Technology
COP	Coefficient of performance
DOD	Depth of discharge
GWI	Global Water Intelligence
IX	Adsorption and ion exchange
MF	Micro-filtration
MPPT	Maximum power point tracker
MSF	Multi stage flash desalination
NF	Nano-filtration
PV	Photovoltaic
PVT	Photovoltaic thermal system
PWM	Pulse width modulation
RE	Renewable energy
RO	Reverse osmosis
RR	Recovery ratio
SAHP	Solar assisted heat pump system
SD	Solar distillation
STC	Standard test conditions
SWD	Seawater desalination
TDS	Total dissolved parts
TE	Thermoelectric
TE_c	Thermoelectric cooler
TE_G	Thermoelectric generator
UF	Ultra-filtration
VC	Vapour compression
WHO	World Health Organization
WWD	Waste water desalination

Terms	Definition/Explanation
A	Area (m^2)
AC	Alternating current (Amp)

C_p	Specific heat (kJ/Kg. K)
d	Day of the year
DC	Direct current (Amp)
$E_{\lambda b}$	Energy emitted per unit area
f	Circumsolar horizontal incident radiation flux
h_f	Enthalpy (kJ/kg)
I	Current (Amp)
I_{bh}	Horizontal incident beam flux
I_{cs}	Closed circuit current (A)
I_d	Incident diffuse flux
I_s	Solar constant (W/m^2)
I_T	Total incident radiation on tilted surface (W/m^2)
K_m	Thermal conductance ($W \cdot K^{-1}$)
L	Latitude
$\dot{m}$	Mass flow rate (kg/s)
N	Number of semiconductor Pairs
P_n	Number of PV panels
Q	Heat energy (kJ)
Q_b	Quantity of brine produced (m^3/day)
Q_{max}	Maximum load of TE module
R_m	Electric resistance (Ohms/ Ω)
S	Entropy (kJ/kg)
T	Temperature (^oC) or (K)
T_c	Cold sides temperature of TE module
T_h	Hot sides temperature of TE module
V	Voltage (Volt)
V_{max}	Maximum voltage of TE module
V_{oc}	Open circuit voltage (v)
W	Work input (Watt)
ZT	Figure of merit

Greek symbols	**Definition/Explanation**
ε	Emissivity
η	Efficiency
α	Solar altitude angle
z	Azimuth angle (˚)
β	Incident angle (˚)
θ	Tilt angle from horizontal

θz	Zenith angle (˚)
ω	Hour angle
ρ_g	Ground reflectivity
α_s	Seebeck coefficient
α	Electric conductivity (S/m)
σ	Declination angle

CHAPTER ONE

Introduction

1.1. Problem statement

The problem statement of this research can be broken down into the following points:

- Current solar thermal water purification systems developed at the Cape Peninsula University of Technology (CPUT) and elsewhere so far work well only on sunny days. No such purifier works on cold cloudy days and/or at night.
- There are no well-established performance indicators for solar water purifiers.
- Apart from units developed at CPUT, there are no known commercial solar thermal water purifiers on the continent.

Therefore, this research will comprise the design, construction and testing of a solar water purification system that can produce purified water during cloudy days and at night. The system will use two different heat pump systems to pump heat to the distillation unit in order to maintain the temperature at as high a level as possible. A PV system will be used to power the heat pump systems and other electronics. This will be a novel approach to water distillation/purification technology.

1.2. Objectives

Water is a precious commodity: the expression “water is life” is one of the most truthful messages all humans bear witness to (Thairu, 2018). Sources of fresh water are limited on earth. Therefore, governments and societies face the challenge of providing people with their potable water needs. Water treatment plants consume a vast amount of energy, which has a negative impact on the economy and environment. In remote areas, the limited access to the public line water supplier or national grid has led the residents to rely on natural resources such as wood and charcoal to treat their needs of fresh water, and therefore, the use of solar water purification technology is a promising solution to provide small communities with a sufficient amount of fresh water. In this respect, the objectives of this research are as follows:

- To invent novel solar water purification systems that can work in cloudy weather and at night for small rural homesteads.
- To introduce two novel ways of complementary heating in solar water purification systems.
- To overcome the shortcomings of the conventional solar still systems.
- To enhance the socioeconomic status of developing and remote region residents which can be achieved by reducing the risks of consuming contaminated water and reducing dependence on fossil fuels in terms of energy production.

- To design the system such that it will utilize solar energy to power the heat pumps, which increases the productivity of the distillate water during cloudy days.
- To define and compare key performance indicators for solar water purification units. thereby providing a scientific concept for further projects to upscale the system.
- To present an energy backup system that can be used for different configurations of solar water stills.

1.3. Water and life

Water is one of the essential needs of life on planet earth. It plays a crucial role in the welfare of societies around the globe and affects the sustenance of every human. It is the most widely distributed substance that covers more than 70% of the earth surface. However, 97.5% of that amount is salty water, leaving only 2.5% as consumable water, which can be found in rivers, fresh water lakes, and deep underground aquifers or as soil moisture, and the large amount of that fresh water representing about 70% is confined in glaciers (WHO, 2015). In recent decades, massive growth in population and modern life has led to a significant expansion in the agricultural and industrial production. The associated increase in energy demands and urbanization expansion have increased the stress on the fresh water resources, oceans and seas. These activities have led to the destabilization of natural ecosystems and the deterioration of water supply systems (Perk, 2013).

Recent research and studies on potable water warn that fresh water sources are becoming scarce and most countries are suffering from water contamination due to climate change, human activities, and long-term droughts (Chong et al., 2010; Inyinbor et al., 2018). By 2050, the world population is expected to reach up to 9 billion, therefore, the demand on fresh water will increase and this lead to put more stress on water resources. Srinivasan et al. (2012) reported that regions such as India, China and North and sub-Saharan Africa will face water crises. Moreover, water policies have a tremendous impact on the economy. In 2011, the Chinese government announced that investments in water protection and improvements of about 600 billion US dollars for the following ten years (Yu, 2011). In the commercial capital of Tanzania, Dar es Salaam, people pay more for water than residents of New York City (Chamberlain, 2008).

1.4. Water quality

From a scientific perspective, water has a molecular weight of 18. It has a simple structure with two hydrogen atoms and an oxygen atom. This gives water unique features (large latent heat for phase changes, heat capacity, and it is a good solvent),

allowing it to behave differently compared with other compounds of similar characteristics (Boyd, 2000).

The term water quality could be used to describe the suitability of water for human consumption and the health ecosystem. It describes the biological, chemical, and physical characteristics of water. The biological constituents (living organisms) include viruses, bacteria, phytoplankton, protozoans, insects, and plants. The most common chemical constituent (dissolved substances) include gases (e.g., nitrogen and carbon dioxide), metal (e.g., iron and lead), pesticide (e.g., atrazine and endosulfan) and other organic compounds. The physical characteristics of water include taste, colour, odour, temperature, and turbidity (Kati & Angelo, 2010).

Rivers, lakes, and natural springs, which are all potential sources of drinking water, are subjected to a wide range of climatic conditions that might degrade their quality, and as a result, all water sources need to undergo some kind of treatment in order to be safe for human use (Ahuja, 2013). Government agencies and regulatory groups are responsible for setting water quality standards. The World Health Organization (WHO) for example has established guidelines for drinking water standards. It suggests that there should be legal international standards for drinking water quality in all countries (WHO, 2008; Krantzberg, 2010).

1.5. Water quality and public health

Dating back to the middle of the 19th century, it was thought that diseases such as cholera and typhoid were transmitted by breathing miasma and vapor released from decaying carcasses. Later, at the end of the century, scientists could identify the relationship between the contamination of water and waterborne diseases (Crittenden et al., 2012). As a better understanding of water and health was gained, a sanitary system revolution was achieved. Hence, the advancement of water purification technologies and sanitation management has resulted in numerous positive effects on human health (Bartram & Baum, 2015).

The contamination of drinking water resources is a problematic issue facing governments around the globe. In terms of the health sector, waterborne diseases contribute to high rates of mortality and morbidity, after respiratory infections. It is estimated that more than 60 million cases of gastrointestinal infection occur annually (Chigor et al., 2012) and cause death for about 24000 children (Chamberlain, 2008; Kalita et al., 2016). The most common health hazards associated with water contamination are the infectious diseases caused by pathogenic bacteria and viruses. Chemical contamination in drinking water has less impact on human health than microbial contamination. Its effects appear after a prolonged period of consumption, but there are some hazards associated with massive leakage of chemicals into the water supply (WHO, 2008).

1.6. Water and security

Water plays a significant role in the stabilization of societies. Water shortages can cause threats to the security, economic and political situation of countries and destabilize them. Throughout the history of the civilisations and nations, competition for fresh water resources has taken place very early and therefore disagreement and conflicts were raised, and in many cases moved to violence (Chellaney, 2013). Nowadays, water-related conflict is very common in many countries and it is expected to be more intense in the coming years (Gehrig & Rogers, 2009). Figure 1.1 shows the number of major events reported since 1931.

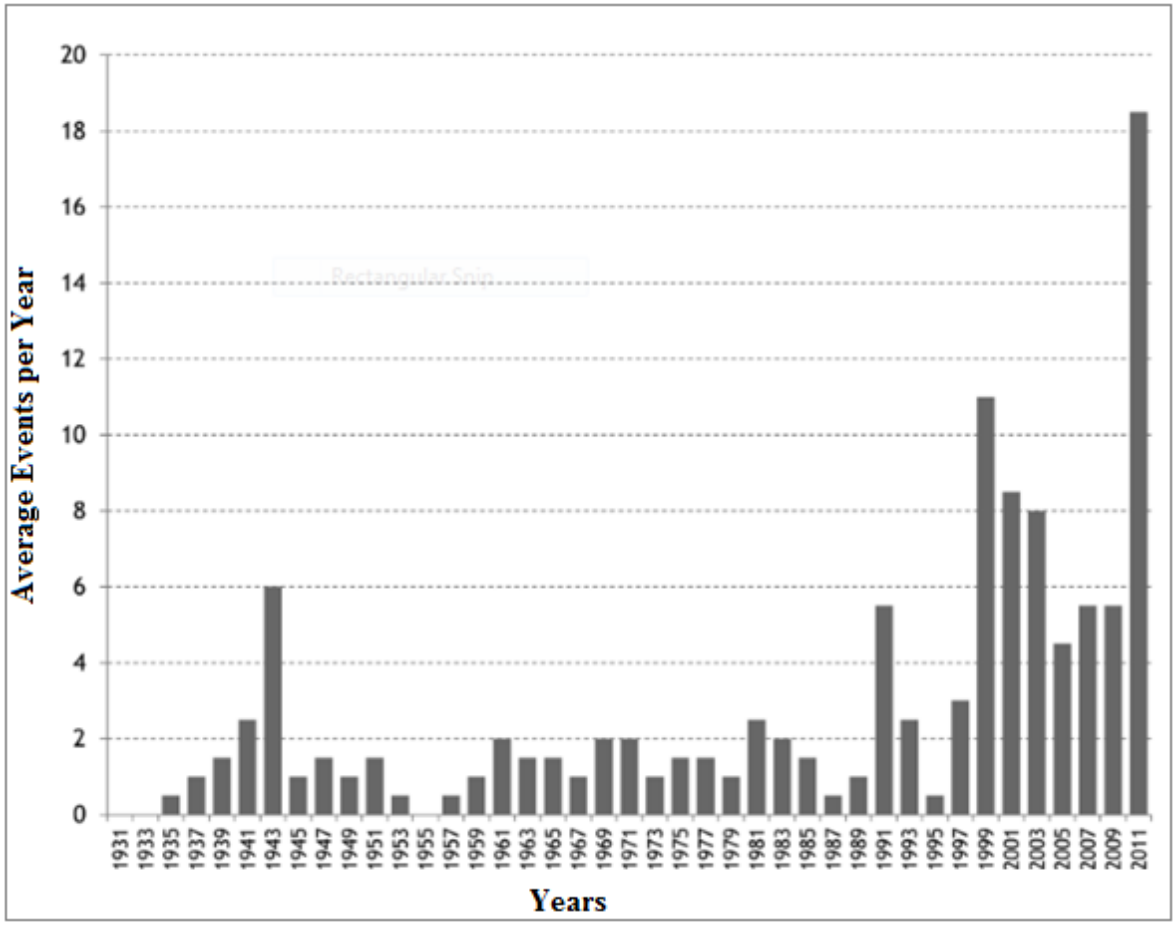

Figure 1. 1 Number of major reported water conflict events per year

(Adapted from (Gleick & Heberger, 2011)

The most recent conflict issue which evokes political tension in Africa is a dispute over water in the Nile basin. In 1999, the Nile Basin Initiative (NBI) was initiated by 9 out of 10 riparian countries with the support of major donor institutions, and achieved some success in its attempts to strengthen cooperation. But in 2015, two downstream riparian nations (Egypt and Sudan) disagreed with upstream riparian Ethiopia when the latter began the construction of the Renaissance dam. Negotiations are still in progress so far (Detges et al., 2017).

1.7. Water treatment process

Water treatment refers to the processing of water to achieve a water quality that meets specified standards set by consumers, communities and organisations through regulatory agencies (Liang et al., 2014). Thus, the main goal of water treatment is to remove turbidity as well as chemical and pathogenic contaminants. The contamination of water can be varied, depending on the source of the pollutant (Ambashta & Sillanpää, 2010). In fact, groundwater is considered much cleaner than surface water, therefore it does not require the same processes of treatment. Surface water resources are more easily contaminated because they are exposed to direct wet weather runoff and atmosphere (Shammas & Wank, 2016).

The following gives a brief explanation for most common methods of water treatment technology:

- **Sedimentation**

In this process, the turbid water is placed in basins and left for a while. Gravitational forces settle particles out of solution because they are large enough to settle out. Surface water mineral particles usually have densities ranging from 2 to 3 g/cm^3 and will settle out readily by gravity, while other organic particles with densities less than 2 g/cm^3 need more time to settle out. In some cases, sedimentation can be employed as the first stage of different stages of water treatment processes (Shammas et al., 2007).

- **Rapid granular filtration**

Filtration is the process of removing solid particles from suspension by passing through a porous medium. It is the most common type encountered in wastewater and drinking water treatment (Benjamin & Lawler, 2013). In rapid granular filtration, the porous medium is a thick bed of granular materials such as sand and coal. This process is faster than low sand filtration by a rate of 50 to 100 times. The key features of rapid filtration include granular media processed to a more uniform size than typically found in nature.

- **Membrane filtration**

The objective of membrane filtration is similar to rapid granular filtration. In this process, the filter media is a thin synthetic material less than 1 mm in thickness. The material contains a small pore that the water can pass through. Membrane filtration can compete with rapid granular filtration in terms of productivity but it is still expensive technology. The main advantage of this process is that it does not need chemical additives or thermal input. It can purify water even at the ionic level. Reverse osmosis (RO), nano-filtration (NF), ultra-filtration (UF) and micro-filtration (MF) are examples of membrane filtration technologies (Das et al., 2014).

The RO process for example is used to separate dissolved solutes from water. The osmosis process occurs when two different concentrated solutions are separated by a semipermeable membrane (Eisenberg & Middlebrooks, 2013). This method is commonly used for the desalination of sea water and brackish ground water.

- **Adsorption and ion exchange**

Adsorption and ion exchange (IX) are treatment processes where solutes (dissolved contaminants) are removed from water by transferring them to the surface of a solid. Activated carbon is the most common adsorbent material in drinking water which can be used in either a granular or powdered form. Zeolite, ferric hydroxide and activated alumina are other options of adsorbent materials. On other hand, synthetic resins are specifically engineered to be used as ion exchange materials.

- **Air stripping and aeration**

The principle of this method is utilizing mass transfer to move volatile substances between liquid and gaseous phases. In this process, water and air are brought into intimate contact to transfer volatile substances such as methane, trichloroethylene and petroleum hydrocarbons from the water to the air (Chellam, 2002). The main objectives of air stripping and aeration treatment are to improve the taste and odour of water and remove potential carcinogens.

- **Advanced oxidation**

Advanced oxidation is a chemical transformation process. The chemical change has led to destroying or modifying the undesirable components and making them more biddable for separation by one of the above processes of water treatment. Another category of oxidation called conventional oxidation can be employed to remove specific contaminants by using a specific oxidant. Chlorine, ozone, chlorine dioxide, hydrogen peroxide and potassium permanganate are examples of conventional chemical oxidants. The main goal of the advanced oxidation process is to produce hydroxyl radicals in water (Bekbolet, 2011).

- **Multi-stage flash desalination**

The basic principle of multi-stage flash (MSF) desalination is that seawater is heated and evaporated in a cascade of chambers (flash chambers); the vapour condenses in the upper parts of these chambers leaving highly concentrated salty water (brine) behind. The MSF plants work at a temperature range of 90-120 ^{o}C to avoid corrosion and scale formation. They are usually established with power plants on a cogeneration configuration (Khawaji, et al., 2008; Woldai, 2015).

The water treatment technologies mentioned above are suitable for cities and large communities where the infrastructure such as electricity and pipelines are facilitated. In rural areas, access to these facilities is difficult and costly, therefore solar energy is a promising technology that can be utilized for the water treatment process. A water

desalination unit can be run directly using solar energy to evaporate water, or indirectly by converting solar energy into heat or electricity

1.8. Significance of the research

The important points of this research are summarized as follows:

- WHO and UNICEF: >780 million people have no access to clean water resources and most of them live in rural areas in Africa.
- This research presents an innovative solution for water treatment technology. It presents a stand-alone solar purification system that can provide houses and small communities with the fresh water they need.
- The system is environmentally friendly and easy to install. It is not complicated, therefore an unskilled person can operate it.

1.9. Outputs

Solar water purification systems utilizing heat pumps as a backup system should be able to produce pure water at night and on cloudy days where other similar systems have stopped producing in the absence of solar radiation. Therefore, this system can ensure an adequate amount of water for the homestead.

The results of the parametric study of solar purifier performance based on the type of heat pump utilized would be used to categorise the system in terms of efficiency and cost.

1.10. Research design and methodology

This project will be divided into different parts as follows:

- **System design**

During the design of the solar water purification system, some considerations have been taken such as the geometry and dimensions of the purification unit, and type and cost of materials. The weather conditions of target areas are considered as well. Two categories of solar radiation collectors will be used. One is a thermal collector which consists of a painted basin and photovoltaic collectors. The system basically consists of two parts; the first one is an advanced solar water purification system with a vapour-compression heat pump system attached to it. The second one is a solar PV system used to power heat pump system and other electronic devices. Another solar purification system utilizing a thermoelectric heat pump (Peltier module) will be designed, constructed and tested as well.

- **System construction**

A water purification system will be built in the Mechanical Engineering Department laboratories at the Cape Peninsula University of Technology. Appropriate material will be used to build the system considering the weight and the cost. PV system will be sized to meet the energy requirements during cloudy days.

- **Working principle**

The purification processes will include three techniques, sedimentation, evaporation and condensation, and filtration. The solar still will harness the cooling and heat effect of a heat pump. The condenser of the heat pump system will be installed inside the basin so that it will heat up the contaminated water. The evaporator will be installed in insolated cold water reservoir. The cooled water will be circulated around the condensation surface of the still unit in order to increase the condensation rate. A small DC pump will be used to circulate the water. A filtration system will be attached to the outlet of the still condenser. In the thermoelectric heat pump system, the hot side of the Peltier module will be attached to the bottom of the basin.

1.11. Organization of the dissertation

The research comprised theoretical and experimental studies, as reported in different chapters of this dissertation. The thesis consists of six chapters which are summarized as follows:

Chapter one discusses the low efficiency of solar water purifiers and the objectives of the current work. It also discusses the water shortage and water quality and standards, as well as the relationship between water quality and public health. Further, the safety, security and stability problems associated with fresh water scarcity are also covered. A brief discussion of water treatment processes is given as well. And finally the significance, output and methodology of the research work are presented.

Chapter two reviews the fundamentals of solar energy and solar radiation components, as well as the important methods required to calculate the solar radiation incident on the tilted surfaces. The solar energy harvesting technologies are discussed in this chapter. The heat pump system, particularly vapor compression and thermoelectric heat pumps are presented. Also, the chapter addresses the desalination processes adopted around the globe, as well as the environmental considerations of desalination technologies. Solar water distillation processes and the efficiency of the solar stills are presented. The chapter ends with the economic point of view of the photovoltaic system and the prediction of energy price futures.

Chapter three describes the prototype design, construction and modification of the advanced solar distillation unit based on the fundamental of heat transfer and thermodynamic principles, as well as the configuration of the vapour compression heat

pump system as a heat recovery system for the solar still. The materials and equipment required to construct the prototype are presented. The sizing of the PV system required to power the heat pump system is demonstrated. The chapter concludes with a description of the final assembly of the advanced still.

Chapter four addresses the experimental protocol and setup procedure of the advanced solar still tests. The required tools and equipment are described. Different test conditions are discussed in order to evaluate the performance of the advanced still.

Chapter Five presents a summary of the results gained from the various long term experimental tests that were performed outdoors with the solar distillation prototype and model.

Chapter Six provides a conclusion of this work and recommendations for future work

1.12. Publication

As a result of the work that was done for this research, the author has made the following contributions to the existing body of literature in the topic of solar water distillation.

1. Alkilani, F.M. and Kanyarusoke, K.E., 2019, October. Solar Water Purification at Night: design of a suitable heat pump. In *IOP Conference Series: Earth and Environmental Science* (Vol. 354, No. 1, p. 012007). IOP Publishing.
2. Fouad Alkilani, Ouassini Nemraoui, Fareed Ismail. Performance evaluation of solar still integrated with thermoelectric heat pump system[J]. *AIMS Energy*, 2023, 11(1): 47-63. doi: 10.3934/energy.2023003

CHAPTER TWO
Fundamental and Theoretical Background

2.1. Solar energy

The sun provides most of the energy sources on Earth directly or indirectly (except nuclear power and geothermal energy). Solar light is known as solar energy or radioactive energy. It is exploited by constantly evolving technologies such as solar photovoltaic panels, solar water heating, solar fruit dryers, etc. It is one of the most important sources of renewable energy available on earth or in space applications (Narasimhan et al., 2016) (Kosmopoulos et al., 2015). Figure 2.1 shows the common uses of solar energy.

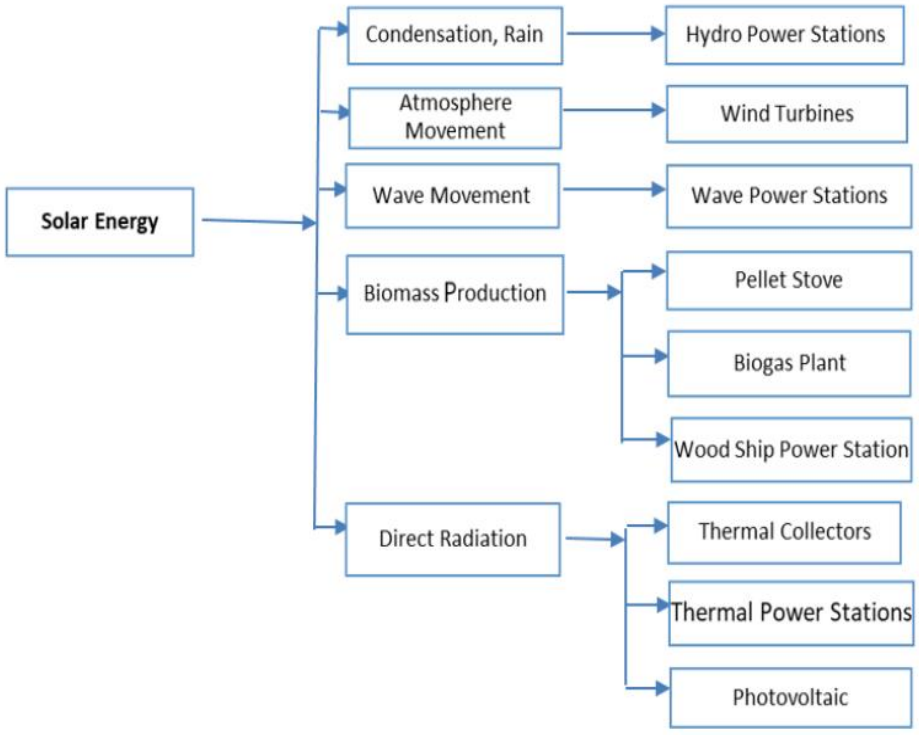

Figure 2. 1: Various possibilities for the use of solar energy (Mertens, 2014)

2.2. Solar radiation

Solar radiation is composed of millions of high energy particles called photons. It is the dominant energy input to the Earth system. About 70% of total solar radiation reaching the earth is absorbed by the atmosphere, land and water, with the remaining 30% being reflected back to space (Rottman et al., 2007).

The radiation power emitted by the sun is estimated at around 3.845×10^{26} W in all directions. The Earth, that is located about 15 million km from the sun, receives a small fraction of that huge amount of energy. The following equation is assumed to calculate the value of solar energy on the earth's surface:

$$Is = \frac{Psun}{4 \times \pi \times {r_{se}}^2} \tag{2.1}$$

$$= \frac{3.845 \times 10^{26} W}{4\pi(1.496 \times 10^{11} m)^2} = 1367 W/m^2$$

In the above equation, it is assumed that the sun has a radius of r = r_{SE}, while solar power (instantaneous energy flux) is a description of the term irradiance. The amount of solar energy falling on a unit area over a stated time (day/year) is an expression of the term solar irradiation (J/m²). The result of 1367 W/m² is called the *solar constant*. The solar constant is the energy from the sun per unit time received on a unit area of the surface perpendicular to the direction of propagation of the radiation at a mean earth-sun distance outside the atmosphere (Duffie & Beckman, 2013; Mertens, 2014). The amount of solar radiation reaching the earth's surface is affected by factors such as clouds, aerosols and water vapour. Figure 2.2 shows the influence of these factors.

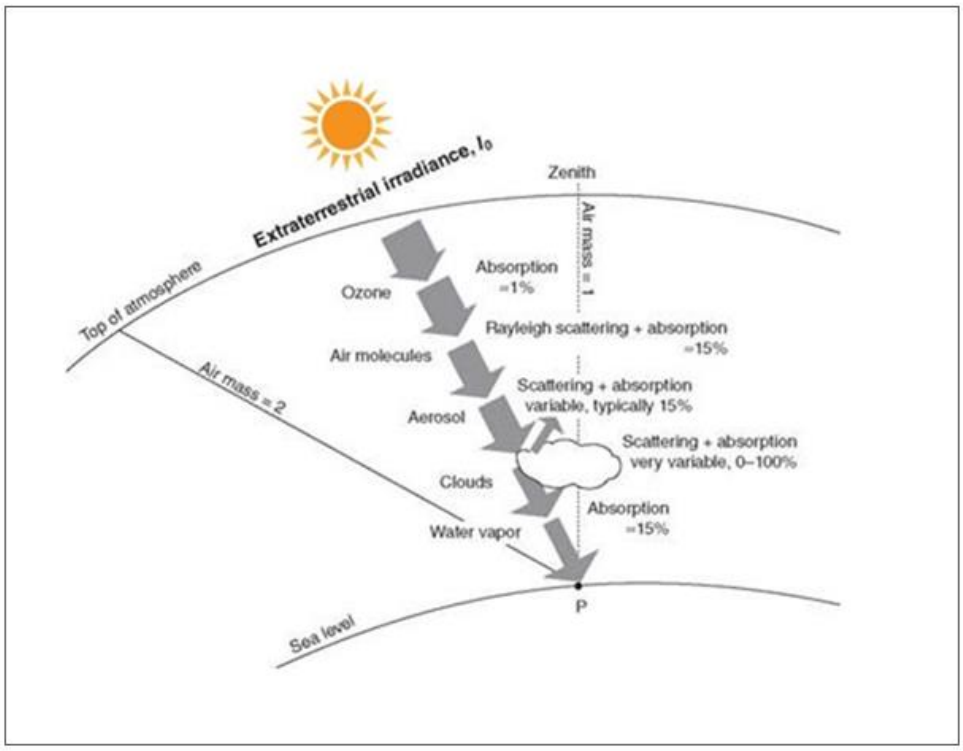

Figure 2. 2: The main processes influencing solar radiation in the atmosphere (Lovegrove & Stein, 2012)

2.2.1. The spectrum of the sun

The sun is considered as a gigantic fusion reactor with an interior temperature estimated at 8×10^6 to 40×10^6 K, its surface temperature is about 5778 K. Despite the physical structure and temperature gradient of the sun, it does not represent a perfect black body at a fixed temperature. Therefore, the emitted solar radiation is a combination of emitting and absorbing radiation of various wavelengths (Tiwari, 2002). According to Planck's Law of Radiation, the surface temperature of the sun leads to an idealized black body spectrum and, therefore the solar irradiance of black body as a function of wavelength can be calculated as:

$$E_{\lambda b} = \frac{C_1}{\lambda^5[exp\{C_2/(\lambda T)\} - 1]} \qquad (2.2)$$

Where $E_{\lambda b}$ is the energy emitted per unit area, C_1 and C_2 3.742×10^8 W.μm^4/m^2 and 14387.9 μmK respectively.

Figure 2. 3 shows the maximum spectral intensity occurs at about 480 nm wavelength.

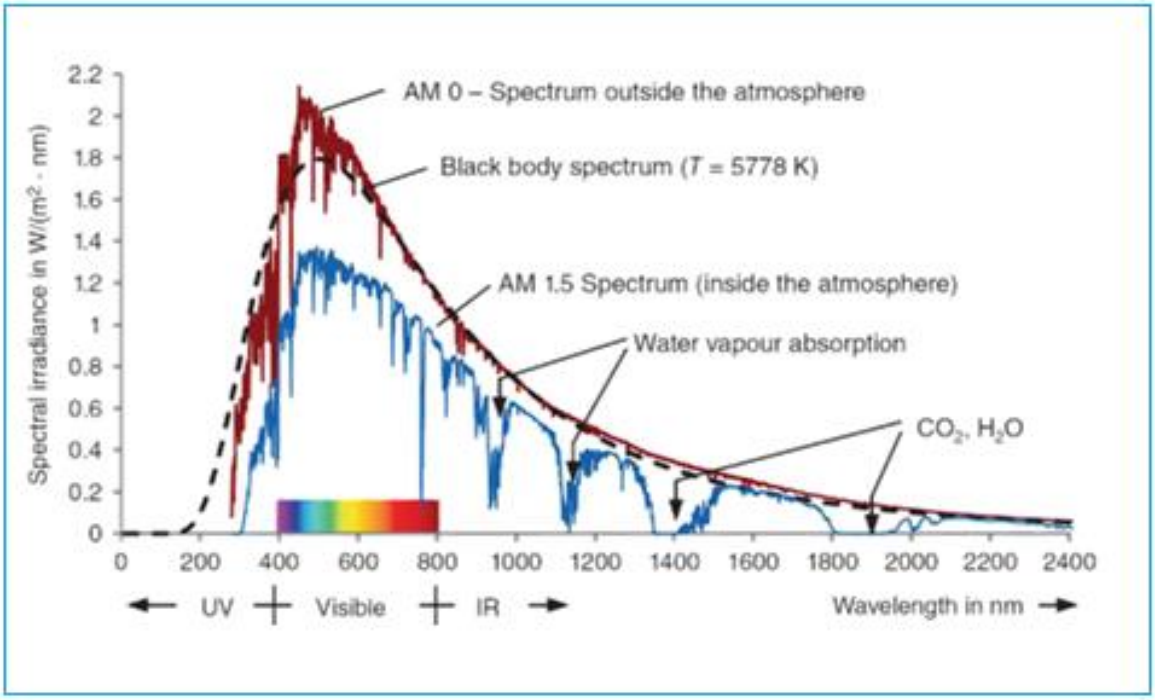

Figure 2. 3: Spectrum outside and inside the atmosphere (Mertens, 2014)

The term AM 0 refers to the air mass 0 which means that the light has not passed through the atmosphere. The spectrum measured is approximately following the idealized (dashed) line. When sunlight passes through the atmosphere, the spectrum changes as well as a result of the following factors:

- Reflection of light
- Absorption of light
- Rayleigh scattering
- Scattering of aerosols and dust particles

2.2.2. Solar radiation on tilted surfaces

Before going through the details of the calculation of solar radiation on a tilted surface, some definitions have to be reviewed.

- **Declination**

The declination (δ) refers to the angular distance of the sun's rays (north or south) of the equator. In the southern hemisphere, declination varies from 0˚at the spring equinox to -23.45˚ at the summer solstice and 0˚ at the fall equinox to 23.45˚ at the winter solstice. The following equation is assumed to calculate the declination for any day of the year (*N*) (Duffie & Beckman, 2013).

$$\delta = 23.45 sin\left[\frac{360}{365}(248 + N)\right] \qquad (2.3)$$

- **Hour angle**

The hour angle (ω) refers to the angle where the earth would turn to bring the meridian of the point directly under the sun. The hour angle can be obtained using the following equations:

$$\omega = \pm 0.25(number\ of\ minutes\ of\ local\ solar\ noon) \quad (2.4)$$

The plus and negative signs apply for afternoon and morning hours respectively.

$$\omega = (AST - 12)15 \quad (2.5)$$

Where, *AST* is apparent solar time.

- **Solar altitude angle**

The solar altitude angle (α) refers to the angle between the sun's rays and a horizontal plane. It can be calculated by the following equation:

$$\sin(\alpha) = \sin(l)\sin(\delta) + \cos(l)\cos(\delta)\cos(\omega) \quad (2.6)$$

Here, *L* local latitude

- **Azimuth angle**

The azimuth angle (z) refers to the angle of the sun's rays measured in horizontal plane from the north for the southern hemisphere, or from the south for the northern hemisphere. The azimuth angle can be obtained by the following equation:

$$\sin(z) = \frac{\cos(\delta)\sin(\omega)}{\cos(\alpha)} \quad (2.7)$$

- **Incidence angle**

The incidence angle (θ) is the angle that the sun's rays make with a line perpendicular to the surface. The mathematical expression of the incidence angle is as follows:

$$\begin{aligned}\cos(\theta) = {} & \sin(l)\sin(\delta)\cos(\beta) - \cos(l)\sin(\delta)\sin(\beta)\cos(zs) \\ & + \cos(l)\cos(\delta)\cos(\omega)\cos(\beta) \\ & + \sin(l)\cos(\delta)\cos(h)\sin(\beta)\cos(zs) \\ & + \cos(\delta)\sin(\omega)\sin(\beta)\sin(zs)\end{aligned} \quad (2.8)$$

Where, Zs is the surface azimuth angle, β is the tilt angle from the horizontal.

Figure 2.4 shows the different solar angles which are considered important to calculate the overall solar radiation on a tilted surface.

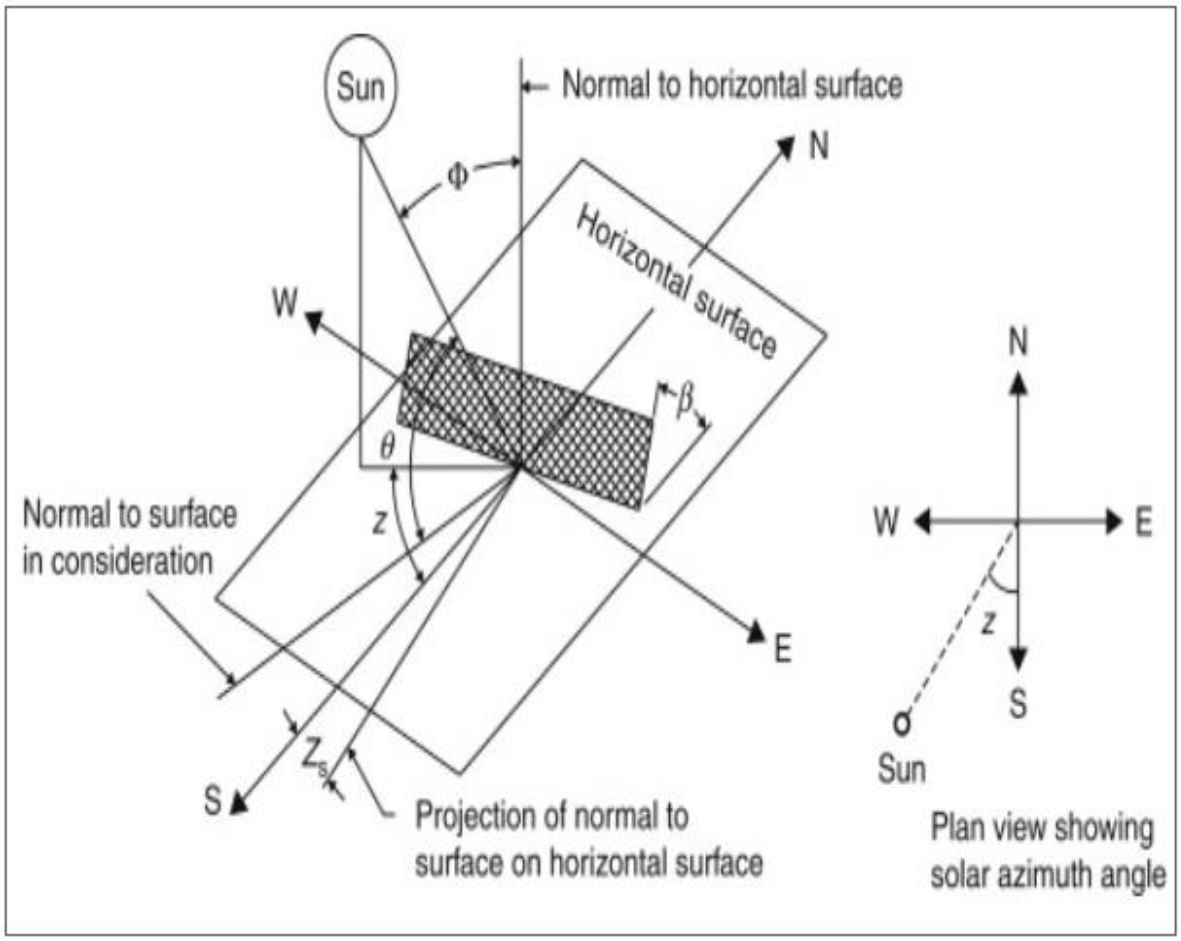

Figure 2. 4: Solar angles diagram (Duffie & Beckman, 2013)

The total solar radiation incident on a tilted surface is the sum of the beam and the diffuse. The diffuse is a combination of isotropic diffuse, circumsolar diffuse, horizontal brightening and reflected radiation. Therefore, the mathematical expression will be as follows:

$$I_T = I_{T,b} + I_{T,d,iso} + I_{T,d,cs} + I_{T,d,hb} + I_{T,d,g} \quad (2.9)$$

To estimate the solar radiation on a tilted surface, Perez formula (Perez et al., 1990) is assumed. The expression of the formula as follows:

$$I_T = I_b R_b + I_d \left[(1 - f_1) \left(\frac{1 + cos\beta}{2} \right) + F_1 \frac{a}{b} + F_2 sin\beta \right] + I_h \rho_g \left(\frac{1 - cos\beta}{2} \right) \quad (2.10)$$

a and *b* take into account the incidence angle of the sun on the sloped and horizontal surfaces. *F1* and *F2* are circumsolar and horizon brightness coefficients. These factors can be computed using the following equations:

$$a = max\,(0, cos\theta i) \quad (2.11)$$

$$b = max\,(cos\,85^{o}, cos\theta z) \quad (2.12)$$

$$F_1 = max\left[0, \left(f_{11} + f_{12}\Delta + \frac{\pi\theta_z}{180} f_{13}\right)\right] \quad (2.13)$$

$$F_2 = \left(f_{21} + f_{22}\Delta + \frac{\pi\theta_z}{180} f_{23}\right) \quad (2.14)$$

The factors *F11, F12, F13, F21, F22* and *F23* were derived by Perez based on a statistical analysis of the clearness.

2.3. Solar energy collectors

Solar collectors are devices used to collect, concentrate and convert solar radiation from the sun into another sort of energy (Hanania, et al., 2018). There are two categories of solar energy collectors, thermal and electrical collectors.

- **Solar thermal collectors**

The principle of solar thermal collectors is the conversion of solar radiation into thermal energy. This process of heat transfer creates mechanical energy which can be used to generate electricity or water heating for domestic use. The different types of solar thermal collectors are explained in the following sections:

- **Flat plate collectors**

The flat plate collector basically is a metal box painted a dark colour and covered with transparent glazing. The sides and bottom of the compound are usually covered with insulation to minimize heat losses. Solar radiation passes through the transparent glazing material and hits the absorbent surface. It heats up the panel, and the heat is transferred either to the water or air trapped between the glazing and absorption. Sometimes, these coated panels are coated with special layers designed to absorb and retain the heat better than conventional dark paint. These panels are usually made of good conductive metal (aluminum/copper).

- **Thermodynamic collectors**

Thermodynamic collectors are a newly developed technology in solar thermal concepts. They use the same principle of heat pumps in their design but are deployed on the surface or walls like regular flat plate collectors and do not have to face the sun. The concept behind a solar thermodynamic collector is that it operates like a reverse refrigeration system and differs from a conventional flat thermal collector in that it does not use solar radiation to heat up the transferring liquids. The plates contain a refrigerant that passes through and absorbs heat. Then the heat passing through the plate will become gas. The gas that is heated is then compressed and then passed to the heat exchanger inside the hot water container (Rois, 2007; Li, 2014).

- **Evacuated tube collectors**

The evacuated tube is constructed of two overlapping glass tubes with a vacuum trapped between them. This combination allows solar radiation to pass into the heat

pipe at the center, and prevents heat from dissipating. The heat pipe consists of a long copper tube containing a small quantity of the working fluid such as acetone, methanol, ethanol, etc. (Kotb et al., 2019). The system is made up of a frame, manifold and series of vacuum tubes depending on the size of the hot water reservoir. The internal metal tube uses a suction plate carrying the heat collected from the sun into the water. This heated tube contains liquid that is under very specific pressure. At this pressure, the hot tip of the tube contains boiling liquid while the cold end contains the condensation vapour. This allows thermal energy to move more efficiently from one end of the tube to the other. Once the heat from the sun passes from the hot end of the heat tube to the condensation end, the thermal energy is transferred to the water that is heated for use.

- **Concentrating solar power collectors**

The concentrating solar power collector uses a combination of reflective materials such as mirrors or lenses to concentrate direct solar radiation to produce thermal energy. There are two different categories of concentrating collectors. The first category is a line focus collector (parabolic). This system consists of parabolic-shaped, highly reflective material connected to a long trough. A long pipe located at a focal point of the parabolic carries a circulating liquid at high temperature. These are very high powered collectors and are thus generally used to generate steam for solar thermal power plants and are not used for domestic applications. The second category is a point focus collector. It uses the same principle of the first category but solar radiation is focused onto a single point. This system is commonly used to drive Stirling engines (He et al., 2020).

- **Photovoltaic Collectors**

The photovoltaic cells (PV) are made up of semiconductor materials that convert solar energy into electricity. When sunlight strikes the cell, a portion is absorbed within the semiconductor material, stimulating electrons to move. This movement produces electrical current. Sets of PV cells are connected together to create a PV module. The module can be connected in series or in parallel to meet the voltage or current required. The three basic types of PV applications are stand-alone, grid-connected and hybrid systems (Duffie & Beckman, 2013).

2.4. Heat pump system

The term heat pump refers to the device that extracts heat from one place and transfers it to another using different sorts of energy input (mechanics, heat, etc.). In the 19th century, Lord Kelvin proposed using a heat engine in reverse mode as a heat pump. Kelvin's idea came to practical life in the twentieth century when refrigeration systems became commonly used. Thus, the main objective of a heat pump is similar to the objective of refrigeration (Dincer & Kanoglu, 2010) . The most common examples of

heat pumps are vapour-compression systems (Brodowicz et al., 2013). Heat pump systems can be classified, depending on heat source, into four common configurations (Silberstein, 2015):

- Air to air systems
- Air to liquid systems
- Liquid to air systems
- Liquid to liquid systems

Heat pump systems have high energy efficiency and low environmental impact, particularly in industrial processes. They are competent in recovering low temperature waste heat to useful level, which otherwise would be rejected to the ambient.

2.4.1. Vapour compression heat pump

Most heat pump systems in use today utilize the same principle of the vapour compression cycle. In this respect, the main components of the vapour compression heat pump are similar to those of the vapour-compression refrigeration system, namely, compressor, condenser, evaporator and throttling device (Althouse et al., 2000). The difference between these two systems is that the heat pump system transfers heat from lower ambient temperature to the higher temperature level, therefore it is identified as reverse-cycle refrigeration system, whereas the refrigeration system transfers heat from lower temperature to the higher level (ambient) (Dincer & Kanoglu, 2010). The thermodynamic analysis involved in heat transfer processes is governed by the first and the second law of thermodynamics. The first law of thermodynamics (energy conservation) is expressed as follows:

$$\sum \mathrm{Q_i} + \mathrm{w} = 0 \qquad (2.15)$$

Where, Q_i is the amount of heat energy exchanged at temperature T_i, and w is work input.

The law of energy conservation is applied to a closed heat pump cycle and allows reckoning of the heat exchange between the components and the ambient.

The second law establishes the direction of heat flow. Thus, for reversible processes it can be written as:

$$\sum \frac{\mathrm{Q_i}}{\mathrm{T_i}} = 0 \qquad (2.16)$$

The amount of energy transferred by the heat pump is the sum of the work input and amount of energy at temperature T1, thus the first law can be written as:

$$Q_1 + W = Q_2 \qquad (2.17)$$

The first law of thermodynamics can be applied to each process of vapour-compression shown in Figure 2.5 for steady-flow operation, neglecting change in kinetic and potential energy.

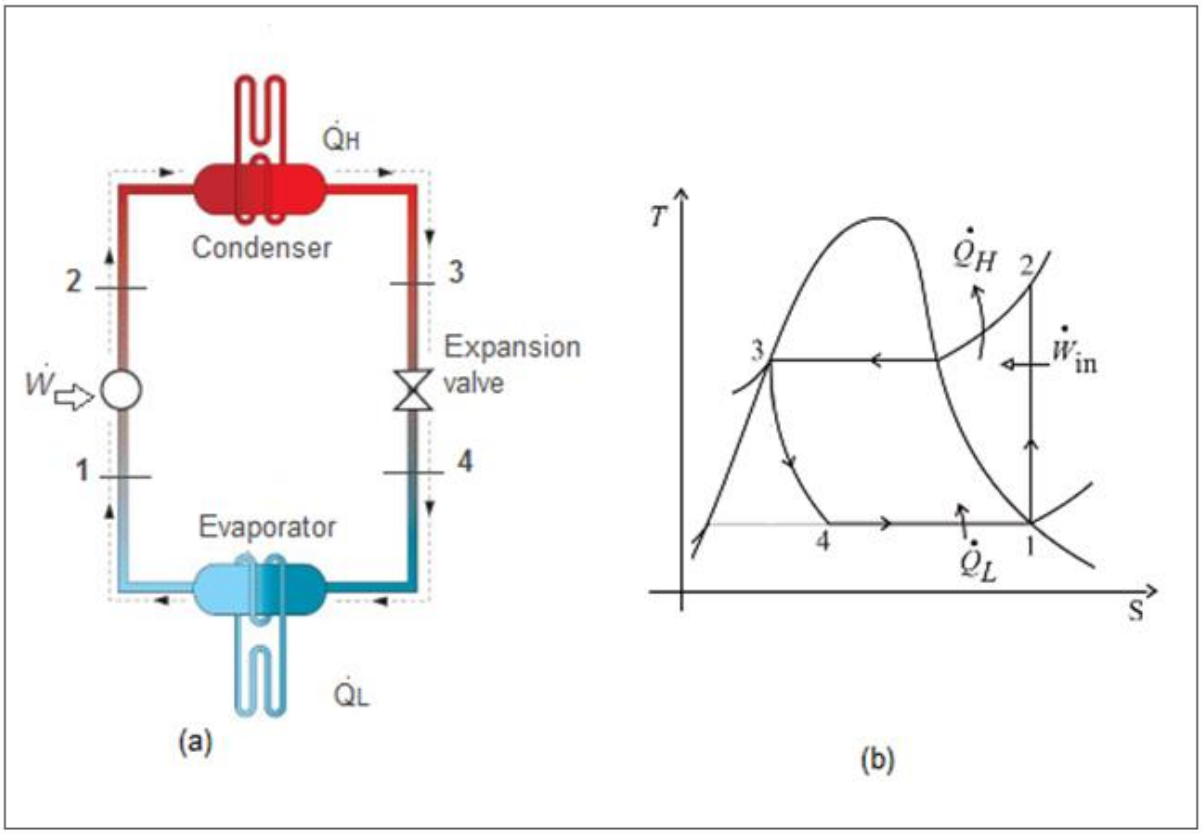

Figure 2. 5: Ideal vapour compression heat pump cycle and its temperature-entropy diagram (Dincer & Kanoglu, 2010)

Therefore, for each process the law can be written as:

For compressor

$$\dot{W} = \dot{m}(h_2 - h_1) \quad (2.18)$$

For condenser

$$\dot{Q}_H = \dot{m}(h_2 - h_3) \quad (2.19)$$

For throttling device

$$h_3 = h_4 \quad (2.20)$$

For evaporator

$$\dot{Q}_L = \dot{m}\,(h_1 - h_4) \quad (2.21)$$

The energy balance if the system gives

$$\dot{W} + \dot{Q}_L = \dot{Q}_H \quad (2.22)$$

Therefore, the coefficient of performance (COP) of a vapour-compression heat pump can be expressed as:

$$COP = \frac{\dot{Q}_H}{\dot{W}} \quad (2.23)$$

2.4.2. Thermoelectric heat pump

The thermoelectric phenomenon refers to the conversion of thermal energy into electrical energy, or vice versa (lee, 2017; Sun et al., 2019). The thermoelectric effect was discovered by Thomas Seebeck early in the nineteenth century by applying heat to the junction of two dissimilar materials, electromotive force can be produced. Thirteen years later, Peltier discovered reverse process of the Seebeck effect. He passed an electrical current through a semiconductor material to produce heating or cooling, depending on the direction of the current (Elsheikh et al., 2014; Pourkiaei et al., 2019).

The thermoelectric module basically consists of n-type and p-type semiconductor materials connected electrically in series and thermally in parallel (Xuan, 2003). These thermoelectric elements and their electrical interconnects are typically mounted between two ceramic substrates in order to hold the overall structure together as shown in Figure 2.6.

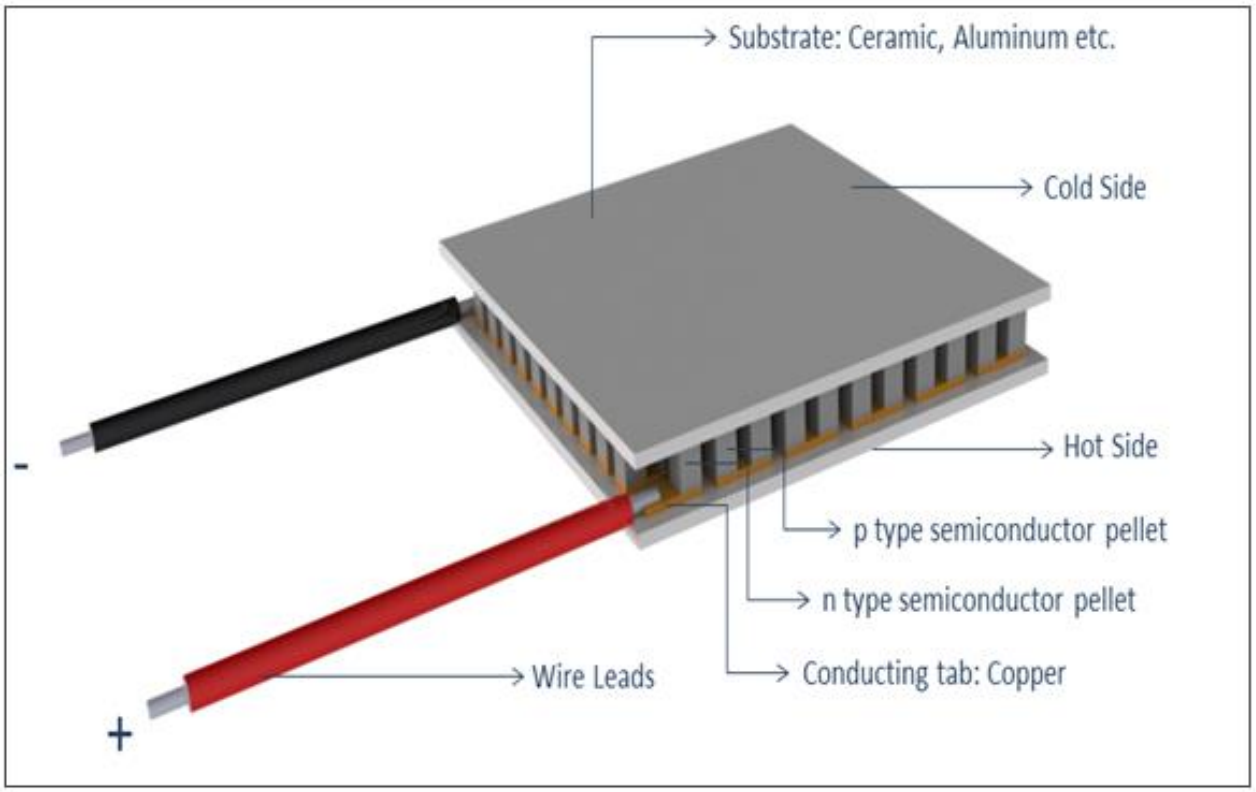

Figure 2. 6: Thermoelectric module components

Thermoelectric modules can be used as a heat pump when operated in the Peltier mode (Min, 2018; Wang et al., 2014). The efficiency of the module can be expressed as

$$\eta = \frac{l}{l + 2rl_c}\left(\frac{T_c}{T_h - T_c} \frac{\left(1 + \frac{Z\dot{T}l}{n+l}\right)^{1/2} - \frac{T_h}{T_c}}{\left(1 + \frac{Z\dot{T}l}{n+l}\right)^{1/2} + 1} - \frac{rl_c}{l} \right) \quad (2.24)$$

$$COP_{max} = \frac{T_C}{T_H - T_C} \times \frac{\sqrt{1 + ZT} - \frac{T_C}{T_H}}{\sqrt{1 + ZT} + 1} \quad (2.25)$$

Here, *n, r* and l_c commercial module dimensions. T_h and T_c are the hot and cold side temperature of the module. $Z = 2.8\times10^{-3}K^{-1}$. Ṫ is temperature average. *ZT* is a figure of merit that is used to evaluate the transport property of thermoelectric material. It is expressed as:

$$ZT = \frac{\sigma\alpha^2 T}{k} \quad (2.26)$$

Here, σ is the electrical conductivity, *α* the Seebeck coefficient, T the absolute temperature and *k* the thermal conductivity.

The coefficient of performance (COP) of thermoelectric heat pump can simply be defined as:

$$COP = \frac{Q_h}{Q_h - Q_c} \quad (2.27)$$

$$Q_h = \alpha_m I T_h - K_m(T_h - T_c) + \frac{1}{2} R_m I^2 \quad (2.28)$$

$$Q_c = \alpha_m I T_c - K_m(T_h - T_c) - \frac{1}{2} R_m I^2 \quad (2.29)$$

Where:

Q_h is the flow of heat to the heat sink,

Q_c is the flow of heat from the heat source,

α_m is the Seebeck coefficient,

I is applied current,

T_h the temperature of the hot side of the module,

T_c the temperature of the cold side of the module,

K_m thermal conductance and

R_m electric resistance.

The aforementioned parameters (α_m, K_m and R_m) depend on the thermoelectric materials, the number of modules and the thermoelectric module geometry. They can be given as follows:

$$\alpha_m = N(\alpha_p - \alpha_n) \quad (2.30)$$

$$K_m = N(\lambda_n + \lambda_p)\frac{A}{L} \tag{2.31}$$

$$R_m = N(\rho_n + \rho_p)\frac{L}{A} \tag{2.32}$$

Here, *N* is the number of semiconductor pairs, λ is the thermal conductivity, ρ is the electric resistivity, *L* is the thermoelement leg length and *A* is the cross-sectional area of the thermoelement leg (Feng et al., 2018). The properties of thermoelectric materials (λ, α, and ρ) are temperature dependent variables (Diaz de Garayo et al., 2022).

Figure 2.7 shows the relationship between the coefficient of performance of the module and the t length of thermoelement.

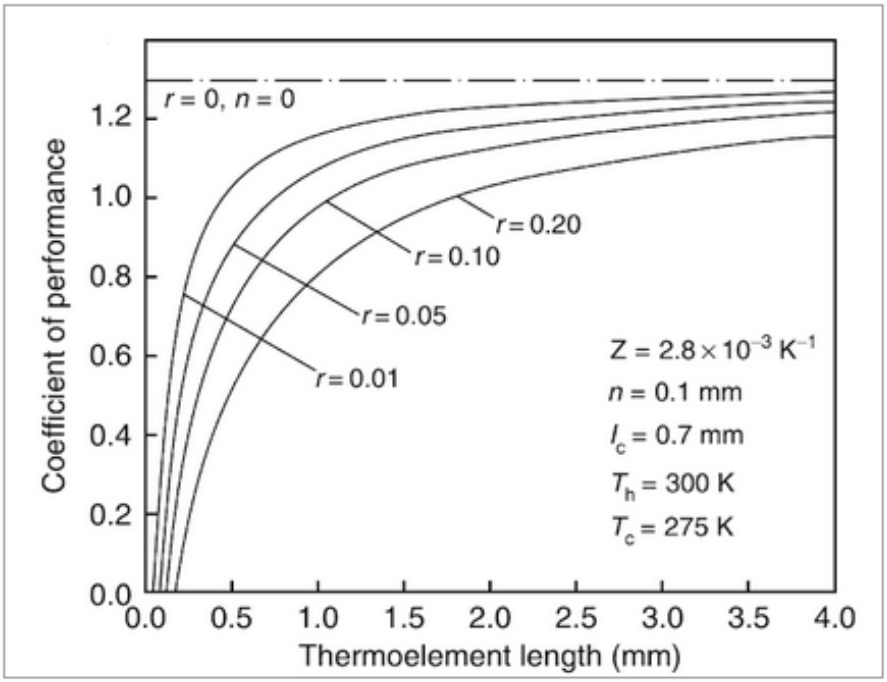

Figure 2. 7:The COP as a function of thermoelement length (Min, 2018)

To achieve desirable cooling performance, the temperature difference between the hot and cold sides of the module should be controlled. Therefore, a heat sink is recommended to be attached to the hot side. Figure 2.8 shows the relationship between temperature difference and the COP of the thermoelectric module.

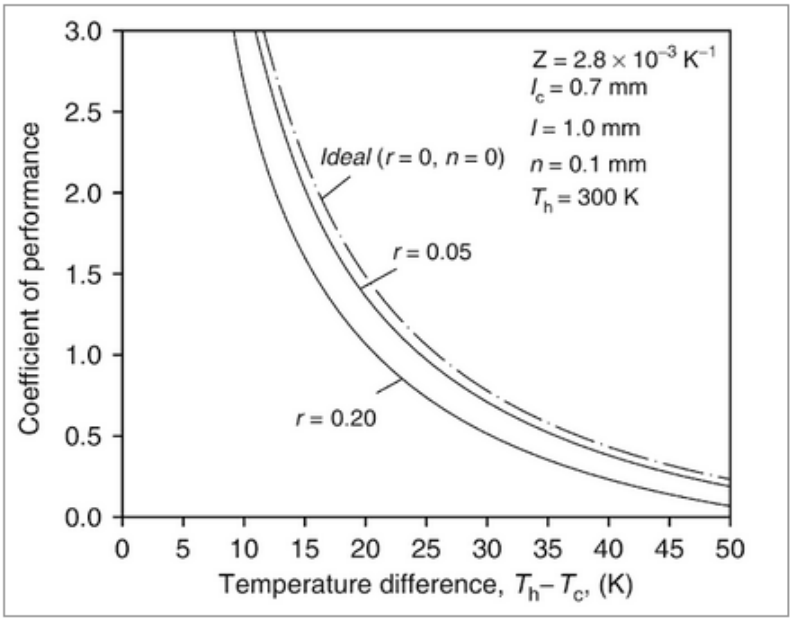

Figure 2. 8: The COP of thermoelectric module as a function of temperature difference (Min, 2018)

Thermoelectric device technology has recently been widely used in many applications such as aerospace, modern vehicles, cooling and heating purposes, etc. (Muñoz-García et al., 2013; Nami et al., 2017; Arora et al., 2016; Gao et al., 2018; Azahar et al., 2020; Balasubramanian, 2020 and Nohay et al., 2020). As aforementioned, the COP of the thermoelectric module is considerably low and therefore many attempts have been made to boost the efficiency which is related to the properties of fabrication material and the system arrangement (Goldsmid, 2021). Materials such as polymers, ceramics and semiconductors are commonly used to fabricate thermoelectric modules (Tan et al., 2017; Tani & Kido, 2005; Tsubota et al., 2008; Zhu et al., 2014).

Many experimental works have been conducted in order to investigate the performance of thermoelectric heat pumps for various applications (Yamashita, 2008; Yamashita, 2009; Meng et al., 2009; Saifizi et al., 2018; Ebrahimi & Derakhshan, 2018; Duan, et al., 2021; Mengmeng et al., 2018).

To connect the Peltier modules electrically, some technical specifications have to be considered, including V_{max} of the module, which refers to the DC voltage that would deliver the maximum temperature difference (ΔT) between the junction of the module. At operation voltage above V_{max} the power dissipation within the Peltier device begins to increase the system temperatures and diminish the temperature difference. I_{max} refers to the DC current level that would achieve the maximum ΔT across the TE module. Operating the module above Imax leads to increasing the system temperature and diminishing ΔT due to power dissipation (I2R). Q_{max} is a specification that is commonly used as an indication of load line on the performance graphs of the module. ΔT_{max} is the maximum possible ΔT across the TE module at a given T_{Hot}. It occurs at a

thermal load equal to zero watts. On the performance graph, it represents the endpoint for load lines. As mentioned above, the Peltier modules are temperature dependant, therefore the modules have a positive temperature coefficient with respect to resistance, ΔT_{max} and Q_{max}.

Hereinafter, the most common methods to control the thermoelectric heat pump system are proposed. One of the more affordable modes of temperature control is (on/off) thermostatic operation. In this approach, the system oscillates back and forth between two temperature points and therefore the cycle time can be slow. To avoid potential thermal stress of the Peltier module, it is preferable to maintain the cycle time in the range of 10 minutes. Another electronic method to control the thermoelectric system efficiently is utilizing pulse-width modulation (PWM) (Arzarello, 2014). The main advantage of this approach is that it reduces the power dissipation through the electric circuit, especially when metal oxide semiconductor effect transistors (MOSFETs) are used for switching. A precaution has to be taken while using PWM to avoid potential thermal stress and electromagnetic interference in the Peltier heat pump system, therefore it is recommended to keep the frequency at 2000 Hz or higher, and proper wire insolation should be used. A linear controller such as a bipolar junction transistor (BJT) driver can be used to regulate the temperature of the thermoelectric heat pump system. The driver must be connected in series with the Peltier module to regulate the power supply introduced to the module.

Finally, an Arduino Uno board can be programmed and used as an auxiliary circuit to control the power supplied to the Peltier heat pump system. A simple Arduino control circuit consists of an Arduino board, breadboard, TE module, LED indication light, switcher, resistors and LM35 temperature sensor. In applications where the precise temperature is required, the layout and the coding of the Arduino are more complex (Introini & Kos, 2018).

2.5. Heat pump systems and energy conservation

In residential and industrial situations, about 60% of energy production is used for heating and cooling purposes (Xi et al., 2011). The fluctuation in fuel costs and global warming concerns become a problematic facing the whole world. In terms of heating and cooling, heat pump systems represent high efficiency energy-saving and environmentally tolerant applications for domestic and industrial use. They are the only systems that can circulate environmental and waste heat back into useful use (Chua et al., 2010). Using heat pump systems in water heating in both residential and commercial applications is a promising technology in term of energy saving (Hepbasli & Kalinci, 2009). Neksa (2002) reported that the energy consumption for residential heat pump water heating at 60 ˚C can be reduced up to 75% compared to electrical and gas-fired water heaters. He tested CO_2 as an alternative working fluid for a vapour-

compression heat pump for domestic purposes. According to Neksa's experimental findings, a CO_2 heat pump water heater can achieve a heating rate up to 90 ˚C without operational problems. Yokoyama et al. (2007) tested CO_2 heat pump water heating system performance. They used a numerical simulation model to evaluate the performance of each component of the system. The model results in a set of nonlinear differential algebraic equations, and it was solved by a hierarchical combination of the Runge–Kutta and Newton–Raphson methods. The configuration of their system is shown in figure 2.9. The heating performance of the system varies between 75 - 85 ˚C, depending on ambient and city water temperature. They conclude that with increases in ambient temperature the COP increases and the operating time become shorter.

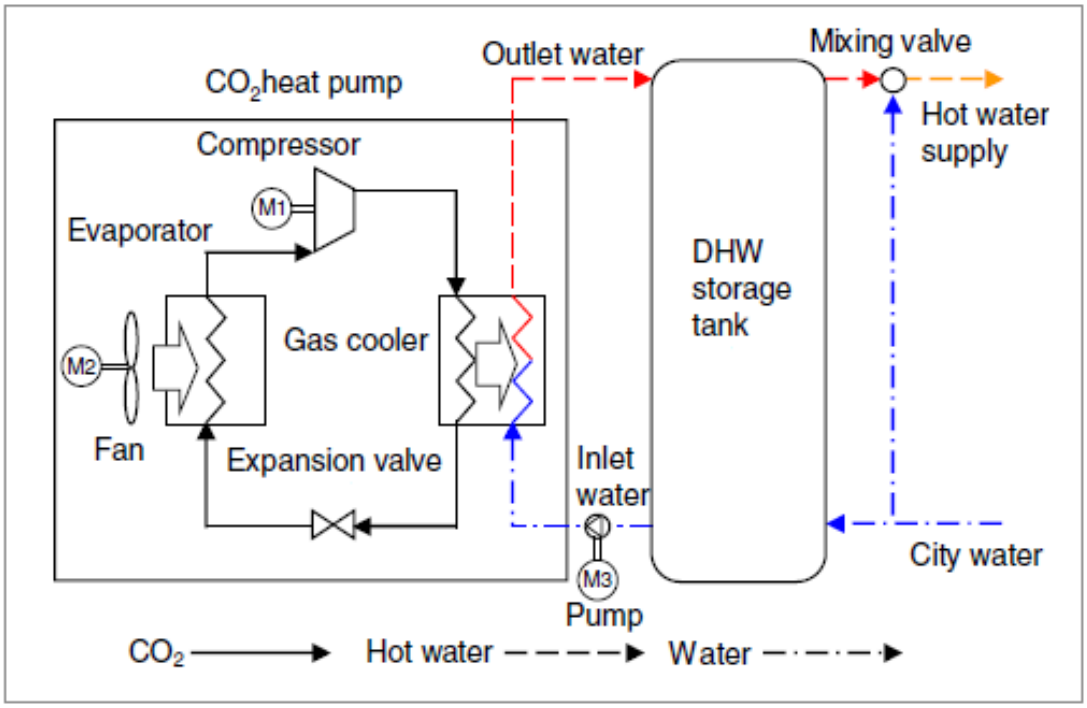

Figure 2. 9: CO_2 heat pump water heating system (Yokoyama et al., 2007)

Along with the energy conservation benefits of utilizing heat pump systems, it contributes to carbon footprint reduction when employing renewable energy resources. In particular, solar assisted heat pump systems (SAHP) are promising technology that can be used in domestic water heating and space comfort (Mohamed et al., 2017), (Wang et al., 2018). In the research field, various types of solar energy collectors integrated into heat pump systems have been experimented in order to evaluate the performance of the heat pump system. Chen, et al., (2018) introduced a PV/T module integrated with heat pump system to provide hot water for domestic use. The experimental results showed that the daily average values of electrical, thermal efficiency, COP_{th}, and $COP_{PV/T}$ are 12.2%, 33.9%, 2.78, and 3.40 in heating mode, respectively, while the values are 12.9%, 25.3%, 1.96 and 2.52 in heat charging mode.

A novel solar photovoltaic-loop heat pipe (PVLHP) heat pump system for water heating was designed and tested in order to investigate the overall efficiency of the system. Under the given experimental parameters, the electrical, thermal and overall efficiency of the system was 10%, 40% and 50% respectively, while the COP was about 8.7 (Zhang et al., 2013). Further research work analyzed the energy consumption and the environmental benefits of utilizing a solar photovoltaic-assisted heat pump. It is concluded that the energy consumption and CO_2 emission reduced by 55% and 73% respectively compared to conventional heat pump system (Li & Sun, 2019). Recently, environmentally friendly and energy efficient modern houses that can save up to 90% of energy consumption compared to current houses were constructed in Germany and the USA. A combination of solar photovoltaic system, ventilation and space comfort devices, high quality insulation, and optimized orientation and design were the key factors in building the modern house (Passive House) (Ferrell, 2021).

2.6. Desalination process

The water desalination process can be defined as a physical procedure of separating undesirable levels of salts from brackish and sea water to decrease the concentration level of the salts to be suitable for domestic and industrial uses (Belessiotis et al., 2016; Jones et al., 2019). Historically, the desalination process was aimed at extracting the salt from sea water rather than producing fresh water, considering that salt was a valuable commodity. Aristotle (384 - 422 BC) explained the desalination process. He noticed that when seawater heated up and turned into vapour, the condensed vapour is fresh water (Chua & Rahimi, 2017). At that time, the desalination of seawater using distillation became an early method to obtain drinkable water. During long distance sea trips, sailors boiled seawater in a brass vessel and suspended a sponge from the mouth of the vessel to catch the vapour and condense it to produce fresh water (Kalogirou, 2005) and (El-Dessouky & Ettouney, 2002). In the 17^{th} to the 19^{th} centuries, basic desalination processes were taking place on American naval ships to provide the crews with their fresh water needs. Over the past century, desalination technologies have attracted more attention. In 1912, six desalination units with a capacity of 75 m^3/day were established in Egypt. During the period 1929-1937, more desalination units were established, and thereafter the total production capacity increased due to the development of the oil industry in the Middle East. In the 1940s, the development of desalination technology took a giant leap forward in order to provide military bases and troops with fresh water in remote areas during WWII (Lotatidou et al., 2017). In water scarce areas, especially the Arabian Gulf, the population increased dramatically, and therefore, commercial desalination plants were established by the 1960s. Later on, bigger desalination units with a capacity of 8000 m^3/day were installed in various

regions of the world. Nowadays, desalination processes have become a fully commercial enterprise and there are around 18000 plants in operation globally with a capacity of 90M m^3/day of fresh water for the provision of municipal and industrial facilities (Chua & Rahimi, 2017).

In general, desalination technologies can be classified into two main categories based on the phase change of the treated water as shown in Figure 2.10. The first category is a desalination process with phase change. In these processes, thermal energy is utilized to produce fresh water by evaporation and condensation. The most common method of thermal desalination technologies is multi-stage flash (MSF), multi-effect distillation (MED) and vapour compression distillation (VCD). The second category is a desalination process without phase change. In this process, mechanical energy is utilized to separate undesirable salt ions from the water through membranes. Reverse osmosis (RO) is the most common membrane technology used (Elsaid et al., 2020).

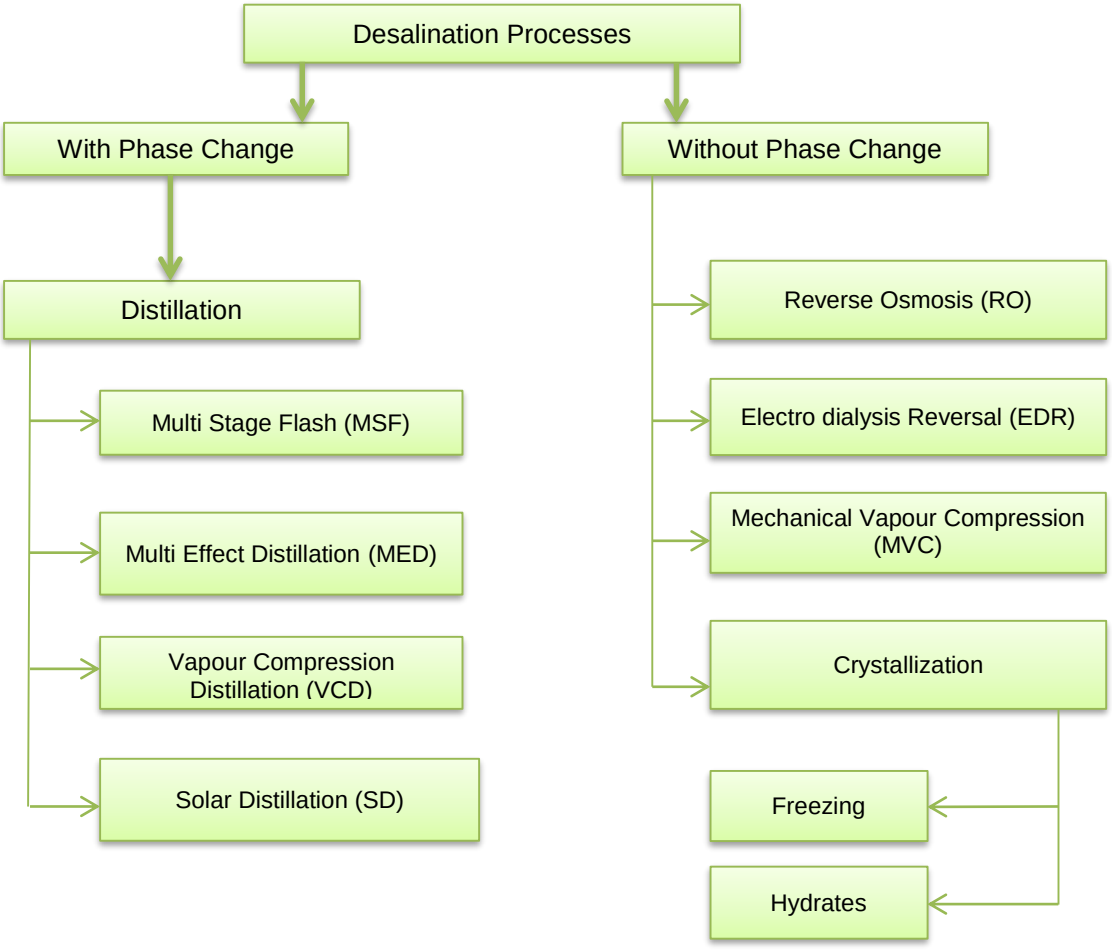

Figure 2. 10: Desalination processes

In terms of operation cost, desalination processes require a significant amount of energy to achieve a proper separation of salt from the saline solution. Developed and

rich countries can therefore afford such systems, while others cannot be due to the high capital cost and limited energy source availability. Moreover, there is a negative impact on the environment through the intensive use of fossil fuels. It is estimated that, in thermal desalination treatment processes, 1 m^3 of fresh water requires 2.6 to 10.6 kWh. Furthermore, the amount of carbon dioxide emitted to the environment must be taken into consideration. Further, membrane desalination treatment processes are prone to fouling and scaling of the membrane. Fouling can occur as a result of biological growth in the membrane vessels. Scaling occurs from the precipitation of sparingly soluble salts in the system (Sethi & Wetterau, 2011).

As mentioned above, conventional desalination technologies are energy-intensive and subject to high capital cost of the investment due to the cost of build and operation. Therefore, many attempts have been made to find another alternative to power desalination plants and to increase energy efficiency. In this regard, solar distillation processes are promising technologies to produce fresh water to satisfy the human need for pure water for small/medium communities.

2.6.1. The global adaptation of desalination technologies

The global desalination production of fresh water has witnessed a dramatic increase during the last 15 years. It is estimated that the total desalination capacity in 2005 was 35 million m^3/day (Gleick et al., 2006) and in 2019 has tripled to over 95 million m^3/day (Jones et al., 2019). Furthermore, it is expected to exceed 192 million m^3/day in 2025 (Darre & Toor, 2018). As the threat of water scarcity worldwide continues to rise, several desalination technologies have been adopted worldwide. These technologies rely on phase change (thermal), are pressure driven, electrically-based, while chemical and hybrid processes are used to relieve the stress on limited fresh water resources and to assure water safeguard for societies. The desalination technologies can be classified based on feed water sources into seawater desalination (SWD), brackish water desalination (BWD), and waste water desalination (WWD) (Al-Obaidi et al., 2020). The number of desalination plants is therefore distributed according to the type of feed water as 71%, 21% and 8% for SWD, BWD and WWD respectively (Elsaid et al., 2020). The economic cost reduction of desalination processes associated with new technological advancements has enabled desalination to become a cost-effective and attractive option to meet domestic and municipal water needs. In terms of statistical survey, there are 15906 desalination plants currently operating, distributed across 177 countries (Jones et al., 2019). Figure 2.11 shows the increase in the number of desalination plants and the capacities based on main desalination technologies over the last 60 years.

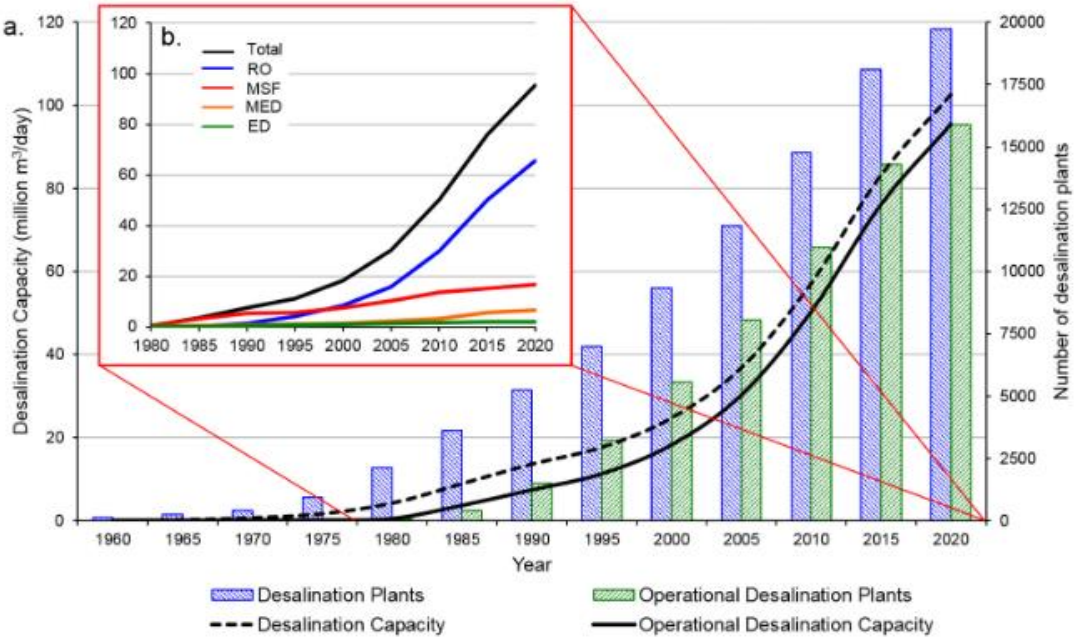

Figure 2. 11: **Number of the desalination plant and the total capacities (Jones et al., 2019)**

The geographical distribution of the desalination facilities shows that most of them are located in fresh water scarce areas such as the Middle East, Australia and North Africa, and in high population countries such as China and the USA. The early facilities utilized phase change (thermal) technologies. Thermal technologies tend to be used in high salinity feed water where there is a low cost of energy (Xu et al., 2013), and usually they are integrated with power plant facilities, especially in oil-rich countries.

2.6.2. Environmental considerations

To produce fresh water using desalination, three main stages have to be implemented: pre-treatment, pure water extraction, and brine disposal. Each stage has disadvantages for the environment. Pre-treatment can be determined depending on the feed water conditions. According to Global Water Intelligence (GWI), feed water is categorized as river and waste water (500-3000 parts per million (ppm) total dissolved solids (TDS)), brackish water (3000-20000 ppm TDS), seawater (20000-50000 ppm TDS) and brine (< 50000 ppm TDS). Pre-treatment is crucial for high salinity feed water to adjust pH, remove suspended matter and avoid corrosion, foaming and fouling (Alshahri et al., 2019). In this process, chemical substances are added to feed water such as biocides (sodium hypochlorite, chlorine, etc.), coagulants (aluminium salts, ferric salts, polyelectrolytes, etc.), acids, corrosion inhibitors and anti-scaling agents (Sutzkover-Gutman & Hasson, 2010; Anis et al., 2019). All the chemical agents added during pre-treatment processes are disposed of with the brine stream. However, it can

cause severe harm to the marine life inhabitants on the coastline where desalination facilities are concentrated.

As mentioned, desalination processes are energy-intensive. In the membrane desalination process for instance, it is estimated that the energy requirements are 0.4-3 kWh/m^3 and 2-7 kWh/m^3 for sea water and brackish water respectively (Ghalavand et al., 2014), (Voutchkov, 2018) and (Zarzo & Prats, 2018). Most of the energy consumed in the membrane process is used to drive the feed water and hydraulic pumps. On the other hand, thermal desalination requires higher energy than membrane technology. The conventional thermal desalination methods such as MSF and MED require energy ranging from 40 to 80 kWh/m^3 excluding the pumping energy requirements (Semiat, 2008) and (Darwish, 2013). Problematic environmental issues are associated with the high energy consumption of the thermal processes caused by tremendous heat losses to the environment (ambient and feed water source) and greenhouse effects resulting from the burning of fossil fuels.

One of the major challenges of desalination processes is brine disposal management. Brine is a term that refers to the waste water produced from desalination. It is highly concentrated in salt and heavy metals. Moreover, brine is a high temperature solution. The quantity and the quality of the brine can be determined according to many factors such as the feed water conditions, type of desalination process and capacity, pre-treatment procedure, and the recovery ratio (RR) (Darre & Toor, 2018; Jones et al., 2019).

The recovery ratio of treated water is used to determine the daily quantity of brine as:

$$Qb = \frac{Qd}{RR} \times (1 - RR) \tag{2.33}$$

$$RR = 1 - \frac{Sf}{Sb} \tag{2.34}$$

Here *Qb* is the quantity of brine produced (m^3/day), *Qd* is the capacity of the desalination facility (m^3/day), *Sf* is the feed water salinity (mg/l for TDS), *Sb* is brine salinity (mg/l), and *RR* is the recovery ratio.

In most reverse osmosis (RO) technologies, the recovery ratio ranges from 42% to 85%. 42% for sea water, 65% for brackish and 85% for river water (Qasim et al., 2019). On the other hand, thermal technologies have a lower recovery ratio than membrane technologies. In general, the recovery ratio increases as the feed water salinity decreases.

According to Jones et al. (2019), the daily production of brine is about 141 million m^3, most of it concentrated in the Middle East and North Africa. Furthermore, the common method to dispose of brine is to discharge it back into the water source (Kampf & Clarke, 2013). A high salinity brine (1.5 – 2 times higher than sea water) causes a major threat to the marine environment associated with depletion of dissolved oxygen. In

addition, the high temperature of the brine and the chemical agents added in pre-treatment processes increase the mortality of sea water organisms and contribute to toxic compound formation. It therefore requires post-treatment to meet international standards to enable sea discharge. Other conventional methods for brine management such as deep well injection and dilution of brine by blending it with lower salinity wastewater have been used to mitigate the environmental concerns associated with the direct discharge of brine into water bodies.

Costlier advanced techniques such as bipolar membrane electro dialysis can be used to extract acids and valuable metals from brine. In some cases, two or more desalination facilities can be combined in a hybrid configuration such as RO with thermal technology, and thereafter the brine produced from RS can be fed to a thermal desalination plant (Hamed, 2005).

Renewable energy technologies are a key component that has great potential to reduce energy cost and minimize environmental impacts of the desalination processes. Electric energy produced from renewable energy sources can be used to power high pressure hydraulic pumps in membrane technologies. Wind power generation units were coupled with RO and MVC desalination demonstration plants in Germany and Spain (Forstmeier et al., 2006). Experimental research was conducted in the Canary Islands to operate an RO unit directly from a wind turbine (Garcia-Rodriguez, 2003). In particular, a photovoltaic-powered RO unit has achieved competitive cost at about 2 $/m^3 compared with other techniques (Ghermandi & Messalem, 2012). A solar pond storage system coupled with an MED system produced 14000 m^3/year in Qatar (Mohamed & Bicer, 2019).

Due to the negative environmental impacts of brine disposal, artificial solar evaporation ponds technology is utilized in brine treatment and solid salts extraction, especially in inland desalination plants (Morillo et al., 2014).

Thermal desalination technologies based on solar-driven systems have proven to be effective in remote areas whereas infrastructure not facilitated. Despite the low productivity of solar desalination systems, they are still the most reliable method of water treatment in such regions due to their low cost and simplicity (Esfahani et al., 2016).

2.7. Solar water distillation

Solar water distillation is a process of utilizing incident solar energy to produce fresh water from contaminated water based on differences in volatility. It imitates the natural hydrological phenomena of the water cycle shown in Figure 2.12. The only difference is that solar water distillation is a controlled process (closed-loop system) while the natural water cycle is an open-loop system (Tiwari & Sahota, 2017).

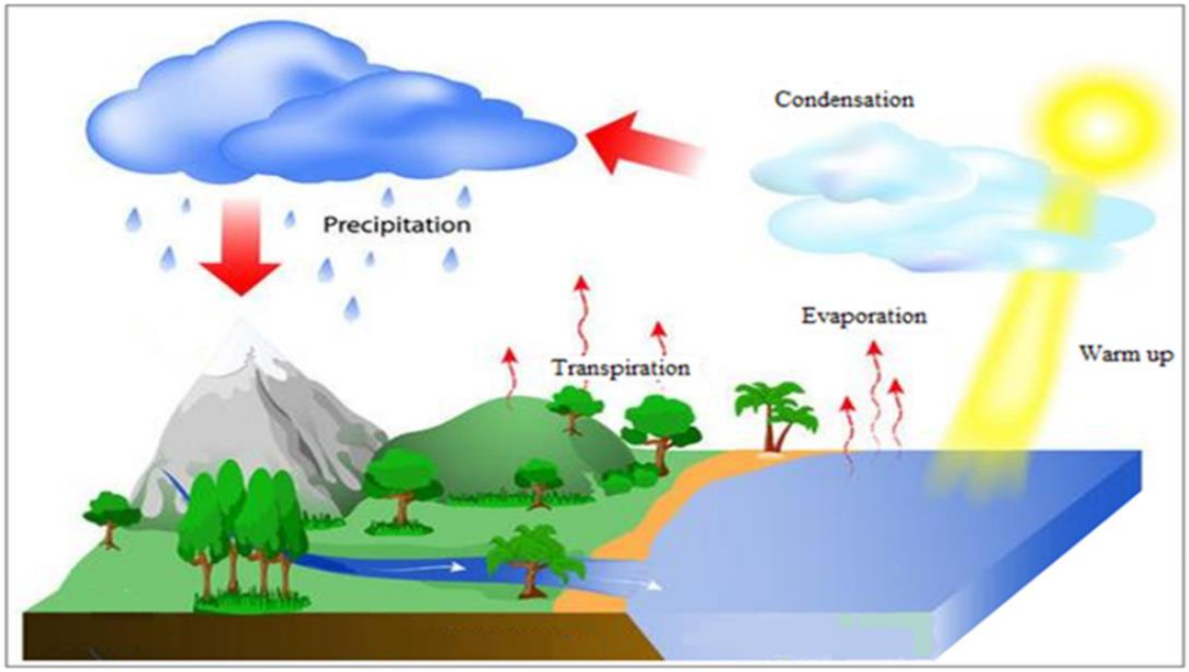

Figure 2. 12: Natural water cycle

In practical terms, the solar water distillation process uses a device called a solar still where contaminated water is fed into a basin covered with a transparent sheet of glass or plastic. The condensation occurs on the inner surface of the cover when the solar energy heats up the contaminated water and creates a temperature difference with the cover. The evaporated solvent, which has higher volatility than the solute, is collected through a channel. Solar water distillation technologies are commonly used to treat low and medium contaminated water such as sea water, underground water and some sorts of low contaminated surface water in remote areas. The first practical application to obtain pure water using solar energy was designed and developed in 1872 by Swedish engineer Carlos Wilson in the northern desert of Chile. The purifier units operated for three decades to provide miners and their families and the animals used at the nitrate mines with drinking water (Duffie & Beckman, 2013). The stills were made of wood and timber and were covered with glass sheets. The total surface area of the glazing was 4450 m^2 and a productivity of 22.7 m^3/d of fresh water was achieved. To feed the stills, high salinity water from a nearby saltpetre mine was transferred to the purification system (Kalogirou, 2005). In 1945, Maria Telkes, a researcher from the Massachusetts Institute of Technology (MIT), designed a portable solar water still for emergency and camping uses. The unit consists of an air-inflated container with a transparent plastic top cover and a felt pad at the bottom. Once the felt pad is soaked with seawater, solar radiation heats up the water, thus generating vapour, which then condenses on the inner surface of the plastic cover. The distilled water flows into the container attached to one side of the plastic cover (Zaragoza et al., 2012). In 1951 more research was conducted at the University of California in a seawater conversion

laboratory, which led to the construction of a solar distillation system on the engineering testing field. One year later, the United States Government established the Office of Saline Water in Florida (Talbert et al., 1970). By the 1970s, better understanding in terms of thermodynamic analysis of solar still performance led to more developed solar stills such as forced convection stills, external condensation stills and tilted wick stills. Moreover, better materials were used to prolong the period of operation of the stills and minimise the maintenance required during that period (Zaragoza et al., 2012). Since then to date, more than 200 scientific works have been published on solar distillation systems, demonstrating the development in the design, modification and performance as well as validation models of the thermodynamics of the stills.

2.8. Solar stills

A solar still is basically an air-tight container that can be made from various materials (metal, plastic, cement and wood) covered with a transparent sheet (glass or plastic). Contaminated water is fed into the basin. Once the solar still is expose to solar radiation, the basin (absorber) absorbs the incident radiation and heats up the water. Then the evaporation takes place, and the generated vapour reaches to the condensation surface and creates water drops. The water drops then slide down and collect at lower end of the glass cover. The result is distilled water which can be used for domestic purposes. Basically, solar stills are classified into two main categories as single and multi-effect solar stills. Furthermore, and based on thermal energy supply, those categories are subdivided as passive and active stills (Pandey et al., 2019). Passive solar stills do not require a backup thermal energy source, as the evaporation and the condensation occur directly inside the system. Active solar stills utilise an auxiliary device such as a solar collector, heat element and heat exchanger in order to carry out the evaporation of the water.

2.8.1. Single effect solar still

The most common and simple type of solar water still is single effect solar still (Pathak et al., 2018). It is the origin of solar stills; it can be called a basin-type solar still. In this system, the glazing consists of one layer of transparent material. Thus, the efficiency of the still is limited as a result of thermal energy losses through the cover (Kiatsiriroat et al., 1987). Many experimental works have been conducted to improve its efficiency, and different factors have been investigated. It has been concluded that cover material type, thickness and inclination, basin liner, water depth, insulation material and weather elements all have a direct influence on the performance of the still. The efficiency of this type of solar still is estimated at 30 - 40% (Kabeel & El-Agouz, 2011). The daily yield of distillate water of theses systems is about 2 - 3 L/m^2 (Tiwari & Sahota, 2017). This system has few advantages such as simplicity of construction, cost-effectiveness,

and easy maintenance and operation. Figure 2.13 shows a simple single-effect solar still.

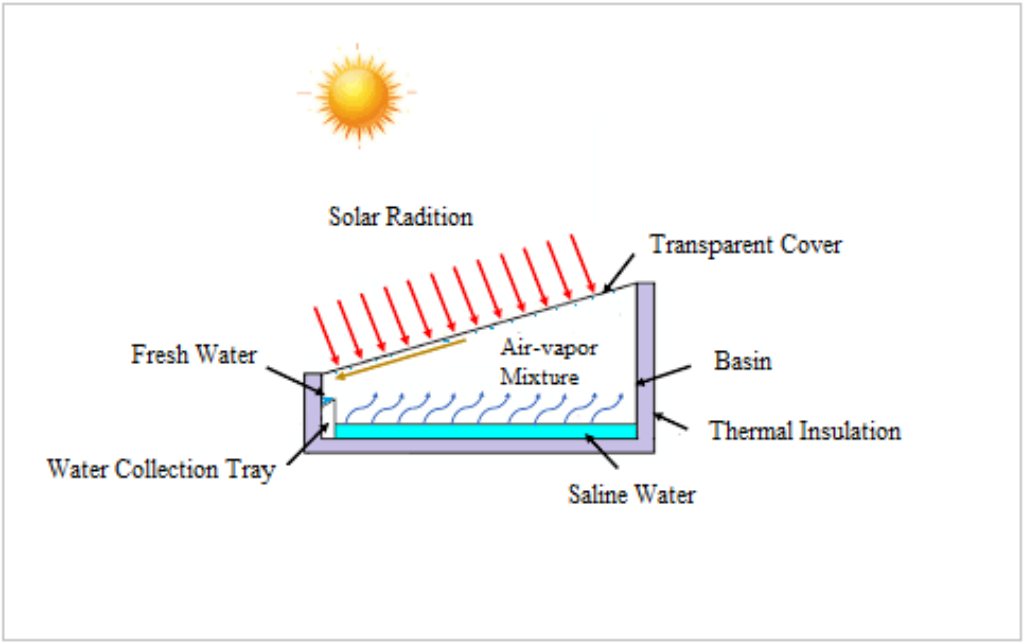

Figure 2. 13: Single-effect solar still

The basin-type solar still illustrated above consists of a shallow basin that can be made of locally available material (metal, plastic, and wood). The base of the still is called the basin liner. It has high absorptivity and high resistance to hot water and corrosion. The basin is covered with a transparent sheet made of (plastic/glass). The cover and sides of the basin are sealed properly in order to minimise vapour losses. The cover angle is an important feature that affects fresh water productivity. It should be set up at a proper slope to allow the condensed water to flow to the collection channel. In order to monitor the performance of the still, thermocouples are required to measure temperature at different places (ambient and still). An anemometer is also required to measure wind speed and a heliometer to measure the incident solar radiation.

In more detail, a single-effect solar still can be categorized into two types, a passive and an active solar still. In the first one, the thermal energy provided to carry out the evaporation is the internal source. There are different types of passive solar still which include:

- Wick solar still
- Basin solar still
- Spherical solar still
- Rectangular solar still
- Weir-type solar still
- Diffusion still

- Tubular solar still

In the second category, the thermal energy provided to carry out the evaporation is external. It comes from different sources such as solar collectors or industrial waste heat. There are different types of active single-effect solar still, which include:

- Industrial waste heat recovery solar still
- Solar still coupled with solar collector
- Air-bubbled solar still
- Regenerative solar still
- Solar still with solar heater
- Hybrid system active solar still
- Solar still integrated with heat exchanger

2.8.2. Multiple effect solar still

Multi-effect solar still systems are more efficient than single-effect solar still systems in terms of thermal energy use. These systems circulate the energy released from the condensation process to the next stage of the treatment. The multi-effect solar still is a device that has multiple operation stages, therefore the latent heat released is utilized to heat up the water mass in the next stage of the upper basin (Tiwari & Singh, 2009). The effect of different stages allows for efficient use of input thermal energy, and hence the yield of distilled water is higher (Estahbanati et al., 2015).

The multi-effect solar still is also subdivided into two types, active and passive stills based on their design and configuration. There are different configurations of the multi-effect solar still, which include:

- Double basin solar still
- Multi-stage evacuated solar still
- Waste heat recovery still
- Multi-effect vertical solar still
- Solar still integrated with heat exchanger
- Solar still coupled with solar collector

Figure 2.14 shows a multi-effect solar still coupled with a solar collector. This system consists of two basins constructed one above the other. A solar collector is attached to the lower basin to enhance the evaporation rate. The system employs the thermosiphon method.

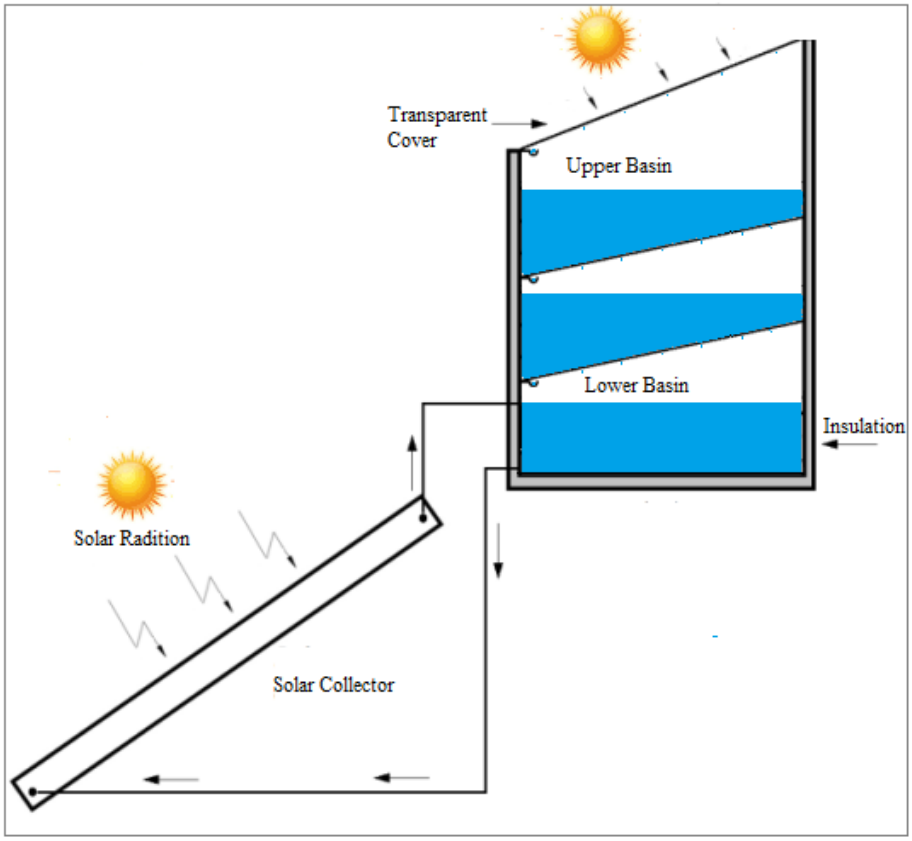

Figure 2. 14: A schematic view of the multi-effect solar still

Many researchers have reported that the number of stages influences the solar flux received by each basin. Therefore, the performance of the still depends on the number of effects. The studies have included an increasing number of stages up to nine effects. They have observed that the seven stage system gives the optimum performance. Beyond that, the yield becomes insignificant (Tiwari & Singh, 2009; El-Sebaii & El-Bialy, 2015). The disadvantages of the passive stills such as low operation temperature and ineffective night operation are overcome by employing the idea of an active solar still (Zheng, 2017).

2.9. The efficiency of solar stills

Solar water distillation technologies have been used for more than a century to obtain fresh water for domestic purposes. Valuable researches have been conducted to estimate the performance of several types of solar stills. The influence of variable factors such as wind speed, incident solar radiation, ambient temperature and glazing inclination on the performance of solar stills has been addressed. In general, the productivity of distilled water in a solar still depends on the intensity of solar radiation and the optimum design of the still. Single-basin solar stills are the most common type of solar still. It is simple, easy to operate and cost-effective. The main drawback of this type is the low yield of fresh water due to heat loss through its cover. Many attempts to enhance its efficiency have therefore been made. Sampathkumar & Senthilkumar (2012) tested a single slope solar still coupled with an evacuated tube solar water

heater system. They found that the productivity of the coupled still is double that of a simple solar still. Badran (2007) investigated the effect of different operational parameters on a single slope solar still. He concluded that using asphalt as basin liner increased efficiency up to 29%; moreover, the change in water depth from 3.5 to 2 mm increased productivity by 26%. Singh & Tiwari (2004) evaluated the monthly performance of a solar still. They used numerical computations to analyse climate and design parameters. They concluded that the annual performance of the solar still could be maximised when the inclination of the glazing was equal to the latitude of the place. A hemispherical solar still with a water cooled cover was designed and tested by Kumar et al. (2015). They found that the system efficiency increased by 42% compared with an uncooled hemispherical solar still. Tanaka (2009) performed outdoor experiments to investigate the performance of a single basin solar still with external and internal reflectors in the winter season. He concluded that the daily yield can be improved by 70% when using solar reflectors. Many valuable research works have addressed different types of solar stills and discussed their performances (Kanyarusoke, 2018; El-Sebaii & El-Bialy, 2015; Kumar et al., 2015; Tiwari & Sahota, 2017).

2.9.1. Thermodynamic analysis of the solar still

The energy analysis of a single basin solar still shown in figure 2.15 demonstrates that the total solar radiation received by the still is (I_t). The reflected fraction at the cover is $R_c(I_t)$ and the amount absorbed by the cover is $\alpha_c(I_t)$. The transmitted solar radiation $t_c(I_t)$ is absorbed by the brackish water $B_w(I_t)$, while a small fraction is reflected by brackish water surface $R_w(I_t)$. Finally, solar radiation reaches the basin liner. Most of the energy is transferred to water mass as convection. A small fraction is dissipated through the side walls to the ambient as conduction transfer.

Once brackish water is heated up, three modes of heat transfer occur from water mass to the cover. Latent energy is released as a result of condensation on the inner surface of the cover. Distilled water flows through the channel at a rate (m_p) and specific enthalpy (h_p).

Some assumptions are proposed to simplify the analysis, which include:

- The inclination of the cover is in the optimum position;
- The absorbed thermal energy by the side walls are negligible;
- There is no temperature gradient along the side walls and bottom;
- The still is vapour-leakage proof.

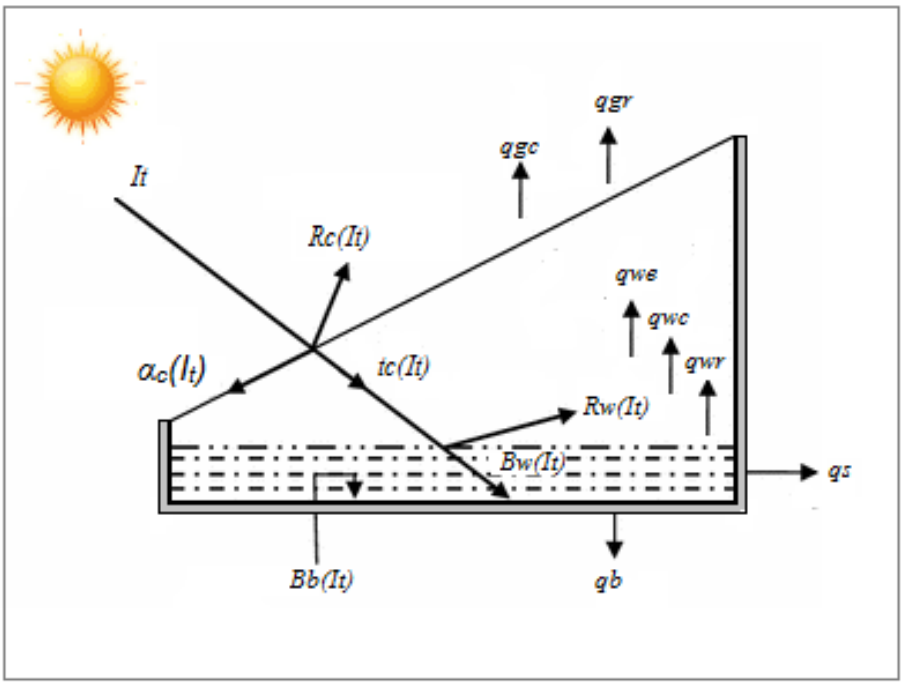

Figure 2. 15: **Energy analysis of single solar still**

The thermal energy gained by the cover (from the sun and brackish water) is equal to the sum of energy lost to the atmosphere and the energy gained. Therefore, the energy balance equation for the cover can be written as:

$$(I_t)\alpha_c A_c + q_{we} + q_{wc} + q_{wr} = q_{gc} + q_{gr} + m_c C_{pc}\left(\frac{dT_c}{dt}\right) \quad (2.35)$$

The energy gained by brackish water is equal to the sum of the three mode heat transfer from water to cover and the energy gained. It can be written as:

$$(I_t)t_c\alpha_w A_w + B_b = q_{we} + q_{wc} + q_{wr} + m_w C_{pw}\left(\frac{dT_w}{dt}\right) \quad (2.36)$$

The energy gained by the basin liner is the sum of convective energy to the brackish water and lost energy through the walls. It can be expressed as:

$$(I_t)\alpha_b R_w R_c A_b = m_b C_{pb}\left(\frac{dT_b}{dt}\right) + B_b + q_{b+s} \quad (2.37)$$

Here, (dT_c), (dT_w) and (dT_b) are the increase in cover, brackish water and basin liner temperature respectively. These values are computed every time interval (dt).

The absorptivity of each component can be calculated as:

$$\alpha_c = (1 - R_c)\alpha_{Tc} \quad (2.38)$$

$$\alpha_w = (1 - R_c)(1 - \alpha_{Tc})(1 - R_w)\left[1 - \sum \mu j \; exp(-\eta j d_w)\right] \quad (2.39)$$

$$\alpha_b = \alpha_{Tb}(1 - R_c)(1 - \alpha_{Tc})(1 - R_w)\sum \mu j \; exp(-\eta j d_w) \quad (2.40)$$

Here, α_c, α_w and α_b are the absorptivity of the cover, brackish water and the basin liner respectively. The values of μj and ηj are given in index 1.

The thermal energy transfer between basin liner and brackish water is given as:

$$B_b = h_{cb} A_b (T_b - T_w) \tag{2.41}$$

The thermal energy transfer between brackish water and the cover is given as:

$$q_{wc} = h_{wc} (T_w - T_c) \tag{2.42}$$

The convective heat transfer coefficient is calculated by using the Dunkle formula (Tiwari, 2002). It is expressed as:

$$h_{wc} = 0.884 \left[T_w - T_c + \frac{(P_w - P_c)(T_w + 273)}{268.9 \times 10^3 - P_w} \right]^{1/3} \tag{2.43}$$

$$P_T = exp\left[25.317 - \left(\frac{5144}{273 + T} \right) \right] \tag{2.43a}$$

The radiative heat transfer factor between the brackish water surface and the cover is expressed as:

$$q_{wr} = h_{wr} A_w (T_w - T_c) \tag{2.44}$$

Where, h_{wr} is the radiative heat transfer coefficient which can be expressed as:

$$h_{wr} = \epsilon_{eff} \sigma [(T_w + 273)^2 + (T_c + 273)^2](T_w + T_c + 546) \tag{2.45}$$

The rate of evaporative heat transfer between the brackish water and the cover is expressed as:

$$q_{we} = h_{we} A_w (T_w - T_c) \tag{2.46}$$

Where, h_{we} is the evaporative heat transfer coefficient. It can be expressed as:

$$h_{we} = 16.237 \times 10^{-3} \, h_{wc} \frac{P_w - P_c}{T_w - T_c} \tag{2.47}$$

The heat lost through the side of the basin can be expressed as:

$$q_{b+s} = U_{b+s} A_b (T_b - T_a) \tag{2.48}$$

Where T_a is atmosphere temperature. The heat loss coefficient (U_{b+s}) is equal to 14 W/m^{2}K (Velmurugan, et al., 2009).

The radiative heat through the cover to the atmosphere is expressed as:

$$q_{gr} = h_{gr} A_c (T_c - T_a) \tag{2.49}$$

Here, h_{gr} is the radiative heat coefficient. It is expressed as:

$$h_{gr} = \varepsilon \sigma \left[(T_c + 273)^4 - \left(T_{sky} + 273 \right)^4 \right] / (T_c - T_a) \tag{2.50}$$

Here, T_{sky} is the sky temperature. It can be obtained as:

$$T_{sky} = T_a - 6 \tag{2.51}$$

The convective thermal energy from the cover to the sky is expressed as:

$$q_{gc} = h_{gc} A_c \left(T_c - T_{sky} \right) \tag{2.52}$$

Here, h_{gc} is the convective heat transfer coefficient. It is expressed as:

$$h_{gc} = 2.8 + 3V \tag{2.53}$$

Where V is the wind speed in m/s.

2.9.2. Overall thermal efficiency of solar still

The thermal efficiency of a passive and active solar still can be obtained as:

$$\eta_i = \frac{Q_e}{I(t)} \tag{2.54}$$

$$\eta_p = \frac{\sum m_w L}{A_s \int I(t)dt} \times 100 \tag{2.55}$$

$$\eta_a = \frac{\sum m_w L}{A_s \int I(t)dt + nA_c \int I(t)dt} \times 100 \tag{2.56}$$

Here, η_i is the instantaneous thermal efficiency, n is the number of collectors, A_c is the area of the collector and L is the latent heat of evaporation, which can be obtained as:

$$L = 3.1615 \times 10^6 (1 - 7.616 \times 10^{-4} T) \tag{2. 57}$$

Here, L in J/kg, for temperature above 70 °C.

The instantaneous efficiency can be expressed as shown:

$$\boldsymbol{\eta_i = \frac{m_w L}{I(t) A_s}} \tag{2.58}$$

2.10. Factors influencing the efficiency of a solar still

The temperature difference between the brackish water and the condensing surface is the key factor in production of the distilled water. A higher difference gives a greater distilled water yield. The other factors that affect thermal energy gain can be classified into two main categories. The first one consists of controllable factors such as condensing material, basin liner type, water depth and type of insolation. The second one consists of uncontrollable factors such as wind speed and solar radiation intensity.

2.10.1. The effect of condensing surface material

The effect of different condensation surface materials on the productivity of distilled water has been addressed by many researchers. The most common condensing material is glass. It is abundant and high in transmittance. Conversely, it is heavy, fragile and expensive. Plastic is the other option of condensing material. It is light, durable and easy to handle. But it has a lower transmittance rate compared to glass. One of the important features of the condensing surface is the contact angle with the droplet. The contact angle determines the shape of the droplet. A film-wise condensation (flat droplet) results from a low contact angle. A drop-wise condensation

(hemispherical droplet) results from a high contact angle. Bhardwaj et al. (2013) reported that the formation of the droplet starts as a heterogeneous nucleation, subsequently creating the insolation and finally taking the final shape by coalescence process. They compared two different condensing surfaces: a polyethylene terephthalate (PET) and glass of the same thickness of 2 mm. The results showed that the condensation on the PET was shinier than on the glass, and therefore it was more reflective, although the water temperature of the still with the glass cover was higher. They concluded that the low contact angle of the glass allowed more solar radiation to pass through, leading to an increase in the productivity of distilled water. An experimental study on the effect of wettability alteration of the condensation surface using nanoparticles was performed by Zanganeh et al. (2020). They found that the use of a nano-coated condensation surface improved the solar still efficiency significantly. Eldalil (2010) installed a resonator on a solar still structure in order to excite the droplet formed on the condensing surface to slide down to the collecting channel, and avoid falling back to the brackish water as a result of overgrowing. He improved the daily efficiency of the still by 60%.

2.10.2. The effect of cover thickness and inclination

The transparent cover performs different functions. It works as a condensing surface, as a receiver and transmitter of solar radiation, and also suppresses thermal energy escaping to the environment. The selection of the proper type and thickness of the transparent cover is therefore significant in terms of efficient design and operation of the solar still.

Many research works have been conducted to compare different thicknesses of the transparent cover. They concluded that lower thickness increases the average of distilled water due to the increase in transmittance rate (Ghoneyem & Ileri, 1997; Panchal, 2016). A double-glazed solar still consisting of two 4mm glass sheets and a 10mm air gap was tested by Khechekhouche et al. (2019). They confirmed that the efficiency of a double-glazed solar still is lower than the efficiency of a single-glazed solar still by 55.7% due to the lower temperature difference between the condensing surface and brackish water of the double-glazed still.

The inclination angle of the transparent cover is selected according to the latitude angle of the location of the solar still (Selvaraj & Natarajan, 2018). The optimum yield varies according to the season and the place. Therefore, the tilt angle is optimised according to the annual yield and the rigid structure of the solar still.

2.10.3. The effect of basin water depth

The amount of brackish water in the basin has a significant effect on the productivity of distilled water. A large amount of water needs a large amount of thermal energy to heat up, and more time to start condensation. Phadatare & Verma (2007) tested solar stills

with different basin water depths varying between 2-12cm. They found that the maximum distilled yield obtained at a water depth of 2 cm and solar still efficiency was 34%. Rajamanickam & Ragupathy (2012) elevated the daily yield of a double slope solar still from 2.76 L/m^2 to 3.07 L/m^2 by reducing the basin water depth from 2 cm to 1 cm.

2.10.4. The effect of wind velocity

The effect of wind velocity on the performance of solar stills was investigated in the early 1960s by many researchers (Lof et al., 1961; Cooper, 1969). Their conclusions show contradictions. Cooper reported that the efficiency of a solar still increased by a small fraction at high wind velocity, while the results from Lof and others showed a decrease in efficiency with an increase in wind velocity. Tiwari & Singh (2009) reported that the rate of evaporation was increased by an increase in wind velocity, which caused a high temperature difference between brackish water and the condensing surface. El-Sebaii (2000) investigated the effect of wind velocity on five different types of solar stills. He found that the daily yield of the stills increased with the increase of wind velocity until a specific value. The value of wind velocity was seasonally dependent.

2.10.5. The effect of absorber type

The absorbing materials of solar stills can be classified into two types: coated and uncoated absorbers. The former includes coated basin liners, black floating plates and coated porous media. The latter includes organic dyes, charcoal particle beds, black volcanic rocks and uncoated porous media (wick materials) (Panchal & Shah, 2012; Abdallah et al., 2009). The main purpose of using different types of absorbing materials is to improve the daily yield of solar stills due to the increase of temperature difference between brackish water and the condensing surface. The absorber materials also work as thermal energy storage media. During the sun's absence, they release the stored energy to heat up the water.

2.10.6. The effect of enhancement devices

One of the drawbacks of single-effect solar stills is the low yield of distillate productivity. Attempts to enhance the thermal efficiency of the stills have therefore been made in many research works. Devices such as internal and external reflectors, flat plate collectors, evacuated tubes, parabolic solar concentrators and heat elements have been used to boost the thermal energy gain (Kumar et al., 2015). An external condenser with and without a suction fan is used to increase the rate of condensation. In order to modify the condensing surface, devices such as a wiping system, resonator and water cooling system have been used. Considerable improvement has been achieved in the daily yield of distilled water.

2.11. Atmospheric water generation

Atmospheric water generation (AWG) technology refers to harvesting fresh water from atmospheric humidity condensation (Tu & Hwang, 2020; Moghimi et al., 2021). As water vapour is one of the components of the atmosphere, it can be condensed due to the phase change process from the gaseous phase to the liquid phase, and can be harvested utilizing devices called water generators and dew collectors. The approaches include fog water collection and dew water collection. Fog water collection is subdivided into a conventional method (fog collector) and modern method (biomimicry inspired). Dew water collection is subdivided into a radiative cooling condensation (passive system), solar-regenerated desiccants, and the active cooling condensation method (Jarimi et al., 2020). In water vapour condensation technology, a cooled surface is required in order to initiate dew water formation. While in fog water collection technology, a simple traditional technique depends on exposing a mesh-like structure to the atmosphere in order to harvest fresh water. The following sections provide a brief review of recent technologies used in atmospheric water harvesting.

2.11.1. VCC and TEC atmospheric water harvester

One of the atmospheric water generation technologies is water harvesting using condensation. Condensation process requires heat pump system to achieve (Zhang, et al., 2016). It employs a vapour compression cycle (VCC) or thermoelectric cooler cycle (TEC) to create a cold surface in order to condense the water vapour. VCC can be utilized directly to harvest water vapour or as a water vapour coo-generator in a vapour compression air conditioning cycle (AC and AWG integrated system) (Magrini et al., 2015; Zolfagharkhani et al., 2018; Tu & liu, 2019; Tu & Hwang, 2019). In a VCC collector, the ambient air stream is withdrawn through the condensation exchanger, cooled down and dehumidified. The system is capable of producing water in the ambient temperature range of 25 to 40 ºC and relative humidity between 30 to 100%. Different system designs and configurations have been proposed to capture water vapour using VCC (Solís-Chaves et al., 2018; Zolfagharkhani et al., 2018; She et al., 2014).

In recent years, the thermoelectric effect has drawn attention in the energy sector research field, meant to be used as a power generator and/or cooler and for space comfort. This technology has proven the characterization of the cooling capacity and satisfied efficiency of a heat pump system (Tassou et al., 2010; Enescu & Virjoghe, 2014; Xuan, 2003). Further, the thermoelectric cooling system is used as a humidifier to capture water vapour from the atmosphere depending on condensation technology (Yao et al., 2017). The humidifier consists of thermoelectric modules raw. The TEC is

arranged to create a cooling channel. The hot side of the modules is connected to the heat sink to avoid overheating. A cooling fan is preferable to increase heat dissipation. The humid air passes through the cooling channel, and condensation takes place. The fresh water is then collected through a plumbing system. Different designs and configurations of the TEC water vapour generator have been proposed, tested and investigated (Yao et al., 2017; Joshi et al., 2017; Liu et al., 2017; Shourideh et al., 2018; Eslami et al., 2018; Jradi et al., 2012; Tu & Hwang, 2020).

2.12. Hydro panel system

The hydro panel is a compound system that uses solar photovoltaic and thermal collectors to extract pure water from the air. The system shown in Figure 2.16 consists of three main sections: a solar PV panel, solar thermal collector and air filtration system. It works by drawing atmospheric air into the system. The hygroscopic material adsorbs vapour from the air, then the thermal collector desorbs the vapour from the hygroscopic material into the amplified vapour cycle to format the condensation. The collected water flows into the water reservoir and then through mineral packs to improve its taste and health criteria. The performance of the system can be monitored by connecting it to a phone application. The system is applicable to satisfy the water needs of commercial and residential facilities.

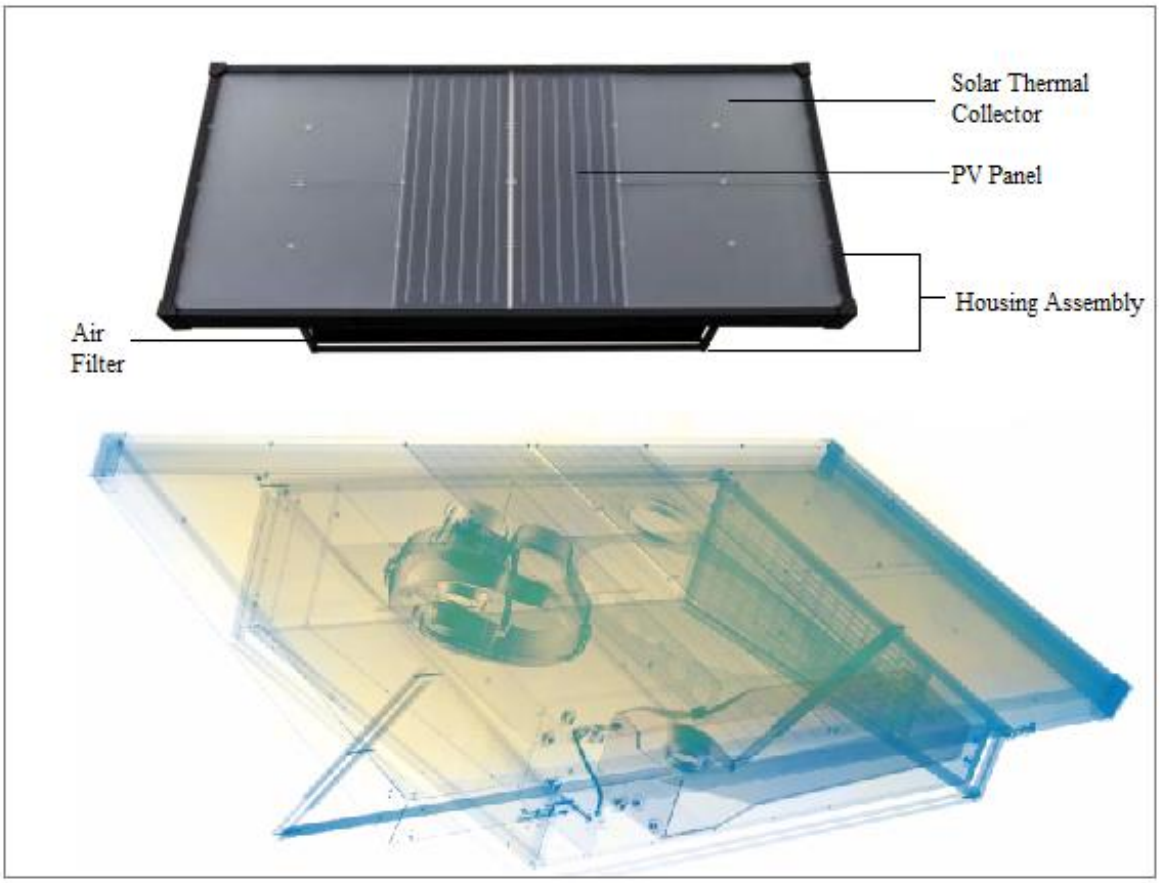

Figure 2. 16: **Hydro panel system (Markham, 2020)**

The main drawbacks of the system are:

- Noisy: the vapour cycle fan makes a loud noise.
- Expensive: it costs around 5500-6500USD to install s system that produces about 2-8 L/d.
- Strong mineral taste in the first month of operation.
- Low to zero production on very dry days.

2.13. Economic perspective of PV systems

In 1839, Alexander Becquerel discovered the photovoltaic effect when exposing a conductive solution to light (Fraas, 2014). After many years of experimentation and research, the first conventional photovoltaic cells were manufactured in the late 1950s and achieved an efficiency of 10% (Mukerjee & Thakur, 2011). In 1963, the first photovoltaic module was produced by Sharp Corporation made out of silicon cells. In the early 1970s, large companies were established and commercial business and sales started. Twenty years later, photovoltaic systems were designed for telecommunication applications, refrigerators, vaccine and medical equipment, water pumps and other applications. The beginning of the 21st century has witnessed tremendous changes in photovoltaic market share. Many companies in the industry have been listed on stock exchanges. Large renewable energy corporations have been established in Germany and Japan, and there has been a significant increase in the number of MW utility-scale PV power plant installations (Lenaidic, 2016; Young, 2011). The annual increase in installations of photovoltaic systems during that period is shown in Figure 2.17.

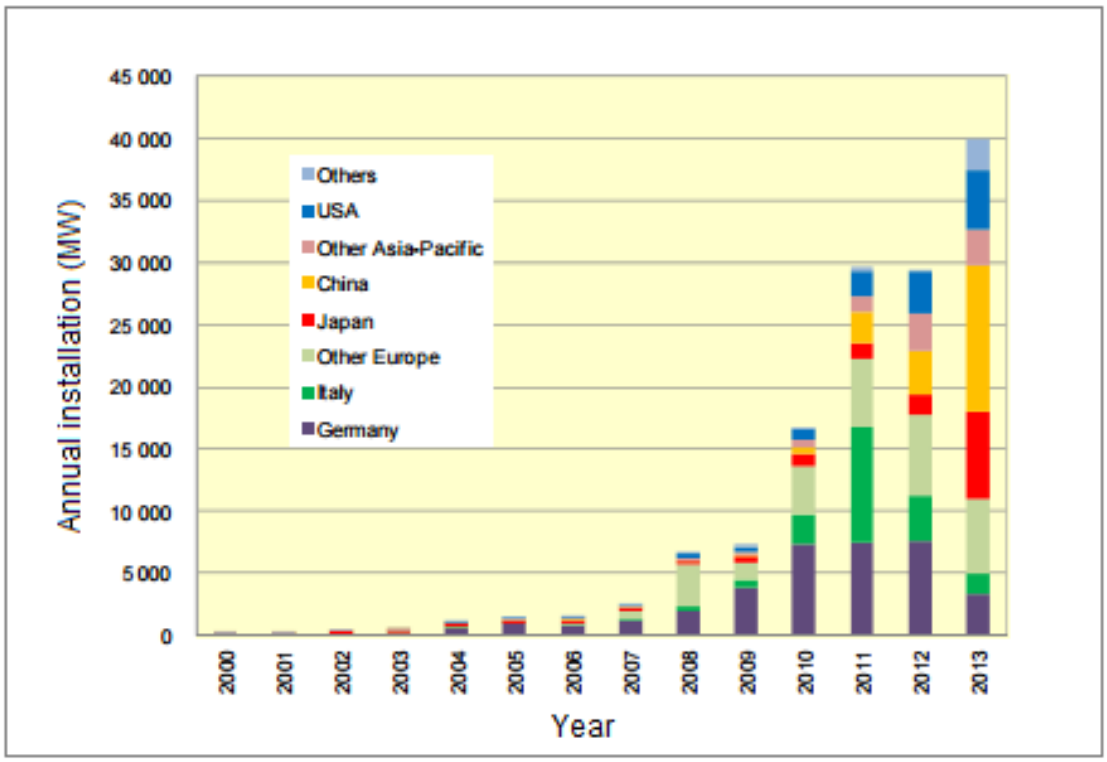

Figure 2. 17: **Annual PV installation (IEA & PVPS, 2015)**

The cost per watt during 40 years of development has decreased drastically. It was around 77 USD compared to the current value which is about 0.33 USD and it is continuing to drop. In the United States, the average residential PV level cost of energy (LCOE) reached 0.15 USD/kWh in 2017. By 2030, the US Department of Energy is targeting PV cost reduction up to 0.09 USD/kWh for residential systems (Ardani et al., 2018). In economic terminology, residential photovoltaic systems cost is categorised into hardware and soft costs. The hardware cost includes components such as modules, charge regulators and inverters. The soft cost includes factors such as customer acquisitions, installation labour, site and government regulations (O'shaughnessy et al., 2019).

As the global photovoltaic market continues to grow, China has implemented policy changes in order to contribute to PV cost reduction. It prioritizes the renewable energy concern as one of seven strategic industries, and therefore it has dominated the photovoltaic industry market (Chung et al., 2016).

Currently in 2020, photovoltaic systems have demonstrated substantial efficiency improvements. Most of the PV modules available have an efficiency of between 15% to 20%, and more expensive modules have reached 23%. The theoretical experimentation however has not stopped at 23% efficiency; they have achieved around 30% for silicon PV modules (Ferrell, 2020). Scientists at the National Renewable Energy Laboratory (NREL) have revealed a solar cell with an efficiency of 47.1% (Geisz et al., 2020). Figure 2.18 shows the relationship between the module efficiency and price based on the SunShot initiative launched by the US Department of Energy in 2011 (Jones-Albertus et al., 2016).

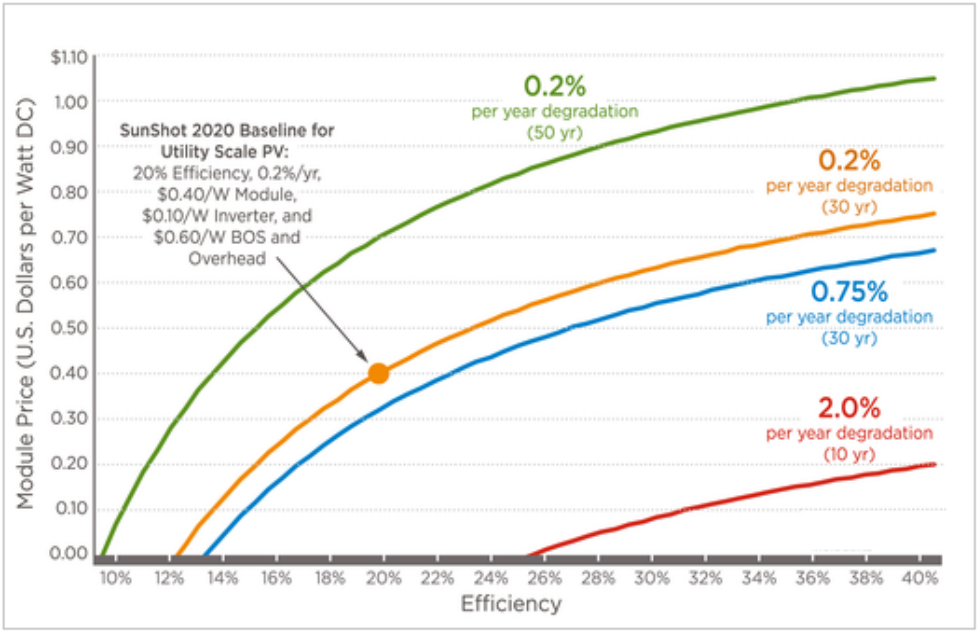

Figure 2. 18: **The relationship between the module price, efficiency, degradation and life span**

The goal of achieving a low carbon society hinges on the future of renewable energy sources. Interest has grown from society and non-governmental organization stakeholders in decarbonising the energy system. A quantum leap in the electric transport sector is taking place these days. Intense competition between electric vehicle manufacturers has combined with the establishment of thousands of eco-friendly vehicle recharge stations. Energy storage and transmission systems have had a tremendous effect on greenhouse gas emission reductions and the cost of photovoltaic installations, therefore efficient larger capacity storage systems are used to ensure an instant stable electrical supply system. The most common electrochemical storage used in PV technologies is rechargeable batteries such as lithium-ion (Zsiborács et al., 2018). It is expected that the electrochemical energy storage cost will significantly decline by 2030 as the demand and global market share continues to grow (May et al., 2018). Moreover, the worldwide adaptation of feed-in tariffs has accelerated the investment in renewable energy technologies and promoted the mass penetration of photovoltaic technologies in power generation (Manabe, 2016; Abdin & Noussan, 2018; Clark, 2017).

CHAPTER THREE

Advanced Solar Stills Design and Construction, Equipment and Instrumentation

3.1 Introduction

This chapter describes the design, construction and modification of the models of both advanced solar distillation units based on the fundamentals of heat transfer and thermodynamic principles, along with the technologies of vapour compression and thermoelectric heat pump systems. The manufacturing, construction and assembly processes are also discussed.

Machining processes, required tools, equipment and test devices are presented. Both heat pump systems (vapour compression and thermoelectric) were designed and constructed at the CPUT Mechanical Engineering laboratory. The construction material and the required components were available at local vendors and suppliers. Criteria such as quality, functionality and cost effectiveness were considered. Safety and security factors were implemented during the solar distillation unit manufacturing and construction.

3.2 Advanced solar still

Advanced single-effect solar stills were designed aiming to increase the daily yield of distilled water. They are basically consisting of three systems named above: a conventional single-effect solar still, heat pump system and solar photovoltaic system. The conventional still was integrated with the heat pump system as a thermal energy recovery system, and a simple PV system was used to power the heat pump system. All of them were built as a compact solar purification unit. Two different heat pump systems were proposed in this research, namely vapour compression and thermoelectric heat pump systems. The advanced solar stills were developed and constructed in Cape Peninsula University of Technology, Mechanical Engineering Department laboratory.

3.2.1. Single-effect solar still

A single-effect basin type solar still consists of a metal basin, water cooled transparent cover and plumbing layout, as shown in Figure 3.1.

To construct the basin, two aluminium sheet size 2800 $\times$1500 $\times$1mm were used. The advantages of using aluminium material are high corrosion resistance, longevity, light weight, and ease of cleaning, handling and bending.

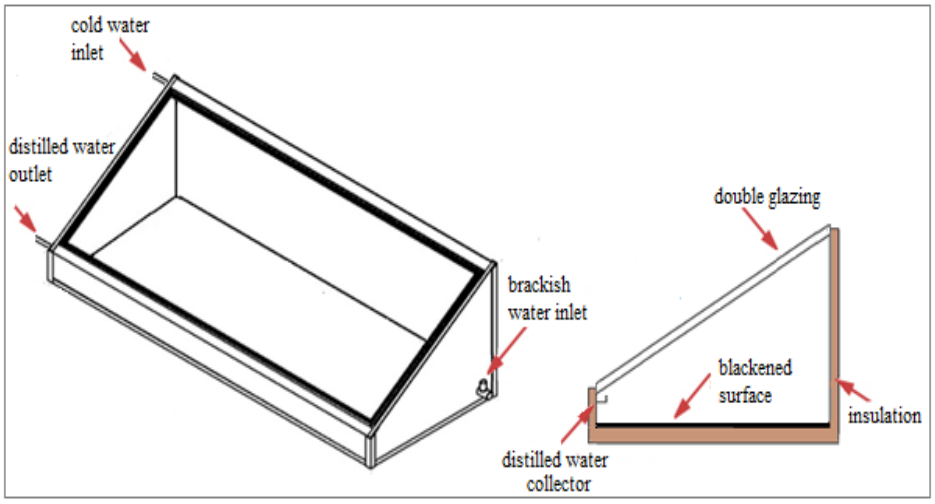

Figure 3. 1: A single-effect basin type solar still

To avoid losing the construction material, the aluminium sheet was cut as shown in Figure 3.2. The dimensions are illustrated as well. The sheet was folded to form the final shape of the solar still using the available bending machine in the mechanical engineering workshop. The outside edges of the structure were joined and enforced using L-shaped aluminium channel size 40×40mm. U-shaped channel size 40×40×40mm was used as a distilled water collector. It was mounted along to the inside front wall using rivets.

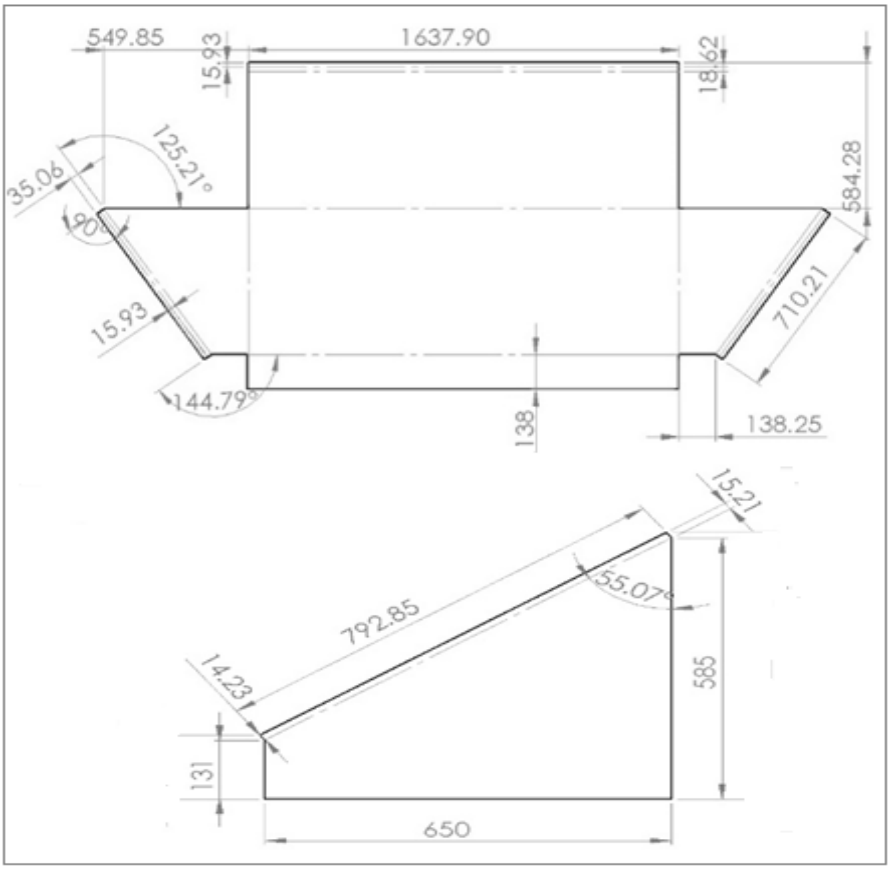

Figure 3. 2: Solar still dimensions

A polystyrene board with a thickness of 15mm was used as a thermal insulator. It was sandwiched between the aluminium sheets on each side of the solar still. Polystyrene is considered a good insulation material with thermal conductivity of 0.03 W/m.K, along with the enhancement of rigidity of the solar still structure.

The basin liner was painted black using waterproof and high heat-resistant paint. To avoid leakage, the inner corners of the still were sealed with waterproof silicon sealant. The transparent cover was made of polycarbonate sheet size 1638 $\times$793 $\times$1 mm. A composite pipe consisting of three layers of different materials was used to run the cold over the sheets. Holes of 5 mm in diameter were drilled with a space of 7 cm to ensure even cold water flow.

3.2.2. Vapour compression heat pump system

A vapour-compression heat pump was designed to be used as a heat recovery system. It consisted of four major components, namely a DC compressor, evaporator, expansion device, and condenser. From a thermodynamic point of view, a heat pump system is an energy-efficient thermal device. It produces more useful thermal energy compared with traditional heating systems.

The heat pump system used in this research employed a renewable energy source to power the compressor and, therefore it has a low operational cost and is environmentally friendly. The system has two main functions: firstly, to pre-heat the contaminated water in the early morning hours, and secondly to cool down the condensation surface in order to increase the temperature difference between the basin water and the condensation surface.

The water to water heat pump system shown in Figure 3.3 consists of two cycles, a vapour compression heat pump cycle and cooling water cycle. In order to construct the system, a DC compressor 12V/24V was used to circulate the R134a refrigerant. The compressor size was selected to have a higher capacity than the total required heat load to avoid overloading the compressor motor. Technical data, specifications and the capacity at different rpms are shown in Appendix A.

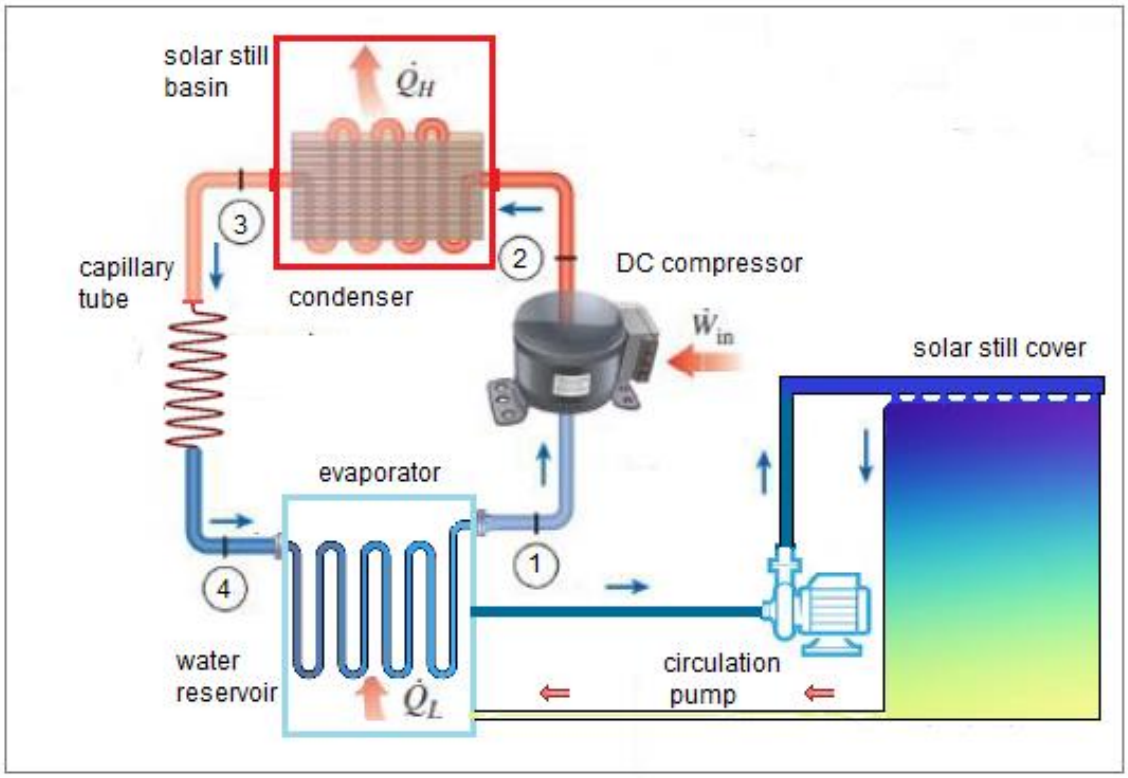

Figure 3. 3: Vapour-compression heat pump cycle

The low temperature heat exchanger including a flat type evaporator made of aluminum was installed in a small insolated compartment. The evaporator was formed to take the compartment shape to ensure even heat transfer. The volume of the compartment was 20 L. The high temperature heat exchanger included a finned condenser made of aluminum. The condenser was painted with black coat and installed inside the solar still. A capillary tube made of copper was used as a throttling device. To determine the dimension of the capillary tube, a cap tube conversion chart was used. A filter drier was attached between the capillary and the condenser coil. The main function of the drier was to avoid refrigerant contamination and, therefore it was installed vertically with the refrigerant flow in the downward direction to work as a liquid seal for the capillary tube. Oxy-acetylene gas welding was used to braze the heat pump system components. In order to charge the system with refrigerant, a vacuum pump was used to apply vacuum in the system cycle. The evacuation of the pipeline was imperative to remove moisture and other contaminant (non-condensable) results from brazing. Another advantage of the evacuation is that it would indicate if there was any leak in the system, therefore the minimum time required was about 15 minutes, maintaining a constant reading at the vacuum gauge indicator. To charge the system, the manifold gauge was attached to the service port of the compressor. The other end of the gauge was attached to the R134a refrigerant canister. An accurate scale was used to weigh the canister in order to measure the amount of refrigerant entering the system.

The cold side of the heat pump system (evaporator) was combined to the cold water compartment. A polystyrene board was used to insulate the compartment. A 12V DC water pump was used to circulate the water between the cold water compartment and the condensation surface. The pipeline of the system was insulated properly using thermal pipe insulation.

3.2.3. Solar PV system

A small solar photovoltaic system was utilized to power the mechanical vapour-compression heat pump and the other components. The total power consumed by the system was equal to the power of the DC compressor and the power of the circulation pump. The total load calculated was about 65-80 W for the DC compressor which depended on the running speed which was indicated on the datasheet of the compressor specifications. The load of the DC water pump was 10 W. Table 3.1 shows the expected power consumption required for each appliance per day.

Table 3. 1:Vapor compression heat pump power requirements

Appliances	Input wattage	Hour/Day	Watthour/day
DC compressor	80W	4h	320Wh/d
DC pump	10W	4h	40Wh/d
			360Wh/d
DC compressor	80W	6h	480Wh/d
DC pump	10W	6h	60Wh/d
			540Wh/d

Manual and online calculations were done in order to select the right components of the solar PV system. In the calculation, some assumptions were proposed such as the working hours of the heat pump, the minimum operating temperature of the battery bank and the depth of discharge of the battery. The calculation shows that the total watt per day was 360 Wh/d for 4 hour of operation, the capacity of the battery bank was 986 watthours and the average sun hours were 8 h.

For these small requirements, a simple PV system was sized to power the components. The system consisted of monocrystalline solar panel peak power (Wp) of 180 W, a pulse width modulation (PWM) charge controller of 20 A, a deep cycle battery capacity of 105Ah, cabling and circuit protection. See Appendices B, C and D for the specification of each component. The wiring diagram is shown in Figure 3.4. The PWM charge controller is relatively basic, cost-effective, and suitable for a small system, programmable to match battery type and monitor battery charging and temperature.

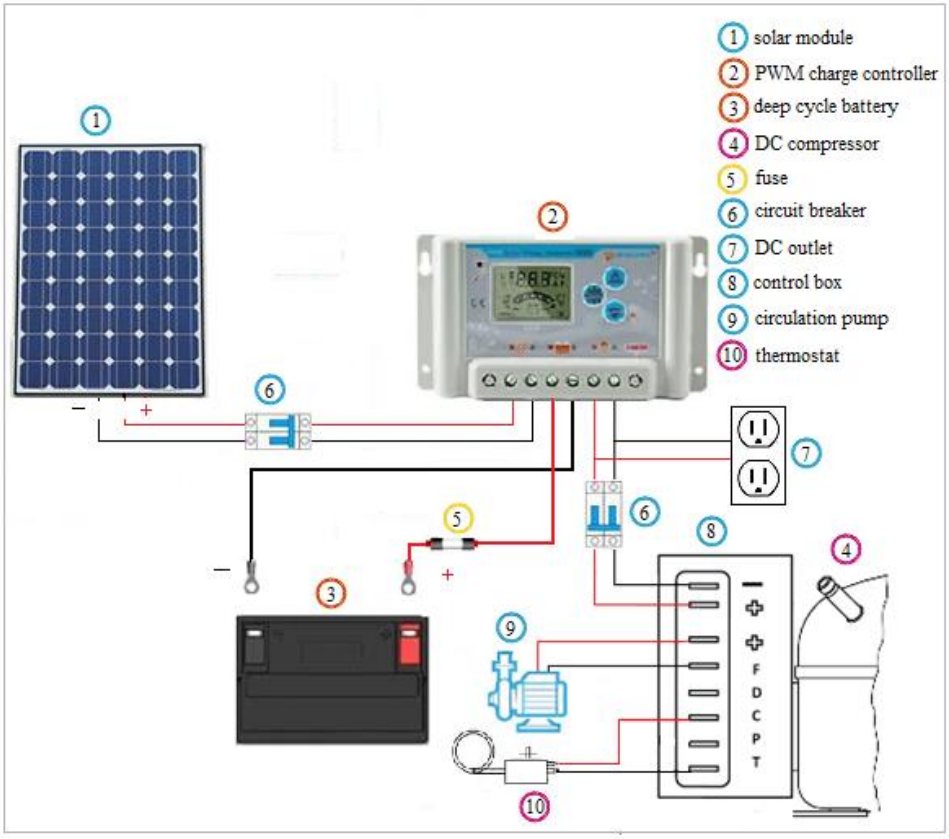

Figure 3. 4: Heat pump wiring diagram

In general, the PV system used in this research is very straightforward to install, cheap and safe, and the components have an appropriate warranty period. It is therefore simple equipment with a low chance of electric shock hazards that an unskilled person can use safely.

3.3 The solar still based on a vapour compression heat pump system

The three main systems mentioned above were installed on a metal frame made of mild carbon steel section sets. The sections were welded to form the required structure then painted with anti-corrosion paint. The whole assembly was mounted on the roof of the building for the purpose of experimentation. Figure 3.5 shows the schematic diagram of the advanced solar still. The DC compressor, cold water reservoir, circulation pump and battery were installed underneath the collectors in order to be protected from the weather conditions. The compressor was installed on the same frame section as the basin. It acted as a resonator to avoid big drop formation on the condensation surface. Water filter and/or mineral packs could be added to improve distilled water taste and quality.

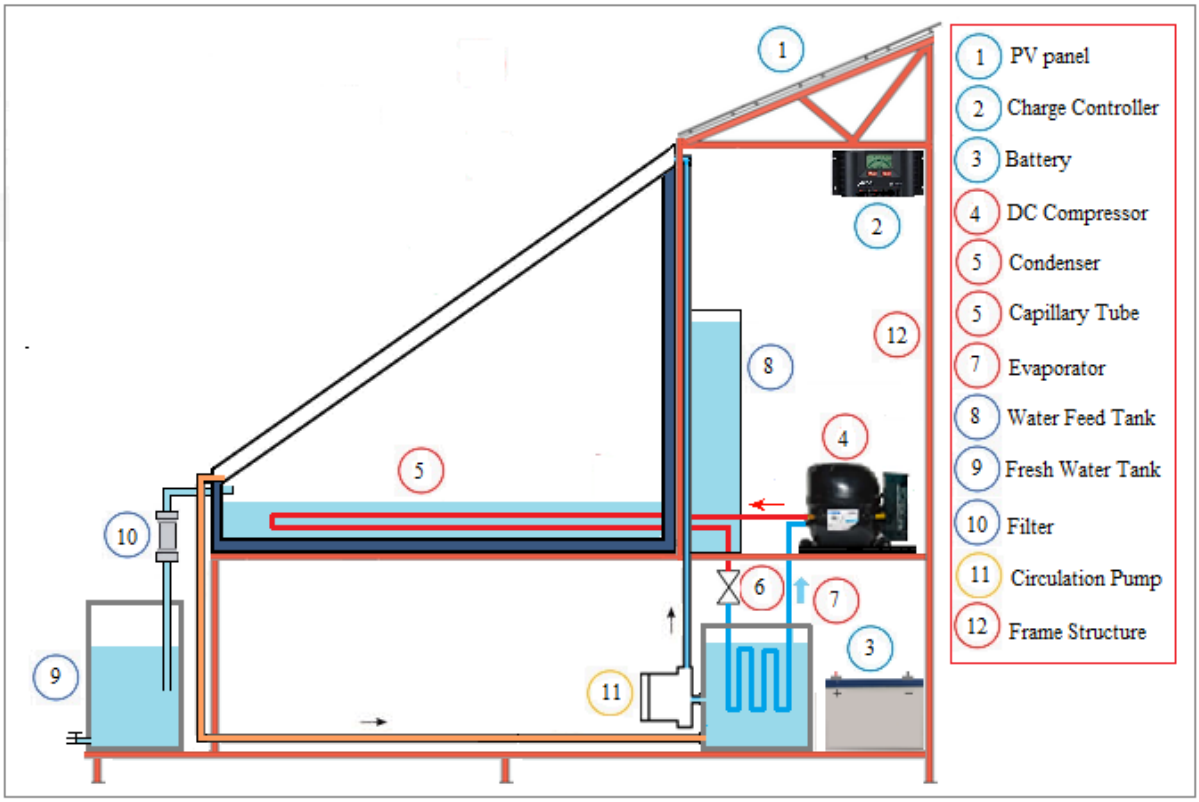

Figure 3. 5: schematic diagram of advanced solar still

3.4 Thermoelectric heat pump system

A thermoelectric cooler (TE_C) described in chapter two, sometimes named a thermoelectric module or Peltier cooler, is a semiconductor-based electronic component that operates as a heat pump for cooling and heating purposes. It can be found in different applications including military equipment, medical devices, industrial applications and telecommunications. The module utilizes low DC voltage to pump thermal energy from one side to the other. Therefore, one side will be cooled while the other simultaneously will be heated. The direction of heat flow can be reversed by changing the polarity of the applied DC voltage. The minimum and maximum operating temperature of the cold and hot sides of the thermoelectric module ranged from -50 to 138 ºC respectively. Its size was approximately 2.5 to 50 mm in length and width respectively and 2.5 to 5 mm in height. The smaller and bigger sizes could be manufactured with regard to extra cost due to machining requirements. The thermoelectric heat pump was governed by the same thermodynamic principle as the mechanical heat pump described above in this chapter. Here, the thermal energy was transferred through the movement of electrons from the lower energy level at a P-type junction to the high energy level at an N-type junction. The transferred thermal energy then was dissipated in the heat sink as shown in Figure 3.6.

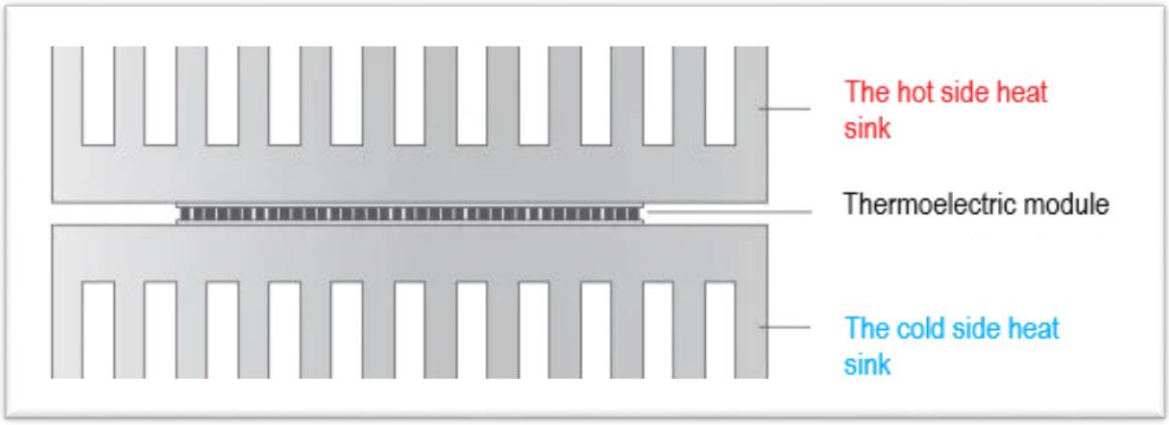

Figure 3. 6: Thermoelectric heat sinks configuration

Some of the advantages of the thermoelectric cooler are that it has no moving parts so that it has noiseless operation, accurate temperature control, compact size, lightweight, direct energy conversion and expected lifespan of 200.000 h (Pourkiaei et al., 2019; Kumar et al., 2020; Enescu & Virjoghe, 2014). The single-stage thermoelectric module can pump thermal energy up to 6 W/cm^2 of module surface area. This amount can be boosted once the modules are thermally connected in parallel. In general, the thermoelectric cooling system has a thermal energy removal capacity ranging from mill watts up to a couple of thousands of watts. One of the major components of the TE_C heat pump system that affects the overall system performance is heat sink selection. Therefore, the design of the heat sink should be considered carefully. Different types of heat sinks are available comprising forced convection, natural convection, heat pipe cooling and liquid-cooled (Zhu et al., 2013). An adequate design of the heat sink depends on the thermoelectric cooling application configurations and constraints. In this research, a water-cooled heat sink was designed in order to be employed as a heat backup system. A thermoelectric heat pump system consisting of six TE_C modules, two water-cooled heat sinks and two 10 W DC water pumps was constructed. Figure 3.7 illustrates the thermoelectric heat pump system configuration and the water cooled heat sinks construction.

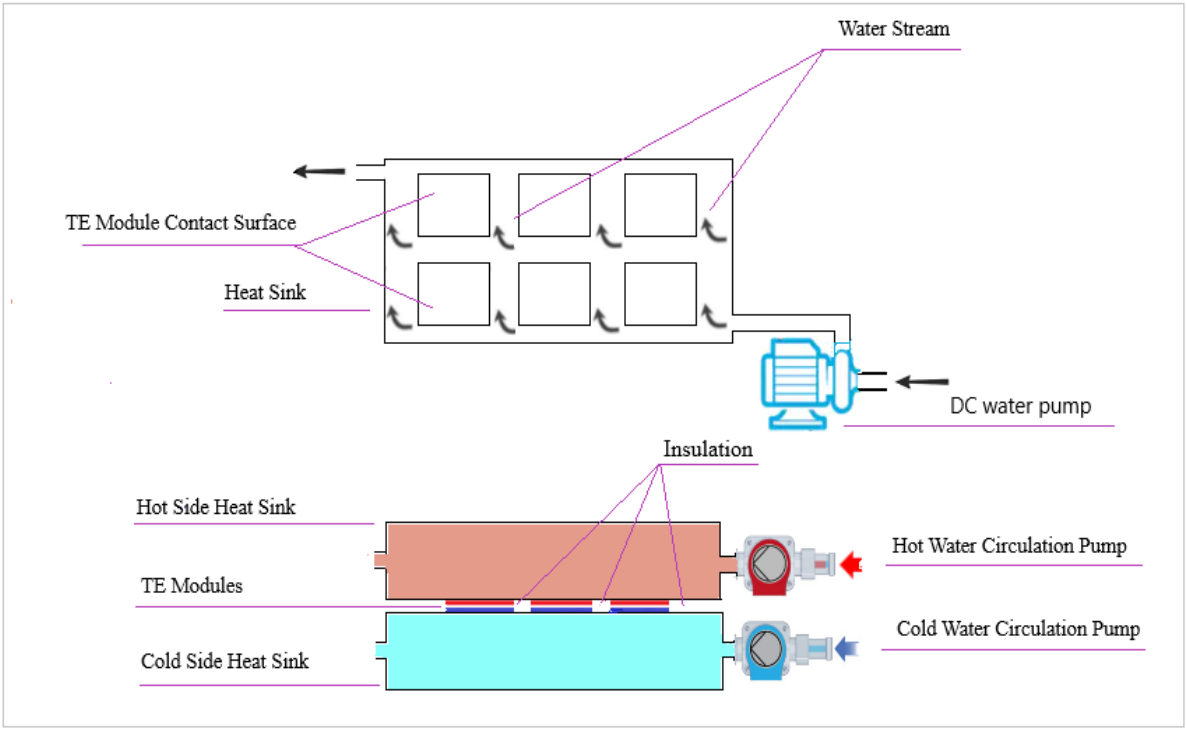

Figure 3. 7: Thermoelectric heat pump configuration

The heat sinks were made of two aluminum tanks with a capacity of 1500 ml each. A thermal paste was used to attach the thermoelectric modules to the heat sinks, and the heat sinks were compressed to each other mechanically. To identify the hot and cold side of each module, different methods could be followed:

- The module might have a printed indication mark that would show the hot and cold sides or a brand name printed on the hot side.
- In case of no print indication, place the module on an even surface so that the wire terminal is pointing towards the experimenter with the positive lead (red) wire on the left hand side and the negative lead (black) wire on the right hand side. In this orientation the cold side will be facing down and the hot side will be facing up.
- In the case of an unsealed module, the hot side can be identified by looking at the soldered joint attached to the corner of the module; the side that the wire is soldered to is the hot side.
- Finally, a direct measuring test can be done to verify the hot and cold sides of the module. Connect the module to the DC power supply to ensure that the polarity is correct, then apply a voltage to the device which is approximately 10% of the V_{max} value indicated on the data sheet. A temperature difference can be sensed using the tips of the fingers.

For better thermal performance, it is important to ensure that the contact surface of the heat sink has proper flatness. It is recommended to be 1 mm/m and may need machining such as lapping and wet sanding and grinding to meet the flatness

specifications. A good insulation material was used to minimize heat loss. High thermal resistance sealant (insulation cotton washers) were used to prevent moisture formation inside the TE module and the enclosure between modules, as shown in Figure 3.8.

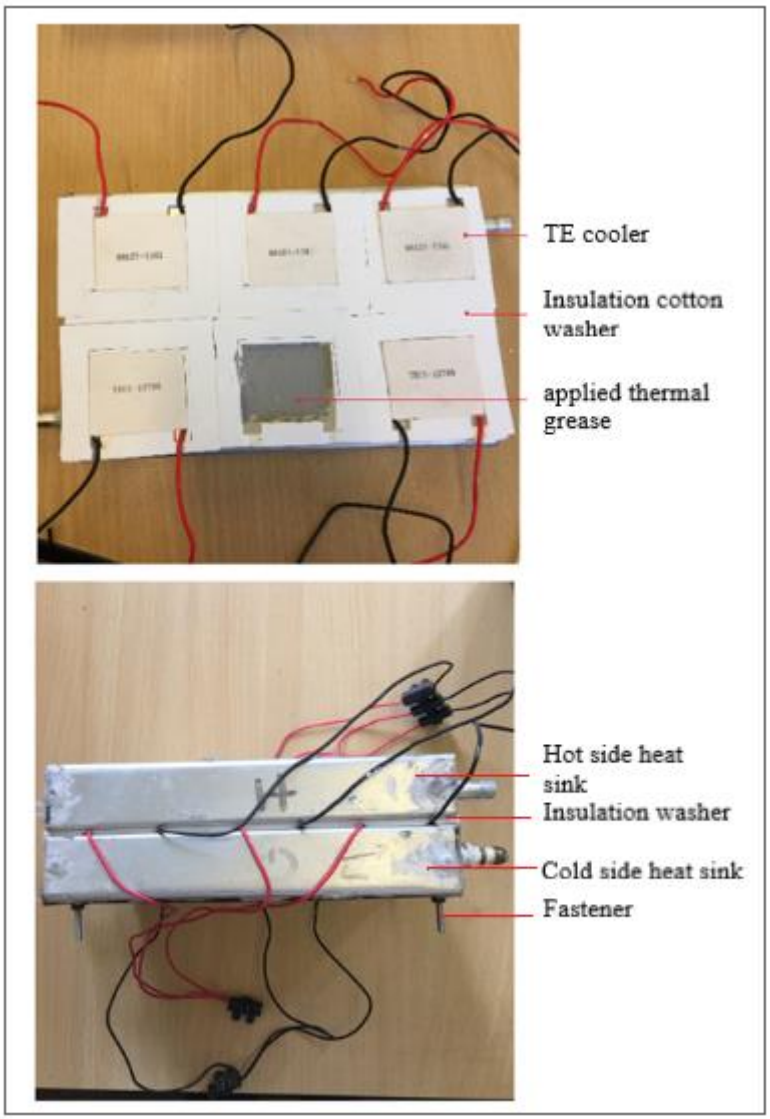

Figure 3. 8: **Thermoelectric modules insulation method**

The thermoelectric heat pump system used in this research consisted of TEC1-12706 modules connected electrically in series/parallel configuration to provide the system with sufficient voltage and current as 12 V DC solar photovoltaic was used as a power source. Figure 3.8 illustrates the wiring configuration of the TE modules.

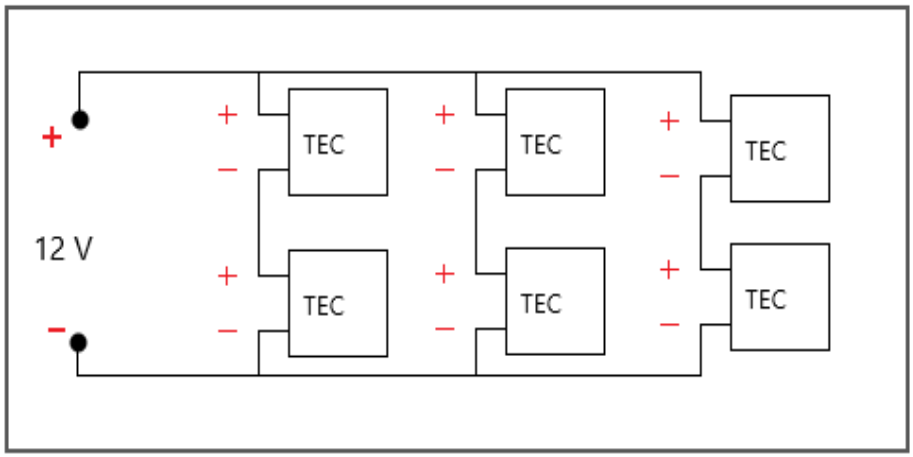

Figure 3. 9: The wiring connection of TE cooler

In this arrangement, every module receives 6 V which is under the maximum operating voltage V_{max}. For the purpose of simplicity, a thermostatic control operation was used to regulate the power supplied to the modules. The water pump power supply circuit was separated from the Peltier circuit. The reason for that is when the power was disconnected from the Peltier circuit, the circulation pumps kept operating for a certain period of time to cool down the Peltier hot side to avoid potential thermal stress.

For smoothness purposes, wet sanding was performed for both contact surfaces of the heat sinks. After that, rubbing alcohol was used to wipe any residual material.

Typical fasteners can be used to mount the modules to the heat sink and in this case, thermally conductive grease is recommended to be applied to coat the interfaces of the heat sink and TE modules. A sufficient pressure (15 kg/cm^2) is required to maintain proper contact between the TE heat pump system assembly. Polyurethane board insulation thickness of 20 mm was used to insulate the water heat sinks. A layer of aluminum sheet was attached to the insulation board to protect the heat sink assembly from changing climate conditions and it added rigidity and durability to the system construction. Rubber pipe insulation was used to insulate the piping system of the model.

3.5 The solar still based on a thermoelectric heat pump system

The thermoelectric heat pump system described in the previous section was integrated into the conventional single-effect solar still in order to utilize it as a thermal energy backup system. On sunny days, it was employed to pre-heat the saline water in early morning hours of the day and cool down the condensation surface during the rest of the operating hours of the day. The system was fully operational system on cloudy days and at night.

3.5.1. Photovoltaic system sizing

A solar photovoltaic system was designed and sized to power the thermoelectric heat pump system components. It consisted of a PV panel, circuit breaker, PWM charge

controller and deep cycle batteries. In order to maintain the power supply to the Peltier heat pump system, the photovoltaic system was sized carefully. The Peltier heat pump system consisted of two circulation pumps, six thermoelectric modules (type TEC - 12706) and a control circuit. Table 3.2 shows the system electrical load per day.

Table 3. 2: Thermoelectric heat pump energy requirement

Appliances	No	Input power	Hour/day	Wh/day
Thermoelectric module	6	Max (70 W)	4h	1680 Wh
Circulation pump	2	10 W	4h	80 Wh
				1760 Wh

The maximum voltage V_{max} required for the Peltier module was 12 V at a maximum power 72 W. in this experiment, the wiring configuration powers the modules with 6 v meant that the power would be about 45 W.

To determine the number of PV panels, the PV generator factor was taken in the calculation as follow:

$$PV_{gf} = S_l \times I_{hs} \qquad 3.1$$

$$P_n = \frac{L_t}{PV_{gf}} \qquad 3.2$$

Where: PV_{gf} is the PV generator factor, S_l is the losses factor, I_{hs} is the average daily radiation hours, P_n is the output required from the PV panels, and L_t is the daily electric load required.

The number is given as:

$$PV_N = \frac{P_n}{W_p} \qquad 3.3$$

Here, PV_N is the number of modules, W_p is the power rate of PV panel

Therefore,

$$PV_{gf} = 0.65 \times 7 = 4.55$$

$$P_n = \frac{1760}{4.55} = 386.8\,W$$

For a 270W PV panel:

$$PV_N = \frac{386.8}{270} = 1.43$$

Here, two panels were selected.

In order to size the battery bank, a few points were considered which included one day of autonomy: the maximum load is 1760 Wh/day, the depth of discharge is 70% and the battery efficiency is 85%.

The battery bank capacity is given as

$$B_c = \frac{L_t}{B_e \times D_d \times B_v} \times n_{au} \qquad 3.4$$

Here, B_c is the battery bank capacity, L_t is the total electric load, B_e battery efficiency, D_d is the depth of discharge, B_v is the battery voltage and n_{au} is days of autonomy.
Therefore,

$$B_c = \frac{1760}{0.85 \times 0.7 \times 12} \times 1 = 246.5\ Ah$$

A lead-acid deep cycle battery rate of 105 Ampere hour was selected.
In case of 6 V wiring configuration, the total power would be 1160W, the number of panels is one and the battery capacity is 162.4 Ah.
A pulse width modulation charge controller (PWM) rated at 12V/24V and 20 A was selected to regulate the power supplied to the battery bank and protect the system from overcharging and discharging.

3.5.2. Solar still model construction

In order to construct the advanced solar still system, the hot side of the heat sink of the thermoelectric heat pump was connected to the heat exchanger run inside the basin of the solar still in order to heat up the brackish/saline water. A 3 m copper pipe with a diameter of 9 mm was used to make the heat exchanger. A pipe bender was used to form the shape of the heating coil. Figure 3.9 shows the interior components of the single-effect solar still based on the Peltier heat pump backup system.

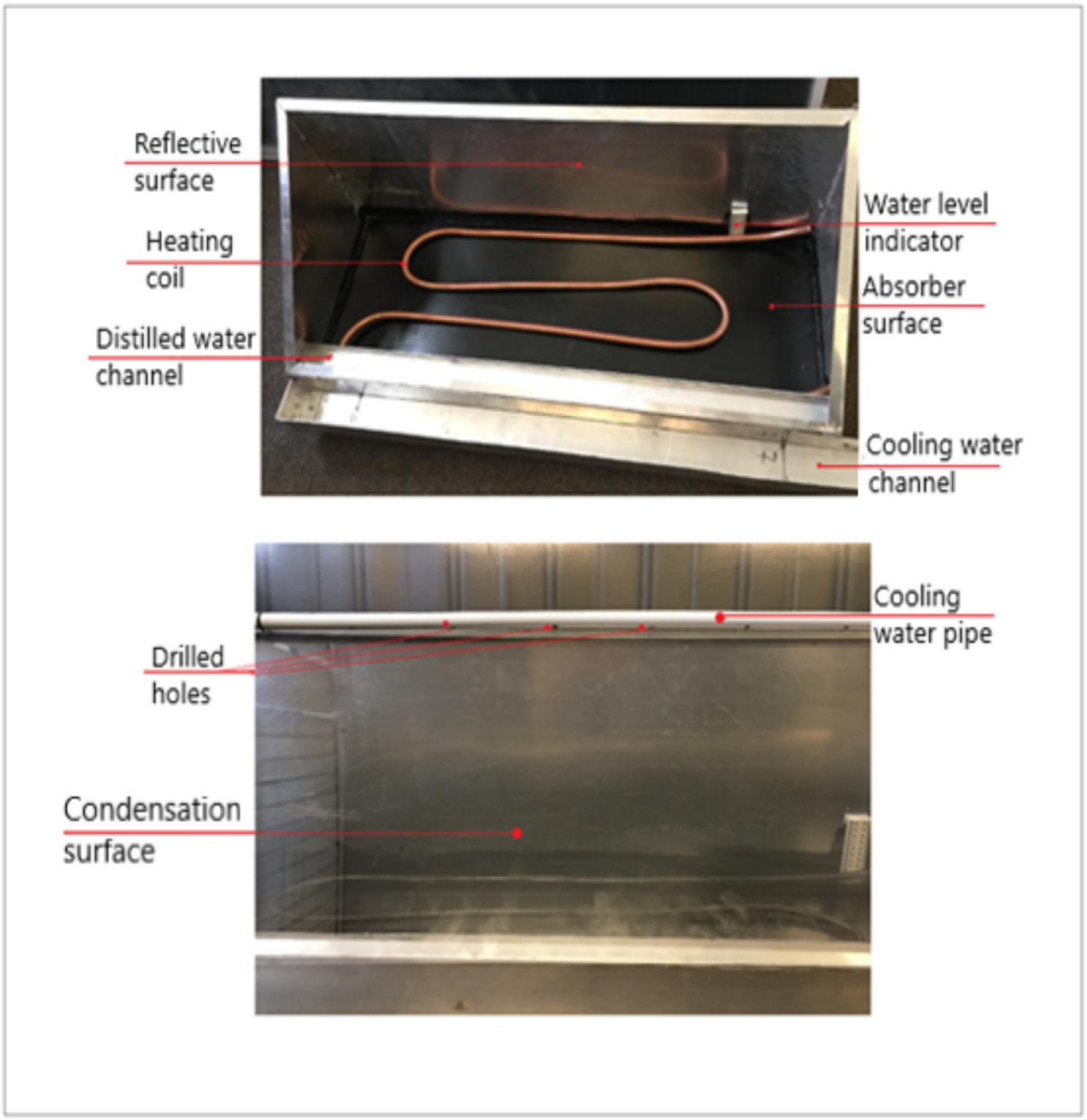

Figure 3. 10: The single-effect solar still construction

The heat exchanger and the absorber plate were painted with a black coat. The cold side was connected to the condensation surface of the still in order to cool it down and create a temperature difference with the brackish water. The condensation surface was made of polyurethane transparent plates with a thickness of 1 mm. A holed water pipe ran along the upper side of the condensation surface, and, therefore uniform cold water flow ran over the plate to cool it down homogenously. A U-shaped channel made of polyvinyl chloride plastic (PVC) was connected to the lower side of the condensation surface to collect the flowing water from the surface and deliver it to the circulation pump. The channel worked as a water reservoir to avoid air bubbles interring the water pump which could affect its pumping efficiency. The power supplied to the circulation pump was controlled via thermostatic operation in the separate electric circuit from the

Peltier module control circuit. Figure 3.11 shows the single-effect solar still integrated with thermoelectric heat pump as thermal energy recovery system assembly.

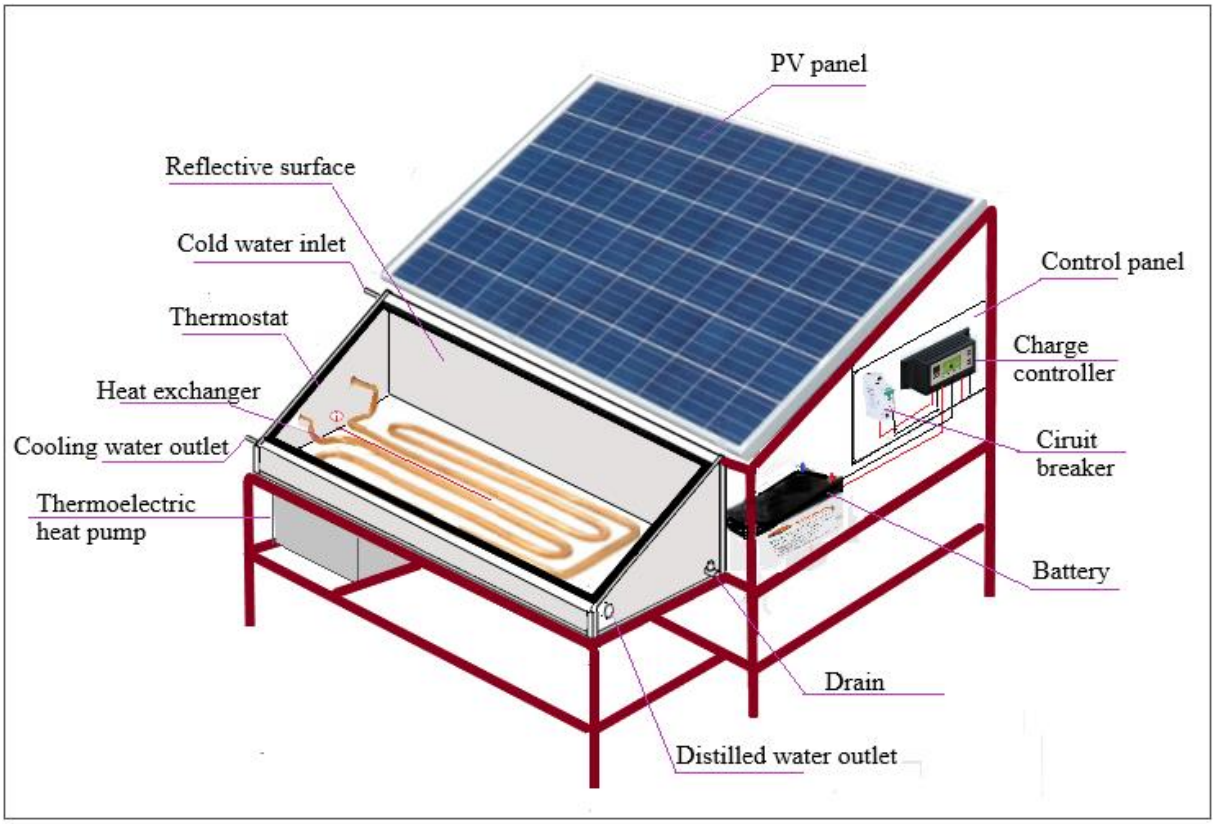

Figure 3. 11:The components of the solar still integrated with thermoelectric heat pump system

The metal frame was used to hold and protect the component. It allowed easy handling and operating of the solar still as a united compact system.

3.6 Instrumentation

During the construction and the manufacturing of the solar still systems, different instruments, machines and devices were used. A metal sheet cutter was used to cut the aluminium sheets, and two bending machines were used to bend the sheets which were used to construct the stills, the water reservoir and the heat sinks. A pipe bending machine was used to form the heating coil and vapour compression pipe system. Oxyacetylene gas welding was used to weld the components of the vapour compression components. A refrigerant manifold was used to charge the system with the required amount of refrigerant. A bench DC power supply was used to power the Peltier modules in order to optimize the wiring configuration. A digital multi-meter was used to monitor the electric circuit continuity and voltage, and a clamp multi-meter was used to monitor the current. An infrared thermometer was used to monitor each side of the Peltier modules, and a set of K-type thermocouples was inserted into different check points. Adjustable circulation pumps were used to regulate the flow rate in and

out of the heat sinks. The daily yield of distilled water was measured by a graduated glass jar. The weather elements were monitored by the weather station mounted at the top of the Mechanical Engineering building.

3.6.1. Thermocouples calibration

Thermocouple calibration is an essential aspect of temperature measurement accuracy, so all the thermocouples used in this research were calibrated. They were tested at the freezing point of the water and close to boiling point. The test was performed by adding 600 ml of ice and water into a lab beaker. A thermometer was used as reference. The thermocouple and the thermometer were placed in the beaker. The beaker was heated up to the water boiling point using lab electrical heater. Figure 3.12 shows the calibration procedure setup.

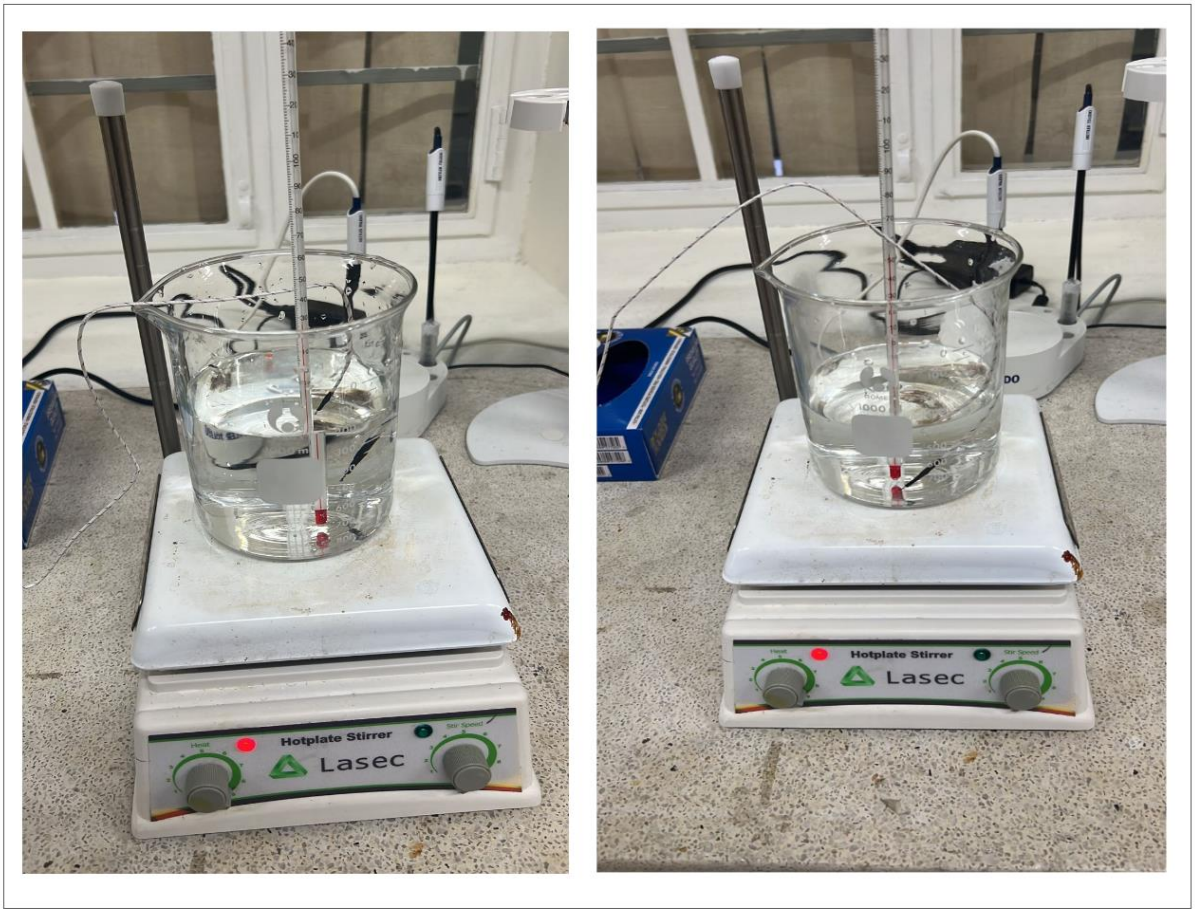

Figure 3. 12: Thermocouple calibration

Chapter Four
Experimental Protocol

4.1. Introduction

This chapter presents the experimental protocol for the testing procedures of the advanced single-effect solar still systems. Two different systems were tested outdoor under changeable atmospheric conditions. The experiments were conducted in different weather seasons in Cape Town, South Africa. A comparison between the advanced solar still and the conventional one is described. The performance of the heat pump system models (vapour compression/ thermoelectric) was evaluated. The comparison focused on the daily yield of distilled water, heat loss through the glazing and the temperature gradient performance.

The experimental protocol as indicated below upheld the rules of the research ethics requirements of the Cape Peninsula University of Technology. Hazards and risks to the environment, animals and humans were avoided. Precautions and discipline adhered to the safety procedures, university facilities and data management.

4.2. Testing of the advanced solar still prototype and model

4.2.1. Test location

The experiments were conducted on the roof of the CPUT Mechanical Engineering building, Bellville campus, Cape Town. The site is located at 33.92˚ S, 18.4˚ E. Elevation is about 68.5 m above sea level. Obstacles such as tree and building shadows were avoided in order to have the actual solar radiation, thermal and electrical energy yield. Table 4.1 indicates the weather elements average at the mentioned location.

Table 4. 1: The average values of weather elements in Cape Town

Month of the year	Daily sunshine (Avg)	A temp (Avg)	Humidity (Avg)	Wind speed	A pressure
Sep.	7 h	24 ºC	75 %	15 km/h	1020 mbar
Oct.	9 h	26 ºC	65 %	15.9 km/h	1017 mbar
Nov.	10.5 h	27 ºC	69 %	17.5 km/h	1015 mbar
Dec.	13.5 h	28 ºC	68 %	17.3 km/h	1014.3 mbar

4.2.2. Tools and equipment

The required tools and equipment used to monitor and evaluate the performance of the advanced solar still and weather elements detectors are listed below.

- Digital multi-meter to measure the circuit voltage
- Clamp meter to measure the current

- Sets of K-type thermocouples with a temperature range of -50˚C to 204˚C
- Thermometers
- Gradual water containers
- Campbell scientific weather station including a Kipp & Zone CMP6 pyranometer, SP-LITE Silicon pyranometer and 03101 Young three-cup anemometer
- Manifold refrigerant gauge leak detector
- Water test sample container

4.2.3. The experimental setup of the solar still integrated with vapour compression heat pump system

The advanced solar still model, consisting of a single-effect basin type integrated with a vapour-compression heat pump as a heat recovery system, was assembled outdoors for experimental purposes. The experimental works aimed to investigate the different factors named: the effect of cooling down the condensing surface; the effect of pre-heating the basin water; the effect of the resonator on droplet formation; the performance of the system in early morning hours and on cloudy days; and the evaluation of the coefficient of performance of the heat pump system. To achieve that, the system was mounted on the roof to be exposed to random weather change, and faced north to achieve the highest energy yield.

A small solar photovoltaic system was used to power the vapour compression heat pump system. It consisted of a monocrystalline PV panel peak power (Wp) of 180W, a pulse width modulation (PWM) charge controller of 20 Amp, deep cycle battery capacity of 105 Ah, circuit breaker and fusers. The PV panel was fixed incline at an angle of 34º facing north.

In order to facilitate data collection, a pre-test was done to monitor the operation condition of the system and observe any possible malfunction of the still components. The basin of the still was filled with 15 L of tap water until the condenser was submerged to avoid excessive heat. The heat source reservoir was filled with 6 L of distilled water to avoid rust and corrosion formation in the water-cooled cycle. The system ran for two days. During the pre-test period, it was checked for water vapour and water leaks, and the refrigerant pressure was monitored as well. The results were satisfactory. Another purpose the per-test was that to clean the system of residual material, the effect of the new coat of paint and the odours of adhesive materials and sealants that could affect the distilled water characteristics.

To facilitate the measuring instruments, sets of thermocouples were calibrated and attached to each component of the solar still and the heat pump system, as shown in Figure 4.1. The weather elements data were collected using a weather station mounted close to the advanced solar still system.

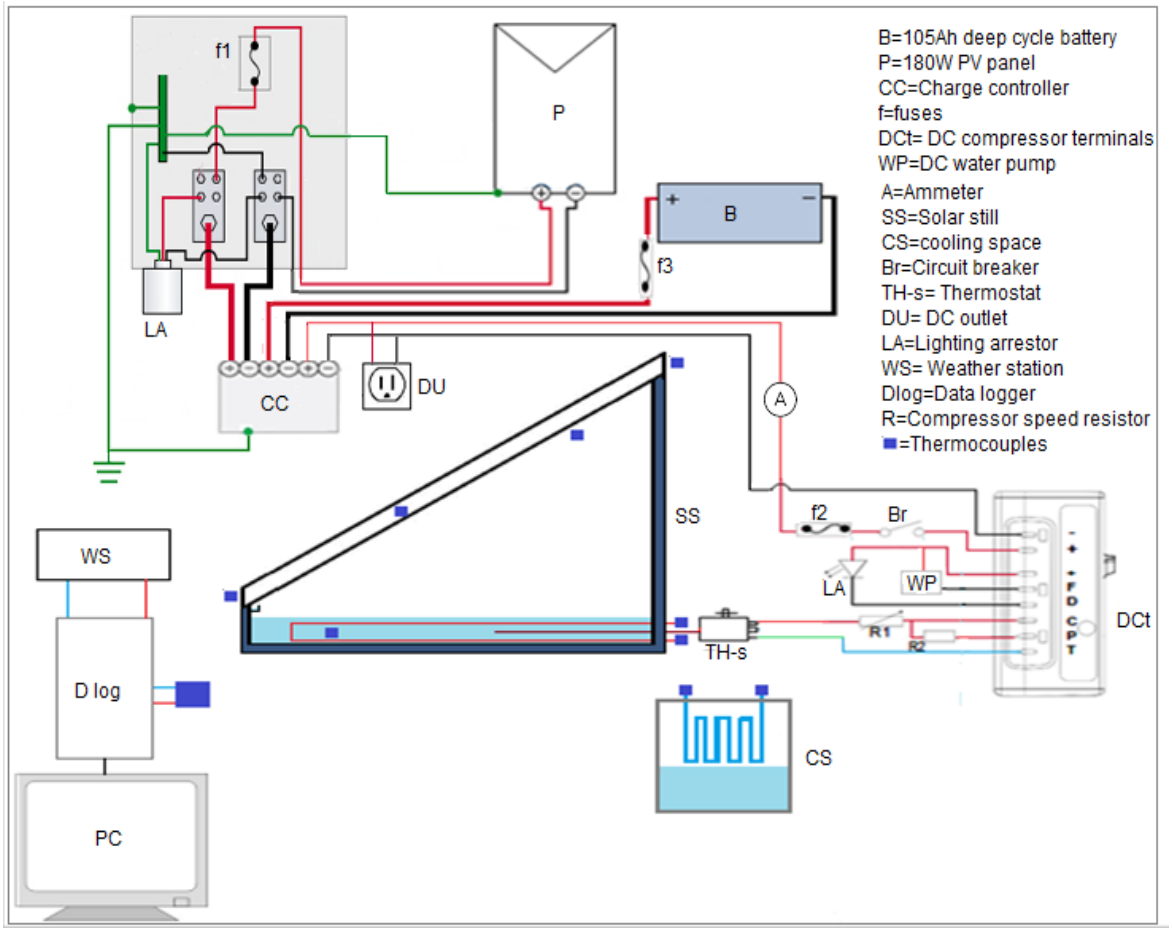

Figure 4. 1: Experimental setup of the solar still integrated with vapour compression heat pump

4.2.3.1. Testing the system without cooling of the condensation surface

The purpose of this test was to investigate the effect of water flow on the condensation surface which could minimize the transmittance of solar radiation into the water basin. To perform that, the circulation pump was disconnected, therefore there was no water flow on the condensation surface. The still was filled with 20 L of water until the condenser was submerged. Distillate water was added to the cold water compartment in order to provide the heat pump system with the required thermal energy source. The experiment was run on a sunny day from 07:00 am to 19:00. The water level in the still was kept at about 2.0 cm depth. Temperature readings were recorded each half-hour. The daily yield of distilled water and the power consumed by the heat pump system were also recorded.

The confirmation experiments were conducted in the following days. Before performing each test, the brine water was flushed from the system. The initial temperatures of the different reading points were recorded.

4.2.3.2. Full operation of the heat pump system

In this experiment, both sides of the vapour-compression heat pump were involved. The circulation pump was connected to the compressor circuit so that the water cooling system ran simultaneously with the DC compressor. The thermostat was adjusted to 60˚C, and the water depth to about 20 mm. The water amount at the cold water compartment reservoir was kept at 4L and the battery was fully charged. During the 8 hours of daily experimentation, the weather elements were automatically recorded every 15 minutes on the data logger. The electrical current was recorded manually. The charging voltage and the battery temperature were displayed on the charge controller screen. The formation of the droplets on the condensation surface was evaluated.

4.2.3.3. Comparison with a conventional solar still

The third experiment was performed with intention of comparing the performance of the advanced still with the conventional still. A conventional single-effect basin type with a similar dimension and cover inclination to the one used in the advanced still was utilized in these experiments. Both units were filled with the same amount of water and operated at the same time in the same location. The temperature reading of the conventional still was taken manually for different locations. To ensure accuracy, the reading was taken twice. One with thermocouple and the other with a laser non-contact digital infrared thermometer. The water level was kept at about 20 mm for both systems. The experiments were performed in summer and winter so that the stills were exposed to different weather conditions, including cold cloudy days.

4.2.3.4. Night operation test

The advanced solar still was tested at night in order to evaluate the performance of the vapour compression heat pump. The still was filled with water at a level of 20 mm. The battery bank was fully charged and the thermostat was adjusted at 55 ºC. The performance of the advanced still was evaluated in summer and winter seasons.

4.2.4. The experimental setup of the solar still integrated with Peltier heat pump system

A conventional single-effect solar still integrated with a thermoelectric heat pump was constructed in the CPUT Mechanical Engineering laboratory and experimentally tested on the roof of the department building in order to investigate and evaluate the system performance under different seasonal weather conditions. A schematic of the experimental model is shown in Figure 4.2. A photograph of the experiment setup is given in Figure 4.3.

An identical conventional single-effect solar still was used for the purpose of comparison with the advanced one. A solar photovoltaic system was used to power the

thermoelectric heat pump system. Pre- experiments were conducted to investigate any system malfunction, and water and steam leaks, as well as to clean the system of any residual materials resulting from new coat of paint, adhesive and sealant that could affect the distilled water characteristics.

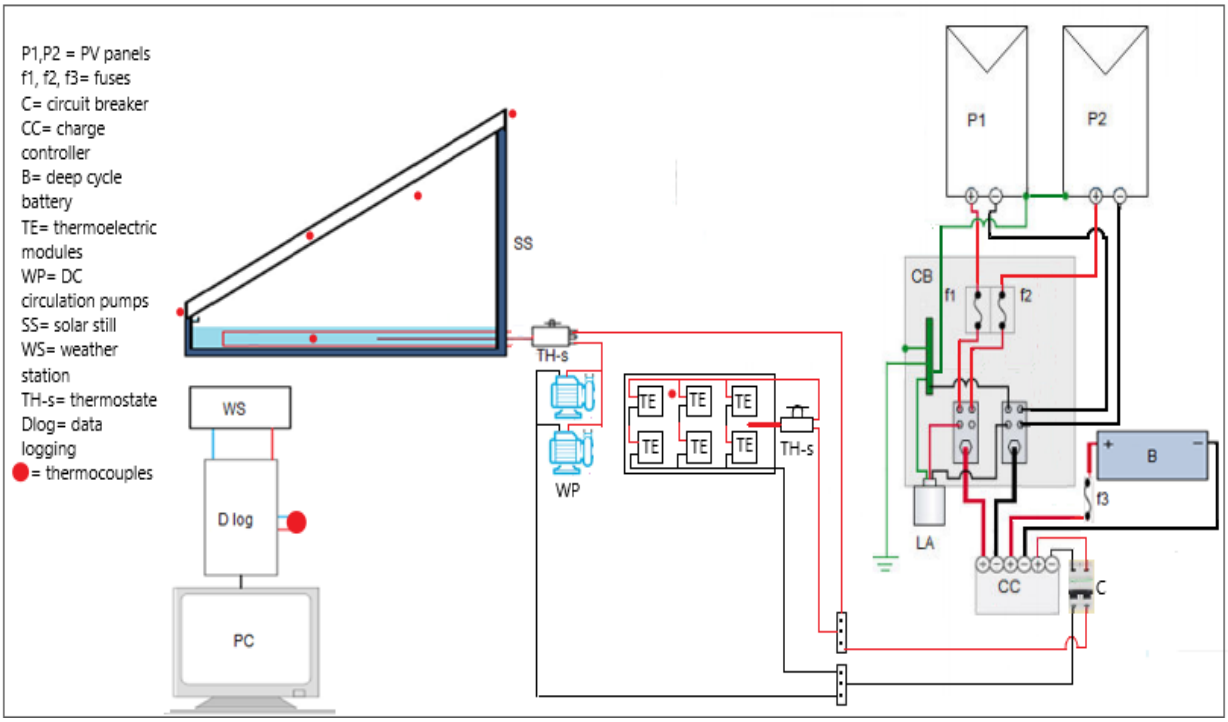

Figure 4. 2: The experimental setup of the solar still integrated with thermoelectric heat pump

A set of thermocouples was positioned at the different checkpoint at the solar still and the heat pump system, as indicated in Figure 4.2. Weather elements including ambient temperature, solar radiation and wind speed were monitored using existed data weather station at the test location. A time interval of 15 minutes was selected to monitor weather data. The power consumption of the thermoelectric heat pump was monitored in order to avoid thermal stress on the Peltier modules. The distilled water output was recorded hourly, and the temperature was recorded half hourly. The data of the experimental tests are presented in Appendix G. The data obtained then was used to evaluate the solar still performance to determine the coefficient of performance of the heat pump system.

Figure 4. 3: Photograph of experiment setup

CHAPTER FIVE
Results and Discussion

5.1 Introduction

This chapter presents and discusses the experimental results of various tests that were conducted with two different types of advanced single-effect stills: a conventional solar still integrated with a vapour compression heat pump and another one integrated with thermoelectric heat pump recovery systems. The consequences of the modification of both systems that affected the stills performance and the variation of the coefficient of performance of the heat pump systems are also discussed. A comparison between the conventional solar stills and the advanced stills was discussed from a thermodynamic point of view. A graphic summary of results was presented while the numerical results are indicated in Appendix E. Microsoft Excel and MATLAB software were used to analyse and visualize the data.

5.2 Experimental results of the solar still integrated with the vapour compression heat pump system

In this research, two types of heat pump systems were used as thermal energy recovery systems in two different experiments during the research program. First, various experimental tests were conducted to evaluate the performance of a single-effect solar still integrated with vapour compression heat pump system. Outdoor experiments were performed under different weather conditions for the year 2019 and the first two months of 2020. Then the experimental work was suspended for three months due to the Covid-19 pandemic which caused the national lockdown. The experiments then were resumed at the end of 2020 and continued throughout 2021 to test and evaluate the single-effect solar still model based on a thermoelectric heat pump system.

5.2.1. The meteorological conditions of the test location

During the long period of experimentation, the weather conditions at the location of the experiment were monitored using a weather station mounted at top of the Mechanical Engineering building at the Bellville campus of CPUT. Samples of the weather conditions over the course of the testing period are illustrated in Figures 5.1 to 5.4.

Figure 5.1 shows the variation of the ambient temperature with respect to time on 24 April 2019 and the three following days. The data recording period was 7:00 to 19:00. It can be observed that the highest ambient temperature recorded during the day was 37.21 ºC on 26 April 2019.

Figure 5.2 shows the fluctuation of wind speed, which ranged between 0.01 and 11.05 m/s in April. It was noticed that the wind speed is seasonally dependent. It was found that an increase of wind speed increased the temperature difference between the basin water and the condensation surfaces.

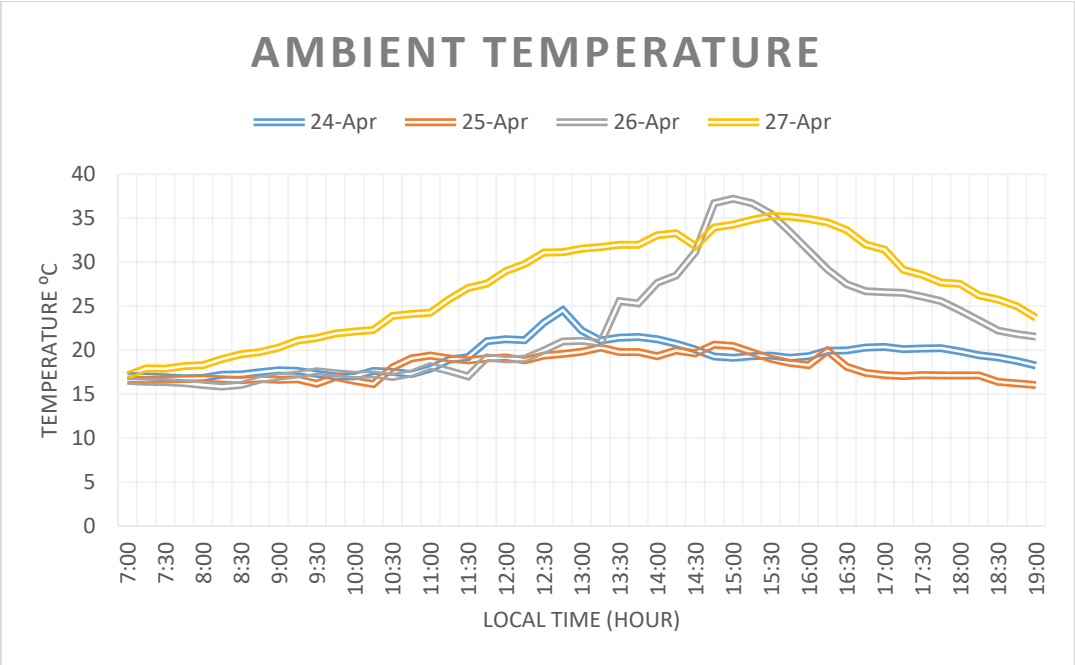

Figure 5. 1: The variation of ambient temperature in April 2019

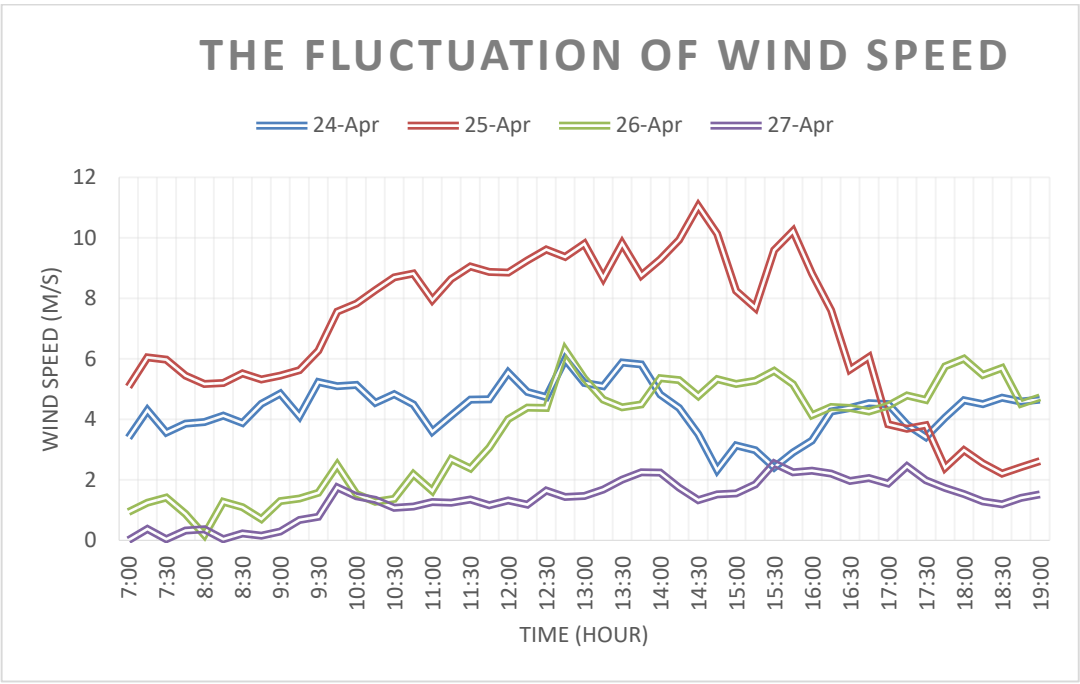

Figure 5. 2: The variation of wind speed in April 2019

Figure 5.3 displays a sample of available solar radiation on a horizontal surface during the month of April 2019 at the test location. The maximum solar radiation recorded was a noon value of 725 W/m^2. The incident diffuse radiation on respective days is demonstrated in Figure 5.4. Further, the beam solar radiation showed the same trend as the horizontal solar radiation with its peak noticed at noon at a value of 719 W/m^2.

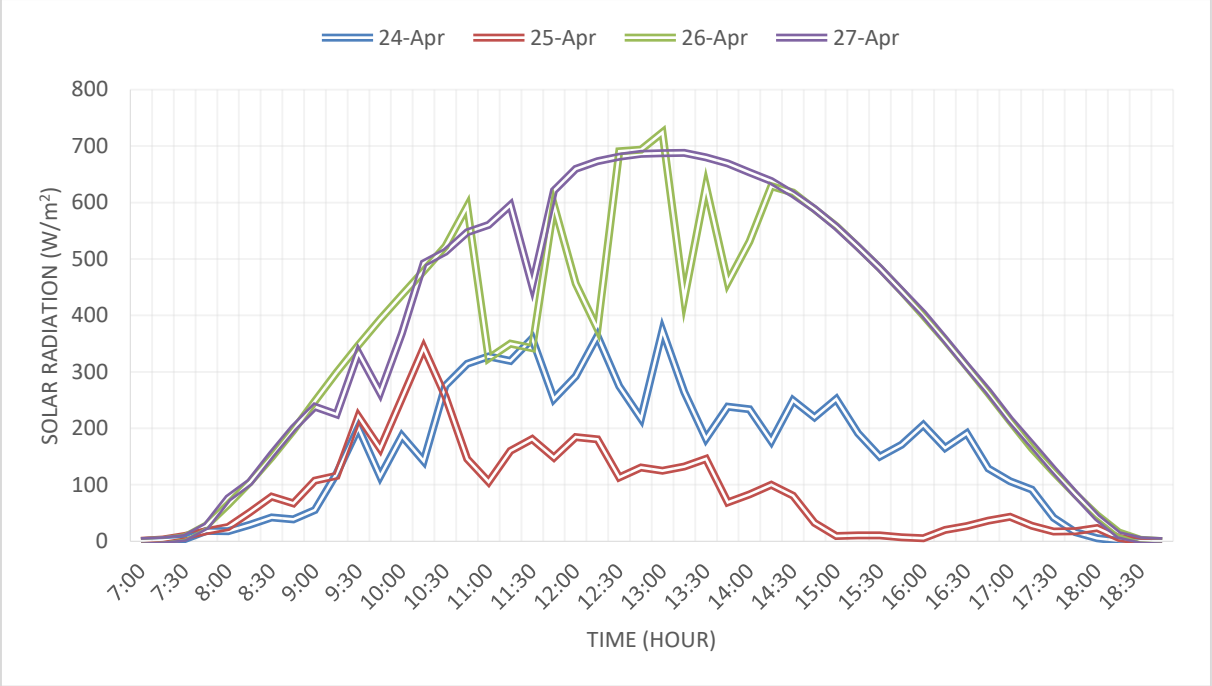

Figure 5. 3: Total solar radiation on a horizontal surface in April 2019

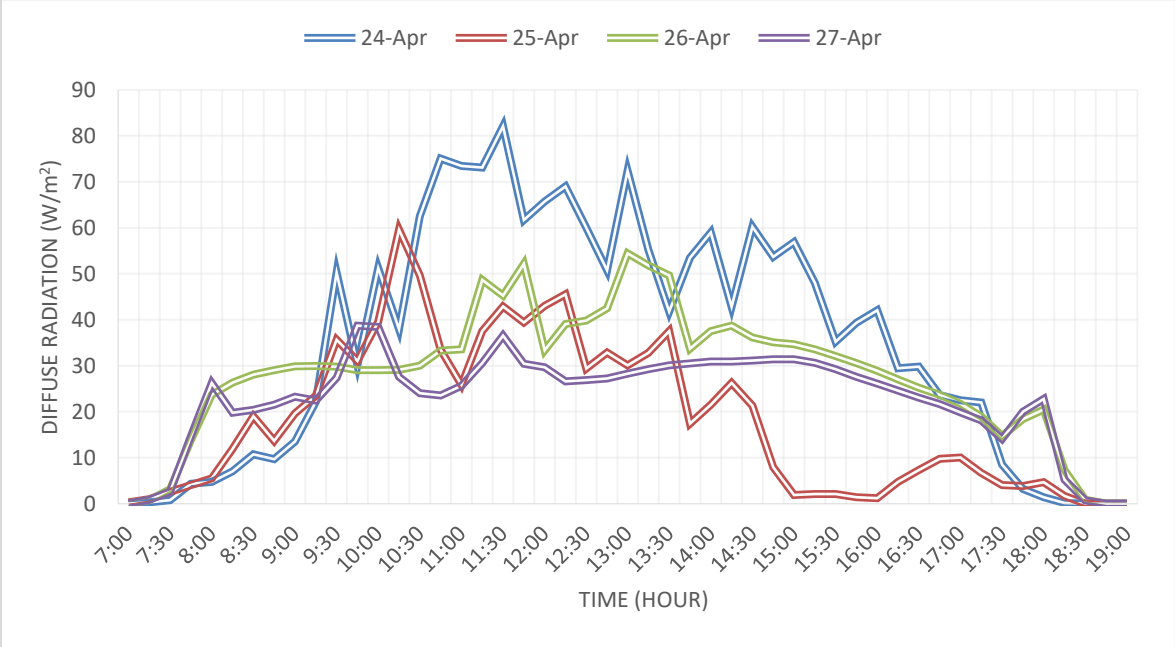

Figure 5. 4: Diffuse radiation level in April 2019

The incident solar radiation on the glazing of the solar still is presented in Figure 5.5. The tilted angle of the cover is 35º; Perez formula (2.10) was used to compute the solar radiation on the tilted surface. From analysis of the graph, it can be observed that the incident solar radiation on the solar still cover fluctuated on the 25th due to the effect of semi-cloudy weather. The maximum value computed was about 401 W/m^2. Furthermore, on the 27th the incident solar radiation became more stable and satisfactory for a test location, considering the relatively high latitude in the southern hemisphere. The incident solar radiation was computed at the maximum value of 890 W/m^2.

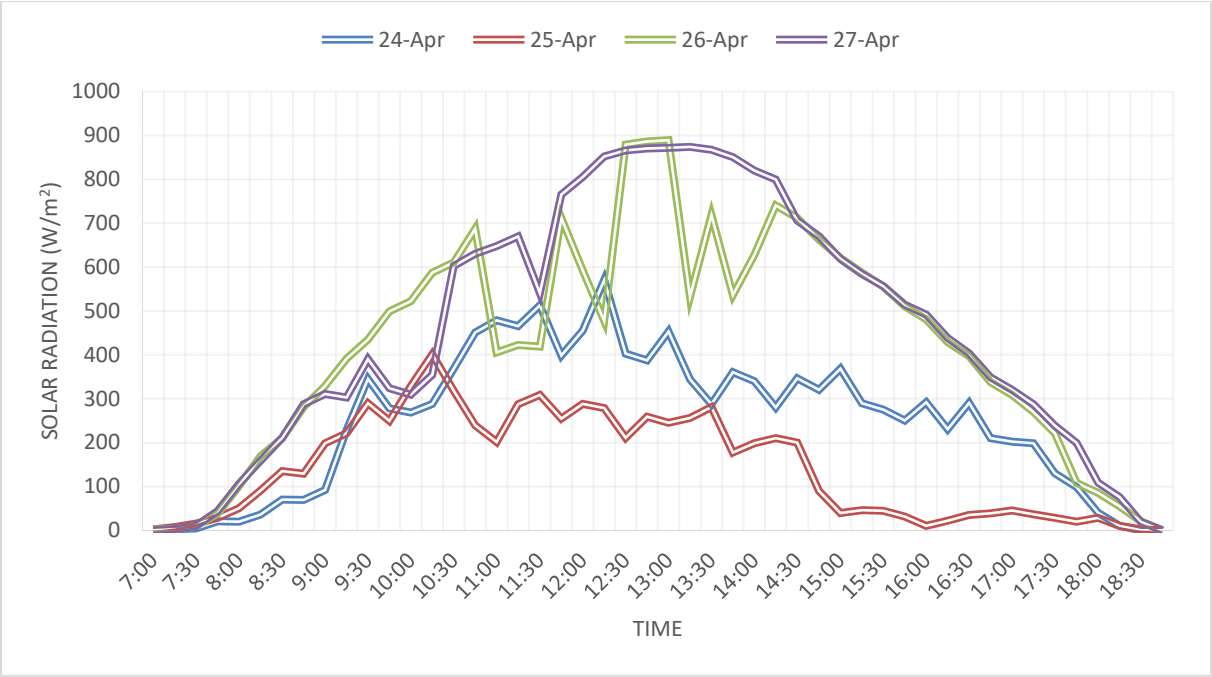

Figure 5. 5: **Variation of incident solar radiation on the tilted surface in April 2019**

5.2.2. The performance of the advanced solar still

5.2.2.1. First experimental results (without cooling down the condensation surface)

To evaluate the performance of the solar still based on the vapour compression heat pump, various tests were performed. The first test aimed to investigate the effect of cooling down the condensation surface. During the test, the circulation pump was disconnected so that the condensation surface was cooled by the atmospheric air. The solar still was filled with 20 L, and, therefore the water depth was 21 mm. Figure 5.6 shows the still's performance during a clear sky day on 23 April 2019.

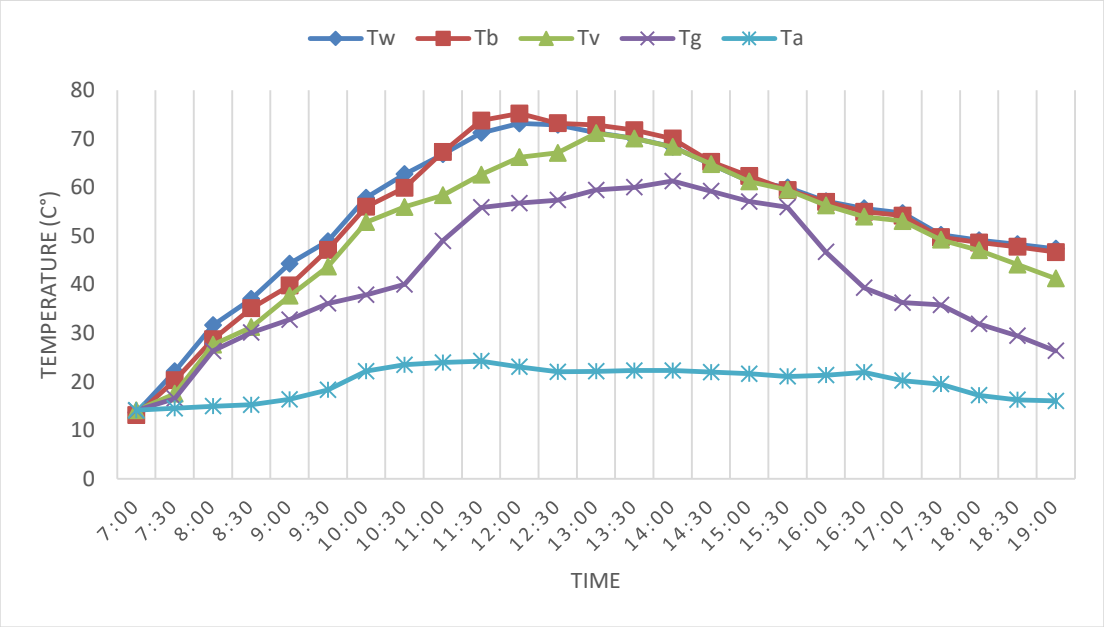

Figure 5. 6: **Advanced solar still performance in 23 April 2019**

The highest basin water temperature recorded was 73.2 ºC and the correlating basin temperature was 74.3 ºC. It was observed that the condensation surface temperature was relatively high due to a lack of a cooling process. It reached the maximum value of 60 ºC at noon (14:00) which was undesirable due to its minimizing the temperature difference between the basin water and the condensation surfaces.

Figure 5.7 presents the accumulative distilled water yield and the incident solar radiation on the still surface on 23 April 2019. The total distilled water yield was 4250 ml/m^2 (4.25 L/m^2) after 12 hours of daily operation.

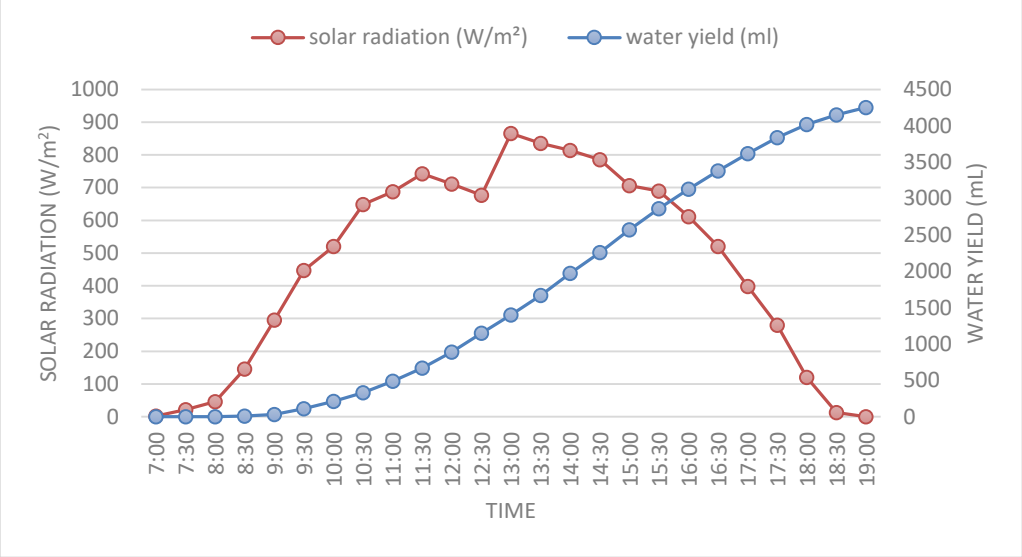

Figure 5. 7: Hourly solar radiation and the accumulative distillate yield in 23 April 2019

The energy analysis of the vapour compression heat pump cycle is described in chapter 3. The coefficient of performance (COP) of the cycle can be defined as the ratio of the thermal energy delivered on the work input. Figure 5.8 shows the COP of the cycle during 23 April 2019.

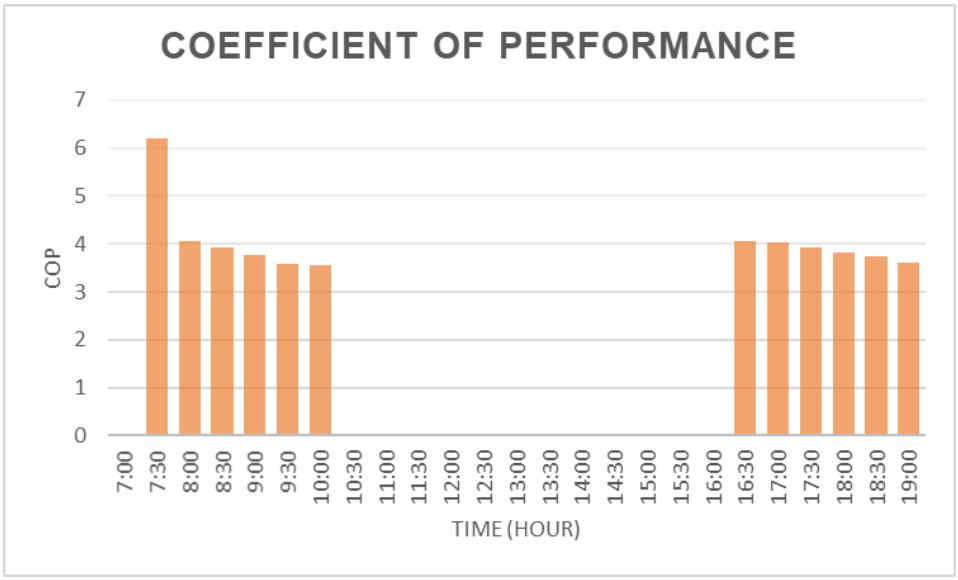

Figure 5. 8: The coefficient of performance of the VC heat pump on 23 April 2019

The maximum value of the coefficient of performance estimated was 6.2 and the minimum was 3.55. It can be observed from the graph that from 10:30 to 16:00 the value of the COP has not represented; this was because the heat pump system was in off mode because the basin water temperature was above 58 °C. The incident solar energy was sufficient to maintain the basin water temperature at the desirable level.

The power consumed by the 12 V DC compressor of the heat pump system is presented in Figure 5.9. The maximum power consumption recorded was about 55 W. The power consumption is a function of rotation speed (rpm); the energy consumption increases as the rotation speed increases (see the compressor specification in Appendix A).

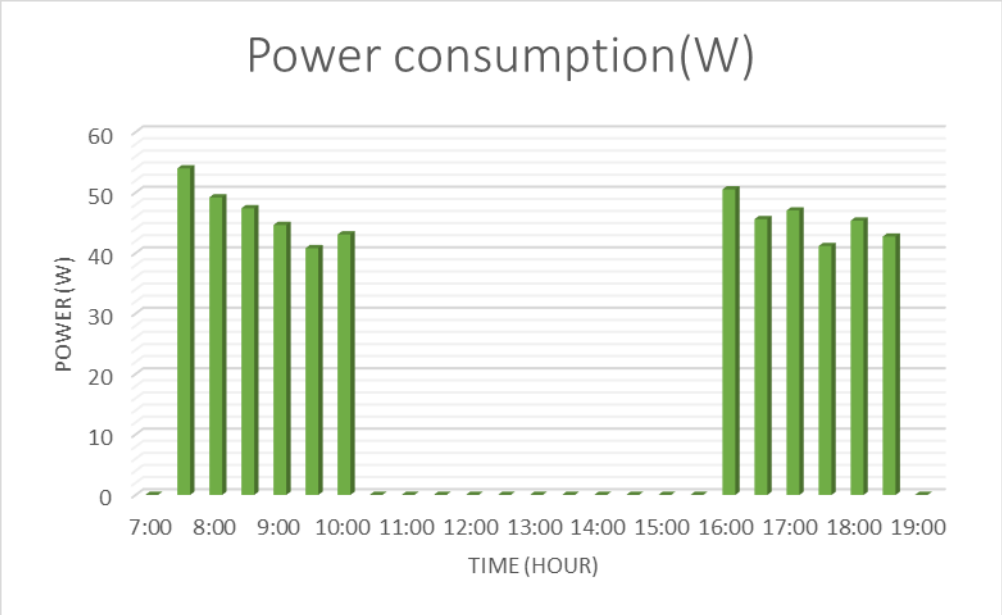

Figure 5. 9: Power consumption of the DC compressor

5.2.2.2. The experimental results from the second test (full operation of heat pump system)

The second test was performed in order to investigate the effect of cooling the condensing surface on the daily distillate water yield. As mentioned in literature, the temperature difference between the condensation surface and the basin water has a great impact on the daily yield of the distillate water. The higher the temperature difference achieved, the greater the water yield. Therefore, the second experimental test aimed to indicate and explain the effect of cooling down the condensation surface and to evaluate the performance of the vapour compression heat pump system.

Figure 5.10 presents the trend of the temperature of the advanced solar still system elements. As indicated on the graph, the basin water temperature reached a desirable level at 10:30. The maximum basin water temperature recorded at noon (13:00) was 62 °C. The condensation surface temperature varied from 16 to 28 °C. The maximum ambient temperature recorded was about 23.2 ºC, which is relatively low. The

maximum temperature difference between the contaminated water and the condensing surface achieved was about 32 ºC. During the test period, it was noticed that the heat pump system was operating most of the day due to low incident solar radiation which was not sufficient to maintain the temperature inside the still at the desirable level. Therefore, the heat pump system was maintained above 50 °C until the end of the experiment.

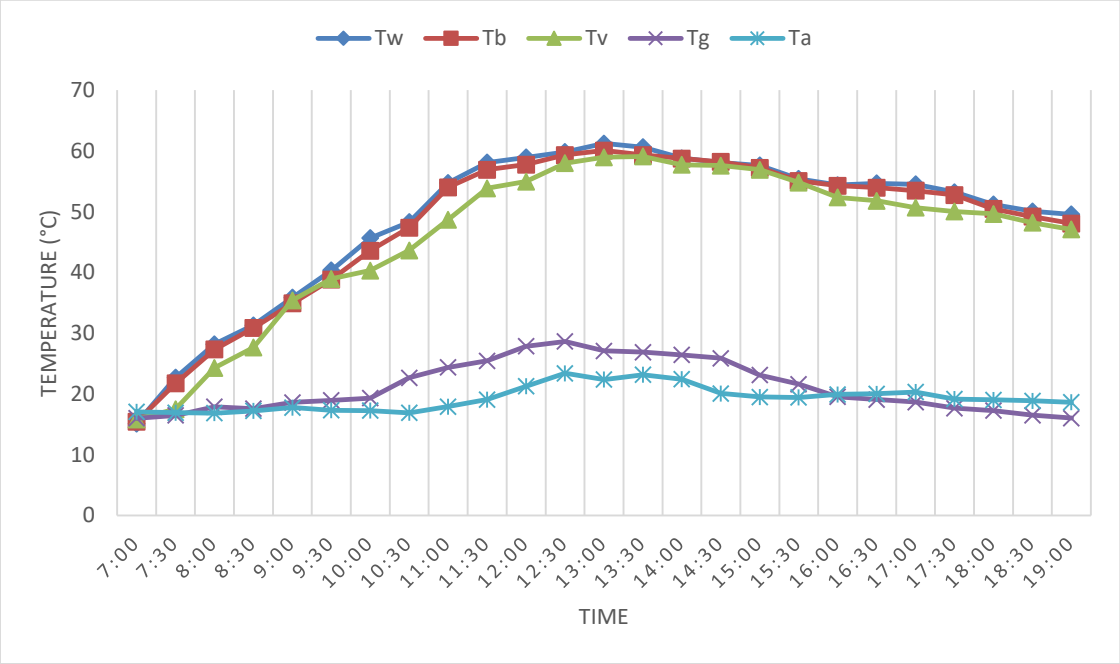

Figure 5. 10: **Temperature trend of the vapour compression solar still components**

The COP of the heat pump system and the compressor power consumption are shown in Figure 5.11. The average COP was about 3.5 and the average power consumption was about 50 W.

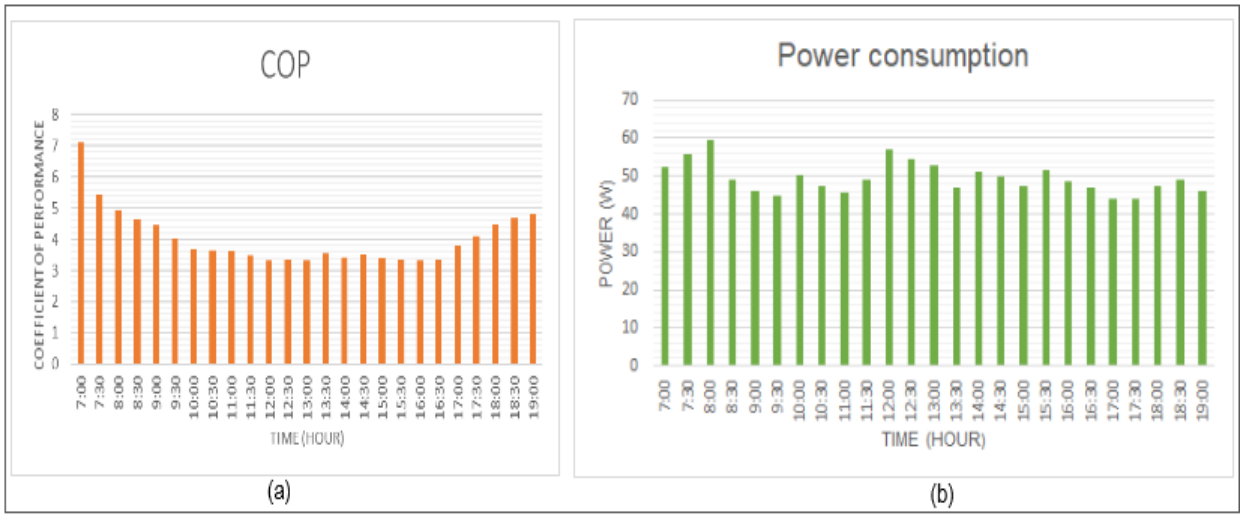

Figure 5. 11: (a) the coefficient of performance of VC heat pump system; (b) the energy consumption of the DC compressor

The incident solar radiation on the solar still and the daily distillate yield is presented in Figure 5.12. As it can be seen on the graph, the maximum computed incident solar radiation was about 630 W/m^2 and the accumulative water yield was 5750 ml (5.75 L/day).

Clearly, the improvement of the advanced solar still performance was accompanied by a cooling down of the condensing surface. Although the incident solar radiation was relatively low during the second experiment compared to the first experiment, the daily distillate yield was better.

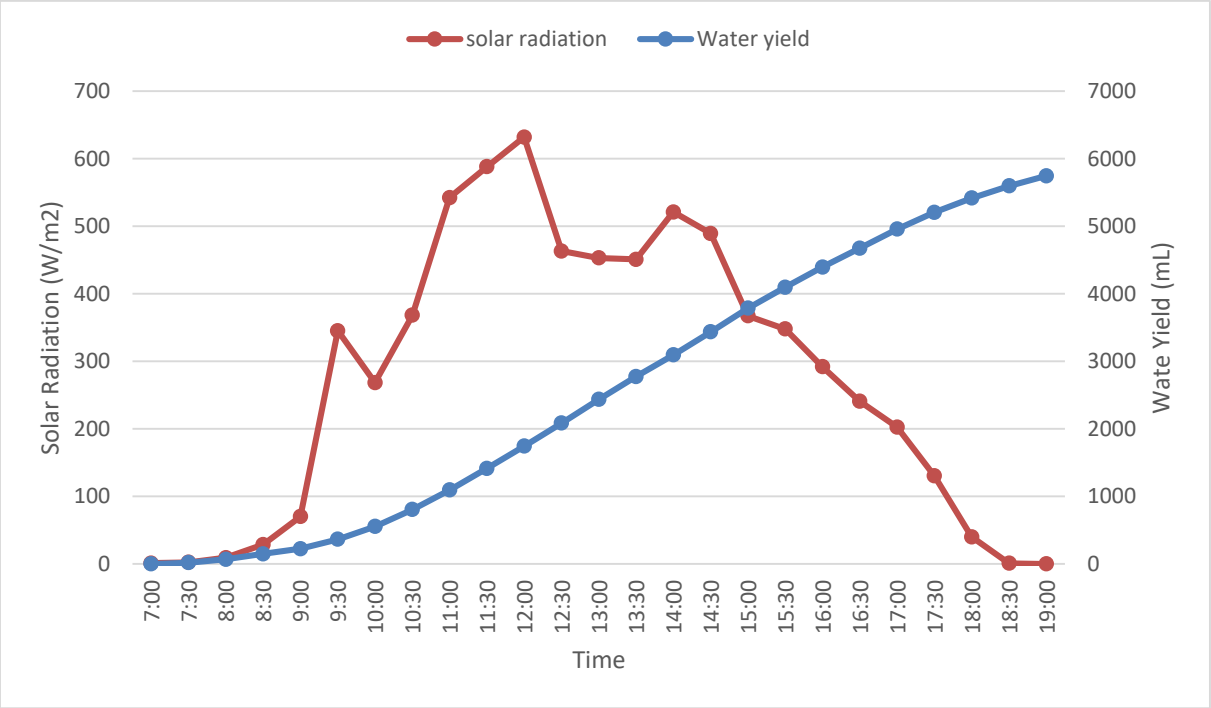

Figure 5. 12: The incident solar radiation and the accumulative distillate water during the second experiment

5.2.2.3. The experimental results from the third test (comparison between the advanced and the conventional stills)

An experimental work was performed in order to compare the advanced solar still with the conventional solar still. In order to investigate the performance of the stills, two identical stills were tested at the same time in different seasons (summer and winter). Both stills were filled with 20 L of water to a depth of 20 mm. Figure 5.13 shows the weather condition at the experimental site on 25 November 2019 (summer in the southern hemisphere). The maximum ambient temperature recorded was about 34 ºC and the maximum wind speed was about 7.7 m/s.

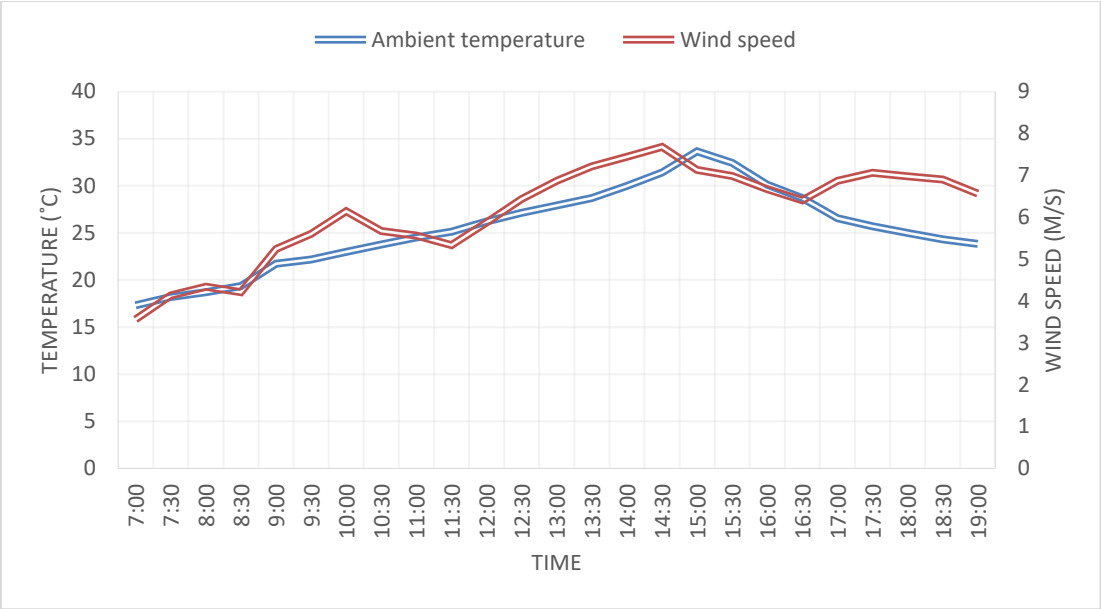

Figure 5. 13: Variation of wind speed and ambient temperature on 25 November 2019

The temperature trend of the different advanced solar still components is shown in Figure 5.14. The vapour compression heat pump system was able to preheat the water to the desired level before 9:00 and maintain it above 50 ºC until the end of the experimental test (19:00). The maximum water temperature recorded at noon was 73 ºC. The maximum ambient temperature recorded was 33 ºC. It can be observed from the graph that the condensation surface temperature increased rapidly after 11:30 and then decreased at 15:30. It reached a maximum value of 47 ºC at 13:30. During the stated period, the heat pump system was off. The average of the temperature difference between the basin water and condensation surfaces was 26 ºC. The maximum temperature difference was 34 ºC.

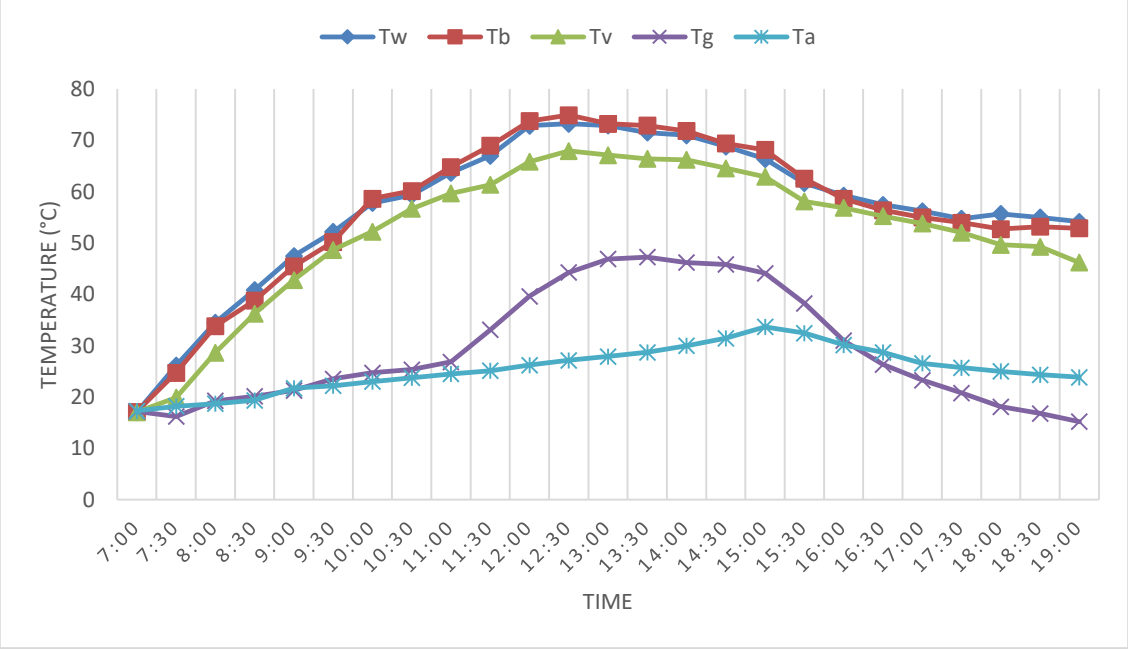

Figure 5. 14: Temperature trend of the advanced solar still (November 2019)

The temperature trend of the different conventional solar still components is shown in Figure 5.15. The maximum basin water temperature recorded at 13:30 was 57.4 ºC. The maximum ambient temperature recorded was 33 ºC. As can be noticed in the graph, the condensation surface temperature has the same tendency as basin water temperature. It reached its peak at 13:30, which was 49.3 ºC, then gradually decreased. The average of the temperature difference between the basin water and condensation surfaces was 8.2 ºC. The maximum value was 9.3 ºC, which is relatively low compared with that achieved by the advanced still as indicated in Figure 5.14.

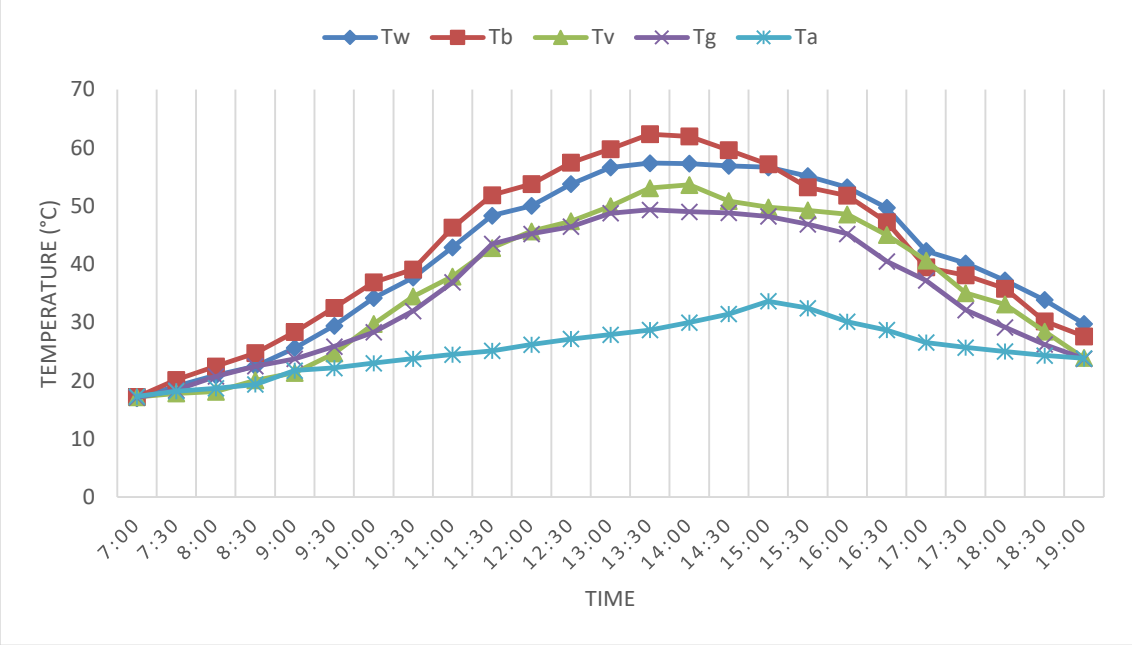

Figure 5. 15: **Temperature trend of the conventional solar still (November 2019)**

The accumulated distillate yield of both solar stills is presented in Figure 5.16 as well as the incident solar radiation on an inclined surface. As can be noticed from the graph, the water yield from the advanced still started early at 7:30, while the conventional still produced water at 8:30. The highest amount of distillate yield was harvested in the afternoon between 13:00 to 13:30 which was 370 and 200 ml for the advanced and conventional still respectively. The corresponding solar radiation on the tilted surface was relatively adequate at the maximum value of 1050 W/m^2. The accumulated daily yield of distillate water at the end of the experiment was 6210 ml/m^2 (6.2 L/m^2) for the advanced still and 2670 ml/m^2 (2.67 L/m^2) for the conventional still. Hence, the vapour compression heat pump system was able to improve the daily yield of distillate water by more than double.

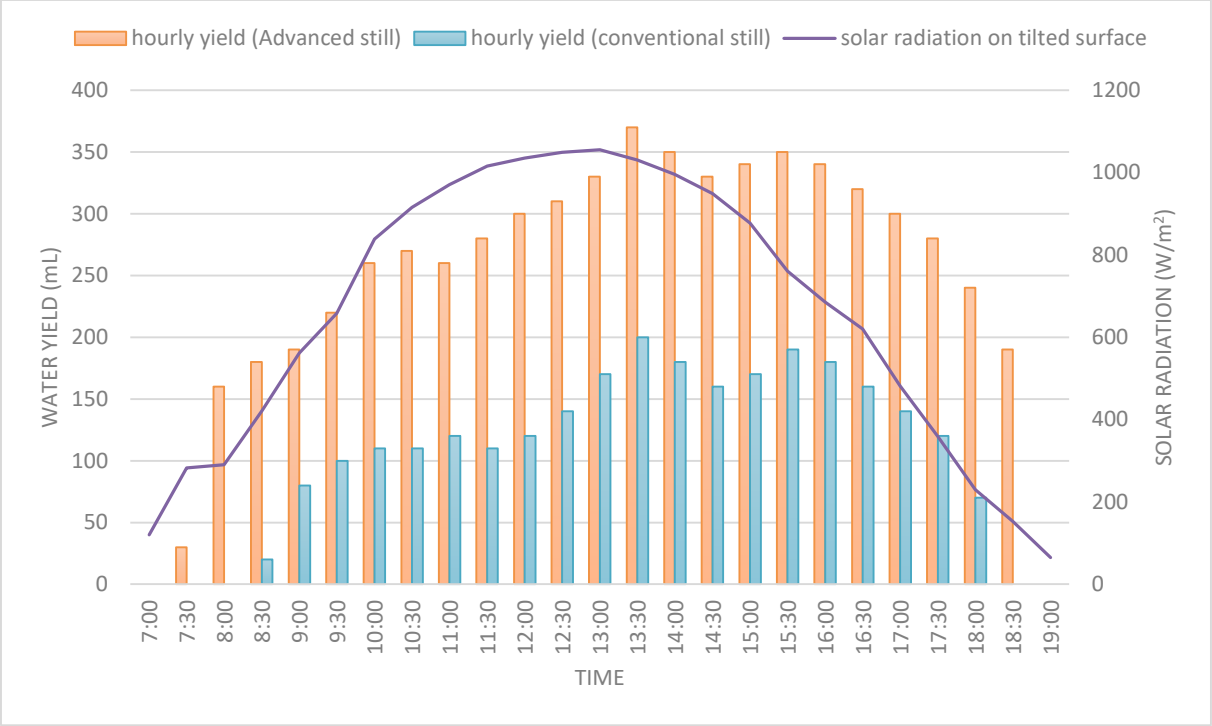

Figure 5. 16: The yield of distillate water from the advanced and conventional solar still on 25 November 2019

An experimental test was performed in winter in July 2020 in order to compare the performance of both stills in harsh weather conditions, and to evaluate the performance of the vapour compression heat pump system. A sample of the weather conditions is presented in Figure 5.17. As it can be seen in the graph, the maximum ambient temperature was 19 ºC and the minimum temperature was about 11 ºC, therefore it was a relatively cold day. The maximum wind speed was about 9.5 m/s.

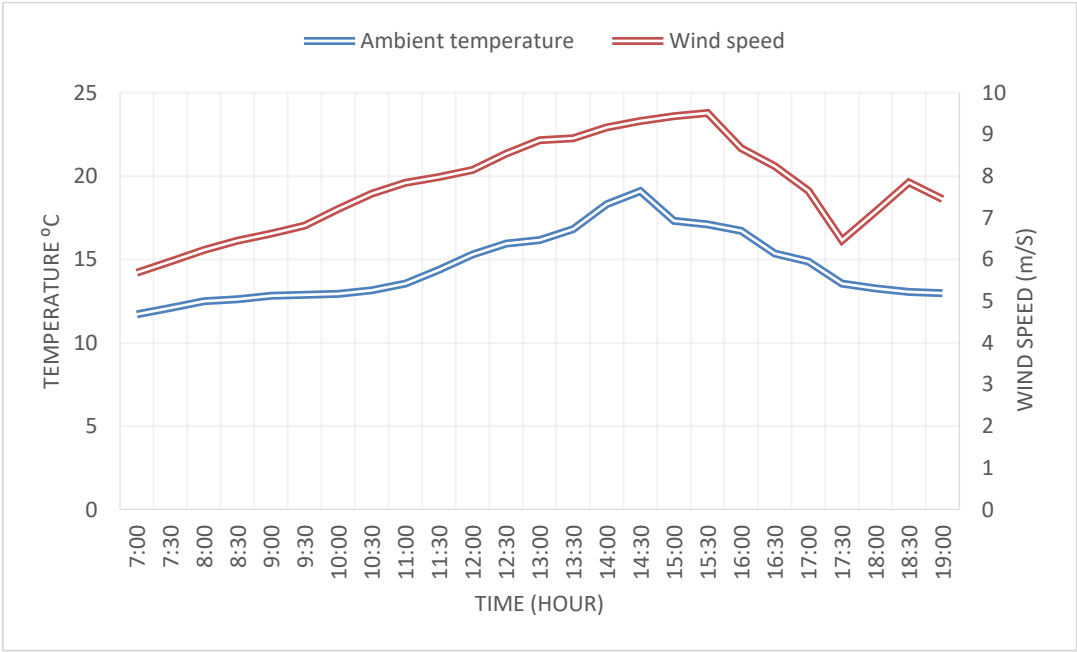

Figure 5. 17: Variation in weather conditions on 14 July 2020

The temperature trend of the advanced solar still components is shown in Figure 5.18. The graph confirms that the vapour compression heat pump system was able to preheat the basin water to the desired level before 10:00 and could maintain it at that level (above 45 ºC) until the end of the test period. The maximum basin water temperature recorded at 14:00 was 59 ºC. The ambient temperature was relatively low during the day, the highest temperature recorded 14:30 was 19 ºC. The condensation surface temperature had tendency to remain low. The highest temperature recorded at 14:00 was 26 ºC. The average of temperature difference between the basin water and the condensation surfaces was 26 ºC.

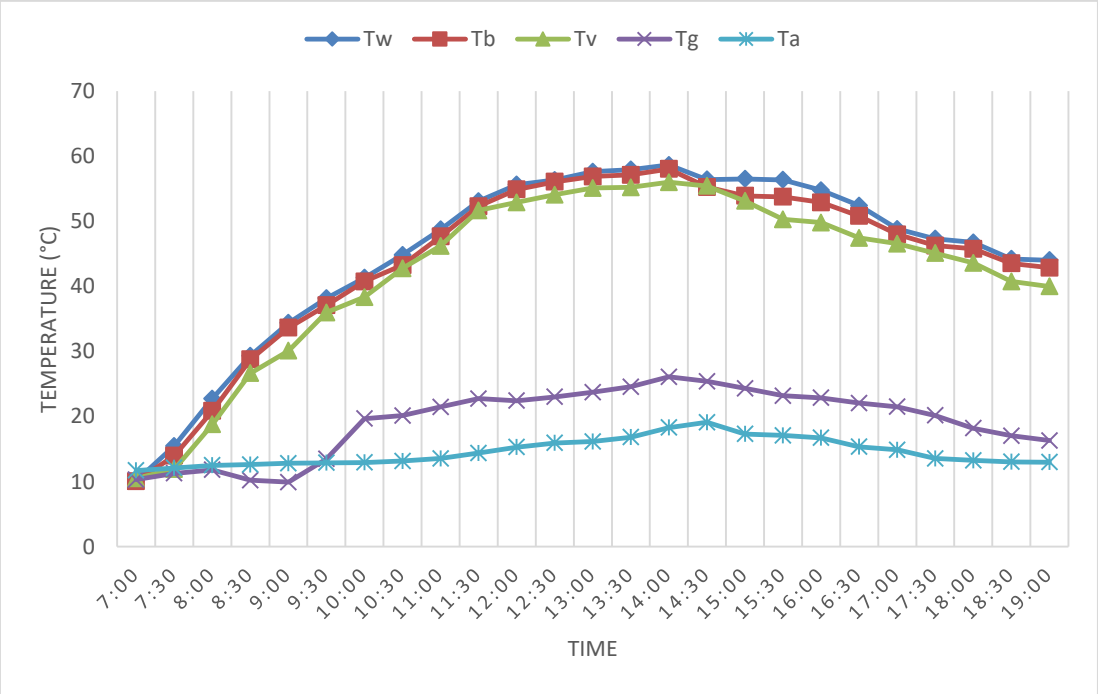

Figure 5. 18: Temperature trend of the advanced solar still on 14 July 2020 (winter)

Figure 5.19 depicts the temperature trend of the conventional solar still components. As can be observed from the graph, the basin water temperature did not increase to the desirable level due to the fluctuation of the incident solar radiation and cold weather (low ambient temperature). The highest basin water temperature recorded was 38.5 ºC. The average of the temperature difference between the basin water and the condensation surfaces was 6.8 ºC.

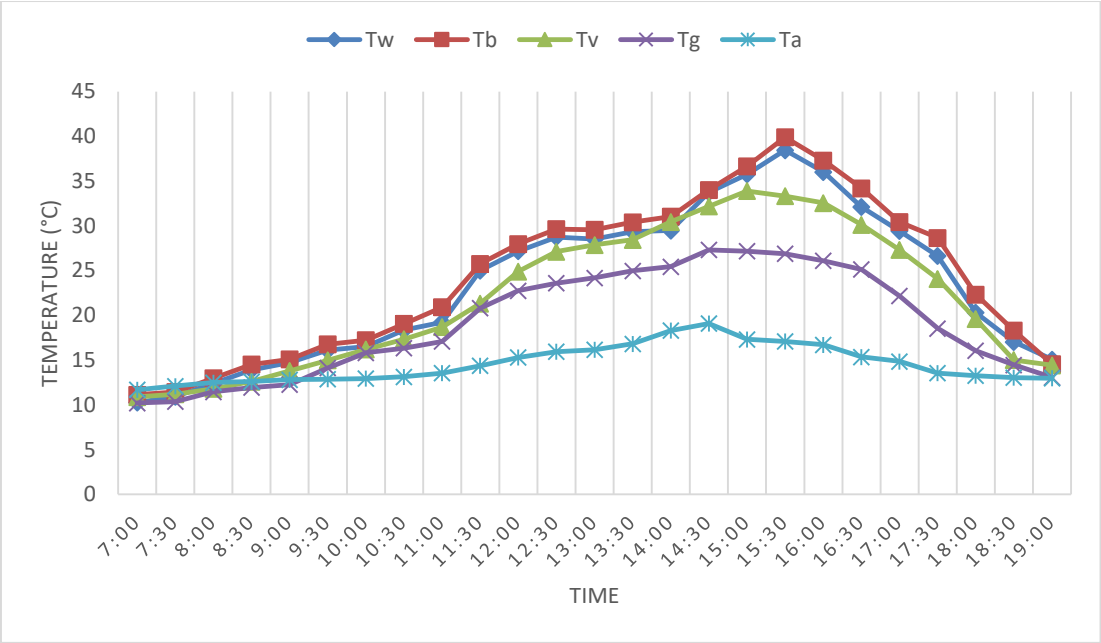

Figure 5. 19: Temperature trend of the conventional still on 14 July 2020 (winter)

The accumulated daily distillate water of both solar stills and the corresponding calculated incident solar radiation is given in Figure 5.20. 14 July was chosen as a typical winter day in the southern hemisphere. As indicated in the graph, the incident solar radiation was fluctuating due to a partially cloudy sky with a maximum value of 452 W/m^2. The daily cumulative distillate water yield from the conventional still was relatively low at the amount of 215 ml/m^2, while the advanced solar still was about 4200ml/m^2.

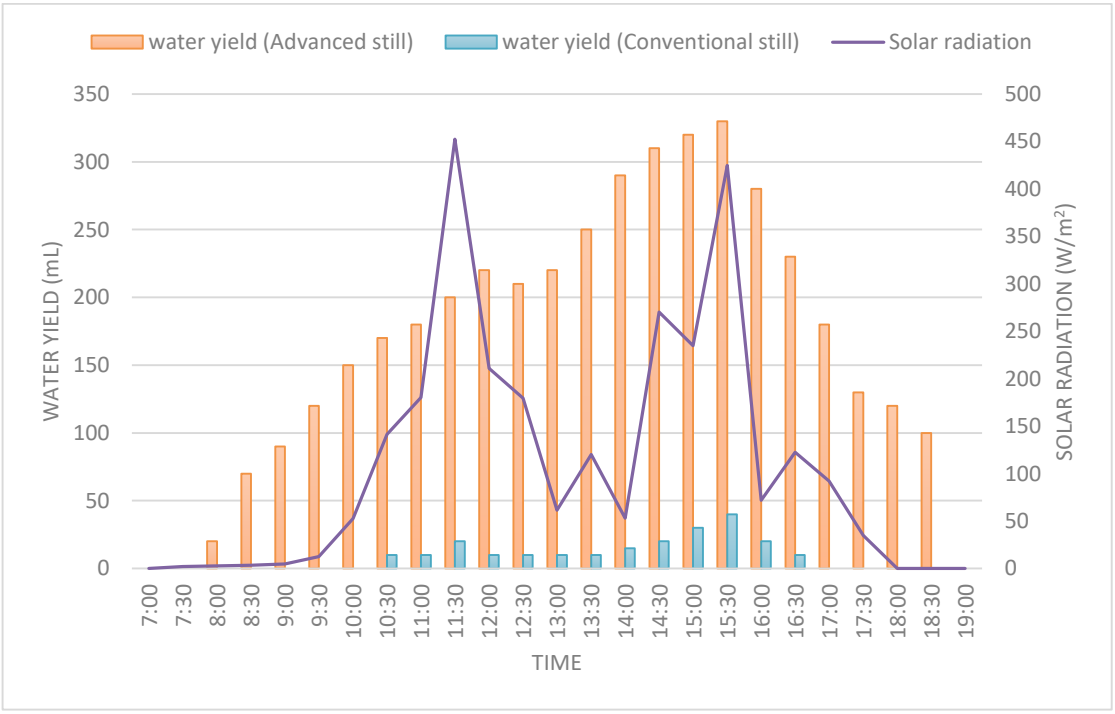

Figure 5. 20: Solar stills distillate water yield on a winter day

The vapour compression heat pump COP during the experimental test in winter time is presented in Figure 5.21. The average COP was rated at 3.5.

Figure 5. 21: The COP of vapour compression heat pump system on 14 July

5.2.2.4. Night operation of the advanced solar still

One of the main objectives of the experimental work was to evaluate the performance of the advanced solar still under adverse conditions (cloudy sky/night period). Figure 5.22 depicts the performance of the advanced solar still during the night operation test in the summer season. During the experimental test, the initial temperature of contaminated water was about 18 ºC and the thermostatic control was set at 54 ºC.

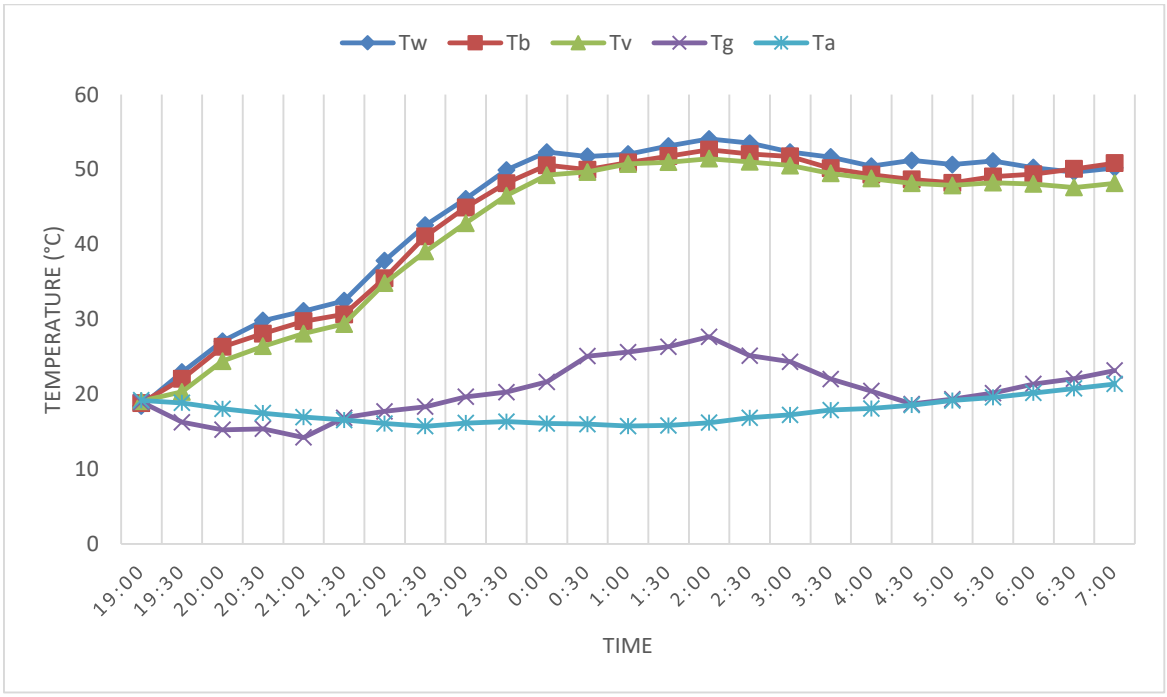

Figure 5. 22: Advanced solar still performance during night test (summer season)

As it can be noticed from the graph, the maximum basin water temperature was 54 ºC. The average of the temperature difference between the basin water and the condensation surfaces was 26 ºC. The accumulated distillate output at the end of the test was 3200 ml/m^2.

The performance of the advanced solar still in the winter season was investigated as well. A sample of data during the night period test is presented in Figure 5.23. The initial temperature of the contaminated water was 14.5 ºC and the water depth was about 16 mm (16 L). The thermostatic control was set at 50 ºC. As can be seen from the graph, the heat pump system was able to maintain the temperature above 48 ºC. The basin water temperature reached the desirable level at 23:00. The average of the temperature difference between the basin water and the condensation surfaces was 28 ºC. The accumulated distillate yield was 2750 ml/m^2.

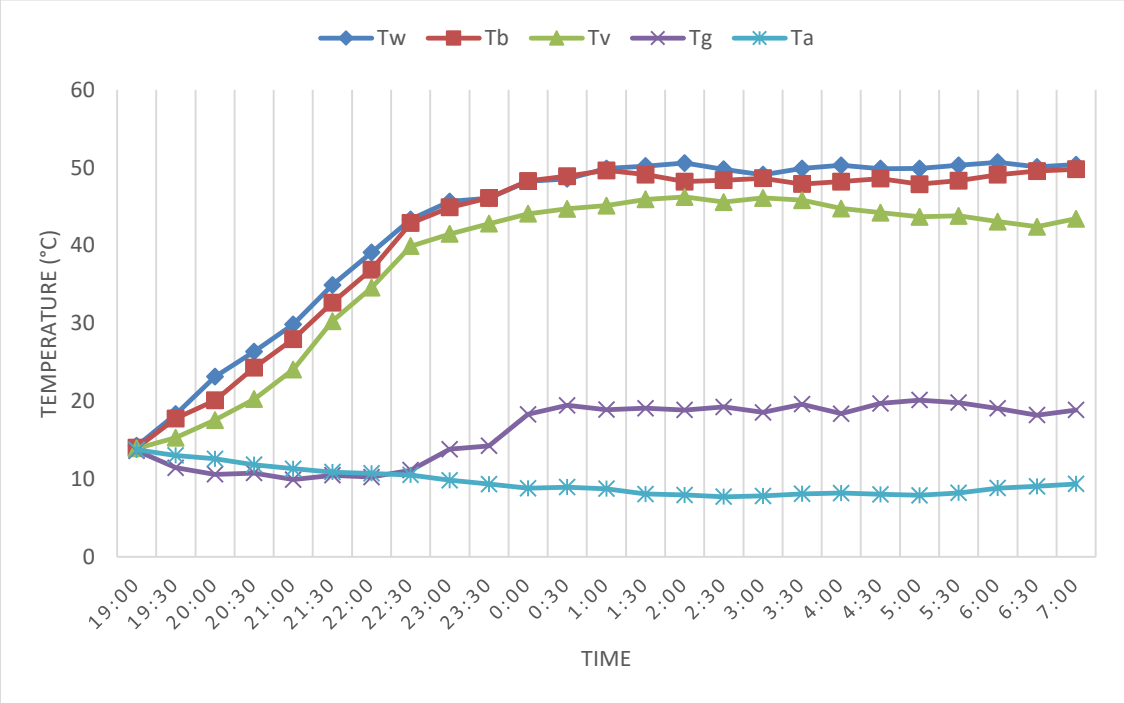

Figure 5. 23: Advanced solar still performance during night test (winter season)

5.2.3. The efficiency of solar still

The hourly efficiency of solar still is basically the ratio of thermal energy used to produce distillate water in a given time span. The useful thermal energy represented in absorbed solar radiation inside the solar still is employed to evaporate the basin water and part of it as a thermal loss through still surfaces. The thermodynamic of the solar is discussed in chapter two. The sample calculation is given in Appendix D. Figure 5.24 illustrates the hourly efficiency of the advanced and the conventional solar stills during the summer season.

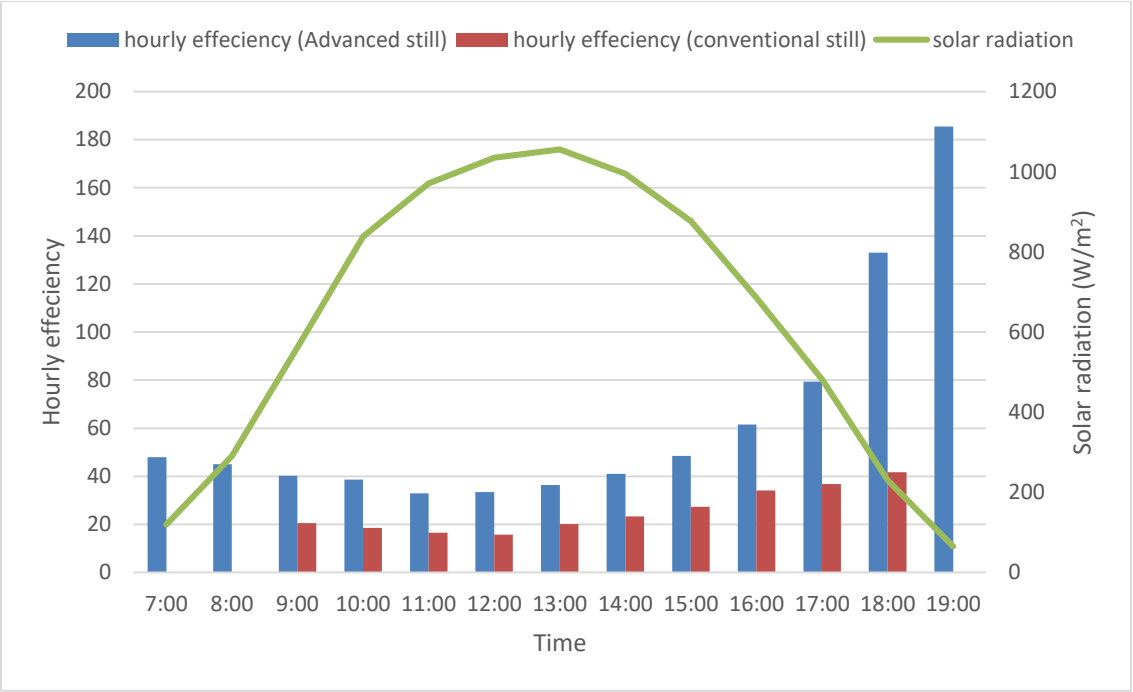

Figure 5. 24: The efficiency of solar still in the summer season

The average of the efficiency of the conventional solar still was 20.77%, while the average of hourly efficiency of the advanced one was 63 %. The high value of efficiency at 19:00 was due to the low value of incident solar radiation.

5.2.4. Factors affects water productivity

The daily/seasonal performance of the solar still and the distillate water yield depends on different factors including climate parameters (ambient temperature, solar intensity and wind speed), design parameters (selected materials, functionality, capability and quality), and the operation parameters (water depth and impurity of feed water). Most of these parameters are studied in different research works, as summarized in chapter two. The other factor studied in this research was the formation of the droplets on the condensation surface. It is noticed that the vibration caused by the compressor and the cooling water flow in the vapor compression heat pump system helps to excite the droplet to slide down toward the collector to prevent the droplet from being overgrown and possibly falling down in the basin, thereby reducing the daily yield. Figure 5.25 shows a photograph of the droplet formation on the condensation surface of both solar stills.

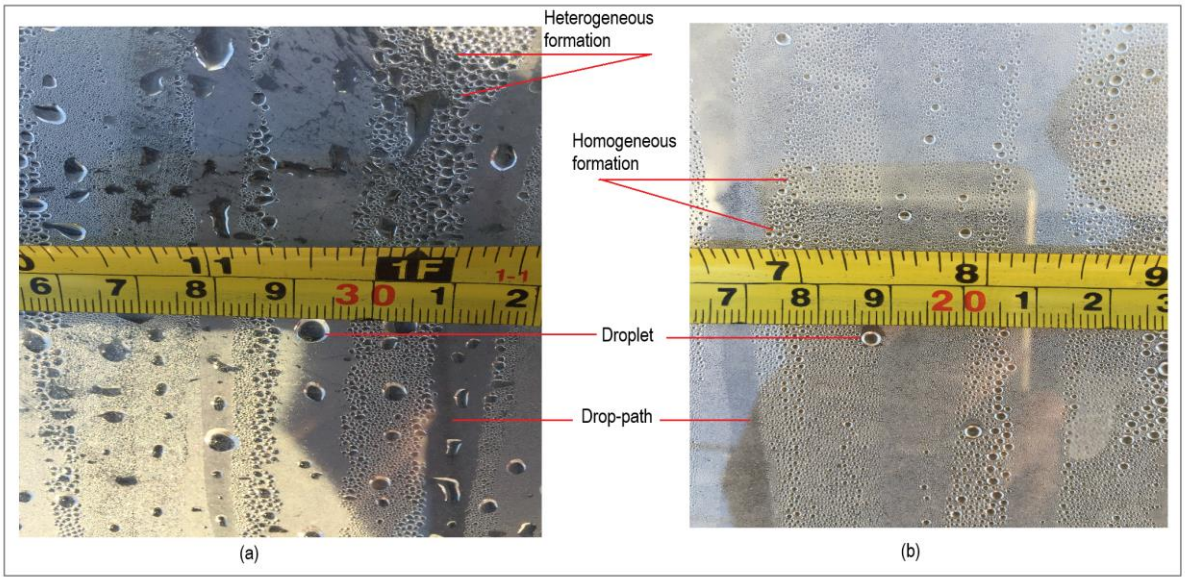

Figure 5. 25: Types of droplet formation on the condensation surfaces. (a) conventional solar still. (b) advanced solar still

Photo (a) represents the droplet formation on the conventional solar still condensation surface. As can be observed from the photo, the droplets continued to grow until reaching the approximate diameter of 5 mm. They were still attached to the condensation surface, meaning that there was the possibility of fall back into the basin. Moreover, the shape of the drops was heterogeneous. Photo (b) represents the droplet formation on the advanced still condensation surface. Here, the droplet diameter was less than 3 mm and they started to slide, as indicated from the drop-paths left behind. Moreover, the drop formation was homogeneous and were more spherical.

5.3 Experimental results of the solar still prototype based on the thermoelectric heat pump system

In this research, two types of heat pump systems were designed and utilized as thermal energy recovery systems in two different experiments during three years of the research program: first, the performance of the vapour compression heat pump system integrated into single-effect solar still, as discussed in previous sections; second, a thermoelectric heat pump system integrated into the single-effect solar still. Various experimental tests were conducted to evaluate the performance the systems. Laboratory experiments were performed in order to optimize the thermoelectric heat pump as well as outdoor experiments conducted under different weather conditions of the year of 2021 in order to investigate the performance of the advanced solar still.

5.3.1. The meteorological conditions

The variations in the computed solar radiation on May and September 2021 are presented in Figure 5.26 and Figure 5.27.

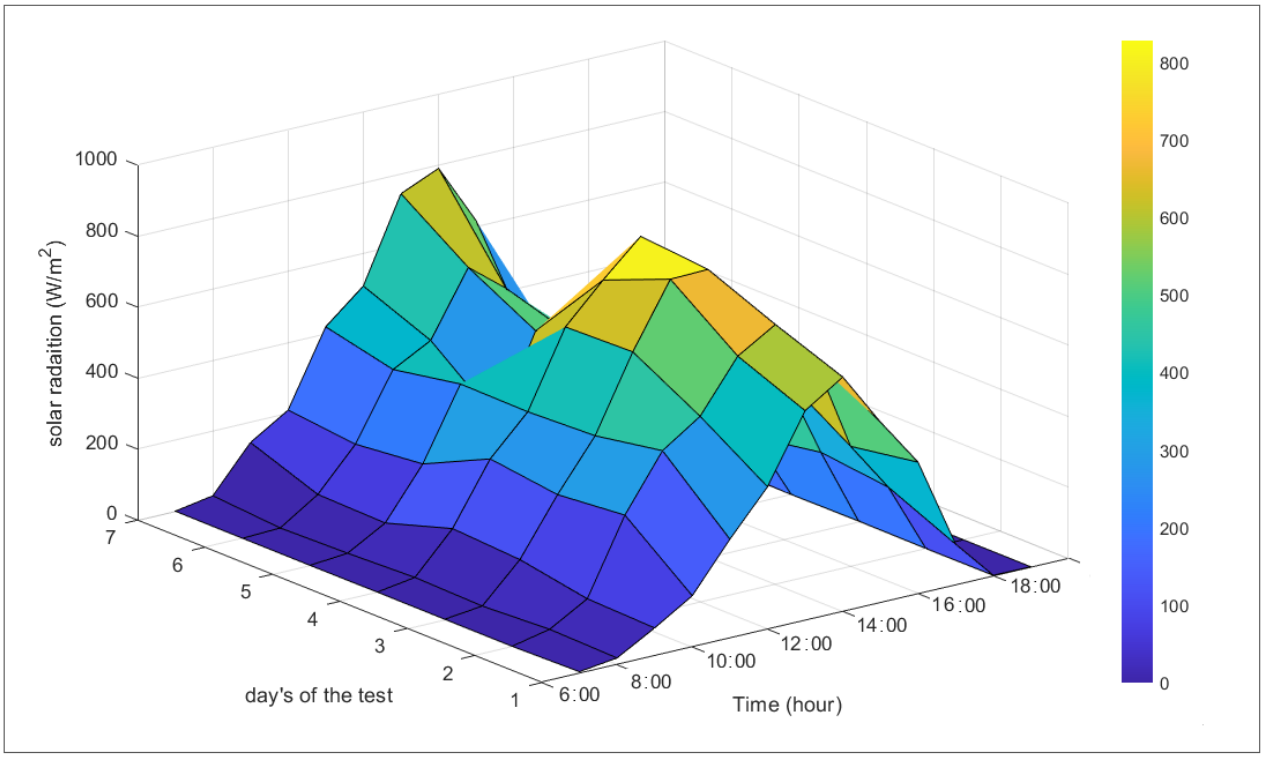

Figure 5. 26: The variation of computed solar radiation on May 2021

As indicated in the graphs, the maximum solar radiation in the late days of May was about 820 W/m^2 and in the early days of September about 630 W/m^2.

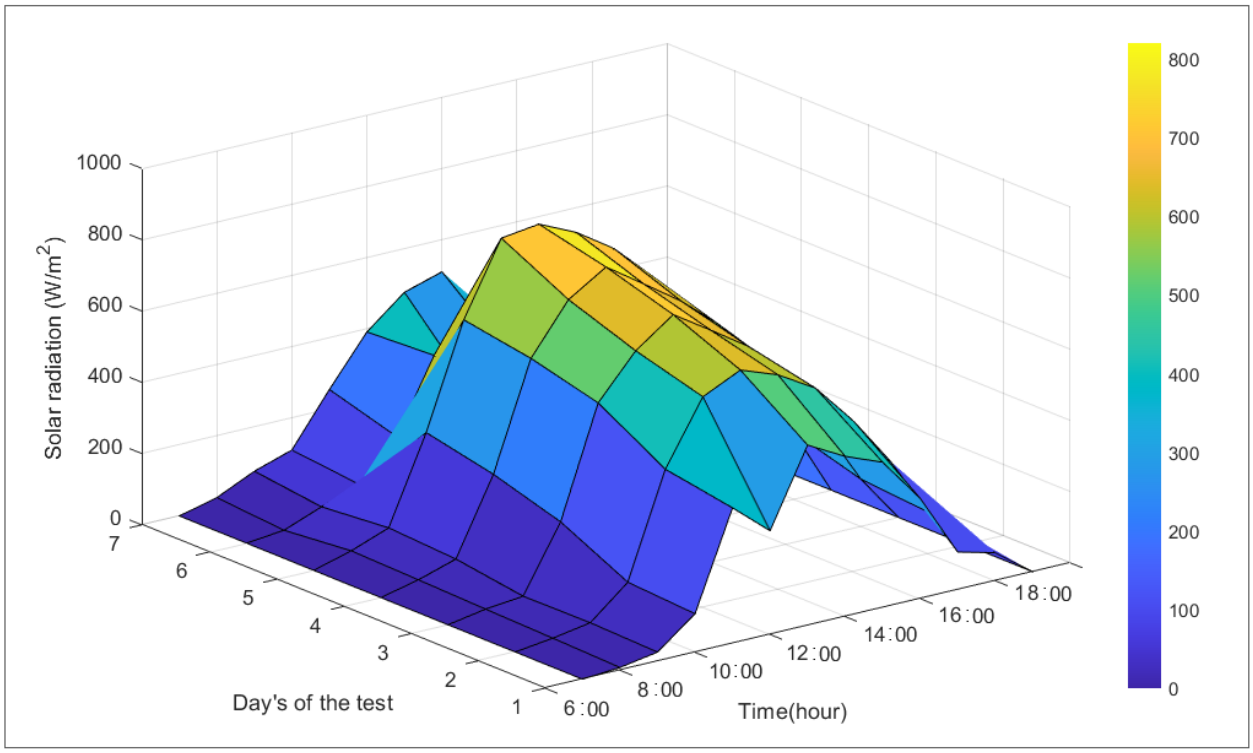

Figure 5. 27: The variation of computed solar radiation on September 2021

5.3.2. The still performance

The performance of the advanced still based on a thermoelectric (TE) heat pump as the thermal energy recovery system was investigated under different weather conditions.

Figure 5.28 presents the temperature trend of the developed solar stills components. The ambient temperature recorded at the beginning of the experiment was 17 ºC, which then increased to 26 ºC at midday. The initial temperature of the basin water was 16 ºC, and then increased to 45 ºC in 3 h. At midday, the basin water temperature reached 60 ºC. It was maintained above 50 ºC till 17:00, then decreased to 49 ºC at the end of the experiment. The sharp increase in basin water temperature was due to the input heat delivered from the TE heat pump system. The vapour temperature showed the same trend as the basin water temperature. It reached 54 ºC at midday.

The temperature difference between the basin water surface and condensation surface is the key force of the solar still. It was maintained above 20 ºC. The highest value recorded was 30 ºC.

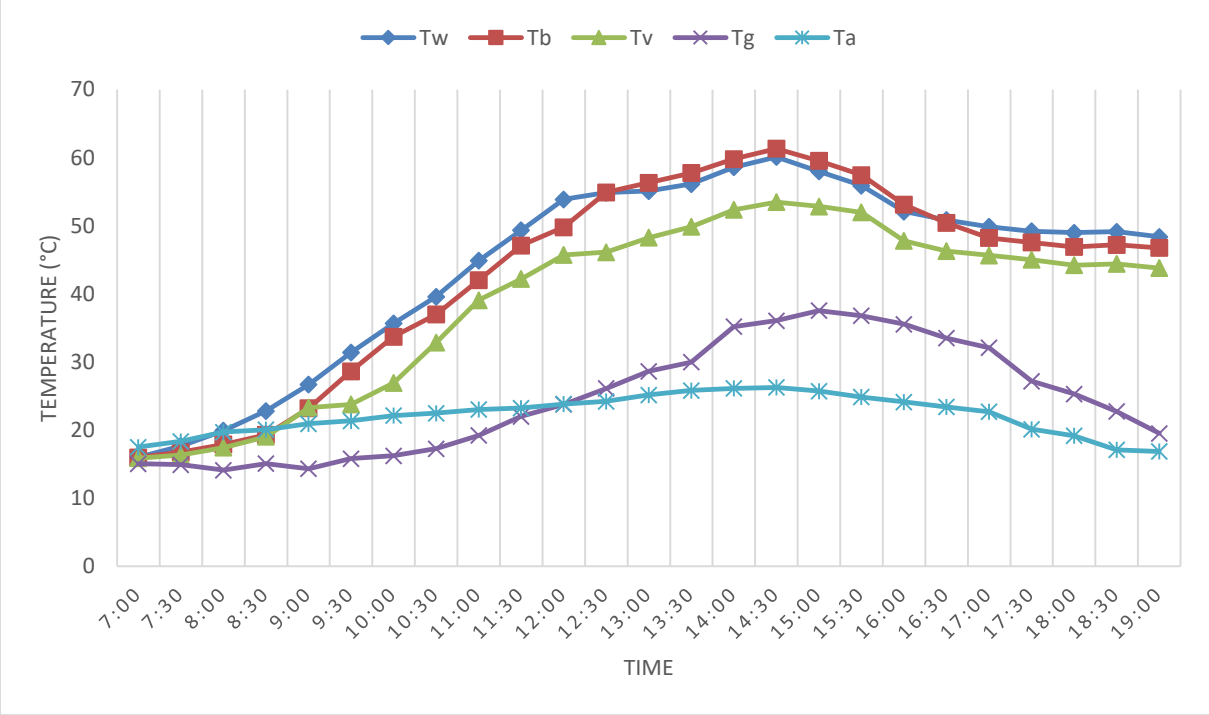

Figure 5. 28: The temperature trend of the thermoelectric solar still

Figure 5.29 presents the temperature trend of the conventional solar still. The ambient temperature recorded at the beginning of the experiment was 17 ºC, and then increased to 26 ºC at midday. At the end of the experiment, the ambient temperature decreased to 18 ºC. The initial temperature of the basin water was 16 ºC, and within 3 h, it reached 26 ºC. There was a linear increase in basin water temperature until midday, and then a linear decrease tendency was shown. The maximum basin temperature recorded was 53 ºC. The vapour temperature showed similar behavior to the basin water

temperature. It reached 49 ºC at midday. The condensation surface temperature increased with the increase of the vapour temperature. The maximum value recorded was 41 ºC at midday. The temperature difference between the basin water and the condensation surfaces varied from 4 to 14 ºC.

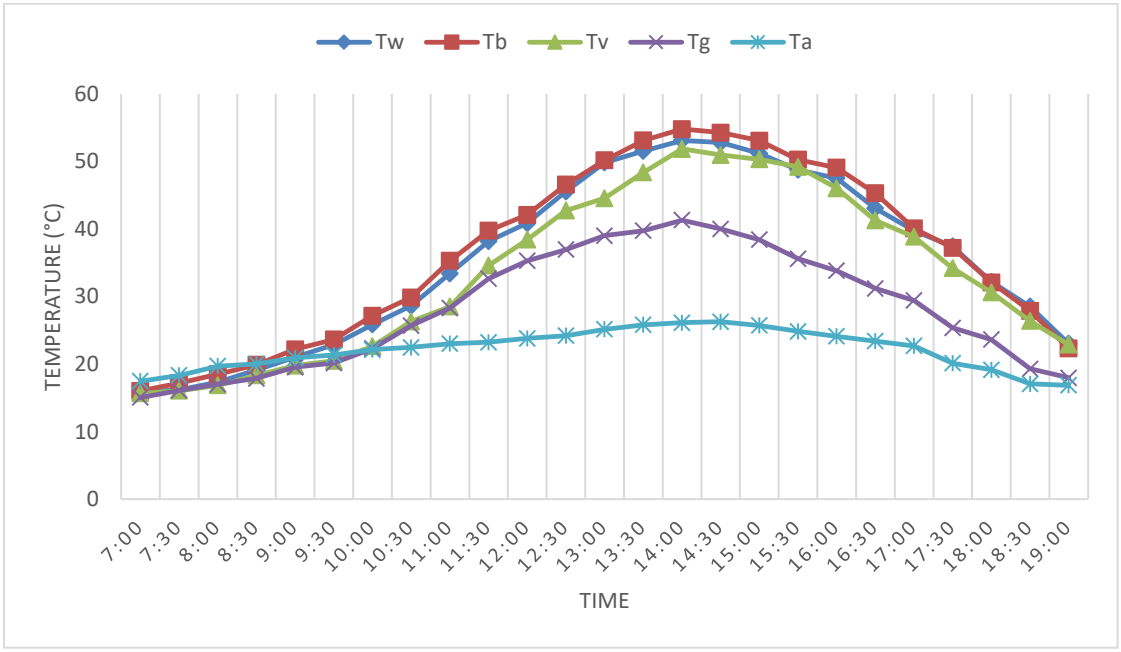

Figure 5. 29: The temperature trend of the conventional solar still

Figure 5.30 depicts the yield of distillate water of both solar stills. As can be observed from the graph, the water yield from the advanced still started early at 8:30, while the conventional still produced water at 10:30. The highest amount of distillate for both stills was collected after 14:00. The incident solar radiation was 660 W/m^2. The accumulated distillate water at the end of the experiment was 2180 ml (4.4 L/m^2) for the advanced still, while the conventional one produced1050 ml (2.1 L/m^2).

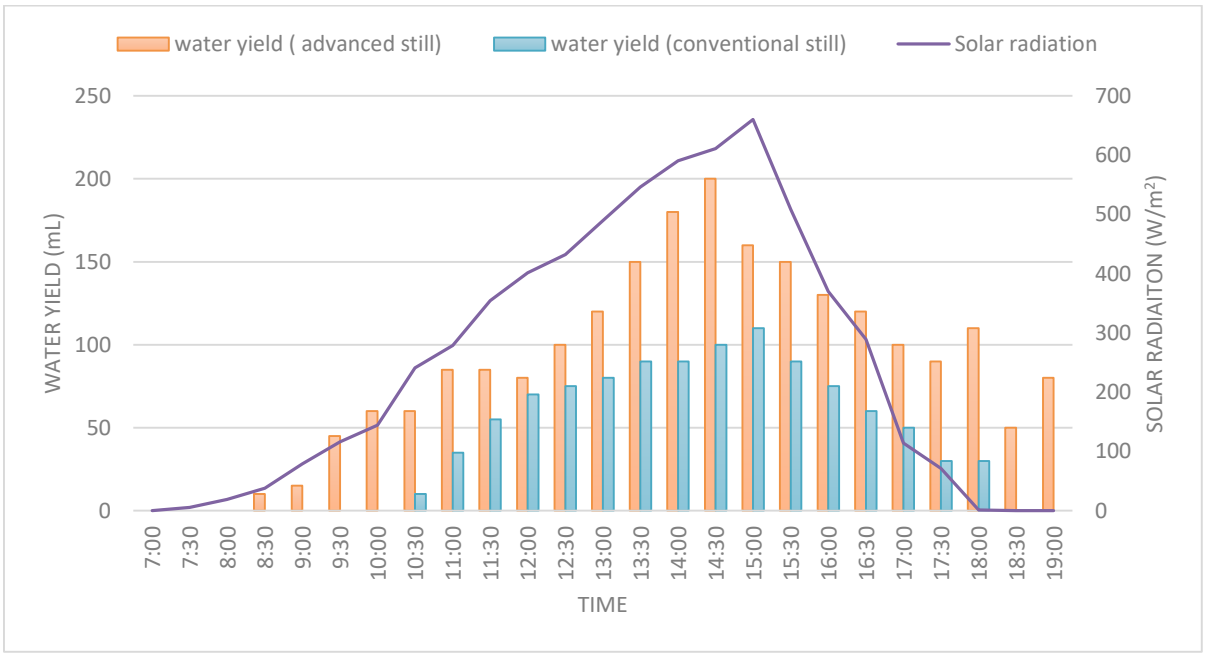

Figure 5. 30: The accumulated water yield from solar stills

The performance of the advanced solar still in September 2021 is presented in Figure 5.31. As it can be observed in the graph, the condensation surface temperature increased gradually after 13:00, due to the fact that the thermoelectric pump was off until 15:30 because of the water temperature was maintained above 52 ºC. The maximum water temperature recorded was 54.8 ºC and the maximum ambient temperature was about 17.7 ºC. The average temperature difference between the basin water and the condensation surfaces was 24 ºC.

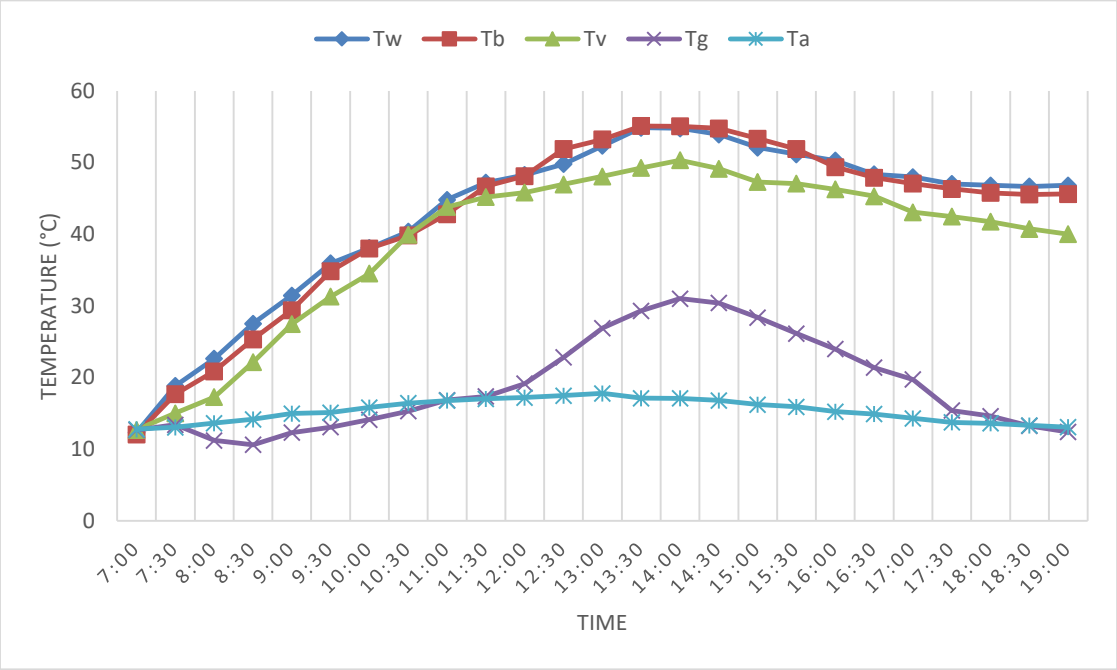

Figure 5. 31: The temperature trend of the TE solar still on September 2021

Figure 5.32 depicts the temperature trends in the counterpart solar still components. The highest temperature of the basin water recorded at 13:30 was 45.8 ºC. The average of the temperature difference between the basin water and the condensation surfaces was 11 ºC.

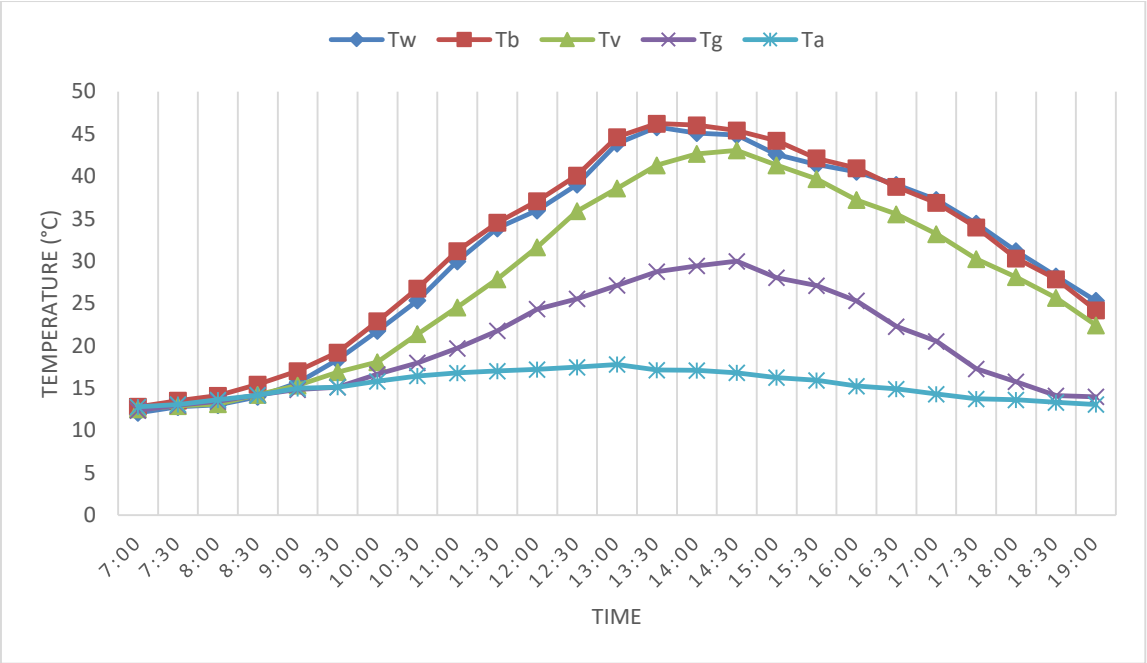

Figure 5. 32: The temperature trend of the conventional solar still on September 2021

Figure 5.33 depicts the accumulated distillate water of both solar stills. As can be observed from the graph, the water yield from the advanced still started early at 9:30, while the conventional still produced water at 11:00. The highest amount of distillate for both stills was collected after 14:30. The incident solar radiation was 530 W/m^2. The ambient temperature was relatively low, the highest value recorded at 13:00 was 17.8 ºC. The accumulated distillate water at the end of the experiment was 2350 ml (4.7 L/m^2) for the advanced still, while the conventional still produced 650 ml (1.3 L/m^2).

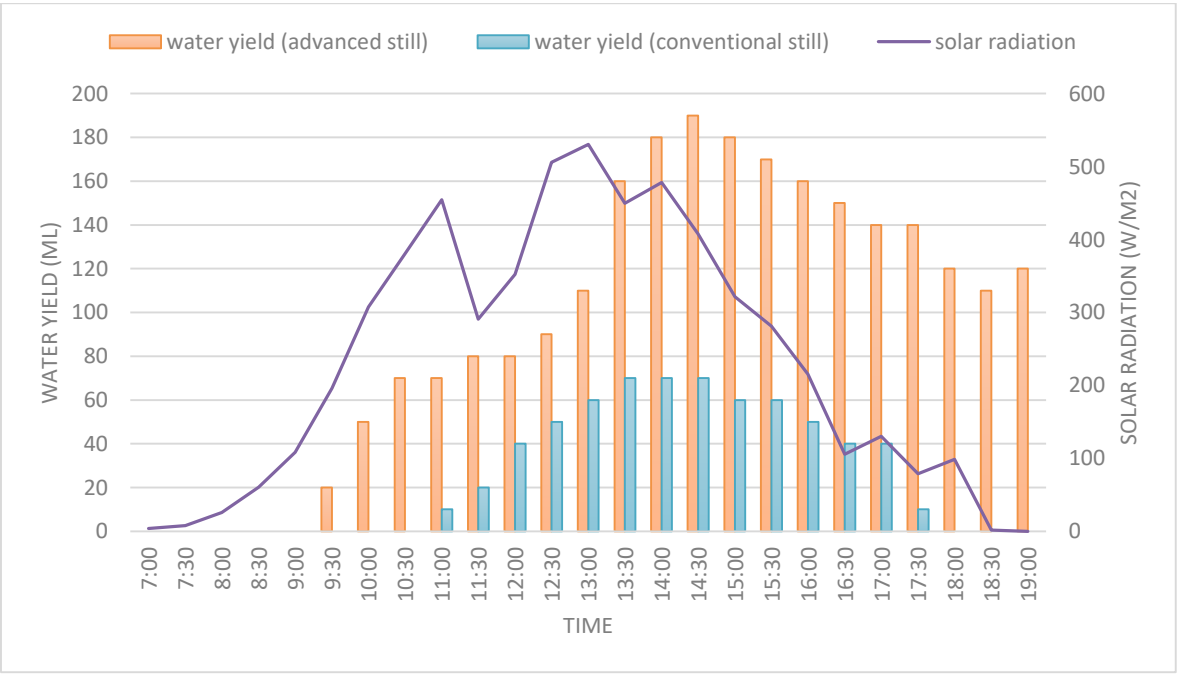

Figure 5. 33: The accumulated water yield of both solar stills

Figure 5.34 shows the variation of the coefficient of performance of the heat pump system at the input current of 5A. It is noticeable that the COP declined with the increase of the cold side temperature of the thermoelectric modules (Tc). At 8:00, the temperature of the cold side of the thermoelectric module was 10 ºC and the hot side was 28 ºC; the value of the COP was 1.9. At 14: 00, the temperature of the cold side increased to 29 ºC and the value of the COP decreased to 0.4 due to the increase in the cooling capacity. At the end of the experiment (19:00), the value of the COP increased again due to the decrease of TC which was 13 ºC. These findings are in agreement with the findings of Diaz de Garayo, et al. (2022).

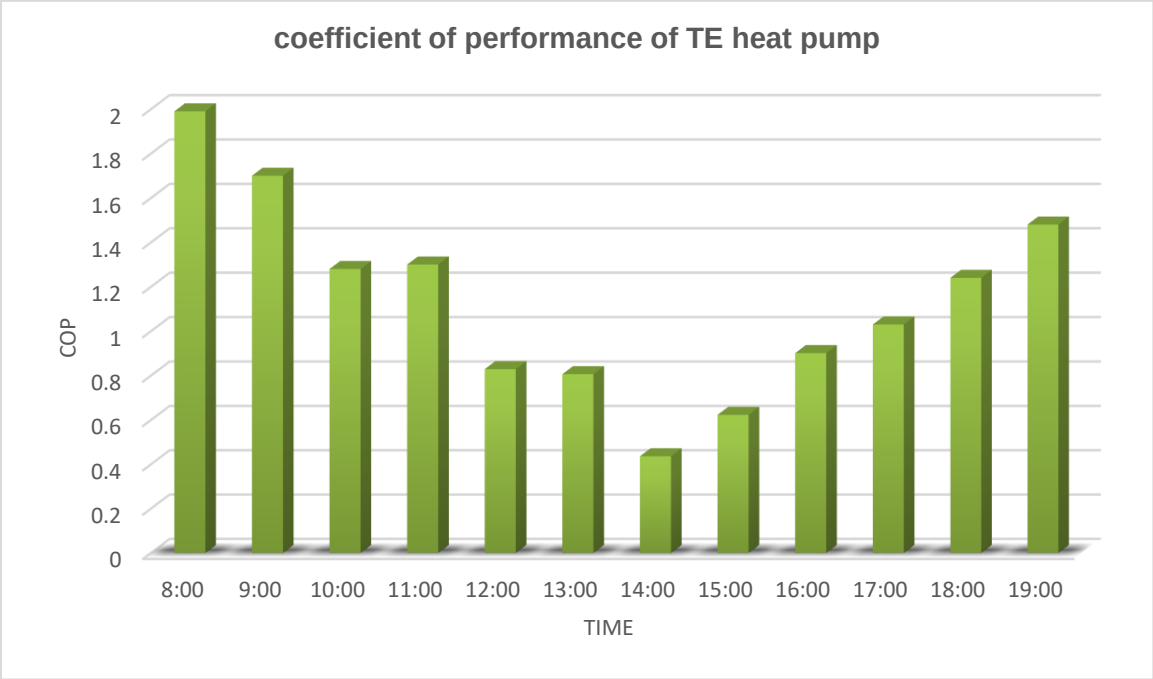

Figure 5. 34: The coefficient of performance of TE heat pump

The performance of the advanced still during a moderate night in May is indicated in Figure 5.35. The basin water temperature reached the desirable level (40 ºC) at 22:00. The highest value recorded was 51.6 ºC. The thermoelectric heat pump system was able to maintain the temperature around 50 ºC until the end of the experiment. The ambient temperature varied between 15.2 to 19 ºC. The average of temperature difference between the basin water and condensation surfaces was 23 ºC. As can be seen from the graph, the condensation took place at 21:30. The accumulated water yield at the end of the test was 1550 ml (3100 L/m^2).

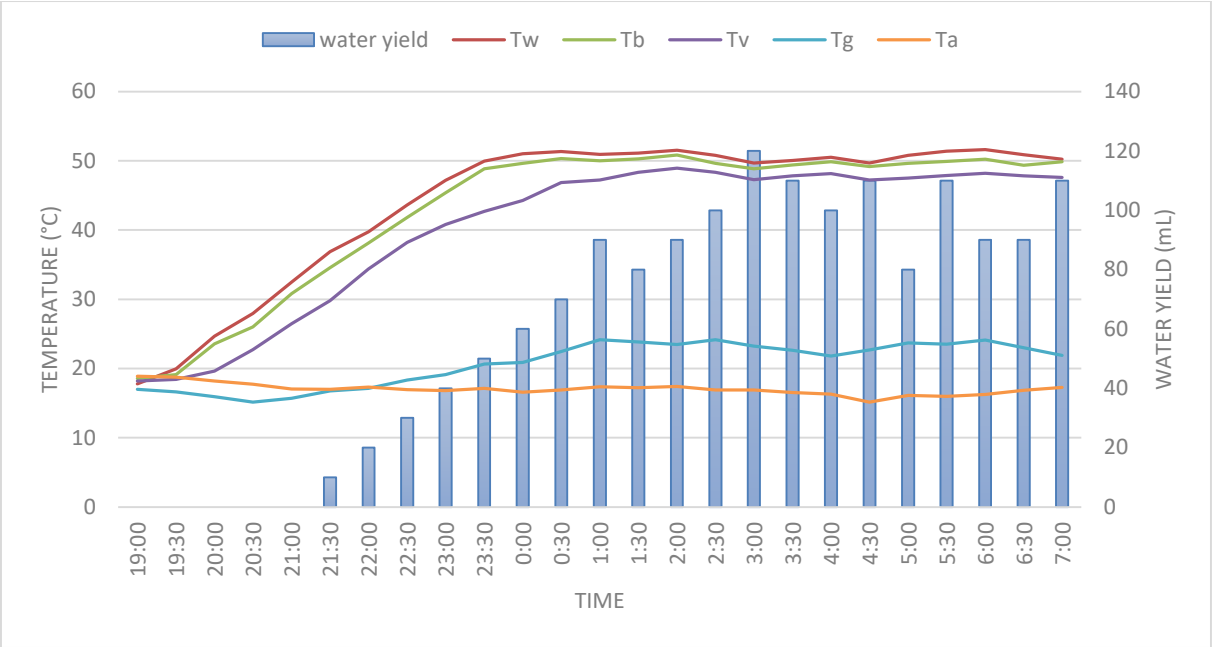

Figure 5. 35: Advanced solar still performance at night (May)

The performance of the advanced still during a relatively cold night in September is indicated in Figure 5.36. The basin water temperature reached 43 ºC at 23:00. The highest value recorded was 50.4 ºC. The thermoelectric heat pump system was able to maintain the temperature around 49 ºC until the end of the experiment. The ambient temperature varied between 11.4 to 16.4 ºC. The average of temperature difference between the basin water and condensation surfaces was 27 ºC. As can be seen from the graph, the condensation took place at 22:00. The accumulated water yield at the end of the test was 1180 ml (2360 L/m^2).

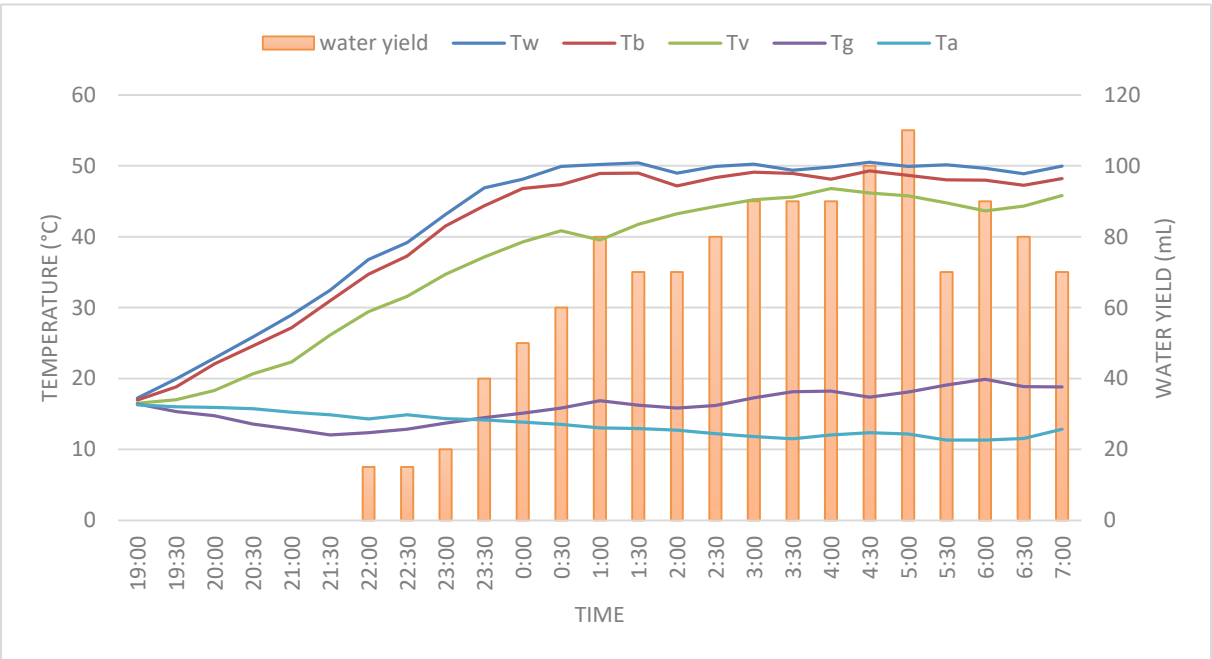

Figure 5. 36: Advanced solar still performance at night (September)

5.3.3. Analysis of the performance of the thermoelectric module

Laboratory experiments were performed in order to optimize the design of the thermoelectric heat pump system and obtain the maximum performance benefit. Different wiring and stacking configuration of the Peltier modules were tested, and multiple DC voltages and currents were applied. Furthermore, the effect of temperature difference on the COP of the thermoelectric heat pump system was investigated. In these tests, the coefficient of performance was determined according to the electric parameters (voltage, current and electrical resistance) and the thermoelectric effect properties (Seebeck coefficient, thermal conductivity and module's number and type). The variations in the cooling capacity (Q_c) and the COP of the TE heat pump system at multiple input current are presented in Figure 5.37.

It was observed that the inlet water temperature for hot and cold sides affected the cooling capacity (Q_c) and the efficiency (COP). In this regard, the cooling capacity of the heat pump system continuously declined with the increase of the inlet water temperature of the TE hot side.

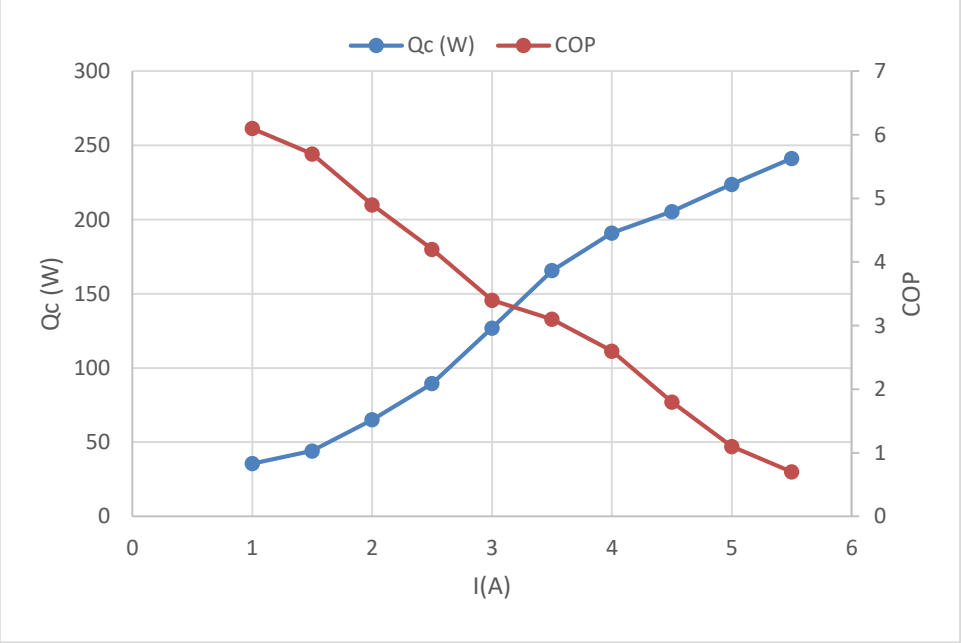

Figure 5. 37: Effect of input current on the performance of TE module

5.4 Seasonal performance of the solar stills

The seasonal performance of solar stills varies depending on the weather elements, especially the intensity of solar radiation and the ambient temperature. It was found that the conventional solar still performance fluctuated between low to zero water productivity in the winter season due to the low rate of solar radiation and cold ambient temperature. Therefore, two types of heat pump systems were proposed to be used as thermal energy recovery systems. The main purposes of the systems were to boost the

energy gain, maintain the temperature inside the still at the desired level and increase the temperature difference between the condensation surface and the basin water to increase the rate of the condensation. Due to an abundance of collected data, samples of the seasonal performance of solar stills are presented in this section in order to form a perspective on how each solar still performed in different seasons. Figures 5.38 and 5.39 show the performance of the advanced solar still based on a vapour compression heat pump and the conventional solar still in the summer season. As indicated in the first graph, the heat pump system was able to heat up the basin water to the desired level from 9:00 and the condensation took place early. The maximum water temperature recorded was 78 ºC on a hot summer day. The heat pump system was also able to maintain the temperature above 50 ºC until the end of the experimental period. The daily distillate yield varied from 5.8 to 6.3 L/m^2. In the second graph, the three-dimensional surface tends to have a gradual increase, peak and sharp decrease. The desirable temperature level and the condensation formation were achieved at 11:00, and the maximum temperature recorded was about 65 ºC. The temperature tended to decrease around 15:30 due to heat dissipation through the glazing material, and therefore the still stopped producing distillate water early. The daily distillate yield varied from 2.2 to 2.8 L/m^2. Note that the data presented as the solar stills' seasonal performance comparison was recorded at the same time for each solar still.

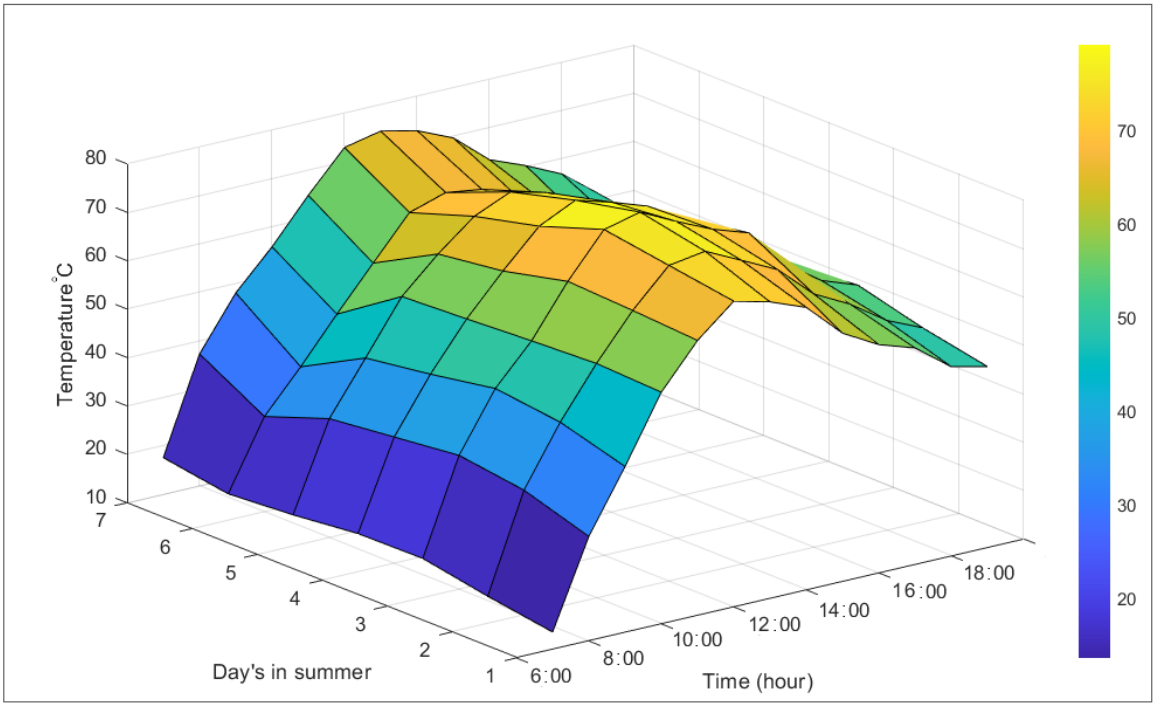

Figure 5. 38: Advanced still seasonal performance (summer)

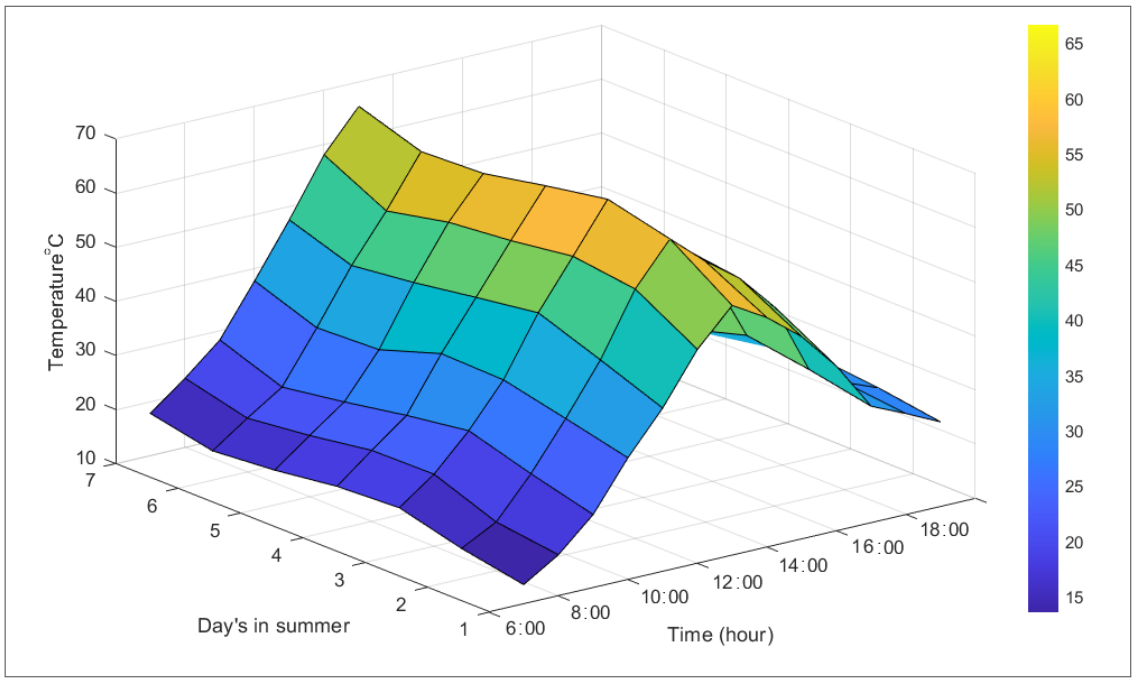

Figure 5. 39: Conventional still seasonal performance (summer)

Samples of seasonal performance data are presented in Figures 5.40 and 5.41. The data was collected in July 2020 (winter season in the southern hemisphere) in order to compare both stills in cold winter conditions. As can be seen in the graphs, the vapour compression heat pump system maintained the basin water temperature above 48 ºC until the end of the daily experimental test, and the maximum temperature achieved was 58 ºC. It was noticed that the daily distillate yield was satisfactory due to the high temperature difference between the condensation surface and contaminated water. The daily distillate yield average was 4.3 L/m^2.

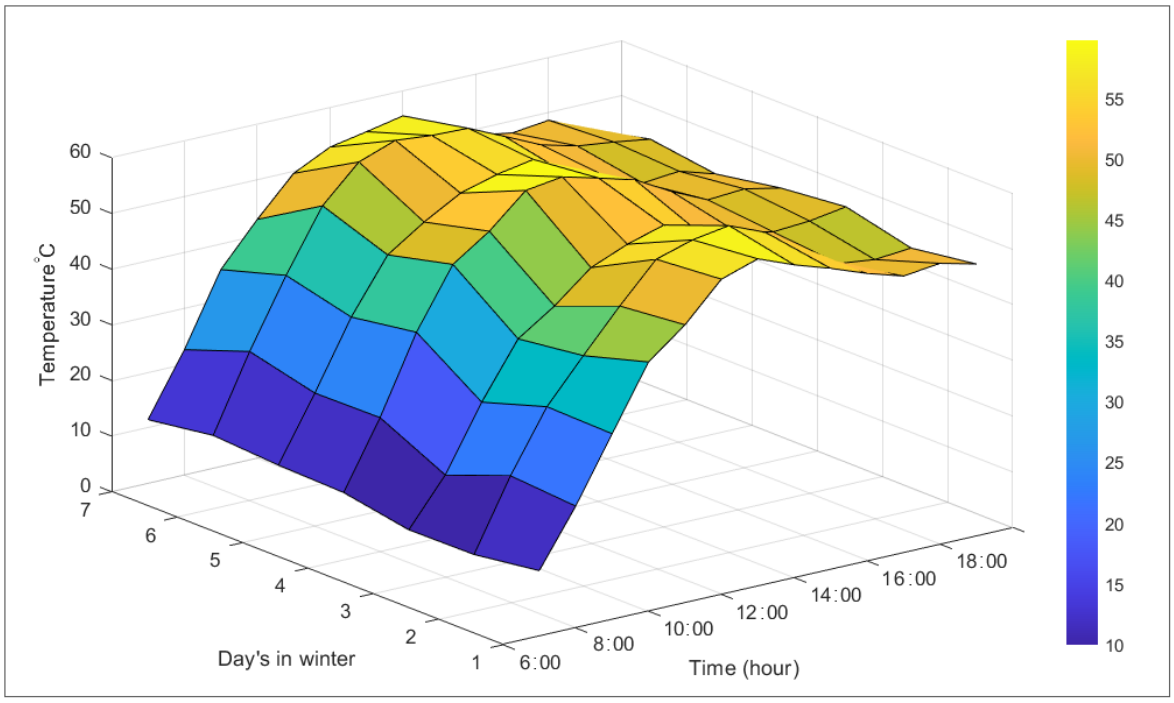

Figure 5. 40: Advanced still seasonal performance (winter)

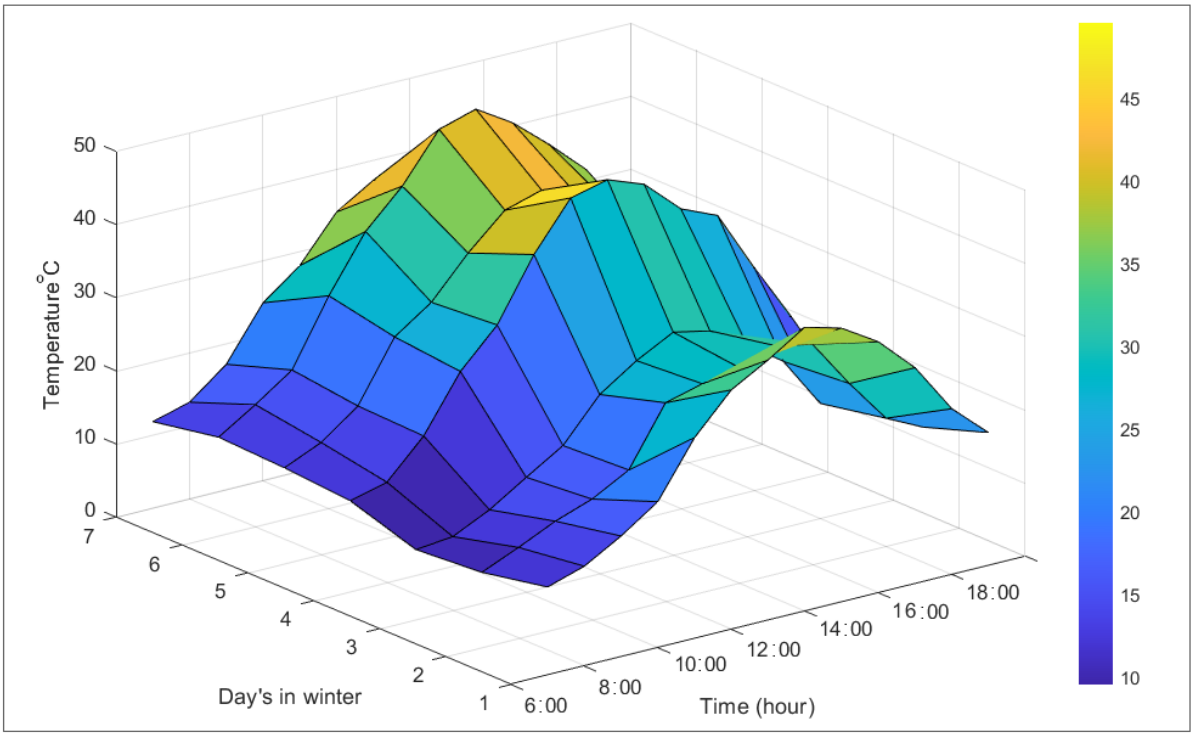

Figure 5. 41: Conventional still seasonal performance (winter)

On the other hand, the conventional still performed inefficiently on cold weather days. In cloudy and partly cloudy days, the distillate output was zero at the highest water temperature of 30 ºC. In July for instance, the maximum temperature recorded was about 47 ºC.

In winter, the temperature of the solar still integrated with thermoelectric heat pump system components had similar tendencies to the solar still integrated with vapour compression heat pump system, while in summer the solar still integrated with vapour compression heat pump system had a higher temperature trend.

As mentioned in the literature, that the driving force of the solar still is the rate of the temperature difference between the basin water and the condensation surfaces, therefore one of the important functions of utilizing a heat pump system in solar distillation technology is to cool down the condensation surface. It was found in this research work that the designed heat pump systems maintained the temperature difference at the desirable level by cooling down the condensation surface. Figure 5.42 shows the variation of the temperature trend for 7 moderate days of an experimental test of the solar still integrated with the thermoelectric heat pump system. The upper 3D surface represents the basin water temperature, while the lower one gives the condensation surface temperature.

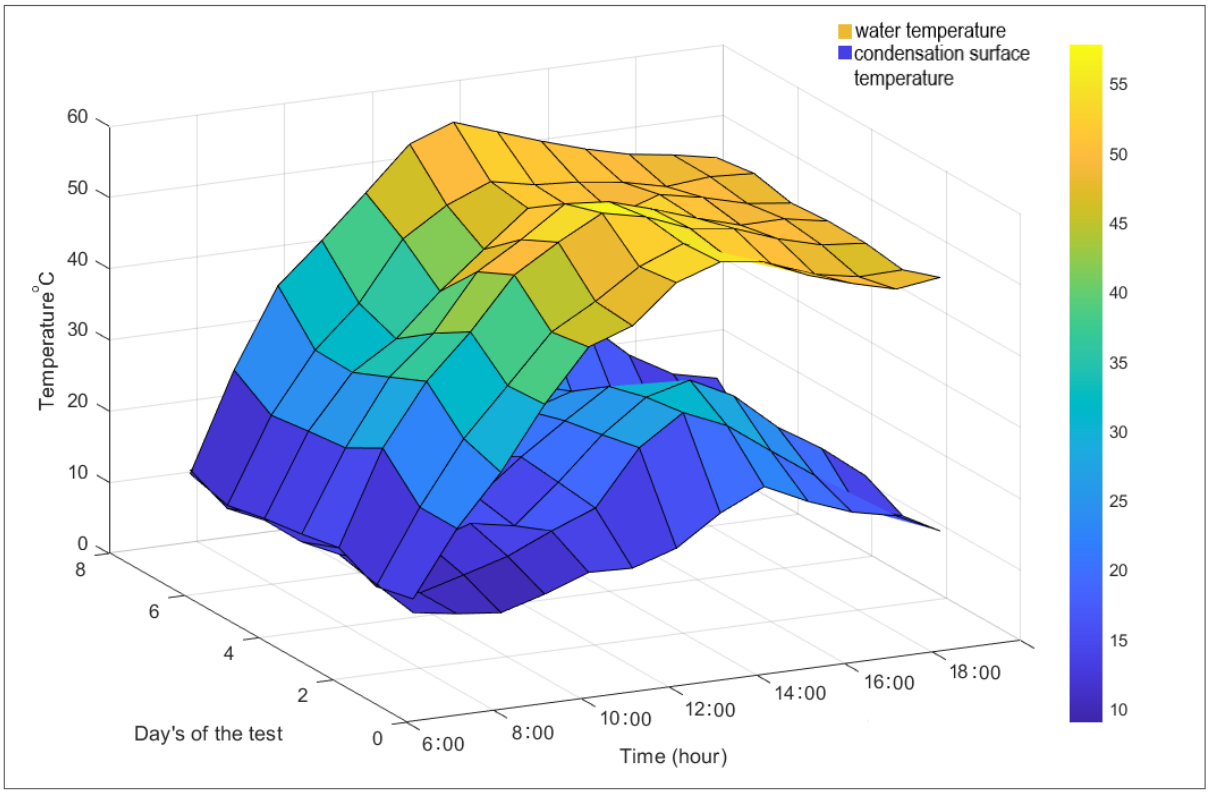

Figure 5. 42: The variation of temperature difference of the TE solar still

Chapter Six
Conclusion and Recommendation

6.1. Conclusion

Due to the rapid growth in population and modern life needs, the over-use of limited natural water resources has increased. In newly emerging and low-income countries, the provision of fresh water to the communities has become a great challenge to the authorities, local authorities and international organizations. In remote areas of such countries, access to clean water sources is limited due to the lack of infrastructure such as water treatment units, electric grids and water pipeline systems. Solar water treatment technologies are the most promising techniques to purify saline and brackish water. Solar distillation is one of the desalination technologies known to be a low-efficiency water treatment process. Therefore, this research work has presented a developed method to enhance the productivity of solar water distillation units. Two different types of heat pump systems were utilized to improve the efficiency of conventional solar still. The experimental study began with an outdoor test to evaluate the performance of a vapour compression heat pump system, then finished with laboratory and outdoor tests to study the performance of a thermoelectric heat pump system. The main functions of the heat pump systems are to:

- Pre-heat the basin water on sunny days so that condensation can take place early;
- Recover the thermal energy loss through the cover;
- Cool down the condensation surface to increase the temperature difference;
- Maintain the temperature inside the still at desirable level;
- Operate during cloudy and cold days and at night.

Two photovoltaic DC systems were designed and sized to power each system. Both PV systems were simple and reliable and were able to sustain the required load during early morning hours, cloudy days and night operation. The findings of the experimental work are concluded as follows:

6.1.1. Conventional solar still integrated with vapor compression heat pump system

Multiple experimental tests were performed to evaluate the performance of the solar still model integrated with vapour compression heat pump system. Outdoor experimental tests were done under different seasonal weather conditions. A weather station located at the site of the experiment was used to record weather elements data at a time interval of 15 minutes. The performance of the solar still was evaluated based on the fundamentals of thermodynamics and the principle heat transfer. The experiments and the results are outlined as follows:

- The results from the first test (testing the model without cooling the condensation surface) indicated that the maximum water temperature recorded on a clear sky day in April was about 73 ºC at peak incident solar radiation of 870 W/m^2 and the inner cover temperature reached 60 ºC due to lack of cooling process. The associated distillate harvest was 4.3 L/m^2.
- The main purpose of the second test was to investigate the effect of cooling down the condensation surface on the efficiency of the solar still. It was found that the greater the temperature difference between water and condensation surfaces, the more distillate could be extracted. The average of temperature difference was rated at about 35 ºC and the average COP of the heat pump system was 3.5. Despite the relatively low rate of the incident solar radiation at the maximum value of 630 W/m^2, the daily distillate yield was about 5.75 L/m^2.
- The results from the comparison between the conventional solar still and the advanced one indicated that on a typical day of November (summer season in the southern hemisphere), the water temperature in the advanced solar still reached 73 ºC while in conventional one it reached 57.5 ºC. The incident solar radiation peak was 1050 W/m^2 and the maximum ambient temperature was 33 ºC. The daily distillate yield was 6.21 and 2.67 L/m^2 for the advanced and conventional solar still respectively. In the winter season, the conventional solar still performed poorly in partly cloudy cold day: the maximum water temperature was about 38.5 ºC and the daily distillate yield was 0.215 L/m^2. The performance of the advanced still was satisfactory: the daily distillate yield was 4.2 L/m^2 at a maximum water temperature of 58.9 ºC.
- The results obtained from the night operation test indicated that the average distillate water yield in summer was 3.2 L/m^2 and the maximum water temperature was 54 ºC. While in winter, the night distillate yield was 2.7 L/m^2 and the maximum water temperature was 50 ºC.
- In typical summer day, the average of the efficiency of the conventional solar still was 20.77%, while the average of hourly efficiency of the advanced one was 63 %.
- Finally, the average COP of the heat pump 3.5. The average of beneficial thermal energy was 4.6 MJ for the advanced still and 3.1 MJ for the conventional still.

6.1.2. Conventional solar still integrated with thermoelectric heat pump system

A laboratory and outdoor test was conducted to evaluate the performance of the single-effect solar still integrated with the thermoelectric heat pump system. The purpose of

the laboratory test was to optimize the thermoelectric module stacking configuration and the optimal required voltage and current. The advanced solar still prototype was tested in two different seasons. The obtained results are outlined as follows:

- In moderate weather conditions in May, the results of the outdoor experiments showed that at incident solar radiation of 660 W/m^2 and the maximum ambient temperature of 26 ºC, the maximum basin water temperature was 60 ºC and the daily distillate yield was 2180 ml (4.36 L/m^2) for the advanced solar still, while the maximum basin water temperature was 53 ºC and the distillate yield was 1050 ml (2.1 L/m^2) for the conventional one.
- In September, on a relatively cold day the highest ambient temperature was 17.7 ºC and the peak of incident solar radiation was 530 W/m^2. The daily yield was 2350 ml (4.7 L/m^2) and the maximum basin water temperature achieved was 54.8 ºC. Regardless of the low average of the incident solar radiation and low ambient temperature, the daily yield was more than the daily yield in summer due to the higher temperature difference between the basin water and condensation surfaces in winter, which was rated at 24 ºC. The highest basin water temperature for the conventional solar still was 45.8 ºC and the accumulated distillate yield was 650 ml (1.3 L/m^2).
- The results of the advanced still during a moderate night in month of May showed that the highest basin water temperature was 51.6 ºC and the accumulated distillate yield was 1550 ml (3.1 L/m^2). On a relatively cold night, the basin water temperature achieved was 50 ºC and the accumulated distillate yield was 1180 ml (2.36 L/m^2).
- The maximum value of (COP) of the thermoelectric heat pump, according to energy balance equations and the principle of thermodynamics for a single-stage heat pump was about 1.9.

The overall outcome of these experimental tests indicated that both heat pump systems were able to preheat the water so that the condensation took place early, maintained the temperature at the desired level throughout the period of experiments and, therefore more distillate yield was extracted. In cold weather conditions and night operation, the performance of the advanced solar stills was efficient and satisfactory while the convention still performed inefficiently and poorly. Both types of heat pump systems can be integrated into the different types of passive solar still – simple modifications may be required for the thermoelectric heat pump layout to match the different designs of the solar stills.

6.2. Recommendations

To avoid calcification formation and corrosion, it is highly recommended to flush the system regularly. Also, maintaining the water temperature below 80 ºC is highly recommended in a sea water desalination process.

Brine is waste water produced from a solar distillation process. It is a highly concentrated solution of salt and heavy metals. Heating brine is an energy-intensive process, and therefore it is recommended that the recovery ratio should range between 50 % to 60 %.

In the case of medium scale solar distillation, brine may be diluted and discharged back to the water source at two different disposal points to avoid the problematic environmental issues associated with the high temperature and salinity of brine.

By looking at the design of vapour compression heat pump system, it can be noticed that the condenser is located inside the solar still, which means that the condensation temperature is relatively high. A simple modification can be made to increase the efficiency of the heat pump cycle. An additional refrigerant sub-cooler can be added to ensure that the hot liquid refrigerant is condensed before entering the throttling device and to avoid flash gas formation through it.

A cascade or multi-stage cycle needs to be investigated for the thermoelectric heat pump so that the coefficient of performance of the system may be boosted. Note that with a multi-stage configuration, the thermal analysis is complicated, and therefore a developed computer model is required.

An automated temperature control device needs to be developed that will avoid any possible thermal stress to the thermoelectric modules and ensure the longevity of the whole system.

It is crucial to use the appropriate materials to construct the solar still. Using inappropriate material in a component such as the coat of absorbing plate could affect the quality and the taste of distillate output.

Finally, public health is an ethical issue, therefore water quality is an important matter for human health. Hence, it should be emphasized that the use of solar distillation technology is suitable for low and medium contaminated water only. More advanced methods should be used for highly contaminated water.

Bibliography

Almusaied, Z. and Asiabanpour, B., 2017. Atmospheric water generation: Technologies and influential factors. In *IIE Annual Conference. Proceedings* (pp. 1448-1453). Institute of Industrial and Systems Engineers (IISE).

B. Asiabanpour, N. Ownby, M. Summers & F. Moghimi, "Atmospheric Water Generation and Energy Consumption: An Empirical Analysis," 2019 IEEE Texas Power and Energy Conference (TPEC), College Station, TX, USA, 2019, pp. 1-6, doi: 10.1109/TPEC.2019.8662164.

Engohang, A.D. & Kanyarusoke, K.E., 2018. Solar water purification: How helpful is double glazing? In Cape Town: 8.

Pauline, J. Koura Mbadinga& Kanyarusoke, K.E. 2015. A solar water purification system for rural areas. Cape Peninsula University of Technology. http://hdl.handle.net/20.500.11838/2612.

Peter, J & Kanyarusoke, K.E., 2019. Design optimisation of pillar-mounted sun tracking solar-water purifiers for large households. In 2019 International Conference on the Domestic Use of Energy (DUE). Wellington, South Africa, South Africa: IEEE: 8. https://ieeexplore.ieee.org/abstract/document/8734289.

References

Abdallah, S., Abu-Khader, M. M. & Badran, O., 2009. Effect of various absorbing materials on the thermal performance of solar stills. *desalination,* Issue 242, pp. 128-137.

Abdin, G. C. & Noussan, M., 2018. Electricity storage compared to net metering in residential PVapplications. *Cleaner Production,* Issue 167, pp. 175-186.

Ahuja, S., 2013. *Monitoring Water Quality: Pollution Assessment, Analysis, and Remediation.* 1st ed. Oxford: Newnes.

Al-Obaidi, M., Kara-Zaitri, C., & Mujtaba, I.M. 2020. Wastewater Treatment by Reverse Osmosis Process (1st ed.). CRC Press.

Alshahri, A. H., Fortunato, l., Ghaffour, N. & Leiknes, T., 2019. Advanced coagulation using in-situ generated liquid ferrate, Fe (VI), for enhanced pretreatment in seawater RO desalination during algal blooms. *science of the total environment ,* Volume 685, pp. 1193-1200.

Althouse, A. D., Turquist, C. H. & Bracciano, A. F., 2000. *Modren Refrigeration and Air Conditioning.* 8th ed. Illinois: The Goodheart-willcox Company, Inc..

Ambashta, R. & Sillanpää, M., 2010. Water purification using magnetic assistance. *Elsevier,* 180(1-3), pp. 38-49.

Anis, S. F., Hashaikeh, R. & Hilal, N., 2019. Reverse osmosis pretreatment technologies and future trends: Acomprehensive review. *Desalination,* Volume 452, pp. 159-195.

Ardani, K., Cook, J. J., Fu, R. & Margolis, R., 2018. *Cost-Reduction Roadmap for Residential Solar Photovoltaic (PV), 2017-2030,* Denver West: NREL.

Arora, R., Kaushik, S. & Arora, R., 2016. Thermodynamic modeling and multi-objective optimization of two stagethermoelectric generator in electrically series and parallel configuration. *Applied Thermal Engineering,* Volume 103, pp. 1312-1323.

Arzarello, D., 2014. *Makezine.* [Online]
Available at: https://makezine.com/2014/03/28/arduino-controlled-tec-coolingheating-system-for-beer-fermentation/
[Accessed 3 6 2021].

Azahar, Arman Hadi; Mohamad, Ramizah Amira; Harun, Mohamad Haniff; Abidin, Amar Faiz Zainal; Shah, Mohd Badril & Nor, Rozilawati Mohd l., 2020. Development and Evaluation of Stove Using Peltier Effect: Connection and Temperature Control. *Fluid Mechanics and Thermal Sciences,* 70(1), pp. 1-12.

Badran, O., 2007. Experimental study of the enhancement parameters on a single slope solar still productivity. *Desalination,* Issue 209, pp. 136-143.

Balasubramanian, R., 2020. Overview of the use of Peltier's modules in technology. *Modern Engineering ,* Volume 1, pp. 11-17.

Bartram, J. & Baum, R., 2015. Introduction. In: J. Bartram, ed. *Routledge Handbook of Water and Health.* NewYork: Routledge, pp. 1-13.

Bekbolet, M., 2011. Fundamentals of Advanced Oxidation Processes. In: V. Naddeo, L. Rizzo & V. Belgiorno, eds. *Water, Wastewater and Soil Treatment by Advanced Oxidation Processes.* Fisciano: Lulu.com, pp. 13-22.

Belessiotis, V., Kalogirou, S. & Delyannis, E. 2016. *Thermal Solar Desalination: Methods and Systems.* London: Elsevier.

Benjamin, M. M. & Lawler, D. F., 2013. *Water Quality Engineering: Physical / Chemical Treatment Processes.* 1st ed. New Jersey: John Wiley & Sons.

Bhardwaj, R., Kortenaar, M. V. & Mudde, R. F., 2013. Influence of condensation surface on solar distillation. *Desalination,* Issue 326, pp. 37-45.

Boyd, C. E., 2000. *Water Quality: An Introduction.* 1st ed. Alabama: Springer Science & Business Media.

Brodowicz, K., Dyakowski, T., Wyszynski, M. L. & Wyszynski, 2013. *Heat Pumps.* 2nd ed. Oxford: Elsevier.

Chamberlain, G., 2008. *Troubled Waters: Religion, Ethics, and the Global Water Crisis.* 1st ed. Maryland: Rowman & Littlefield.

Chellam, s., 2002. Air Stripping and Aeration. In: S. Lingireddy, ed. *Control of Microorganisms in Drinking Water.* Houston: ASCE Publications, pp. 93-104.

Chellaney, B., 2013. *Water: Asia's New Battleground.* 1st ed. Washington: Georgetown University Press.

Chen, H., Niu, H., Zhang, L., Xiong, Y., Zhai, H. and Nie, J., 2018. Performance testing of a heat pipe PV/T heat pump system under different working modes. *International Journal of Low-Carbon Technologies*, *13*(2), pp.177-183.

Chigor, V., Umoh, V. J., Okuofu, C. A., Ameh, J. B., Igbinosa, E. O., & Okoh, A. I. 2012. Water quality assessment: surface water sources used for drinking and irrigation in Zaria, Nigeria are a public health hazard. *Environmental Monitoring and Assessment,* 184(5), pp. 3389-3400.

Chong, M. N., Jin, B., Chow, C. W. & Saint, C., 2010. Recent developments in photocatalytic water treatment technology. *water research,* Issue 44, pp. 2997-3027.

Chua, H. & Rahimi, B., 2017. *Low Grade Heat Driven Multi-Effect Distillation and Desalination.* 1st ed. s.l.:Elsevier.

Chua, K., Chou, S. & Yang, W., 2010. Advances in heat pump systems: A review. *Applied Energy,* Volume 87, p. 3611–3624.

Chung, D., Horowitz, K. & Kurup, P., 2016. *On the Path to SunShot: Emerging Opportunities and Challenges in U.S. Solar Manufacturing,* s.l.: National Renewable Energy Laboratory NREL.

Clark, W., 2017. *Sustainable Cities and Communities Design.* 2nd ed. CA, United States: Butterworth-Heinemann.

Cooper, P., 1969. Digital simulation of transient solar still processes. *Solar Energy,* 3(12), pp. 313-331.

Crittenden, J. C. et al., 2012. *Water Treatment: Principles and Design.* 3rd ed. New Jersey: John Wiley & Sons.

Darre, N. C. & Toor, G. S., 2018. Desalination of Water: a Review. *Current Pollution Repotrs,* 2(4), pp. 104-111.

Darwish, M. A., 2013. Thermal desalination in GCC and possible development. *Desalination and Water Treatment,* Volume 52, pp. 27-47.

Das, Rasel; Ali, Eaqub; Abd hamid, Sharifah; Ramakrishna, Seeram & Chowdhury, Zaira., 2014. Carbon nanotube membranes for water purification: A bright future in water desalination. *Elsevier,* Volume 339, pp. 97-109.

De Garayo, S. D., Martínez, A., & Astrain, D. 2022. Optimal combination of an air-to-air thermoelectric heat pump with a heat recovery system to HVAC a passive house dwelling. Applied Energy, 309, 118443.

Detges, A., Pohl, B. & Adelphi, S., 2017. *reliefweb.* [Online]
Available at: https://reliefweb.int/report/world/editor-s-pick-10-violent-water-conflicts
[Accessed 2 October 2018].

Dincer, I. & Kanoglu, M., 2010. *REFRIGERATION SYSTEMS and APPLICATIONS.* 2nd ed. Chennai: John Wiley & Sons.

Duan, M., Sun, H., Lin, B., & Wu, Y. 2021. Evaluation on the applicability of thermoelectric air cooling systems for buildings with thermoelectric material optimization. Energy, 221, 119723.

Duffie, J. A. & Beckman, W. A., 2013. *Solar Engineering of Thermal Processes.* 4th ed. Wisconsin: John Wiley & Sons.

Ebrahimi, M. & Derakhshan, E., 2018. Design and evaluation of a micro combined cooling, heating, and power system based on polymer exchange membrane fuel cell and thermoelectric cooler. *Energy Conversion and Management,* Volume 171, pp. 507-517.

Eisenberg, T. N. & Middlebrooks, E. J., 2013. *Reverse Osmosis Treatment of Drinking Water.* Tennessee: Elsevier.

Eldalil, M. S., 2010. Improving the performance of solar still using vibratory harmonic effect. *Desalination,* Issue 251, pp. 3-11.

El-Dessouky, H. & Ettouney, H., 2002. *Fundamentals of Salt Water Desalination.* 1st ed. Amsterdam: Elsevier.

Elsaid, Khaled; Kamil, Mohammed; Sayed, Enas Taha; Abdelkareem, Mohammed Ali; Wilberforce & Tabbi; Olabi, A. 2020. Environmental impact of desalination technologies: A review. *Science of the Total Environment,* 748(141528).

El-Sebaii, A. A. 2000. Effect of wind speed on some designs of solar stills. *Energy Conversion & Management,* Issue 41, pp. 523-538.

El-Sebaii, A. & El-Bialy, E., 2015. Advanced designs of solar desalination systems. *Renewable and Sustainable Energy Reviews,* Issue 49, pp. 1198-1212.

Elsheikh, M. Hamid; Shnawah, D. Abdulameer; Sabri, M. Faizul Mohd; Said, Suhana Binti Mohd; Hassan, M. Haji; Bashir, M. Bashir Ali & Mohamad, M. 2014. A review on thermoelectric renewable energy: Principle parametersthat affect their performance. *Renewable and Sustainable Energy ,* Volume 30, pp. 337-355.

Enescu, D. & Virjoghe, E. O. 2014. A review on thermoelectric cooling parameters and performance. *Renewable and Sustainable Energy Reviews,* Volume 38, pp. 903-916.

Esfahani, I. J., Rashidi, J., Ifaei, P. & Yoo, C. 2016. Efficient thermal desalination technologies with renewable energy systems: A state-of-the-art review. *Korean Journal of Chemical Engineering,* 33(2), pp. 351-387.

Eslami, E., Tajeddini, F. & Etaati, N. 2018. Thermal analysis and optimization of a system for water harvesting from humid air using thermoelectric coolers. *Energy Conversion and Management,* Volume 174, pp. 417-429.

Estahbanati, Karimi; Feilizadeh, Mehrzad; Jafarpur, Khosrow; Feilizadeh, Mansoor & Rahimpour, Mohammad. 2015. Experimental investigation of a multi-effect active solar still: The effect of the number of stages. *Applied Energy,* Issue 137, pp. 46-55.

Feng, Y., Chen, L., Meng, F., & Sun, F. 2018. Influences of the Thomson effect on the performance of a thermoelectric generator-driven thermoelectric heat pump combined device. Entropy, 20(1), 29.

Ferrell, M., 2020. *undecided.* [Online]
Available at: https://undecidedmf.com/episodes/2020/7/23/exploring-solar-panel-efficiency-breakthroughs-in-2020
[Accessed 5 November 2020].

Ferrell, M., 2021. *UNDECIDED.* [Online]
Available at: https://undecidedmf.com/episodes/2021/2/17/exploring-passing-house-design-90-energy-savings
[Accessed 26 February 2021].

Forstmeier, M; Mannerheim, F; D'Amato, F; Shah, M; Liu, Yan; Baldea, M & Stella, Albert, 2006. Feasibility study on wind-powered desalination. *Desalination,* Volume 203, pp. 463-470.

Fraas, L. M., 2014. *low-cost solar electric power.* 1st ed. Bellevue: springer.

Gao, Yan-Wei; Meng, Jing-Hui; Liu, Hai-Bo; Chen, Wei-Hsin; Wang, Xiao-Dong. 2018. Transient supercooling behaviors of a novel two-stage Peltier cooler. *Applied Thermal Engineering,* Volume 143, pp. 248-256.

Garcia-Rodriguez, L., 2003. Renewable energy applications in desalination: state of the art. *Solar Energy,* Volume 75, pp. 381-393.

Gehrig, J. & Rogers, M. M., 2009. *Water and Conflict,* Baltimore: Catholic Relief Services.

Geisz, J. F; France, Ryan M; Schulte, Kevin L; Steiner, Myles A; Norman, Andrew G; Guthrey, Harvey L; Young, Matthew R; Song, Tao & Moriarty, Thomas., 2020. Six-junction III–V solar cells with 47.1% conversion efficiency under 143 Suns concentration. *Nature Energy,* Issue 5, pp. 326-335.

Ghalavand, Y., Hatamipour, M. & Rahimi, A., 2014. A review on energy consumption of desalination processes. *Desalination and Water Treatment,* 54(6), pp. 1526-1541.

Ghermandi, A. & Messalem, R., 2012. Solar-driven desalination with reverse osmosis: the state of the art. *Desalination and Water Treatment,* 7(1-3), pp. 285-296.

Ghoneyem, A. & lleri, A., 1997. Software to analyze solar stills and an experimental study on the effects of the cover. *Desalination,* Issue 114, pp. 37-44.

Gleick, P. H. & Heberger, M., 2011. The World's Water Volume 7. In: P. H. Gleick, ed. *World's Water.* s.l.:Island Press/Center for Resource Economics, pp. 159-171.

Gleick, P. H. Wolff, Gary H; Cooley, H; Palaniappan, M; Samulon, A; Lee, E; Morrison, J & Katz, D, 2006. *The World's Water 2006-2007: The Biennial Report on Fresh water Resources.* Oakland: Island Press.

Goldsmid, H. J. 2021. Improving the thermoelectric figure of merit. Science and Technology of Advanced Materials, 22(1), 280-284.

Hamed, O. A., 2005. Overview of hybrid desalination systems — current status and future prospects. *Desalination,* 186(1-3), pp. 207-214.

He, Y. L., Qiu, Y., Wang, K., Yuan, F., Wang, W. Q., Li, M. J., & Guo, J. Q. 2020. Perspective of concentrating solar power. Energy, 198, 117373.

Hepbasli, a. & Kalinci, Y., 2009. A review of heat pump water heating systems. *Renewable and Sustainable Energy Reviews,* Volume 13, p. 1211–1229.

IEA & PVPS, 2015. *Energy from the Desert: Very Large Scale PV Power Plants for Shifting to Renewable Energy Future,* s.l.: IEA.

Introini, V. & Kos, D., 2018. *Temperature Controlled Container for Sample Transportation.* [Online]
Available at: https://create.arduino.cc/projecthub/viola-introini/temperature-controlled-container-for-sample-transportation-3e0155
[Accessed 3 6 2021].

Inyinbor Adejumoke, A., Adebesin Babatunde, O., Oluyori Abimbola, P., Adelani Akande Tabitha, A., Dada Adewumi, O., & Oreofe Toyin, A. 2018. Water pollution: effects, prevention, and climatic impact. Water Challenges of an Urbanizing World, 33, 33-47.

Jarimi, H., Powell, R. & Riffat, S., 2020. Review of sustainable methods for atmospheric water harvesting. *International Journal of Low-Carbon Technologies,* 12(2), pp. 253-276.

Jones-Albertus, R. Feldman, D; Fu, R; Horowitz, K & Woodhous, Michael, 2016. Technology advances needed for photovoltaics to achieve widespread grid price parity. *Progress in photovoltaic,* Issue 24, pp. 1272-1283.

Jones, E; Qadir, M; Vliet, Michelle T.H. van; Smakhtin, V & Kang, Seong-mu 2019. The state of desalination and brine production: A global outlook. *Science of the Total Environment,* Issue 657, pp. 1343-1365.

Joshi, V. P. Joshi, V S, Kothari, H A; Mahajan, M D; Chaudhari, M B & Sant, K D. 2017. Experimental investigations on a portable fresh water generator using a thermoelectric cooler. *Energy Procedia,* Volume 109, pp. 161-166.

Jradi, M., Ghaddar, N. & Ghali, K. 2012. Experimental and theoretical study of an integratedthermoelectric–photovoltaic system for airdehumidification and fresh water production. *INTERNATIONAL JOURNAL OF ENERGY RESEARCH,* Volume 36, pp. 963-974.

Kabeel, A. & El-Agouz, S. 2011. Review of researches and developments on solar stills. *Desalination ,* 1-3(276), pp. 1-12.

Kalita, P., Dewan, A., & Borah, S. (2016). A review on recent developments in solar distillation units. Sadhana, 41(2), 203-223.

Kalogirou, S. A., 2005. Seawater desalination using renewable energy sources. *Progress in Energy and Combustion Science ,* Issue 31, pp. 242-281.

Kampf, J. & Clarke, B., 2013. How robust is the environmental impact assessment process in SouthAustralia? Behind the scenes of the Adelaide seawater desalination project. *Marine Policy,* Volume 38, pp. 50-56.

Kanyarusoke, K., 2018. Solar water purifiers for small rural African homesteads: Evaluation of alternative designs. *IOP Conference Series: Earth and Environmental Science,* 188(1).

Kati, M. & Angelo, M., 2010. water quality regulations and policy development. In: Y. Li & M. Kati, eds. *Water Quality Concepts, Sampling, and Analyses.* 1st ed. New York: CRC Press, pp. 11-21.

Khawaji, A. D., Kutubkhanah, I. K. & Wie, J.-M., 2008. Advances in seawater desalination technologies. *Elsevier,* Issue 221, pp. 47-69.

Khechekhouche, A; Benhaoua, B; Manokar, A. M; Kabeel, Abd Elnaby & Sathyamurthy, R. 2019. Exploitation of an insulated air chamber as a glazed cover of a conventional solar still. *heat transfer-asian research,* 5(48), pp. 1563-1574.

Kiatsiriroat, K., Bhattacharya, S. C. & Wibulswas, P., 1987. Performance Analysis of Multiple Effect Vertical Still with a Flat Plate Collector. *solar & wind technology,* 4(4), pp. 451-457.

Kosmopoulos, P; Kazadis, S; Lagouvardos, K; Kotroni, V & Bais, A. 2015. Solar energy prediction and verification using operational model forecasts and ground-based solar measurements. *Energy,* 2(93), pp. 1918 - 1930.

Kotb, A., Elsheniti, M. B., & Elsamni, O. A. 2019. Optimum number and arrangement of evacuated-tube solar collectors under various operating conditions. Energy Conversion and Management, 199, 112032.

Krantzberg, G., 2010. *Advances in Water Quality Control.* 1st ed. NewYork: ScientificResearchPublishing.

Kumar, P. M; Babu, V. Jagadeesh; Subramanian, A; Bandla, A; Thakor, N; Ramakrishna, S & Wei, He. 2020. The Design of a Thermoelectric Generator and Its Medical Applications. *designs ,* 4(8), pp. 2-26.

Kumar, P. V., Kumar, A., Prakash, O. & Kaviti, A., 2015. Solar stills system design: A review. *Renewable and Sustainable Energy Reviews,* Issue 21, pp. 153-181.

lee, H. S., 2017. *Thermoelectrics: Design and Materials.* 1st ed. Mishigan: John Wiley & Sons,.

Lenaidic, D., 2016. *Power China 2020.* [Online]
Available at: http://www.pvresources.com/en/about.php
[Accessed 4 November 2020].

Lewisvile, C., 1999. *altestore.* [Online]
Available at: https://www.altestore.com/store/calculators/off_grid_calculator/
[Accessed 18 September 2020].

Liang, R., Hu, A. H.-F. M. & Zhou, N., 2014. Fundamental on Adsorption, Membrane Filtration, and Advanced Oxidation Processes for Water Treatment. In: A. Hu & A. Apblett, eds. *Nanotechnology for Water Treatment and Purification.* New York: Springer, pp. 1-44.

Li, H. & Sun, Y., 2019. Performance optimization and benefit analyses of a photovoltaic loopheat pipe/solar assisted heat pump water heating system. *Renewable Energy,* Volume 134, pp. 1240-1247.

Liu, S., He, W., Hu, D., Lv, S., Chen, D., Wi, X., Xu, F & Li, S., 2017. Experimental analysis of a portable atmospheric water generator by thermoelectric cooling method. *Energy Procedia,* Volume 142, pp. 1609-1614.

Lof, G. O. G., Eibling, J. A. & Bloemer, J. W., 1961. Energy balances in solar distillers. *AlChE journal,* 7(4), pp. 641-649.

Lotatidou, S., Mavukkandy, M., Chakraborty, S. & Arafat, H., 2017. what is sustainable desalination. In: H. Arafat, ed. *Desalination Sustainability: A Technical, Socioeconomic, and Environmental Approach.* s.l.:Elsevier, pp. 4-29.

Lovegrove, K. & Stein, W., 2012. *Concentrating solar power technology.* 1st ed. Cambridge: Woodhead Publishing.

Magrini, A., Cattani, L., Cartesegna, M. and Magnani, L., 2015. Integrated systems for air conditioning and production of drinking water–Preliminary considerations. *Energy Procedia*, *75*, pp.1659-1665.

Manabe, Y. 2016. Application of DERs in electricity market. In: T. Funabashi, ed. *Integration of Distributed Energy Resources in Power Systems: Implementation, Operation and Control.* Nagoya: Academic Press, pp. 295-302.

Markham, D., 2020. source. [Online]
Available at: https://www.source.co/how-hydropanels-work/ &
https://www.treehugger.com/solar-hydropanel-can-pull-liters-drinking-water-day-out-air-4858522
[Accessed 22 September 2020].

May, G. J., Davidson, A. & Monahov, B., 2018. Lead batteries for utility energy storage: A review. *Energy Storage,* Issue 15, pp. 145-157.

Meng, F., Chen, L., Sun, F. & Wu, C., 2009. Thermodynamic analysis and optimisation of a new-type thermoelectric heat pump driven by a thermoelectric generator. *International Journal of Ambient Energy,* 30(2), pp. 95-101.

Mengmeng, W; Houcheng, Z; Jiapei, Z; Fu, W & Jinliang, Y. 2018. Performance analyzes of an integrated phosphoric acid fuel cell and thermoelectric device system for power and cooling cogeneration. *International Journal of Refrigeration,* Volume 89, pp. 61-69.

Mertens, K. 2014. *Photovoltaics Fundamentals, Technology and Practice.* 1st ed. West Sussex: Wiley.

Min, G. 2018. Thermoelectric Module Design Theories. In: D. M. Rowe, ed. *Thermoelectrics Handbook: Macro to Nano.* s.l.:CRC Press, pp. 11.1-11.14.

Moghimi, F., Ghoddusi, H., Asiabanpour, B. & Behroozikhah, M. 2021. Is atmospheric water generation an economically viable solution?. *Clean Technologies and Environmental Policy,* pp. 1-18.

Mohamed, A. M. O. & Bicer, Y. 2019. Integration of pressure retarded osmosis in the solar ponds for desalination and photo-assisted chloralkali processes: Energy and exergy analysis. *Energy Conversion and Management,* Volume 195, pp. 630-640.

Mohamed, E., Riffat, S. & Omer, S., 2017. Low-temperature solar-plate-assisted heat pump: A developed design for domestic applications in cold climate. *International Journal of Refrigeration,* Volume 81, pp. 134-150.

Morillo, J; Usero, J; Rosado, D; El Bakouri, H; Riaza, A & Bernaola, Francisco-Javier. 2014. Comparative study of brine management technologies for desalination plants. *Desalination,* Volume 336, pp. 32-49.

Mukerjee, A. K. & Thakur, N., 2011. *photovoltaic system: analysis and design.* 1st ed. New Delhi: PHI Learning Pvt. Ltd.

Muñoz-García, M. A., Moreda, G. P., Raga-Arroyo, M. P. & Marín-González, O., 2013. Water harvesting for young trees using Peltier modules powered by photovoltaic solar energy. *Computers and Electronics in Agriculture,* Volume 93, pp. 60-67.

Nami, H., Nemati, A., Yari, M. & Ranjbar, F., 2017. A comprehensive thermodynamic and exergoeconomic comparisonbetween single- and two-stage thermoelectric cooler and heater. *Applied Thermal Engineering,* Volume 124, pp. 756-766.

Narasimhan, V., Jiang, D. & Yong Park, S., 2016. Design and optical analyses of an arrayed microfluidic tunable prism panel for enhancing solar energy collection. *Applied Energy,* Issue 162, pp. 450-459.

Neksa, P., 2002. CO2 Heat Pump Systems. *International Journal of Refrigeration,* Volume 25, pp. 421-427.

Nohay, J. A; De Belen, J. Karl; Claros, J. Vernon; Lupo, R. Benjo; Jennifer, A Benedict Barrato; Dela Cruz, Jennifer C; Amado, Timothy M & Manuel, M. Christian. 2020. Design and Fabrication of a Portable Solar Powered Thermoelectric Refrigerator for Insulin Storage. *IEEE Xplore,* 183(106581).

O'shaughnessy, E., Nemet, G. F., Pless, J. & Margolis, R., 2019. Contents lists available atScienceDirectEnergy PolicyjouAddressing the soft cost challenge in U.S. small-scale solar PV system pricing. *Energy Policy,* 110956(134).

Panchal, H., 2016. Performance Investigation on Variations of Glass Cover Thickness on Solar Still: Experimental and Theoretical Analysis. *Technology and Economics of Smart Grids and Sustainable Energy,* 1(1), pp. 1-11.

Panchal, H. & Shah, P. K., 2012. Investigation on solar stills having floating plates. *International Journal of Energy and Environmental Engineering,* 3(8).

Pandey, P., Prakash, O. & Kumar, A., 2019. Desalination and Solar Still: Boon to Earth. In: A. Kumar & O. Prakash, eds. *Solar Desalination Technology.* Singapore: Springer, pp. 1-25.

Pathak, A. C. K; Kapil, C; Har, Mohan Singh; V. V. Tyagi; Richa Kothari, S Anand & A. K. Pandey. 2019. Role of Solar Energy applications for Environmental Sustainability. In: R. C. Sobti, N. K. Arora & R. Kothari, eds. *Environmental Biotechnology: For Sustainable Future.* s.l.: Singapore, Springer, pp. 342-370.

Perez, R; Ineichen, P; Seals, R; Michalsky, J & Stewart, R. 1990. Modeling daylight availability and irradiance components from direct and global irradiance. *Solar Energy,* 44(5), pp. 271-289.

Perk, M., 2013. *Soil and Water Contamination.* 2nd ed. London: CRC Press.

Phadatare, M. K. & Verma, S. K., 2007. Influence of water depth on internal heat and mass transfer in a plastic solar still. *Desalination ,* Issue 217, pp. 267-275.

Pourkiaei, S.M., Ahmadi, M.H., Sadeghzadeh, M., Moosavi, S., Pourfayaz, F., Chen, L., Yazdi, M.A.P. and Kumar, R., 2019. Thermoelectric cooler and thermoelectric

generator devices: A review of present and potential applications, modeling and materials. *Energy*, 186, p. 115849.

Qasim, M., Badrelzaman, M., Darwish, N. N. & Darwish, N. A., 2019. Reverse osmosis desalination: A state-of-the-art review. *Desalination,* Issue 459, pp. 59-104.

Rajamanickam, M. R. & Ragupathy, A., 2012. Influence of Water Depth on Internal Heat and Mass Transfer in a Double Slope Solar Still. *Energy Procedia,* Issue 14, pp. 1701-1708.

Rois, P. (2007). Thermodynamic solar energy: Energy saving and efficiency. Solar PST. Retrieved November 11, 2021, from http://www.solarpst.com/files/Catalgo_PST_EN.pdf

Rottman, G., Woods, T. & George, V., 2007. *The Solar Radiation and Climate Experiment (SORCE).* 2nd ed. s.l.:Springer Science & Business Media.

Saifizi, M., Zakaria, M. S., Yaacob, S. & WAN, K., 2018. *Development and Analysis of Hybrid Thermoelectric Refrigerator Systems.* s.l., IOP Conference Series: Materials Science and Engineering 318.

Sampathkumar, K. & Senthilkumar, P., 2012. Utilization of solar water heater in a single basin solar still—An experimental study. *Desalination,* Issue 297, pp. 8-19.

Selvaraj, K. & Natarajan, A., 2018. Factors influencing the performance and productivity of solar stills - A review. *Desalination,* Issue 435, pp. 181-187.

Semiat, R., 2008. Energy Issues in Desalination Processes. *Environmental Science & Technology ,* 42(22), pp. 8193-8201.

Sethi, S. & Wetterau, G., 2011. Seawater Desalination Overview. In: G. Wetterau, ed. *Desalination of Seawater.* Denver: American Water Works Association, pp. 1-15.

Shammas, N. K., Kumar, I. J., Chang, S.-Y. & Hung, Y.-T., 2007. Sedimentation. In: L. K. Wang, Y. Hung & N. K. Shammas, eds. *Physicochemical Treatment Processes.* s.l.:Springer Science & Business Media, pp. 380-395.

Shammas, N. K. & Wank, L. K., 2016. *Water Engineering.* 1st ed. New Jersey: John Wiley & Sons.

She, X., Yin, Y. & Zhang, X., 2014. Thermodynamic analysis of a novel energy-efficient refrigeration systemsubcooled by liquid desiccant dehumidification and evaporation. *Energy Conversion and Management,* Volume 78, pp. 286-296.

Shourideh, A. H; Ajram, W. Bou; Al Lami, J; Haggag, S & Mansouri, A. 2018. A comprehensive study of an atmospheric water generator using Peltier effect. *Thermal Science and Engineering Progress,* Volume 6, pp. 14-26.

Silberstein, E., 2015. *Heat Pumps.* 2nd ed. Boston: Cengage Learning.

Singh, G. & Tiwari, G., 2004. Monthly performance of passive and active solar stills for different Indian climatic conditions. *Desalination ,* Issue 168, pp. 145-150.

Solís-Chaves, J. S; Rocha-Osorio, C M; Murari, A L L; Lira, V. Martins & Filho, A. Sguarezi. 2018. Extracting potable water from humid air plus electric wind generation: A possible application for a Brazilian prototype. *Renewable Energy,* Volume 121, pp. 102-115.

Srinivasan, V, Lambin, E.F., Gorelick, S.M., Thompson, B.H & Rozelle, S. 2012. The nature and causes of the global water crisis: Syndromes from a meta-analysis of coupled human-water studies. *Water resources research,* Volume 48 (10).

Sun, Y., Di, C. A., Xu, W. & Zhu, D., 2019. Advances in n-Type Organic Thermoelectric Materials and Devices. *Advanced Electronic Materials,* 5(11).

Sutzkover-Gutman, I. & Hasson, D., 2010. Feed water pretreatment for desalination plants. *Desalination,* 264(3), pp. 289-296.

Talbert, S. G., Eibling, J. A. & Loef, G. o., 1970. *manual on solar distillation of saline water,* Florida: united states department of the interior .

Tan, H., Fu, H., & Yu, J. (2017). Evaluating optimal cooling temperature of a single-stage thermoelectric cooler using thermodynamic second law. Applied Thermal Engineering, 123, pp. 845-851.

Tanaka, H., 2009. Experimental study of a basin type solar still with internal and external reflectors in winter. *desalination,* Issue 249, pp. 130-134.

Tani, J. i. & Kido, H., 2005. Thermoelectric properties of Bi-doped Mg2Si semiconductors. *Physica B: Condensed Matter,* 364(1-4), pp. 218-224.

Tassou, S. A., Lewis, J. S., Ge, Y. T., Hadawey, A., & Chaer, I. 2010. A review of emerging technologies for food refrigeration applications. *Applied Thermal Engineering,* 30(4), pp. 263-276.

Thairu, L., 2018. *The Importance of Water.* [Online]
Available at: https://www.africa.com/importance-water-waterislife/
[Accessed 26 July 2018].

Tiwari, G., 2002. *solar energy fundamentals, design, modelling and applications.* 1st ed. New Delhi: Narosa Publishing house.

Tiwari, G. N. & Singh, H. N., 2009. Solar Distillation . In: J. Blanoo & S. Malato, eds. *Solar Energy Conversion and Photoenergy System - Volume II.* s.l.:EOLSS Publications, pp. 1-66.

Tiwari, G. & Sahota, L., 2017. *Advanced Solar-Distillation Systems: Basic Principles, Thermal Modeling, and Its Application.* 1st ed. Singapore: Springer.

Tsubota, T., Ohno, T., Shiraishi, N. & Miyazaki, Y., 2008. Thermoelectric properties of Sn1−x−yTiySbxO2 ceramics. *Journal of Alloys and Compounds,* 463(1-2), pp. 288-293.

Tu, R. & Hwang, Y., 2019. Performance analyses of a new system for water harvesting from moist air cycles tha tcombines multi-stagedesiccant wheels and vapo rcompression. *Energy Conversion and Management,* Volume 198, p. 111811.

Tu, R. & Hwang, Y., 2020. Reviews of atmospheric water harvesting technologies. *Energy,* Volume 201, p. 117630.

Tu, R. & liu, L., 2019. *Performance Evaluations of Extracting Water From Dry Air Using Multi-Stage Desiccant Wheels and Vapor Compression Cycle.* Washington, USA, ASME 2019 Heat Transfer Summer Conference.

Velmurugan, V., Kumar, K. J., Noorul Haq, T. & Srithar, K., 2009. Performance analysis in stepped solar still for effluent desalination. *Energy,* Issue 34, pp. 1179-1186.

Voutchkov, N., 2018. Energy use for membrane seawater desalination – current status and trends. *Desalination,* Volume 431, pp. 2-14.

Wang, G., Zhao, Y., Quan, Z. & Tong, J., 2018. Application of a multi-function solar-heat pump system in residential buildings. *Applied Thermal Engineering,* Volume 130, pp. 922-937.

Wang, H., Mccarty, R., Salvador, James. R., Yamamoto, Atsushi & Konig, Jan. 2014. Determination of Thermoelectric Module Efficiency: A Survey. *Electronic Materials,* 43(6), pp. 2274-2286.

WHO, 2008. *guidelines for driking water quality,* Geneva: world health organization .

WHO, U. a., 2015. *Progress on Sanitation and Drinking Water: 2015 Update and MDG Assessment,* USA: UNICEF.

Woldai, A., 2015. *Multi-Stage Flash Desalination: Modeling, Simulation, and Adaptive Control.* 1st ed. New York: CRC Press.

Xi, C., Lin, L. & Hongxing, Y., 2011. Long term operation of a solar assisted ground coupled heat pump system for space heating and domestic hot water. *Energy and Buildings,* Volume 43, pp. 1835-1844.

Xuan, X. C., 2003. Investigation of thermal contact effect on thermoelectric coolers. *Energy Conversion and Management ,* Volume 44, pp. 399-410.

Xu, P., Cath, T. Y., Robertson, A. P., Reinhard, M., Leckie, J. O., & Drewes, J. E. 2013. Critical Review of Desalination Concentrate Management, Treatment and Beneficial Use. *Environmental Engineering Science,* 30(8), pp. 502-514.

Yamashita, O., 2008. Effect of temperature dependence of electrical resistivity on the cooling performance of a single thermoelectric element. *Applied Energy,* 85(10), pp. 1002-1014.

Yamashita, O., 2009. Effect of linear and non-linear components in the temperature dependences of thermoelectric properties on the cooling performance. *Applied Energy,* 86(9), pp. 1746-1756.

Yao, Y., Sun, Y., Sun, D., Sang, C., Sun, M., Shen, L. and Chen, H. 2017. Optimization design and experimental study of thermoelectricdehumidifier. *Applied Thermal Engineering,* Volume 123, pp. 820-829.

Yokoyama, R., Shimizu, T., Ito, K. & Takemura, K., 2007. Influence of ambient temperatures on performance of a CO2 heat pump water heating system. *Energy,* Volume 32, pp. 388-398.

Young, G. W., 2011. *young ideas.* [Online]
Available at: http://www.youngideas.info/index.html
[Accessed 4 November 2020].

Yu, C., 2011. *China's water crisis needs more than words,* Beijing: Macmillan .

Zanganeh, P., Goharrizi, A. S., Ayatollahi, S., Feilizadeh, M., & Dashti, H. (2020). Efficiency improvement of solar stills through wettability alteration of the condensation surface: An experimental study. Applied Energy, 268, 114923.

Zaragoza, G., Alarcon, D. & Blanco, J., 2012. use of passive solar thermal energy for fresh water production . In: J. Bundschuh & J. Hoinkis, eds. *Renewable Energy Applications for Fresh water Production.* s.l.:CRC Press, pp. 79-101.

Zarzo, D. & Prats, D., 2018. Desalination and energy consumption. What can we expect in the near future?. *Desalination,* Volume 427, pp. 1-9.

Zhang, R., Zang, R. & Liu, J., 2016. Study on properties of water extraction from cooled air system under all operating conditions. *Cryogenics&Superconductivity,* 44(1), pp. 51-55.

Zhang, X., Zhao, X., Xu, J. & Yu, X., 2013. Characterization of a solar photovoltaic/loop-heat-pipe heat pump waterheating system. *Applied Energy,* Volume 102, pp. 1229-1245.

Zheng, H., 2017. *Solar Energy Desalination Technology.* 1st ed. Beijing: Elsevier.

Zhu, L., Tan, H. & Yu, J., 2013. Analysis on optimal heat exchanger size of thermoelectric cooler for electronic cooling applications. *Energy Conversion and Management,* Volume 86, pp. 685-690.

Zhu, Y., Wang, C., Wang, H., Su, W., Liu, J. and Li, J. 2014. Influence of Dy/Bi dual doping on thermoelectric performance of CaMnO3 ceramics. *Materials Chemistry and Physics,* 144(3), pp. 385-389.

Zolfagharkhani, S., Zamen, M. & Shahmardan, M. M. 2018. Thermodynamic analysis and evaluation of a gas compression refrigeration cycle for fresh water production from atmospheric air. *Energy Conversion and Management,* Volume 170, pp. 97-107.

Zsiborács, H., Hegedűsné Baranyai, N., Vincze, A., Háber, I. and Pintér, G. 2018. Economic and technical aspects of flexible storage photovoltaic systems in europe. *Energies*, *11*(6), p.1445.

APPENDICES

Appendix A: Technical Data of Hermetic Brushless DC Motor-Compressor (DC 12/24V)

- Compressor specification

Model	QDZH35G
Power supply	DC 12/24 V
Refrigerant	R134a
Throttle device	Capillary
Motor type	Brushless
Ambient temperature	0~43℃
Evaporation temperature	-35~-10℃
Max discharge pressure	3.24Mpa
Max winding temperature	130 ℃
Max condensing temperature	68 ℃
Max housing temperature	95 ℃
Max discharge temperature	110 ℃
Controller ambient temperature	63 ℃
Oil style	Ester oil
Oil density	0.951g/ml(15 ^{0}C)
Viscosity	20~22mm^{2}/S at 40 ℃
Oil volume	160 ±10m
Weight（with oil）	4.6 kg
Diameter of suction tube（inner diameter）	φ6.2 mm
Diameter of discharge tube	φ5.1 mm
Diameter of serves tube	φ6.2 mm
Material of tubes	Copper

Instructions of DC controller

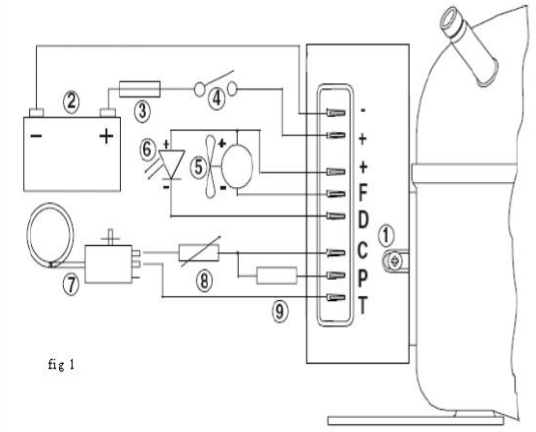

fig 1

Optional battery protection settings（table1）

Resistor (9) KΩ	12Vcut-out V	12Vcut-in V	12Vmax Voltage	24Vcut-out V	24Vcut-in V	24Vmax Voltage
0	9.6	10.9	17.0	21.3	22.7	31.5
1.6	9.7	11.0	17.0	21.5	22.9	31.5
2.4	9.9	11.1	17.0	21.8	23.2	31.5
3.6	10.0	11.3	17.0	22.0	23.4	31.5
4.7	10.1	11.4	17.0	22.3	23.7	31.5
6.2	10.2	11.5	17.0	22.5	23.9	31.5
8.2	10.4	11.7	17.0	22.8	24.2	31.5
11	10.5	11.8	17.0	23.0	24.5	31.5
14	10.6	11.9	17.0	23.3	24.7	31.5
18	10.8	12.0	17.0	23.6	25.0	31.5
24	10.9	12.2	17.0	23.8	25.2	31.5
33	11.0	12.3	17.0	24.1	25.5	31.5
47	11.1	12.4	17.0	24.3	25.7	31.5
82	11.3	12.5	17.0	24.6	26.0	31.5
220	9.6	10.9	17.0	21.3	22.7	31.5

Wire dimensions（table2）

AWG Gauge	Cross setion(mm2)	Max length* 12V DC ft.	m	Max length* 24V DC ft.	m
13	2.5	8	2.5	16	5
12	4	13	4	26	8
10	6	20	6	39	12
8	10	33	10	66	20

*length between battery and electronic unit

Standard battery protection settings（table3）

12Vcut-out V	12V cut-in V	24Vcut-out V	24V cut-in V
10.4	11.7	22.8	24.2

Compressor speed settings（table4）

Motor speed (RPM)	Resistor（8） Ω	C/T voltage V
2000	0	0.87~1.02
2100	51	1.02~1.17
2200	100	1.17~1.32
2300	150	1.32~1.48
2400	200	1.48~1.63
2500	277	1.63~1.78
2600	330	1.78~1.93
2700	400	1.93~2.08
2800	490	2.08~2.24
2900	586	2.24~2.39
3000	692	2.39~2.54
3100	816	2.54~2.69
3200	963	2.69~2.84
3300	1137	2.84~3.0
3400	1331	3.0~3.15
3500	1523	3.15~3.61
stop	>3000	3.61~5

Controller specification

The electronic unit is a dual voltage device. This means that the same unit can be used in both 12V and 24V power supply systems. Maximum voltage is 17V for a 12V system and 31.5V for a 24V power supply system. Max. ambient temperature is 55°C. The electronic unit has a built-in thermal protection which is actuated and stops compressor operation if the electronic unit temperature gets too high.

Installation(Fig.1)

Connect the terminal plug from the electronic unit to the compressor terminal. Mount the electronic unit on the compressor by snapping the cover over the screw head(1).

Appendix B: Charge controller specification

Solar Charge Controller

PV LOGIC intelligent power

10A charger control 12v/24v DC (STCC10) • 20A charger control 12v/24v DC (STCC20)

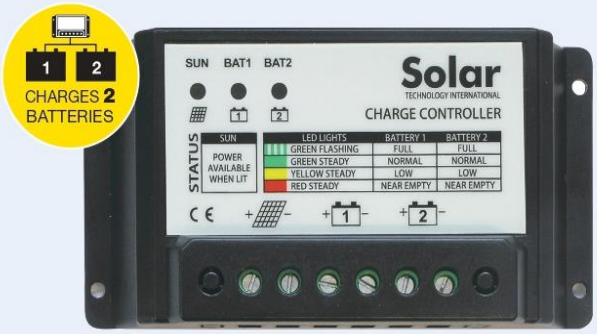

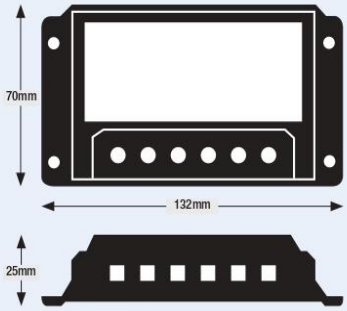

The latest Solar Technology charge controllers provide the very best in power delivery from solar panel to 12v or 24v battery whether charging a single or twin batteries.

These PV Logic Pulse Width Modulation (PWM) controllers deliver sizeable benefits over standard charge controllers by achieving a constant battery voltage and thereby producing a higher charge efficiency, rapid recharging and a longer life expectancy for any battery.

Dual Battery Charging Function - Ideal if twin batteries are used in a caravan or boat or to charge the leisure and vehicle battery in an RV. The dual charge function only occurs when a second battery is connected. In this configuration the controller will still focus its power delivery on the battery connected to the No 1 terminals until that battery is 70% fully charged. Once this is reached power will be delivered to both batteries equally until both are 100% charged.

TECHNICAL SPECIFICATIONS	
Nominal System Voltage	12/24VDC (automatic system voltage recognition)
Battery Voltage Range	6-36V
Rated Battery Current	10A/5A/20A depending on model selected
Charge Circuit Voltage Drop	≤0.26V
Self-consumption	≤6mA
Temperature Compensation Coefficient	-30mV/°C/12V(25° ref)
Over Voltage Disconnect Voltage	16V/32V
Charging Limit Voltage	15.5V/31V
Equalize Charging Voltage	14.6V/29.2V
Float Charging Voltage	13.8/27.2V
Operating temperature	-35°C to +55°C
Overall dimensions	135 x 70 x 35mm
Mounting hole size (in case)	3.8mm
Terminals	6mm2
Net weight	155g
Suitable battery type	Sealed, Flooded and Gel
Solar Panel and battery protection against	Short circuit and reverse polarity, overload, battery r emoval and lightning strike

PRODUCT FEATURES

- 12V/24V AUTOMATIC RECOGNITION ON BOTH BATTERY & SOLAR CONNECTIONS
- UNIQUE SINGLE OR DUAL BATTERY CHARGING FUNCTIONS
- EFFICIENT SERIES PWM CHARGING
- CHARGING & STATUS LEDS
- REVERSE CURRENT PROTECTION

WHICH MODEL?

10AH UP TO MAX OF 150W (10A) OF SOLAR PANEL(S)

20AH UP TO MAX OF 300W (20A) OF SOLAR PANEL(S)

WARRANTY

This Solar Charge Controller is supplied with a 12 month warranty. Should a failure occur during this time Solar Technology International Ltd will repair or replace any faulty part, at its discretion. Solar Technology International Ltd does not accept liability for any 3rd party damage how so ever caused or any costs associated with the return of faulty products. To make a warranty claim please telephone Solar Technology International Ltd on **+44 (0) 1684 774000**.

These warranty conditions in no way affect your statutory rights. A full set of Solar Technology International Ltd terms and conditions are available on request.

Battery connections

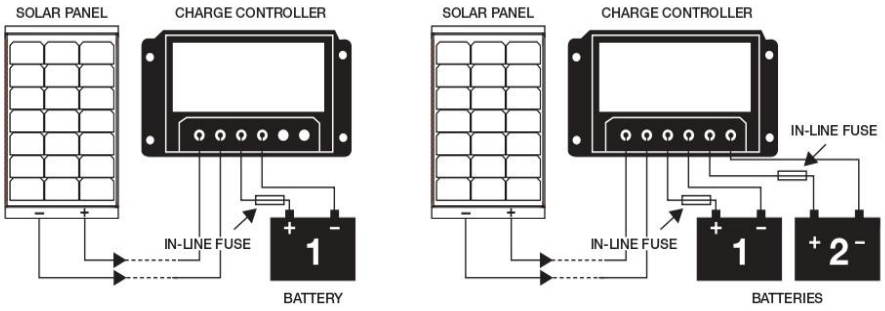

CE

RoHS ✔

Solar Technology International Ltd. Unit 6, Station Drive, Bredon, Nr. Tewkesbury, Glos. GL20 7HH, United Kingdom
Tel: 01684 774000 Fax: 01684 773000 Email: support@solartechnology.co.uk Online: www.solartechnology.co.uk

Solar TECHNOLOGY INTERNATIONAL

Appendix C: (TEC1-12706) thermoelectric module specification

➢ Description

40 mm × 40 mm size single stage module is made of selected high performance ingot to achieve superior cooling performance and greater temperature difference ΔT up to 70 ºC, designed for superior cooling and heating up to 100 ºC applications.

➢ Applications

- Food and beverage service refrigerator
- Liquid cooling
- Photonic and medical systems
- Temperature stabilizer
- Portable cooler box for cars
- CPU cooling

➢ Features

- High effective cooling, heating and efficiency
- No moving parts, noiseless, and solid-state
- Compact structure, small in size, light in weight
- Environment friendly
- Exceptionally reliable in quality
- 200000h life time
- Precise temperature control

➢ Performance Specification Sheet

T_h (ºC)	30	60	Hot side temperature at environment (dry air)
D_{Tmax}(ºC)	70	80	Temperature difference between cold and hot side of the thermoelectric module.
V_{max} (voltage)	15	17	Maximum applied voltage to the module at D_{Tm}
I_{max}(amps)	6	6	Maximum DC applied current I_{max} at D_{Tm}
QC_{max}(Watts)	50	65	Cooling capacity at cold side of the module under D_T= 0 ºC
AC resistance(ohms)	1.37	2.1	Thermoelectric module resistance
Tolerance (%)	±10	±10	Thermal and electricity factor
P_{max} (Kg/cm^2)	10.8	10.8	Maximum vertical static pressure
Flatness (mm)	≤0.05	≤0.05	Contact surface flatness

➢ Geometric Characteristics

The dimensions in millimetres as indicated in the graph.

➢ Sealing

- Solder

BiSn (Tmelt at 138 ºC)

- Ceramics

Alumina (Al_2O_3, White 96%), Aluminium Nitride (AlN)

- Sealant

Epoxy sealant (EPS), Silicon sealant (SS),

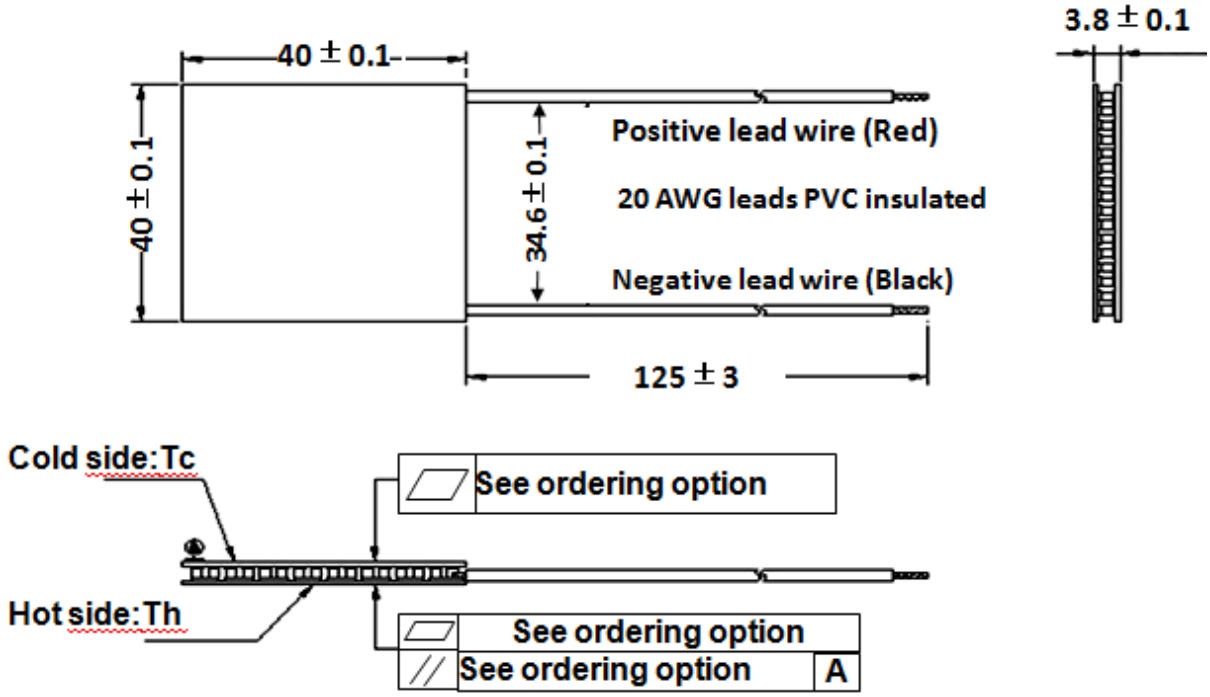

➢ Operation Cautions

- Cold side of the module attached on the object being cooled
- Hot side of the module mounted on a heat sink
- Thermoelectric module storage below 100 ºC
- Operation conditions below I_{max} or V_{max}
- Work under DC

Figure 1 shows the cooling capacity of the TE module at different applied current as a function in temperature difference. Note that Th = 30 ºC. The standard performance of the module at Th =50 ºC is presented in Figure 2.

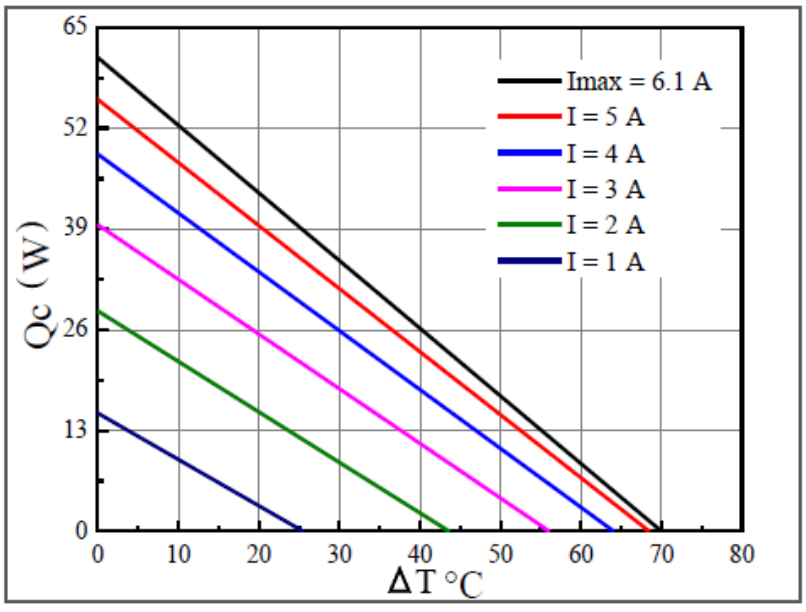

Figure 1: Cooling capacity of TE module at Th=30 ºC

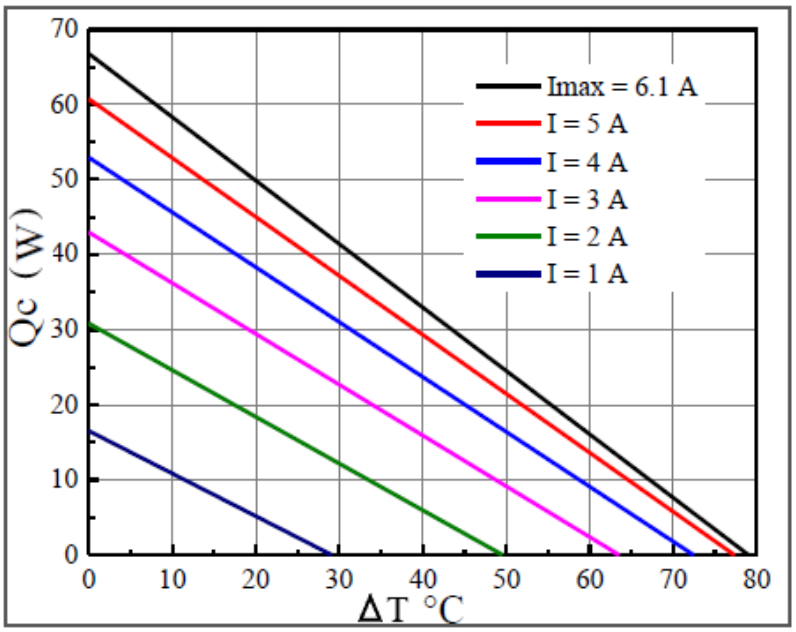

Figure 2: Cooling capacity of the module at Th = 50 ºC

The performance of TE module as a function in voltage and temperature difference is given in Figure 3.

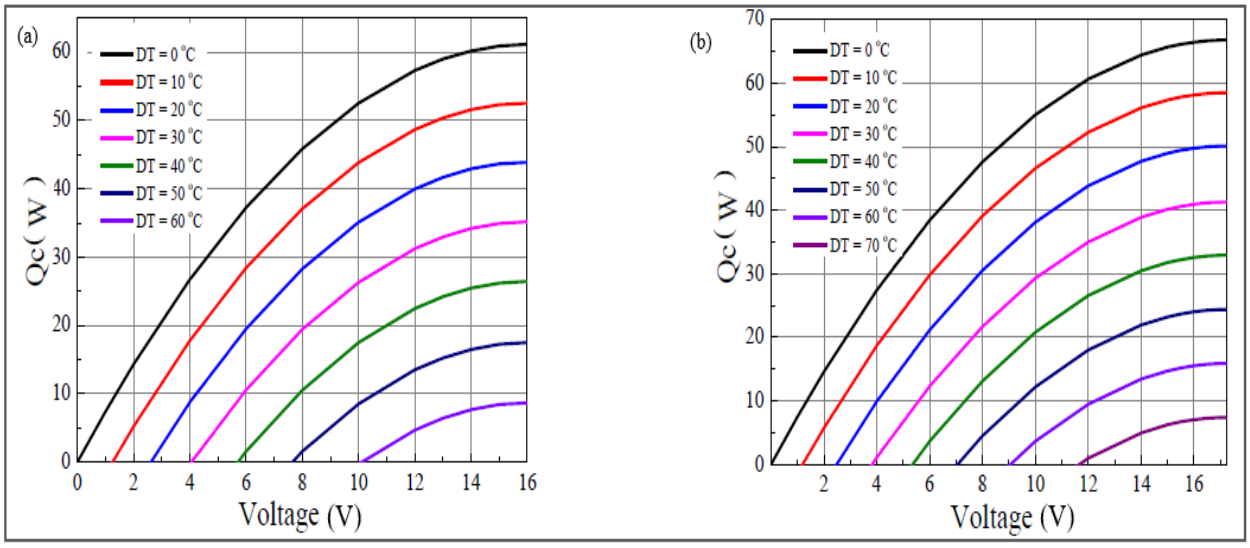

Figure 3: variation of TE module cooling capacity; (a) at Th = 30 ºC, (b) at Th = 50 ºC

Appendix D: Sample calculations

1. Solar radiation on tilted surface

Date of experiment: 6 June 2020

Test location data:

Latitude: L= -33.93º

Longitude: Long=18.46º

Solar constant: I_{sc}=1367 W/m^2

Collector inclined angle: β =34º

The ground reflectance: ρ =0.2

The incident horizontal radiation: Ih = 447.84 W/m^2

The diffuse radiation: I_d = 17.68 W/m^2

The beam radiation $I_b = I_h - I_d$

=447.84-17.68

=430.16 W/m^2

Local time is 11:00

The hour angle is given in equation (2.4)

$\omega = 15(t-t_{noon})$

t_{noon}=720+4 ˣ longitude – equation of time

Equation of time= 9.87sin 2B- 7.53cos B-1.5 sin B

B= 360 ˣ (n-81)/365

On the6 of June, n = 157

Therefore,

B= 360 ˣ (157-81)/365

B = 75.94

Equation of time = 9.87 sin (2 ˣ 75.94) – 7.53 cos (75.94) – 1.5 sin (75.94)

= 1.49

t_{noon} = 720 + (4 ˣ 18.46) – 1.49

= 792.35 minutes

= 13.2 h

ω= 15 (11-13.2)

= -33.08

The declination angle is given in equation (2.2)

δ = 23.45 ˣ sin {360 ˣ (284 + n)/365}

= 23.45 ˣ sin {360 ˣ (284 + 157)/365}

= 23.18º

The incident angle of beam radiation is given as follows:

$\theta_i = \cos^{-1}\{\cos(L+\beta) \times \cos\delta \times \cos\omega + \sin(L+\beta) \times \sin\delta\}$

= cos-1 {cos (-33.93+34) ˣ cos 23.18 ˣ cos -33.08 + sin (-33.93 + 34) ˣ sin 23.18}

$\theta_i = 61.2^o$

The Zenith angle is given as:

$\theta_z = \cos^{-1}\{\cos L \times \cos\delta \times \cos\omega + \sin L \times \sin\delta\}$

$\theta_z = \cos^{-1}\{(\cos -33.93) \times \cos 23.18 \times \cos -33.08 + \sin -33.93 \times \sin 23.18\}$

$= 64.7^o$

The beam ratio is calculated as:

$R_b = \cos\theta_i/\cos\theta_z$

$=\cos 61.2/\cos 64.7$

$= 1.12$

The circumsolar and horizontal brightness coefficients are given in equations (2.12) and (2.13).

$F1 = \max\{0;(f11 + \Delta f12 + \pi\theta_z f13/180)\}$

$F2 = f12 + \Delta f22 + \pi\theta_z f23/180$

Here;

$\Delta = m \times I_d/I_{on}$

$m = 1/\cos\theta_z$

$m = 1/\cos 64.7$

$= 2.33$

$I_{on} = I_{sc}(1+ 0.033 \cos(360n/365) \times \cos\theta_z$

$= 1367(1 + 0.033 \cos(360 \times 157/365) \times \cos 64.7$

$= 566.74\ W/m^2$

Therefore,

$\Delta = 2.33 \times 17.7/566.74$

$= 0.073$

$\varepsilon = \{(I_d + I_{bn})/I_d + 5.535 \times 10E\text{-}6 \times \theta_z^3\}/(1+ 5.535 \times 10E\text{-}6 \times \theta_z^3)$

$I_{bn} = I_b/\cos\theta_z$

$= 430.16/\cos 64.7$

$=1006.4\ W/m^2$

Therefore,

$\varepsilon = \{(17.7+1006.4)/17.7 +5.535 \times 10E\text{-}6 \times 64.7^3)/(1+5.535 \times 10E\text{-}6 \times 64.7^3)$

$= 23.74$

For ε greater than 6.2 (Appendix F), the factors as follow:

f11 = 0.678, f12 = -0.327, f13 = -0.25, f21 = 0.156, f22 = -1.377 and f23 =0.251

Therefore;

$F1 = \{0.678 +(0.073 \times -0.327) + (\pi \times 64.7 \times -0.25/180)\}$

$=0.371$

$F2 = \{0.156+ (0.073 \times -1.377) + (\pi \times 64.7 \times 0.251/180)\}$

= 0.338

The total incident solar radiation is calculated as:

$I_T = R_b \times I_b + I_d\{(1-F1)^x (1 + \cos\beta)/2 + F1(a/b) + F2 \sin\beta\} + I_h \rho_g (1-\cos\beta)/2$

Here, a = max (0;cosθi) and b= max(0; cos θz)

a = 0.48 and b = 0.427

$I_T = 1.12 \times 430.16 + 17.7\{(1-0.371) \times (1 + \cos 34)/2 + 0.331(0.48/0.427) + 0.338 \sin 34\} + 447.8 \times 0.02 \times (1 - \cos 34)/2$

$I_T = 481.6 + 20.1 + 0.765$

$= 502.4\ W/m^2$

2. The coefficient of performance of heat pump

The coefficient of performance of vapour compression heat pump is given in equation (2.22).

$COP = \dot{Q}_H/\dot{W}$

Here, $\dot{Q}H$ and $\dot{W}$ are given in equation (2.17) and (2.18)

Therefore, $COP = (h_2-h_4)/(h_2-h_1)$

At temperature -2.8, 5.13 and 42.6

Using the a134 tables

-4 → 201.6

-2.8 → x

-2 → 200.11

$h_4 = 200.76$

4 → 252.77

5.3 → x

6 → 253.9

$h_1 = 253.41$

42 → 272.12

42.6 → x

44 → 272.95

$h_2 = 272.369$

therefore;

COP = (272.95-200.76)/(272.95-253.41)

=3.77

3. Solar still efficiency

To calculate the convective heat transfer, equation (2.43) and (2.43 a) can be used.

$$h_{wc} = 0.884\left[(T_w - T_c) + \frac{(P_w - P_c)(T_w + 273)}{268.9 \times 10^3 - P_w}\right]^{1/3}$$

$$P_T = exp\left[25.317 - \left(\frac{5144}{273 + T}\right)\right]$$

Here, the water temperature is 52.18 ºC and the inner cover temperature is 23.52 ºC. the calculated incident solar radiation was 658.24 W/m^2

Therefore, $P_w = \exp\left[25.317 - \left(\frac{5144}{273+52.18}\right)\right]$

$$P_w = 13333.95$$

$$P_c = 2890.248$$

$$h_{wc} = 0.884\left[28.66 + \frac{((13333.95 - 2890.248)(52.18 + 273)}{(268.9 \times 10^3 - 13333.95)}\right]^{1/3}$$

$$h_{wc} = 2.93\ W/m^2K$$

The evaporative heat transfer coefficient is calculated by using equation (2.47).

$$h_{we} = 16.237 \times 10^{-3} h_{wc} \frac{P_w - P_c}{T_w - T_c}$$

$$h_{we} = 16.237 \times 10^{-3}(2.93)\frac{(13333.95 - 2890.248)}{(52.18 - 23.52)}$$

$$h_{we} = 17.37\ W/m^2K$$

The thermal energy transferred to the contaminated water is given in equation (2.42).

$$q_{wc} = h_{we}(T_w - T_c)$$

$$q_{wc} = 17.37(52.18 - 23.52)$$

$$= 497.9\ W/w^2$$

Therefore, the efficiency is given as:

$$\eta = \frac{q_{wc}}{I(T)}$$

$$= \frac{497.9}{658.24}$$

$$\eta = 0.756$$

$$= 75.6\%$$

4. The hourly efficiency of solar still

The hourly efficiency of solar still can be found as given on equation (2.55), (2.56) and (2.57).

$$\eta = \frac{\sum m_w L}{A_s \int I(t)dt} \times 100$$

$$L = 3.1615 \times 10^6(1 - 7.616 \times 10^{-4}T)$$

$$L = 10^2\left[2501.9 - (2.40706 \times T_w) + \left(1.192217 \times 10^{-3} \times {T_w}^2\right) - (1.5863 \times 10^{-5} \times {T_w}^3\right]$$

For T_w = 60 °C, m_w =170 ml and I_t =1055 W/m^2

L= 10^2(2501.9 – 801.6 +132.21 – 585.646)

=124.7 *10^3

η = 170*124.7*10^3/1055*1*10^3

= 20.09 %

5. The coefficient of performance of the thermoelectric heat pump

To calculate the coefficient of performance (COP) of thermoelectric heat pump, equations (2.27) to (2.32) were used and the following parameter was considered.

$A_n = \alpha_p$ = 2.03 ×10^{-4}VK^{-1}, K = 0.0176 Wcm^{-1}K^{-1}, the electrical resistance ranged at 1.89 to 2.03 and the number of thermoelements is 127 couples.

The area (A) of the module is 40 mm × 40 mm

At the T_h=50 ºC T_c=10 ºC and I = 4 A

$$Q_h = \alpha_m I\mathrm{T_h} - \mathrm{K_m}(\mathrm{T_h} - \mathrm{T_c}) + \frac{1}{2}\mathrm{R_m}\mathrm{I}^2$$

$$Q_h = 127 \times 4 \times 323 - 0.0176 \times 127 \times (323 - 283) + \frac{1}{2}1.9 \times 127 \times 4^2$$

$$= 165925$$

$$Q_c = \alpha_m \mathrm{I}\mathrm{T_c} - \mathrm{K_m}(\mathrm{T_h} - \mathrm{T_c}) - \frac{1}{2}\mathrm{R_m}\mathrm{I}^2$$

$$Q_c = 127 \times 4 \times 283 - 0.18 \times 127(323 - 283) - \frac{1}{2} \times 127 \times 1.9 \times 4^2$$

$$Q_c = 140919.2$$

Therefore, the maximum coefficient of performance COP = Q_h/Q_h-Q_c

= 165925/165925-140919

= 6.6

The value obtained here agree with the value of COP at the standard condition in the thermoelectric module data sheet.

The second method to determine the coefficient of performance of TEC heat pump is when the thermoelectric modules is operating in solar still system as thermal energy recovery system.

Here, the following equations were proposed:

$$COP = \frac{Q_w}{P}$$

$$Q_w = mC_p(T_2 - T_1)$$

$$P = I \times V$$

Where Q_w is the energy delivered to the water, m is the water mass, C_p is the specific heat of water, I is the applied current and V is the applied voltage.

At 7.00 the initial water temperature was T_1 = 12.32 ºC for 1 hour of operation T_2 =22.64 ºC, the water mass was 5 L, the applied current was 5 A and the voltage was 6 V. Therefore,

P = 5 ˣ 6 =30 W

Qw = 5 ˣ 4186 ˣ (22.64 -12.32)/3600

= 59.9 W

COP = 59.9/30 =1.99 ≈2

Appendix E: Brightness Coefficients Table

Range of ε	f_{11}	f_{12}	f_{13}	f_{21}	f_{22}	f_{23}
1.000-1.065	-0.008	0.588	-0.062	-0.060	0.072	-0.022
1.065-1.230	0.130	0.683	-0.151	-0.019	0.066	-0.029
1.230-1.500	0.330	0.487	-0.221	0.055	-0.064	-0.026
1.500-1.950	0.568	0.187	-0.295	0.109	-0.152	0.014
1.950-2.800	0.873	-0.392	-0.362	0.226	-0.462	0.001
2.800-4.500	1.132	-1.237	-0.412	0.288	-0.823	0.056
4.500-6.200	1.060	-1.600	-0.359	0.264	-1.127	0.131
6.200-∞	0.678	-0.327	-0.250	0.156	-1.377	0.251

Appendix F: Results sample

Table 1: Sample of weather condition data (23 April 2019)

Time	Meteorological Condition					
	Solar radiation (beam) I_b [W/m^2]	Solar radiation (diffuse) I_d [W/m^2]	Solar radiation (total horizontal) I_h [W/m^2]	Solar radiation (total inclined) I_T [W/m^2]	Wind speed (m/s)	Ambient temperature (ºC)
7:00	1.02	0.12	1.14	7.81	1.787	14.1
7:30	7.08	0.639	7.72	21.91	3.421	14.51
8:00	24.87	6.683	31.55	45.78	2.479	14.92
8:30	71.37	17.64	89.01	145.85	2.876	15.21
9:00	171.88	10.27	182.14	295.32	2.366	16.33
9:30	312.72	18.484	331.2	447.21	3.393	18.29
10:00	373.85	16.15	390	520.71	3.371	22.15
10:30	403.52	33.05	436.57	648.32	3.371	23.45
11:00	462.6	55.58	518.18	687.28	3.196	23.92
11:30	593.37	59.1	652.47	742.34	2.808	24.22
12:00	596.67	36.2	632.87	711.61	3.658	23.02
12:30	464.01	62.35	526.36	677.32	3.533	22.0
13:00	688.14	34.96	723.1	865.81	3.021	22.10
13:30	671.42	44.26	715.68	835.31	4.056	22.26
14:00	653.32	35.26	688.58	813.70	3.042	22.28
14:30	596.46	48.34	644.80	785.82	4.125	21.94
15:00	520.7	65.71	586.41	705.78	3.514	21.62
15:30	454.45	58.33	512.78	690.07	3.298	21.07
16:00	373.95	50.14	424.09	611.68	4.097	21.31
16:30	285.39	47.25	332.64	520.31	2.631	21.90
17:00	183.8	51.2	234.81	397.82	2.527	20.20
17:30	84.85	38.77	123.55	280.08	2.241	19.47
18:00	32.78	21.29	53.78	120.39	2.801	17.15
18:30	19.58	12.54	32.12	55.47	2.347	16.25
19:00	10.82	0.25	11.07	17.02	3.827	16.01

Table 2: Stills temperature trend (first test results)

Time	Advanced solar still					Conventional solar still			
	Water temp ºC	Basin temp ºC	Vapour temp ºC	cover temp	Water output ml	Water temp ºC	Basin temp ºC	Vapour temp ºC	cover temp
7:00	13.6	13.08	14.08	14.02	0	13.57	13.27	14.01	14.07
7:30	22.12	20.27	17.51	16.51	0	14.05	14.52	14.54	14.14
8:00	31.60	28.71	27.57	26.31	0	15.24	17.61	14.85	14.92
8:30	37.02	35.08	31.21	30.09	10	17.09	18.69	15.36	15.85
9:00	44.28	39.78	37.67	32.74	30	19.26	20.73	16.96	20.85
9:30	48.91	47.12	43.66	36.08	110	24.3	26.01	22.87	25.06
10:00	57.87	55.98	52.84	37.87	210	26.74	29.85	25.85	29.66
10:30	62.73	59.91	55.97	40.02	330	33.32	36.31	30.12	33.79
11:00	66.81	67.25	58.36	48.98	490	42.01	45.08	34.62	37.21
11:30	71.21	73.74	62.63	55.87	670	47.36	50.22	41.91	40.65
12:00	73.16	75.22	66.21	56.74	890	51.87	54.23	47.48	46.32
12:30	72.88	73.21	67.09	57.37	1150	55.81	56.72	53.8	50.14
13:00	71.25	72.84	71.14	59.44	1400	56.19	57.65	55.78	52.35
13:30	70.09	71.79	70.05	60.02	1670	58.04	59.11	57.37	55.64
14:00	68.36	70.04	68.33	61.31	1970	57.0	57.76	55.64	53.41
14:30	64.77	65.25	64.78	59.21	2260	54.32	55.21	53.21	49.78
15:00	61.28	62.32	61.21	57.07	2570	53.63	53.98	50.01	46.62
15:30	59.97	59.44	59.49	55.91	2860	48.77	50.45	46.35	43.21
16:00	57.16	57.01	56.28	46.7	3130	47.7	48.62	44.18	40.52
16:30	55.66	54.98	53.95	39.26	3380	46.39	46.65	41.76	39.21
17:00	54.72	54.17	53.07	36.24	3620	43.78	44.98	39.80	36.05
17:30	50.22	49.74	49.21	35.78	3840	38.41	39.21	36.61	32.11
18:00	49.09	48.63	47.03	31.85	4020	33.27	33.05	29.14	28.10
18:30	48.27	47.74	44.10	29.41	4150	30.02	29.16	27.85	26.98
19:00	47.36	46.68	41.24	26.33	4250	27.33	25.95	23.06	22.04

Table 3: Second test results

Time	Advanced solar still performance						Meteorological Condition	
	Water temp ºC	Basin temp ºC	Vapour temp ºC	Outer cover temp	Inner cover temp	Water output ml	Solar radiation W/m^2	Ambient temp ºC
7:00	15.13	15.42	15.81	16.02	15.20	0	1.25	17.07
7:30	22.7	21.76	17.52	16.48	15.88	20	2.32	16.92
8:00	28.2	27.33	24.3	17.91	16.41	70	9.25	16.85
8:30	31.32	30.87	27.65	17.58	18.63	150	28.77	17.22
9:00	35.88	34.91	35.41	18.61	19.85	225	70.23	17.78
9:30	40.36	38.85	38.95	18.97	20.11	365	345.25	17.33
10:00	45.68	43.59	40.33	19.32	19.89	555	268.53	17.28
10:30	48.31	47.39	43.65	22.66	24.55	805	368.25	16.90
11:00	54.77	54.02	48.69	24.38	22.41	1095	542.21	17.92
11:30	58.11	56.91	53.85	25.47	23.56	1415	587.95	19.08
12:00	58.94	57.75	54.98	27.86	24.76	1745	631.85	21.27
12:30	59.85	59.33	58.01	28.65	24.97	2085	463.22	23.41
13:00	61.25	60.09	58.98	27.09	24.36	2435	452.98	22.37
13:30	60.64	59.33	59.10	26.89	23.44	2775	450.8	23.18
14:00	58.81	58.77	57.74	26.45	23.14	3095	520.98	22.44
14:30	58.11	58.21	57.60	25.88	22.63	3435	489.2	20.09
15:00	57.64	57.24	56.91	23.13	22.04	3785	367.14	19.51
15:30	55.43	55.07	54.82	21.63	22.18	4095	347.8	19.43
16:00	54.39	54.29	52.37	19.54	22.32	4395	291.89	19.94
16:30	54.68	53.98	51.81	19.08	21.63	4675	240.63	20.05
17:00	54.51	53.46	50.68	18.67	20.52	4955	202.59	20.32
17:30	53.24	52.76	50.04	17.68	20.10	5205	130.23	19.18
18:00	51.20	50.47	49.66	17.26	19.98	5415	40.05	19.04
18:30	50.08	49.21	48.21	16.52	20.73	5595	1.02	18.87
19:00	49.56	48.07	47.09	16.03	20.14	5744	0	18.65

Table 4: Vapour compression heat pump performance

Time	Temperature trend				Heat pump performance	
	evaporator		condenser			
	In ºC	Out ºC	In ºC	Out ºC	COP	Power consumption (W)
7:00	13	12.8	15.1	14.8	7.19	52.56
7:30	2.10	7.9	28.8	22.9	4.95	56.3
8:00	1.02	9.2	35.7	31.8	4.1	59.4
8:30	0.51	8.81	37.2	34.2	3.84	49.2
9:00	0.35	9.1	39.8	35.6	3.72	46.08
9:30	-0.2	8.7	42.3	35.8	4.2	44.64
10:00	0.7	8.9	46.2	38.7	3.95	50.24
10:30	1.2	9.2	55.4	49.1	3.82	47.41
11:00	2.8	10.45	59.7	56.3	4.1	45.85
11:30	1.7	8.85	62.1	58.9	4.92	49.2
12:00	-0.7	7.6	64.02	59.3	4.54	59.04
12:30	-1.05	7.02	63.2	60.2	4.41	54.48
13:00	-2.1	6.65	64.1	61.7	3.9	53.04
13:30	-1.2	8.10	62.3	60.5	4.25	46.8
14:00	-0.5	9.2	61.6	59.4	4.15	51
14:30	-0.6	8.8	60.7	58.6	3.95	49.08
15:00	-0.3	8.12	59.8	57.7	4.3	47.4
15:30	-2.1	8.9	58.1	56.2	4.05	51.6
16:00	-3.0	7.2	57.9	55.08	3.90	48.62
16:30	-2.6	6.8	57.47	55.0	3.76	46.68
17:00	-1.8	6.2	56.3	54.7	3.65	44.05
17:30	-0.9	6.5	56.8	53.8	3.8	47.36
18:00	-0.4	6.2	55.4	53.2	4.01	45.68
18:30	1.02	6.7	54.2	52.8	3.92	48.3
19:00	1.5	6.9	52.6	49.8	3.85	49.5

Table 5: Sample of results from the third test (November 2019)

Time	Weather condition		Advanced still performance			Conventional still performance		
	Ambient temperature (ºC)	Wind speed (m/s)	Water temperature (ºC)	Basin temperature (ºC)	Vapour temperature (ºC)	Water temperature (ºC)	Basin temperature (ºC)	Vapour temperature (ºC)
7:00	17.3	3.56	17	17.1	17.05	17	17.2	17.18
7:30	18.2	4.13	26.1	24.7	19.89	19.05	20.15	17.80
8:00	18.7	4.34	34.51	33.82	28.65	20.91	22.45	18.11
8:30	19.35	4.21	40.82	38.78	36.21	22.48	24.73	20.07
9:00	21.73	5.24	47.46	45.46	42.78	25.61	28.35	21.36
9:30	22.18	5.598	52.18	50.21	48.65	29.44	32.51	24.68
10:00	23	6.145	57.76	58.61	52.19	34.18	36.87	29.75
10:30	23.76	5.672	59.32	60.11	56.64	37.72	39.12	34.46
11:00	24.5	5.56	63.65	64.78	59.66	42.91	46.28	37.91
11:30	25.12	5.331	66.98	68.92	61.32	48.35	51.87	42.80
12:00	26.2	5.879	72.84	73.72	65.83	50.01	53.76	45.66
12:30	27.15	6.43	73.21	74.88	67.91	53.75	57.45	47.38
13:00	27.9	6.87	72.87	73.2	67.08	56.62	59.78	49.95
13:30	28.7	7.21	71.49	72.85	66.37	57.35	62.34	53.07
14:00	29.98	7.44	70.95	71.81	66.18	57.28	61.95	53.61
14:30	31.43	7.677	68.78	69.37	64.55	56.89	59.59	50.85
15:00	33.65	7.128	66.35	68.12	62.89	56.63	57.16	49.78
15:30	32.45	6.981	61.65	62.51	58.10	55.12	53.21	49.24
16:00	30.13	6.673	59.23	58.6	56.84	53.2	51.78	48.57
16:30	28.7	6.4	57.43	56.37	55.21	49.7	47.24	45.01
17:00	26.55	6.871	56.18	54.98	53.78	42.28	39.47	40.65
17:30	25.7	7.06	54.73	53.94	52.01	40.14	38.1	35.05
18:00	25	6.98	55.65	52.71	49.65	37.22	35.82	33.10
18:30	24.33	6.9	54.98	53.16	49.27	33.87	30.21	28.45
19:00	23.84	6.56	54.12	52.86	46.18	29.77	27.62	23.29

Table 6: Distillate output

Time	Inner surface temperature ºC		Distillate output		Incident solar radiation (W/m^2)
	Advanced still (ºC)	Conventional still (ºC)	Advanced still (ml)	Conventional still (ml)	
7:00	17.2	17.1	0	0	120.0
7:30	16.2	18.4	10	0	282.43
8:00	19.25	20.71	40	0	290.34
8:30	20.14	22.48	200	20	420.74
9:00	21.29	23.74	380	40	561.82
9:30	23.52	25.86	570	120	658.24
10:00	24.71	28.31	790	220	838.18
10:30	25.32	31.95	1050	330	915.36
11:00	26.84	36.89	1300	440	970.78
11:30	33.21	43.47	1560	560	1015.46
12:00	39.62	45.21	1840	670	1035.39
12:30	44.25	46.44	2140	790	1048.95
13:00	46.87	48.76	2450	930	1055.62
13:30	47.25	50.17	2780	1100	1030.76
14:00	46.17	51.22	3150	1300	995.38
14:30	45.82	50.55	3500	1480	948.5
15:00	44.11	48.38	3830	1640	877.02
15:30	38.25	46.87	4170	1810	760.87
16:00	30.97	45.21	4520	2000	685.57
16:30	26.32	40.48	4860	2180	620.08
17:00	23.28	37.21	5180	2340	481.8
17:30	20.78	32.14	5480	2480	358.39
18:00	18.09	29.17	5760	2600	230
18:30	16.8	26.21	6020	2670	152.4
19:00	15.21	24.86	6210	2670	64.58

Table 7: The result of the third test (July 2020)

Time	Weather condition		Advanced still performance			Conventional still performance		
	Ambient temperature	Wind speed	Water temperature	Basin temperature	Vapour temperature	Water temperature	Basin temperature	Vapour temperature
7:00	11.7	5.65	10.12	10.07	10.5	10.27	11.14	10.9
7:30	12.1	5.95	15.47	13.98	11.9	10.92	11.45	11.2
8:00	12.5	6.23	22.76	20.85	18.8	12.42	12.98	11.8
8:30	12.61	6.45	29.35	28.77	26.65	13.92	14.52	12.6
9:00	12.82	6.62	34.37	33.65	30.1	14.74	15.09	13.8
9:30	12.88	6.81	38.16	37.08	35.98	16.11	16.78	14.98
10:00	12.94	7.21	41.32	40.75	38.33	16.52	17.24	16.2
10:30	13.15	7.58	44.82	43.25	42.76	18.36	19.06	17.34
11:00	13.55	7.84	48.73	47.65	46.21	19.24	20.92	18.7
11:30	14.38	7.98	53.08	52.31	51.65	25.01	25.76	21.34
12:00	15.3	8.15	55.62	54.88	52.9	27.18	27.98	24.9
12:30	15.95	8.54	56.33	56.07	54.08	28.76	29.65	27.12
13:00	16.17	8.86	57.6	56.88	55.1	28.52	29.58	27.87
13:30	16.82	8.91	57.92	57.12	55.21	29.36	30.41	28.45
14:00	18.31	9.17	58.65	58.04	56	29.48	31.04	30.45
14:30	19.1	9.32	56.41	55.25	55.42	33.76	34.02	32.18
15:00	17.32	9.44	56.5	53.9	53.12	35.76	36.65	33.9
15:30	17.1	9.51	56.35	53.76	50.29	38.45	39.9	33.32
16:00	16.72	8.67	54.76	52.9	48.54	36.03	37.32	32.56
16:30	15.36	8.24	52.4	50.8	47.43	32.12	34.21	30.12
17:00	14.87	7.65	48.81	47.98	46.54	29.43	30.43	27.33
17:30	13.55	6.46	47.31	46.25	45.09	26.65	28.66	24.08
18:00	13.27	7.14	46.75	45.77	43.6	20.32	22.34	19.6
18:30	13.05	7.85	44.21	43.52	40.75	17.04	18.32	15.02
19:00	12.98	7.45	44.01	42.87	39.98	15.07	14.57	14.43

Table 8: Distillate output

Time	Condensation surface temperature ºC		Distillate output		Incident solar radiation (W/m^2)
	Advanced still (ºC)	Conventional still (ºC)	Advanced still (ml)	Conventional still (ml)	
7:00	10.31	10.21	0	0	0
7:30	11.26	10.38	0	0	2.1
8:00	11.82	11.47	10	0	2.62
8:30	10.21	11.95	30	0	3.31
9:00	9.92	12.27	100	0	4.72
9:30	13.47	14.13	190	0	12.38
10:00	19.67	15.82	310	0	52.62
10:30	20.14	16.34	460	0	141.42
11:00	21.48	17.09	630	10	180.28
11:30	22.76	20.82	810	20	452.34
12:00	22.44	22.76	1010	40	210.94
12:30	23.02	23.6	1230	50	179.42
13:00	23.74	24.2	1440	60	61.33
13:30	24.58	24.98	1660	70	120.09
14:00	26.09	25.44	1910	80	52.9
14:30	25.41	27.32	2200	95	270.31
15:00	24.32	27.18	2510	115	234.82
15:30	23.18	26.89	2830	145	424.66
16:00	22.87	26.1	3180	185	71.8
16:30	22.07	25.14	3440	205	122.34
17:00	21.49	22.17	3670	215	92.05
17:30	20.16	18.54	3850	215	34.7
18:00	18.21	16.05	3980	215	0
18:30	17.05	14.46	4100	215	0
19:00	16.31	13.07	4200	215	0

Table 9: Advanced solar still performance during night experimental test
6.1 In summer season

Time	Advanced still temperature				Weather conditions	
	Water temperature (ºC)	Basin temperature (ºC)	Vapour temperature (ºC)	cover temperature (ºC)	Ambient temperature (ºC)	Wind speed (m/s)
19:00	18.42	18.81	19.07	18.94	19.17	3.23
19:30	22.94	22.04	20.31	16.24	18.84	3.58
20:00	27.07	26.31	24.41	15.24	18.03	3.95
20:30	29.82	28.09	26.39	15.36	17.46	4.08
21:00	31.1	29.74	28.08	14.21	16.93	4.21
21:30	32.47	30.66	29.36	16.85	16.54	3.97
22:00	37.84	35.49	34.82	17.69	16.07	4.55
22:30	42.56	41.07	39.05	18.32	15.72	4.86
23:00	46.08	44.92	42.84	19.65	16.14	5.14
23:30	49.92	48.17	46.51	20.26	16.32	5.66
0:00	52.32	50.58	49.25	21.63	16.08	5.29
0:30	51.75	49.98	49.68	25.07	15.98	4.47
1:00	52.04	50.94	50.75	25.6	15.74	4.68
1:30	53.14	51.78	50.98	26.34	15.82	4.32
2:00	54.08	52.65	51.45	27.65	16.19	3.93
2:30	53.53	52.06	51.02	25.14	16.85	3.81
3:00	52.32	51.75	50.53	24.32	17.23	3.77
3:30	51.65	50.17	49.48	22.01	17.86	3.24
4:00	50.44	49.32	48.79	20.41	18.08	3.57
4:30	51.21	48.66	48.16	18.68	18.54	3.40
5:00	50.66	48.21	47.87	19.32	19.16	4.02
5:30	51.13	49.05	48.24	20.14	19.55	4.25
6:00	50.25	49.37	48.08	21.36	20.16	4.66
6:30	49.65	50.08	47.61	22.06	20.75	4.28
7:00	50.21	50.85	48.16	23.14	21.36	4.59

Table 10: The performance in winter season

Time	Advanced still temperature				Weather conditions	
	Water temperature (ºC)	Basin temperature ºC	Vapour temp (ºC)	Inner cover temperature (ºC)	Ambient temperature (ºC)	Wind speed (m/s)
19:00	14.25	14.01	13.92	13.62	13.74	5.74
19:30	18.32	17.76	15.31	11.43	13.02	5.68
20:00	23.14	20.1	17.57	10.6	12.59	5.85
20:30	26.36	24.32	20.26	10.75	11.82	6.12
21:00	29.87	27.98	24.06	9.92	11.31	6.08
21:30	34.92	32.66	30.28	10.46	10.88	8.25
22:00	39.09	36.9	34.57	10.25	10.71	7.12
22:30	43.36	42.88	39.92	11.13	10.5	7.98
23:00	45.65	44.9	41.48	13.82	9.84	9.08
23:30	46.07	46.12	42.81	14.26	9.34	8.87
0:00	48.26	48.3	44.08	18.31	8.8	8.52
0:30	48.55	48.9	44.71	19.46	8.94	7.36
1:00	49.9	49.65	45.12	18.9	8.75	6.91
1:30	50.21	49.12	45.92	19.08	8.07	7.08
2:00	50.6	48.22	46.23	18.85	7.94	6.78
2:30	49.8	48.4	45.58	19.25	7.71	7.25
3:00	49.1	48.65	46.12	18.55	7.82	6.45
3:30	49.9	47.9	45.83	19.61	8.08	6.60
4:00	50.3	48.2	44.76	18.38	8.18	6.12
4:30	49.87	48.6	44.21	19.71	8.02	5.89
5:00	49.9	47.89	43.68	20.14	7.89	5.54
5:30	50.3	48.33	43.81	19.81	8.21	6.13
6:00	50.7	49.1	43.07	19.07	8.83	5.74
6:30	50.1	49.56	42.42	18.21	9.04	5.56
7:00	50.4	49.8	41.93	18.87	9.35	5.73

Table 11: the performance of thermoelectric solar still on May 2021

Time	Advanced still temperature				Weather conditions	
	Water temperature (ºC)	Basin temperature (ºC)	Vapour temperature (ºC)	Cover temperature (ºC)	Ambient temperature (ºC)	Solar radiation (W/m^2)
7:00	16.02	16	15.9	15.07	17.5	0.0
7:30	17.68	16.76	16.33	14.93	18.35	5.68
8:00	19.93	17.9	17.45	14.13	19.72	19.27
8:30	22.81	19.32	19.03	15.1	20.06	38.08
9:00	25.91	23.21	23.31	14.34	20.93	78.85
9:30	27.8	28.65	23.78	15.82	21.37	115.97
10:00	32.91	33.72	26.93	16.24	22.15	144.36
10:30	38.45	36.98	32.85	17.27	22.49	240.85
11:00	42.76	42.02	39.08	19.23	23.03	278.65
11:30	45.27	47.12	42.21	22.03	23.25	354.63
12:00	49.32	49.78	45.72	23.79	23.82	401.25
12:30	52.1	54.9	46.12	26.13	24.22	432.11
13:00	53.16	56.32	48.26	28.65	25.17	489.65
13:30	54.52	57.76	49.87	29.98	25.83	546.36
14:00	58.36	59.8	52.36	35.21	26.14	590.65
14:30	60.08	61.32	53.47	36.07	26.28	610.87
15:00	57.44	59.54	52.85	37.15	25.73	660.36
15:30	54.21	57.44	51.98	36.8	24.86	508.5
16:00	52.08	53.1	49.65	35.56	24.13	370.31
16:30	50.84	50.43	48.22	36.04	23.41	289.28
17:00	49.85	48.21	46.37	32.11	22.7	114.10
17:30	49.21	47.55	45.01	27.18	20.15	71.31
18:00	48.98	46.9	44.21	25.32	19.17	1.25
18:30	49.13	47.2	44.42	22.74	17.1	0.0
19:00	48.37	46.77	43.81	19.54	16.87	0.0

Table 12: The performance of the conventional solar still on May 2021

Time	Conventional still temperature				Weather conditions	
	Water temperature (ºC)	Basin temperature (ºC)	Vapour temperature (ºC)	Cover temperature (ºC)	Ambient temperature (ºC)	Solar radiation (W/m^2)
7:00	15.9	16.04	15.7	15.07	17.5	0.0
7:30	16.21	17.2	16.06	16.12	18.35	5.68
8:00	17.34	18.53	16.87	17.03	19.72	19.27
8:30	19.12	19.9	18.35	17.9	20.06	38.08
9:00	21.03	22.2	19.79	19.55	20.93	78.85
9:30	22.9	23.65	20.5	20.17	21.37	115.97
10:00	25.87	27.18	22.65	22.32	22.15	144.36
10:30	28.65	29.89	26.32	25.71	22.49	240.85
11:00	33.43	35.32	28.54	28.33	23.03	278.65
11:30	38.21	39.76	34.61	32.65	23.25	354.63
12:00	40.87	42.1	38.43	35.32	23.82	401.25
12:30	45.56	46.6	42.76	36.98	24.22	432.11
13:00	49.87	50.2	44.58	39.04	25.17	489.65
13:30	51.56	53.12	48.4	39.76	25.83	546.36
14:00	53.12	54.8	51.87	41.32	26.14	590.65
14:30	52.81	54.3	50.98	40.02	26.28	610.87
15:00	51.2	53.1	50.33	38.43	25.73	660.36
15:30	48.76	50.28	49.21	35.62	24.86	508.5
16:00	47.54	49.1	46.05	33.83	24.13	370.31
16:30	43.08	45.32	41.28	31.21	23.41	289.28
17:00	39.76	40.1	38.86	29.43	22.7	114.10
17:30	37.44	37.23	34.21	25.38	20.15	71.31
18:00	32.21	32.1	30.63	23.65	19.17	1.25
18:30	28.54	27.9	26.39	19.32	17.1	0.0
19:00	23.03	22.32	22.89	17.98	16.87	0.0

Table 13: sample of the result on September 2021(TE solar still)

Time	Thermoelectric solar still temperature				Weather conditions	
	Water temperature (ºC)	Basin temperature (ºC)	Vapour temperature (ºC)	Cover temperature (ºC)	Ambient temperature (ºC)	Solar radiation (W/m^2)
7:00	12.32	12.08	12.71	12.67	12.8	3.87
7:30	18.84	17.69	15.03	13.41	13.07	7.83
8:00	22.64	20.87	17.28	11.22	13.63	25.88
8:30	27.52	25.33	22.14	10.62	14.17	60.41
9:00	31.46	29.41	27.47	12.32	14.98	108.30
9:30	35.95	34.85	31.29	13.08	15.12	195.93
10:00	38.09	38.02	34.52	14.12	15.82	307.71
10:30	40.37	39.83	39.92	15.32	16.43	380.22
11:00	44.8	42.79	43.81	16.85	16.79	454.47
11:30	47.19	46.68	45.19	17.36	17.03	290.85
12:00	48.28	48.11	45.82	19.15	17.22	352.47
12:30	49.79	51.89	46.96	22.81	17.48	505.92
13:00	52.34	53.23	48.06	26.90	17.79	530.20
13:30	54.85	55.11	49.25	29.31	17.13	449.47
14:00	54.77	55.05	50.32	31.02	17.09	478.32
14:30	53.91	54.76	49.13	30.41	16.81	407.62
15:00	52.08	53.34	47.28	28.38	16.24	321.4
15:30	51.16	51.89	47.06	26.14	15.92	281.35
16:00	50.27	49.36	46.25	23.97	15.24	215.23
16:30	48.36	47.89	45.31	21.39	14.91	105.71
17:00	47.99	47.06	43.07	19.73	14.3	130.27
17:30	47.03	46.32	42.46	15.41	13.74	78.69
18:00	46.82	45.78	41.74	14.63	13.62	98.41
18:30	46.66	45.55	40.75	13.25	13.32	1.85
19:00	46.81	45.62	40.01	12.41	13.08	0.0

Table 14: Sample of the results on September 2021 (Conventional solar still)

Time	Conventional solar still temperature				Weather conditions	
	Water temperature (ºC)	Basin temperature (ºC)	Vapour temperature (ºC)	Cover temperature (ºC)	Ambient temperature (ºC)	Solar radiation (W/m^2)
7:00	12.1	12.81	12.5	12.37	12.8	3.87
7:30	12.8	13.52	12.91	12.98	13.07	7.83
8:00	13.02	14.12	13.12	13.43	13.63	25.88
8:30	13.98	15.43	14.22	14.2	14.17	60.41
9:00	15.65	17.03	15.32	14.84	14.98	108.30
9:30	18.34	19.21	16.89	15.12	15.12	195.93
10:00	21.76	22.89	18.08	16.65	15.82	307.71
10:30	25.35	26.77	21.39	17.98	16.43	380.22
11:00	29.98	31.18	24.54	19.7	16.79	454.47
11:30	33.87	34.54	27.87	21.76	17.03	290.85
12:00	35.98	37.08	31.64	24.33	17.22	352.47
12:30	39.03	40.11	35.89	25.54	17.48	505.92
13:00	43.87	44.63	38.58	27.12	17.79	530.20
13:30	45.81	46.23	41.32	28.76	17.13	449.47
14:00	45.11	46.03	42.65	29.43	17.09	478.32
14:30	44.87	45.41	43.07	29.98	16.81	407.62
15:00	42.58	44.21	41.32	28.03	16.24	321.4
15:30	41.39	42.12	39.68	27.11	15.92	281.35
16:00	40.54	40.98	37.21	25.32	15.24	215.23
16:30	39.01	38.76	35.54	22.28	14.91	105.71
17:00	37.23	36.87	33.19	20.54	14.3	130.27
17:30	34.43	33.98	30.25	17.28	13.74	78.69
18:00	31.17	30.32	28.12	15.76	13.62	98.41
18:30	28.21	27.87	25.65	14.12	13.32	1.85
19:00	25.32	24.21	22.43	13.98	13.08	0.0

Table 14: Thermoelectric heat pump performance

Time	TE cold side temperature ºC		TE hot side temperature ºC		Temperature difference ΔT	COP	Distillate output (ml)
	in	out	in	out			
7:00	12.91	12.85	12.42	12.8	3.6		0
7:30	11.32	10.95	18.98	19.94	10.85		0
8:00	12.34	9.85	23.04	24.73	17.98	1.99	10
8:30	11.49	9.07	28.15	29.39	25.68		25
9:00	12.81	9.65	32.14	33.07	27.37	1.70	55
9:30	11.91	8.58	36.75	37.61	30.45		85
10:00	12.68	10.36	38.98	39.79	32.41	1.28	125
10:30	13.13	11.21	41.25	43.11	35.68		210
11:00	14.36	10.75	45.66	46.26	37.25	1.30	320
11:30	15.85	9.89	48.08	48.84	36.14		450
12:00	17.12	10.21	49.87	50.91	35.58	0.829	575
12:30	19.22	11.58	50.21	52.17	38.07		710
13:00	22.40	14.65	53.85	54.94	36.25	0.806	855
13:30	27.52	19.08	55.65	56.14	39.65		975
14:00	28.32	22.39	55.28	56.09	37.65	0.436	1150
14:30	29.04	24.52	54.59	55.85	36.32		1210
15:00	27.91	23.61	52.73	54.38	35.54	0.623	1350
15:30	25.14	21.20	52.06	53.14	36.01		1475
16:00	22.04	19.74	51.42	52.87	34.85	0.901	1600
16:30	20.5	17.22	50.16	51.39	37.47		1720
17:00	19.10	15.08	48.98	49.37	39.89	1.03	1850
17:30	17.52	13.36	48.11	49.05	40.12		1930
18:00	16.22	12.29	47.57	49.17	41.25	1.24	2100
18:30	14.08	11.36	47.25	48.96	42.04		2225
19:00	13.79	10.17	47.38	49.21	38.48	1.48	2390

Table 15: Thermoelectric still performance in May 2021 (Night Operation)

Time	Water temperature (ºC)	Basin temperature (ºC)	Vapour temperature (ºC)	Cover temperature (ºC)	Ambient temperature (ºC)
19:00	17.76	18.56	18.2	17.01	18.9
19:30	19.93	19.1	18.43	16.62	18.76
20:00	24.67	23.54	19.61	15.94	18.21
20:30	27.95	26.01	22.71	15.12	17.75
21:00	32.48	30.8	26.45	15.68	17.04
21:30	36.86	34.54	29.82	16.74	17
22:00	39.72	38.1	34.39	17.14	17.32
22:30	43.61	41.84	38.21	18.32	16.96
23:00	47.18	45.36	40.81	19.14	16.82
23:30	49.95	48.83	42.7	20.63	17.11
0:00	51.03	49.65	44.27	20.86	16.59
0:30	51.34	50.35	46.87	22.46	16.92
1:00	50.95	50	47.24	24.18	17.36
1:30	51.1	50.26	48.32	23.82	17.21
2:00	51.52	50.84	48.92	23.45	17.43
2:30	50.8	49.65	48.36	24.15	16.91
3:00	49.68	48.83	47.28	23.22	16.88
3:30	50.03	49.38	47.85	22.64	16.54
4:00	50.51	49.88	48.15	21.82	16.31
4:30	49.66	49.18	47.23	22.66	15.15
5:00	50.8	49.63	47.51	23.71	16.1
5:30	51.41	49.92	47.87	23.52	15.98
6:00	51.63	50.22	48.2	24.11	16.23
6:30	50.89	49.36	47.81	22.98	16.87
7:00	50.23	49.87	47.59	21.87	17.28

Table 16: Thermoelectric solar still performance in September (Night Operation)

Time	Water temperature (ºC)	Basin temperature (ºC)	Vapour temperature (ºC)	Cover temperature (ºC)	Ambient temperature (ºC)
19:00	17.23	16.94	16.5	16.4	16.3
19:30	19.95	18.83	16.98	15.32	16
20:00	22.87	22.05	18.32	14.73	15.9
20:30	25.84	24.59	20.66	13.57	15.75
21:00	28.96	27.15	22.34	12.87	15.25
21:30	32.44	30.94	26.1	12.04	14.9
22:00	36.76	34.68	29.4	12.33	14.3
22:30	39.16	37.28	31.58	12.85	14.9
23:00	43.15	41.53	34.68	13.71	14.32
23:30	46.89	44.35	37.14	14.48	14.15
0:00	48.12	46.78	39.25	15.12	13.86
0:30	49.93	47.32	40.82	15.82	13.51
1:00	50.19	48.93	39.54	16.86	13.05
1:30	50.43	48.98	41.76	16.24	12.94
2:00	48.98	47.17	43.24	15.83	12.7
2:30	49.92	48.32	44.27	16.21	12.2
3:00	50.23	49.11	45.24	17.28	11.82
3:30	49.36	48.92	45.56	18.13	11.5
4:00	49.83	48.12	46.81	18.23	12.04
4:30	50.51	49.28	46.15	17.36	12.34
5:00	49.92	48.66	45.74	18.1	12.15
5:30	50.13	48.04	44.75	19.07	11.32
6:00	49.66	47.97	43.65	19.87	11.3
6:30	48.87	47.25	44.32	18.87	11.56
7:00	49.98	48.21	45.81	18.83	12.87

Table 17: The temperature difference inside TE solar still

Time	Water temperature ºC						Inner cover temperature ºC					
	day1	day2	day3	day4	day5	day6	day1	day2	day3	day4	day5	day6
7:00	13.54	12.32	14.81	13.76	12.98	13.34	11.63	12.67	13.91	12.66	12.76	13.87
8:00	22.61	22.64	27.98	25.05	24.43	27.09	10.65	10.6	11.76	10.87	11.54	13.03
9:00	29.68	31.46	36.54	34.17	31.88	38.12	9.98	12.32	13.76	9.83	10.76	12.32
10:00	38.43	38.09	42.67	39.49	35.76	43.65	11.76	14.12	15.76	10.43	10.09	15.54
11:00	45.65	44.8	49.85	47.32	41.62	49.52	14.03	16.85	14.62	15.65	13.76	18.6
12:00	47.81	48.28	53.62	51.03	46.7	55.56	13.78	19.25	19.91	20.5	17.65	23.87
13:00	53.06	52.34	56.89	55.23	51.65	57.81	15.76	26.9	25.76	24.76	23.18	29.65
14:00	55.14	54.77	55.54	54.72	50.82	55.64	19.87	31.02	30.22	28.76	25.12	32.18
15:00	54.31	52.08	53.12	52.85	49.08	53.5	22.76	28.38	31.81	26.03	22.79	30.08
16:00	51.64	50.27	52.29	50.77	51.12	51.59	19.87	23.99	28.76	24.21	20.17	27.21
17:00	49.67	47.99	50.02	48.96	49.87	50.02	17.55	19.73	23.54	21.18	18.43	21.82
18:00	48.05	46.82	48.33	49.03	48.22	49.11	16.21	14.23	19.76	17.68	15.32	18.33
19:00	48.87	46.98	47.76	47.88	47.46	47.89	13.28	12.41	15.08	14.52	12.02	14.48

Table 18: The laboratory test results of the thermoelectric heat pump system

Voltage (V)	At T_h= 30 ºC				At T_h= 50 ºC			
	ΔT=60 ºC	ΔT=50 ºC	ΔT=40 ºC	ΔT=30 ºC	ΔT=60 ºC	ΔT=60 ºC	ΔT=60 ºC	ΔT=60 ºC
0	0	0	0	-	0	0	0	-
1	0	0	1.2	-	0	0	5.7	-
2	0	0.5	5.9	-	0	0.9	6.2	-
3	0.25	2.1	6.9	8.2	0	3.6	7.7	8.9
4	0.85	2.7	5.4	7.5	0.9	3.2	7.1	7.4
5	1.5	2.9	4.8	7.1	1.5	3	6	6.6
6	1.9	2.8	4.2	5.2	2.1	2.8	5	5.8
7	1.85	2.3	3.9	4.5	1.9	2.5	4.8	5.2
8	1.7	1.9	3.4	3.8	1.8	2.3	4.2	4.7
9	1.55	1.7	2.7	2.9	1.7	2.1	3.7	4.3
10	1.2	1.6	2.1	2.5	1.5	1.9	3.1	3.9
11	0.9	1.2	1.9	2.1	1.1	1.7	2.8	3.5
12	0.8	1.1	1.8	1.9	0.8	1.5	2.2	2.8

Appendix F: Photos of the systems construction and experiments

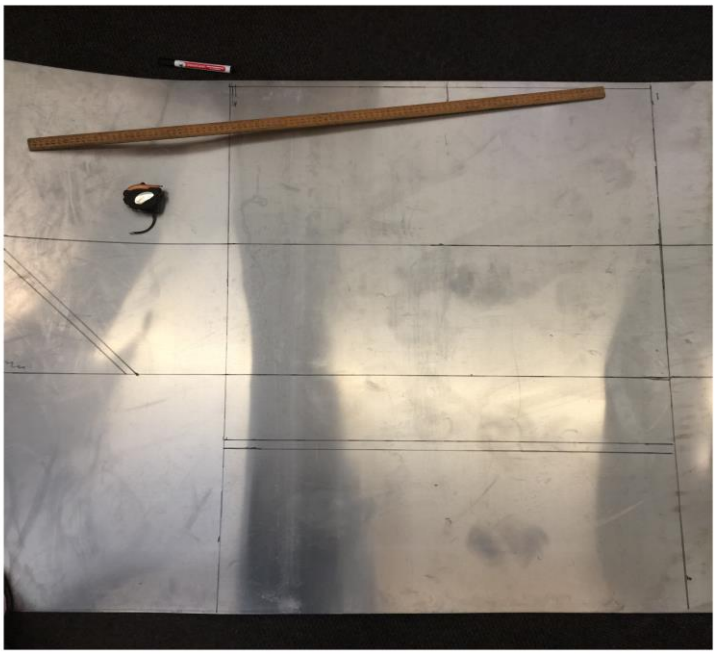

Determine the dimention of the solar still

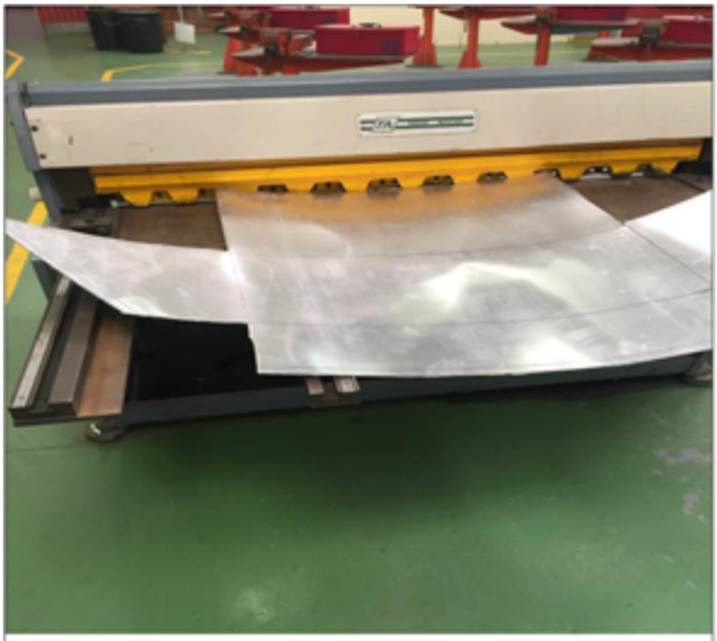

Solar still manufacturing

Bending machine

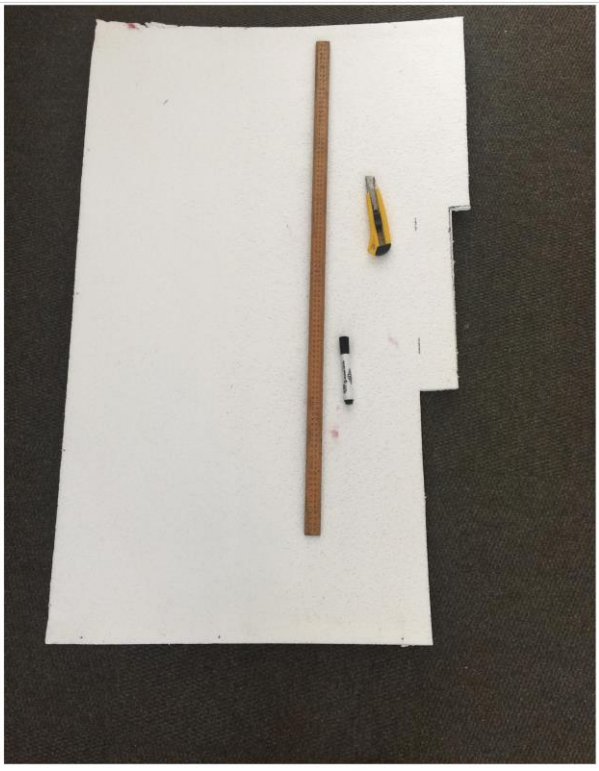

Polyurethane board cutting

Solar still assembly

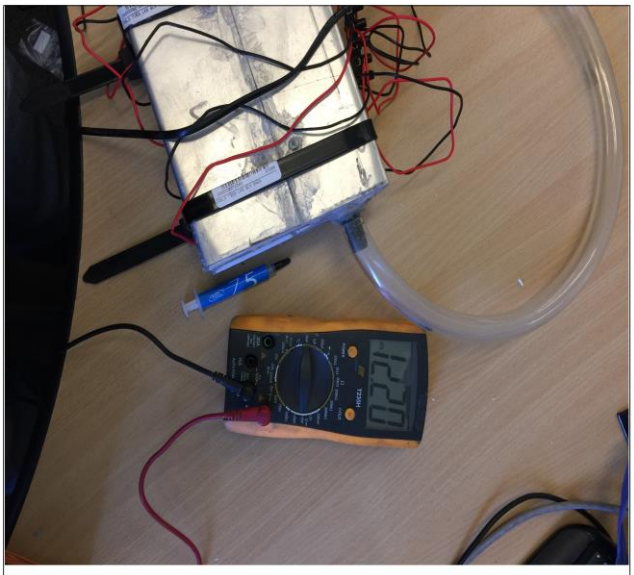

Thermoelectric heat pump pre-test

(a) water temperature of adcanced still

(b) water temperature of conventional still

(a) PV voltage output

(b) battery's temperature

condensation surface's cooling system